



**The dicentric chromosome rob(15;21)c:  
mis-segregation and predisposition to  
cancer**

**Connor Gilkes-Imeson**

Newcastle University  
Biosciences Institute

Doctor of Philosophy

March 2024



## Abstract

---

Robertsonian chromosomes are the most common constitutional translocation in humans, occurring in 1 in 800 of the general population. In 2014 it was discovered that carriers of the rare Robertsonian chromosome, rob(15;21)c, were strongly predisposed to developing a subtype of leukaemia, iAMP21-ALL (with ~2700-fold increased risk). In such cases, rob(15;21)c is dramatically rearranged to form a derivative chromosome that drives leukaemia. *In silico* modelling suggested that this derivative chromosome is produced by a catastrophic DNA damage event, chromothripsis, involving two copies of the rob(15;21)c chromosome. The reason for such a massive predisposition is not currently well understood. Here, I use cell biological techniques to explore the characteristics of the rob(15;21)c chromosome to better understand the mechanism causing iAMP21-ALL development. I show that rob(15;21)c is often actively dicentric, with the ability to assemble two kinetochores per sister chromatid. Despite the fact that rob(15;21)c is stably maintained in the cells of human carriers, I find that rob(15;21)c frequently mis-segregates during mitosis, at a much higher rate than chromosomes 15 and 21. I propose a mechanism in which the dicentricity of rob(15;21)c leads to an increased number of erroneous microtubule-kinetochore attachments which, if not resolved, often cause both rob(15;21)c chromatids to lag during anaphase. If this mis-segregation persists into telophase, then rob(15;21)c chromatids may enter a micronucleus, an environment previously shown to be a facilitator of chromothripsis. In summary, this work suggests that, due to the aberrant segregation tendencies of rob(15;21)c, carriers are predisposed to chromothripsis of rob(15;21)c and, in turn, the development of iAMP21-ALL.

## Acknowledgements

---

Firstly, I would like to thank my supervisor, Jon Higgins, for providing both guidance and freedom. I feel privileged to have undertaken my PhD in a lab where I was allowed to be an independent scientist but with the continuous support of a great supervisor. Jon has provided an environment in which I was not afraid to make mistakes nor ask questions when I was unsure. I would not be the scientist that I am today without the presence of both this environment and Jon's supervision. I would also like to thank my co-supervisors Christine Harrison and Diana Papini for their feedback and advice throughout the years.

My extremely positive experience as a PhD student was largely down to the people around me. I would like to thank both past and present members of the Higgins lab and of the office in which I spent most of my time. You have provided scientific support, emotional support, snacks, and cups of tea, but most importantly genuine friendship that has got me through the more difficult days. Juggling, speed-eating Quavers, pub trips, GeoGuessr and office badminton are some of the highlights, but daily chit-chats are what made each workday feel like hanging out with friends.

Finally, I would like to thank my friends and family for their unwavering support. To my Mam, Dad, and extended family who I know are enormously proud of me. You have always believed in me and supported me, and for that I am forever grateful. Particular thanks to Shannon, I would not be where or who I am today without you. This thesis and PhD have only been possible because of those mentioned above. Thank you all!

# Table of Contents

---

<b>Abstract .....</b>	<b>i</b>
<b>Acknowledgements .....</b>	<b>ii</b>
<b>Table of Contents.....</b>	<b>iii</b>
<b>List of figures .....</b>	<b>vi</b>
<b>List of tables .....</b>	<b>viii</b>
<b>Chapter 1: Introduction.....</b>	<b>1</b>
1.1 Overview.....	1
1.2 Cell cycle .....	1
1.2.1 Introduction to the cell cycle .....	1
1.2.2 Stages of mitosis.....	3
1.2.3 Chromosome segregation .....	5
1.2.4 The mitotic checkpoint and error correction .....	8
1.2.5 Chromosome mis-segregation .....	11
1.3 Dicentric chromosomes .....	13
1.3.1 Robertsonian chromosomes.....	14
1.3.2 Causes and consequences of dicentric chromosome mis-segregation.....	16
1.3.3 Promoting dicentric chromosome stability.....	20
1.4 Chromothripsis.....	22
1.4.1 Complex chromosomal rearrangements .....	22
1.4.2 Micronucleus model .....	25
1.4.3 Breakage-fusion-bridge model .....	28
1.4.4 Intertwined micronucleus and chromosome bridge model.....	30
1.4.5 DNA damage, re-integration and repair .....	31
1.4.6 Chromothripsis in disease.....	32
1.5 iAMP21-ALL.....	34

1.5.1	sporadic iAMP21-ALL .....	35
1.5.2	rob(15;21)c dependent iAMP21-ALL .....	36
1.6	Aims of this project .....	36
<b>Chapter 2:</b>	<b>Methods .....</b>	<b>38</b>
2.1	Genetic testing .....	38
2.2	Cell culture .....	38
2.3	Cloning .....	38
2.4	Flow cytometry.....	39
2.5	Metaphase and Anaphase enrichment .....	39
2.6	Immunostaining.....	40
2.7	Fluorescence In-Situ Hybridisation.....	40
2.8	Chromosome spreads .....	40
2.9	Lentiviral transformation.....	41
2.10	Western blotting.....	42
2.11	Expansion microscopy .....	42
2.12	Correlative Light and Electron Microscopy (CLEM) .....	43
2.13	Correlative immunofluorescence and Fluorescence IN-Situ Hybridisation.....	44
2.14	Fluorescence microscopy.....	44
2.14.1	Confocal microscopy .....	44
2.14.2	Stimulated emission depletion microscopy.....	45
2.14.3	High throughput microscopy .....	45
2.14.4	Live cell imaging .....	45
2.15	Image analysis .....	46
2.15.1	Image deconvolution.....	46
2.15.2	Analysis of centromeric foci .....	46
2.15.3	Mis-segregation analysis.....	46
2.15.4	Metaphase analysis .....	47
2.15.5	Chromosome nuclear location analysis.....	47

2.15.6	Macros used for image analysis .....	48
2.16	Data visualisation .....	48
2.17	Antibodies .....	48
2.18	Primers .....	51
<b>Chapter 3:</b>	<b>Characterising rob(15;21)c .....</b>	<b>54</b>
3.1	Introduction.....	54
3.2	Results.....	56
3.2.1	SNP arrays show the differences between diagnostic and remission samples of the iAMP21-ALL patient. ....	56
3.2.2	L995 and L996 cell lines have no obvious genetic differences from the blood samples from which they were derived. ....	59
3.2.3	iAMP21-ALL patient derived cell line has no obvious genetic differences to the unaffected twin derived cell line .....	64
3.2.4	rob(15;21)c translocation is confirmed in L995 and L996 cell lines .....	69
3.2.5	L995 and L996 cell lines are predominantly diploid.....	72
3.2.6	The dicentric chromosome rob(15;21)c has heterogeneity in its ability to assemble kinetochores .....	78
3.2.7	The rob(15;21)c centromeric heterogeneity does not change across passages ..	86
3.2.8	The rob(15;21)c chromosome has one dominant and one weaker centromere ..	91
3.2.9	Both rob(15;21)c kinetochores have the ability to bind microtubules .....	96
3.3	Discussion.....	98
<b>Chapter 4:</b>	<b>Characterising how rob(15;21)c behaves .....</b>	<b>103</b>
4.1	Introduction.....	103
4.2	Results.....	104
4.2.1	rob(15;21)c frequently mis-segregates during mitosis .....	104
4.2.2	rob(15;21)c mis-segregation rates across passages .....	112
4.2.3	rob(15;21)c mis-segregates into environments that are susceptible to chromothripsis .....	114
4.2.4	Why does rob(15;21)c frequently mis-segregate?.....	118

4.2.4.1	Location of rob(15;21)c in the nucleus.....	118
4.2.4.2	rob(15;21)c centromeric cohesion .....	121
4.2.4.3	CPC activity at rob(15;21).....	124
4.2.4.4	Metaphase plate alignment of rob(15;21)c .....	130
4.3	Discussion .....	133
<b>Chapter 5:</b>	<b>Tagging rob(15;21)c and live imaging of L995 and L996 cells.....</b>	<b>140</b>
5.1	Introduction .....	140
5.2	Results .....	141
5.2.1	Problem 1 – L995/6 move around too much for live imaging.....	141
5.2.2	Problem 2 – Lymphoblastoid cells are difficult to transfect.....	144
5.2.3	Problem 3 – rob(15;21)c needs to be distinguishable from other chromosomes by live imaging.....	147
5.2.3.1	Target identification.....	148
5.2.3.2	CRISPRainbow optimisation.....	152
5.2.3.3	Attempted CRISPRainbow transduction .....	158
5.3	Discussion .....	162
<b>Chapter 6:</b>	<b>Discussion.....</b>	<b>166</b>
6.1	The active dicentricity of the rob(15;21)c chromosome .....	166
6.2	The mis-segregation of rob(15;21)c and mechanisms that may be driving it.....	169
6.3	The difficulty in tagging rob(15;21)c and tracking it throughout cell division.....	172
6.4	Concluding remarks .....	173

## List of figures

---

Figure 1.1.	The eukaryotic cell cycle.....	3
Figure 1.2.	Schematic of the centromere and kinetochore.....	6
Figure 1.3.	Kinetochore-Microtubule attachment types. ....	10
Figure 1.4.	Formation of rob(15;21)c from the acrocentric chromosomes 15 and 21.....	15
Figure 1.5.	Causes of dicentric chromosome mis-segregation. ....	17

Figure 1.6. Consequences of dicentric chromosome mis-segregation. ....	19
Figure 1.7. Schematic of chromothripsis.....	24
Figure 3.1. The diagnostic sample of patient 23299 shows a chromothriptic der(15;21). ....	58
Figure 3.2. L995 cell line is representative of the blood sample from which it was derived...	61
Figure 3.3. L996 cell line is representative of the blood sample from which it was derived...	63
Figure 3.4. Cell lines derived from the iAMP21-ALL twin patient and the unaffected twin patient have no gross chromosomal differences.....	66
Figure 3.5. rob(15;21)c is confirmed in L995. ....	70
Figure 3.6. rob(15;21)c is confirmed in L996. ....	71
Figure 3.7. FISH shows possible tetraploid population in L996 cells.....	73
Figure 3.8. L995 does not have a large tetraploid population. ....	75
Figure 3.9. L996 does not have a large tetraploid population. ....	77
Figure 3.10. rob(15;21)c sometimes appears actively monocentric.....	80
Figure 3.11. rob(15;21)c sometimes appears actively dicentric.....	81
Figure 3.12. Actively dicentric rob(15;21)c inter-centromeric distance can appear short due to chromosome spread variation.....	83
Figure 3.13. Line graphs showing the resolution of CENP-C foci with small inter-centromeric distance. ....	84
Figure 3.14. rob(15;21)c assembles a full outer kinetochore at both centromeres.....	86
Figure 3.15. L995 rob(15;21)c centromeric heterogeneity does not change across passages..	89
Figure 3.16. L996 rob(15;21)c centromeric heterogeneity does not change across passages..	90
Figure 3.17. Actively dicentric rob(15;21)c chromosomes have one stronger and one weaker centromere. ....	91
Figure 3.18. CEN 21 of rob(15;21)c is significantly weaker than other centromeres.....	93
Figure 3.19. Monocentric rob(15;21)c chromosomes specifically retain CEN15.....	95
Figure 3.20. Both kinetochores of rob(15;21)c have the ability to bind microtubules. ....	97
Figure 4.1. Anaphase cell with mis-segregating rob(15;21)c.....	106
Figure 4.2. High throughput analysis of rob(15;21)c mis-segregation.....	107
Figure 4.3. rob(15;21)c mis-segregates frequently.....	109
Figure 4.4. rob(15;21)c sister chromatids often mis-segregate together. ....	111
Figure 4.5. rob(15;21)c mis-segregation rates do not change across passages. ....	113
Figure 4.6. rob(15;21)c in micronuclei.....	114
Figure 4.7. Mis-segregating chromosomes in L995 and L996 cells enter micronuclei. ....	117
Figure 4.8. The interphase location of rob(15;21)c likely does not promote mis-segregation .....	120

Figure 4.9. Cohesin staining at rob(15;21)c is not aberrant.....	123
Figure 4.10. Aurora B staining on rob(15;21)c is not aberrant.....	126
Figure 4.11. INCENP staining on rob(15;21)c is not aberrant. ....	127
Figure 4.12. Survivin staining on rob(15;21)c is not aberrant.....	128
Figure 4.13. Hec1S44ph staining on rob(15;21)c is not aberrant. ....	129
Figure 4.14. rob(15;21)c mis-aligns on the metaphase plate. ....	132
Figure 5.1. Lymphoblastoid cells are difficult to live image due to their movement.....	141
Figure 5.2. Poly-L-Lysine and Cell-Tak do not efficiently stick down lymphoblastoid cells. .....	143
Figure 5.3. Lymphoblastoid cell adhesion is slightly improved by a CC2 coated surface. ...	144
Figure 5.4. Lymphoblastoid L996 cells can successfully be transduced by lentivirus. ....	146
Figure 5.5. Diagram of the CRISPRainbow technique for fluorescently tagging specific loci. .....	148
Figure 5.6. Chromosome 15 and chromosome 21/13 can be tagged in human oocytes. ....	150
Figure 5.7. FISH confirms that sgRNA successfully targets chromosome 21 and chromosome 13.....	152
Figure 5.8. Blasticidin resistance was successfully cloned into a dCas9 containing plasmid. .....	154
Figure 5.9. The U6 promoter, the CCDB gene and 2xPP7 sequences were successfully cloned into a PCP-3xGFP containing plasmid. ....	155
Figure 5.10. The U6 promoter, the CCDB gene and 2xBoxB sequences were successfully cloned into an N22-3xmCherry containing plasmid. ....	156
Figure 5.11. L996 cells transduced with dCas9 containing lentivirus did not express dCas9 protein. ....	159
Figure 5.12. L996 cells can be transfected with a control GFP plasmid by nucleofection....	160
Figure 5.13. Large fluorescent plasmids were not successfully nucleofected. ....	161
Figure 5.14. L996 cells nucleofected with dCas9 containing plasmid did not express dCas9 protein. ....	162

## List of tables

---

Table 2.1. List of primary antibodies.....	48
Table 2.2. List of secondary antibodies .....	50
Table 2.3. List of primers.....	51

Table 3.1. L995 and L996 CNVs compared against the COSMIC database of known cancer genes. ....	68
Table 3.2. L995 and L996 CNVs compared against a database of known chromosome segregation genes from Gene Ontology. ....	68
Table 3.3. Counts of rob(15;21)c with actively monocentric or actively dicentric phenotypes across passages. ....	87



# Chapter 1: Introduction

---

## 1.1 Overview

A seminal study in 2014 highlighted the hugely increased risk that carriers of the dicentric Robertsonian chromosome rob(15;21)c have for developing a subtype of leukaemia, iAMP21-ALL. Although many studies have examined the clinical implications of Robertsonian chromosomes, few have looked at the cell biology that causes them to behave differently from normal chromosomes. Furthermore, rob(15;21)c is rarer than some other Robertsonian translocations and has therefore been less well studied.

The focus of this thesis is to characterise rob(15;21)c, its segregation properties in mitosis, and to better understand why carriers are predisposed to iAMP21-ALL development.

In this introduction, I will outline the mammalian cell cycle, and summarise current knowledge of chromosome segregation and mis-segregation. I will then introduce dicentric chromosomes, with a particular focus on Robertsonian chromosomes and the causes and consequences of dicentric chromosome mis-segregation. As the rob(15;21)c chromosome appears to undergo extensive reorganisation to produce a derivative chromosome that drives leukaemia, I introduce the topic of chromosome rearrangements such as chromothripsis, and the models of how they may occur. Finally, I end the Introduction with information on iAMP21-ALL and its subtypes.

## 1.2 Cell cycle

### 1.2.1 Introduction to the cell cycle

The eukaryotic cell cycle enables the growth and division of a cell to create two identical daughter cells. This process consists of interphase (approximately 23 hours of the ~24 hour cell cycle) and mitosis (approximately 1 hour of the ~24 hour cell cycle); depicted in Figure 1.1. Interphase is split into a first growth/gap phase (G1), a DNA replication phase (S) and a second growth/gap phase (G2), though cells can also exit the cell cycle to become quiescent in G0. Although mitosis is a relatively short process in the cell cycle, it is complex and consists of multiple, highly regulated stages; prophase, prometaphase, metaphase, anaphase and telophase (described in 1.2.2).

The cell cycle is a tightly controlled process, orchestrated largely by complexes consisting of a cyclin and a Cyclin-Dependent Kinase (CDK). As the cell cycle progresses, cyclin levels rise

and fall; when bound to their CDK partner they drive progression through the cell cycle via their kinase activity. CDK4/6 are partnered with D-types cyclins to regulate G1 phase. CDK2 is partnered with cyclin E to regulate the G1-S phase transition, CDK2 with cyclin A to regulate S phase, CDK1 with cyclin A to regulate the G2-M phase transition and CDK1 with cyclin B for mitosis<sup>1,2</sup>. While CDK-cyclin complexes drive a cell through the cell cycle, checkpoints have the ability to halt this progression. Cell cycle checkpoints act to ensure that each phase of the cell cycle is accurately completed before the next begins. Checkpoints are activated by various signals (e.g. the mitotic/spindle assembly checkpoint is triggered by unattached kinetochores, halting cell progression until all kinetochores are bound to microtubules, at which point anaphase can commence).

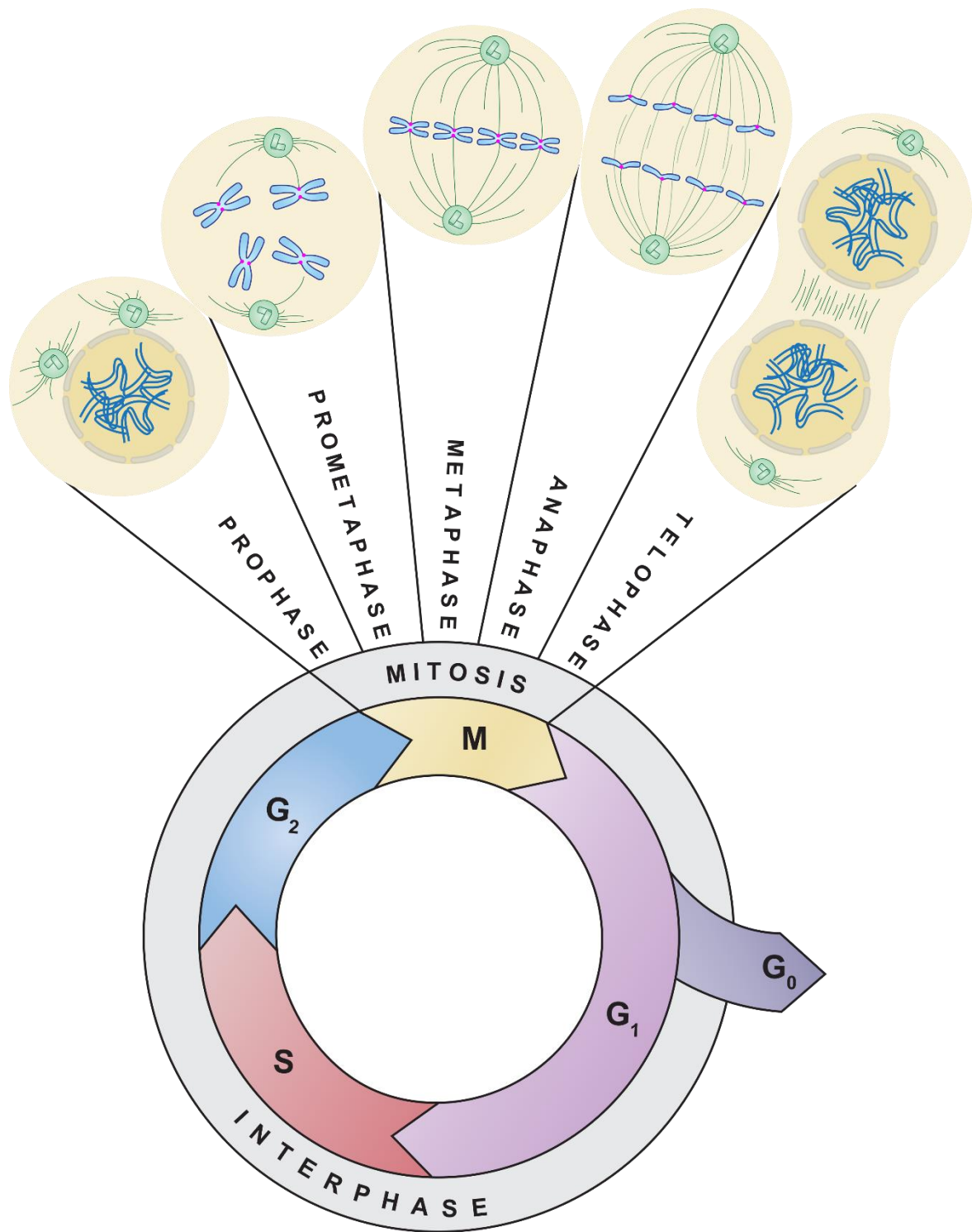


**Figure 1.1. The eukaryotic cell cycle.** Diagram of the eukaryotic cell cycle all stages of interphase and mitosis. Mitosis stages are represented graphically with microtubules labelled in green, DNA in blue, centromeres in magenta, nuclear envelope in grey. Adapted from a PhD Thesis from Beccy Harris<sup>3</sup>.

### 1.2.2 Stages of mitosis

Mitosis, albeit short, is a difficult and high-stakes stage of the cell cycle. Splitting genetic material (previously replicated in S phase) perfectly from one cell into two requires a high

degree of accuracy. Failure of proper chromosome disjunction has the ability to cause aneuploidy and cancer<sup>4-8</sup>. Although mitosis has been well studied, many of its complexities have yet to be fully understood.

Mitosis consists of multiple stages (pictured in Figure 1.1). Firstly, prophase involves the initiation of chromosome condensation. This is coupled with the breakdown of the nuclear envelope and loss of the nucleolus. In prophase, the centrosomes begin travelling toward the cell poles. The cohesin that has been holding sister chromatids together since S phase is now removed from chromosome arms in a cleavage-independent manner (prophase pathway)<sup>9</sup>. However, centromeric and pericentromeric cohesin is retained due to the protection by Shugoshin (and possibly haspin), and sister chromatids are still held together at their centromeres<sup>10,11</sup>.

In prometaphase, chromosomes become fully condensed, and the breakdown of the nuclear envelope is completed. Spindle microtubules continue to grow from the centrosomes as they start to form connections with some kinetochores. Many of these connections may be short lived, though some will persist. As these connections are being formed, some chromosomes will become bioriented, with each kinetochore binding microtubules from opposite poles. This will begin the process of chromosomes lining up on the cell equator.

When all chromosomes are bioriented and lined up on the cell equator (metaphase plate) a cell is described as being in metaphase.

If the Spindle Assembly Checkpoint (SAC) is satisfied (all kinetochores are microtubule-bound), then metaphase is short lived. The now active Anaphase Promoting Complex (APC/C) targets cyclin B1 for destruction, rendering CDK1 inactive<sup>12</sup>. This initiates the onset of anaphase. The APC/C also targets Securin for destruction, which releases (and therefore activates) Separase. Separase acts to cleave the remaining centromeric Cohesin, therefore liberating sister chromatids from each other<sup>13,14</sup>. There is now no inter-centromeric tension and microtubule pulling forces facilitate the movement of single sister chromatids to opposite poles<sup>15,16</sup>. As microtubules shorten, the cell also elongates to aid sister chromatid separation<sup>17,18</sup>.

During telophase, chromosomes reach the poles and begin to decondense. Simultaneously, the nuclear envelope starts to reform, with two distinct nuclear envelopes, one around each set of daughter chromosomes. Nucleoli also reform and spindle microtubules are disassembled.

Cytokinesis then completes the exit of mitosis by cleavage furrow formation, causing the division of cytoplasm into two independent cells through the contraction of an actin and myosin ring at the cell equator<sup>19</sup>. Now there are two identical daughter cells primed for entry into the next interphase; prepared to repeat the whole process again.

### 1.2.3 Chromosome segregation

Given that roughly 300 billion cell divisions take place in a human body every day<sup>20</sup>, and the possibility for a mistake in division to cause drastic effects (e.g. cancer<sup>21</sup>), the segregation of chromosomes must be tightly regulated to ensure high fidelity.

For functional chromosome segregation, there must be a link between the centromeric DNA and the microtubules that will ultimately separate sister chromatids. This job relies on the kinetochore. The kinetochore is a multi-subunit complex made up of over 110 different components<sup>22,23</sup>. A simple schematic of the centromere and kinetochore is shown for reference in Figure 1.2. The inner most part of the kinetochore, the Constitutive Centromere Associated Network (CCAN), binds directly to the histone H3 variant CENP-A and is present throughout the cell cycle<sup>24</sup>. This complex is made up of 16 centromere proteins: CENP-C, -H, -I, -K, -L, -M, -N, -O, -P, -Q, -R, -S, -T, -U, -W and -X that are separated into functional groups with varying roles<sup>25</sup>. One vital role of the CCAN is to provide a structural base for recruitment and assembly of outer kinetochore proteins. Whilst the CCAN is present throughout the cell cycle, most kinetochore proteins are only associated with the centromere during mitosis. Via two distinct mechanisms, CCAN proteins CENP-C and CENP-T recruit the outer kinetochore, with either mechanism being sufficient to build a kinetochore that can allow chromosome segregation<sup>26,27</sup>. The outer kinetochore is made up of the Knl1, Mis12 and Ndc80 complexes; collectively these make up the KMN network<sup>28</sup>. Both the Mis12c and Knl1c start to accumulate at the centromere from S phase onward, with highest levels being reached at metaphase<sup>22</sup>. The recruitment of the Mis12c and Knl1c is facilitated by interactions between CENP-C and the now phosphorylated (and therefore active) Mis12<sup>29</sup>. Upon entry into mitosis (breakdown of the nuclear envelope), Ndc80 is recruited; firstly by the interaction with CENP-C and Mis12<sup>30</sup> and then through interactions with CENP-T (after phosphorylation by CDK1)<sup>31,32</sup>. Although the KMN network is the essential part of the outer kinetochore and directly involved in binding microtubules, other protein complexes are known to be recruited throughout mitosis to mediate microtubule-kinetochore attachments, including the Ska1 complex<sup>33</sup> and formation of the fibrous corona<sup>34,35</sup>.

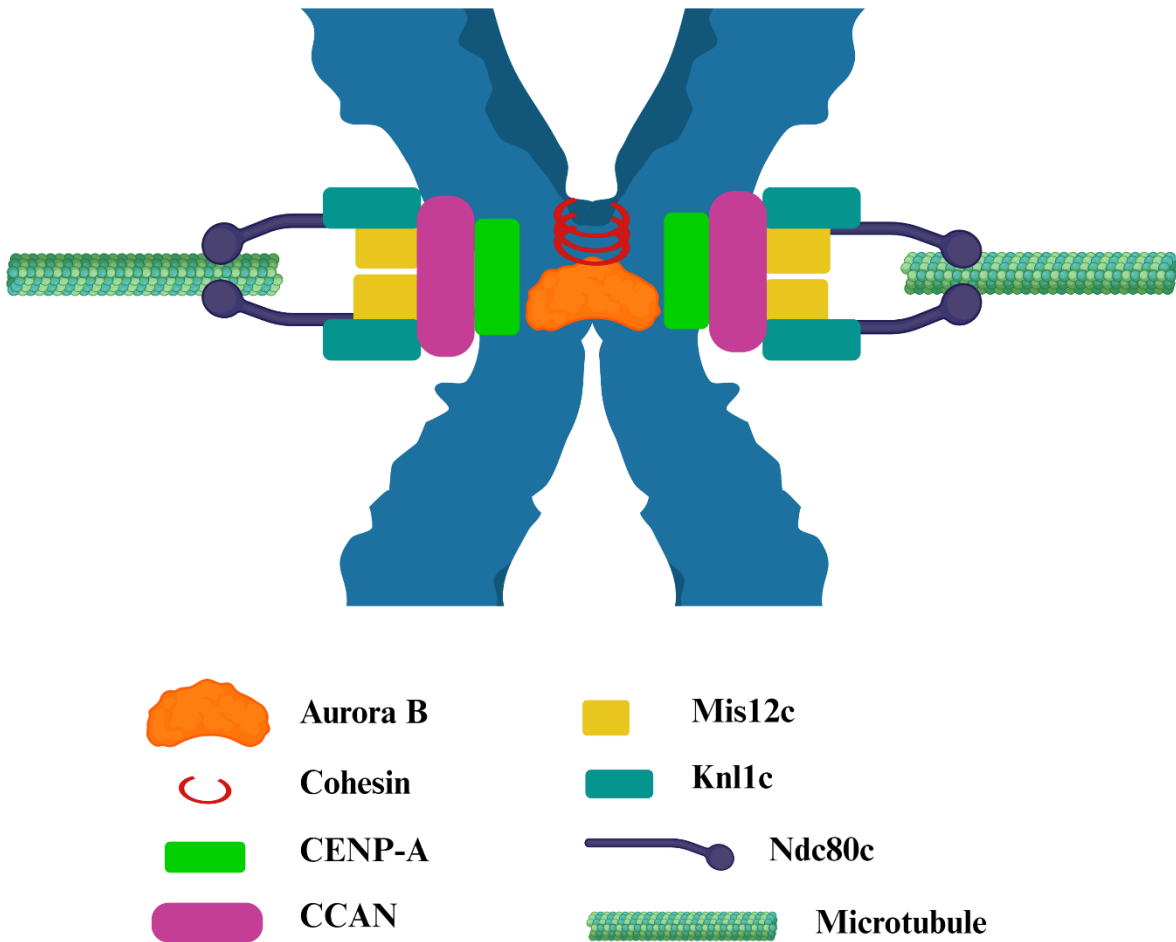


**Figure 1.2. Schematic of the centromere and kinetochore.** An elementary overview of the components that make up the centromere and kinetochore.

The primary role of the kinetochore is to capture microtubules, linking the chromosomes with the spindle poles. For these attachments to cause accurate chromosome segregation, the attachments must be end-on, with the microtubule plus-ends embedded in the kinetochore. Three types of microtubule occur in mitosis: kinetochore microtubules that bind chromosomes, interpolar microtubules that cross over in the centre of the cell and astral microtubules that grow toward the cell cortex<sup>36</sup>.

Microtubule-kinetochore attachments allow for chromosome congression as prometaphase cells transition toward metaphase. Broadly, two types of congression exist. Firstly, peripheral congression occurs when laterally attached chromosomes (where kinetochores interact with the walls of spindle microtubules) are moved toward the pole and then to the equator in a dynein- and CENP-E-dependent manner (described further below). The alternative form of congression is direct congression; this mechanism occurs preferentially when chromosomes are located

between the poles after nuclear envelope breakdown<sup>37</sup>. Direct congression occurs when a chromosome directly forms end-on attachments at the kinetochores without first making lateral attachments.

In order for chromosomes to make initial lateral attachments, crescent-shaped fibrous coronas form as crowns on top of the kinetochores. These structures make the kinetochore larger and more likely to interact with a kinetochore microtubule<sup>38</sup>. Laterally attached chromosomes are firstly moved toward the spindle poles via the minus-end-directed motor protein dynein and then toward the equator via chromokinesins and CENP-E<sup>39-41</sup>. It is here, at the equator, where lateral attachments are converted into end-on attachments. Lateral attachment to end-on attachment conversion is regulated in a spatially dependent manner by Aurora B, BubR1-associated PP2A, and in the late stages of conversion, the Astrin-SKAP complex<sup>42</sup>.

Upon establishment of end-on attachments, depolymerisation of microtubule plus-ends causes a pulling force that is strong enough to move chromosomes<sup>43,44</sup>. However, this microtubule depolymerisation is not the only mechanism by which chromosomes are actively being moved. Pushing forces known as polar ejection forces are exerted by astral microtubules along chromosome arms<sup>45,46</sup>. The balance of the pushing from polar ejection forces and pulling from depolymerisation of kinetochore microtubules causes oscillation in chromosome position. Ultimately, chromosomes are aligned on the equator, forming the metaphase plate<sup>37</sup>. Chromosome congression is proposed to promote mitotic fidelity by causing all chromosomes to start anaphase from the same starting point<sup>47</sup>.

Anaphase then involves the separation of sister chromatids to opposing poles. However, microtubule forces could not accurately separate sister chromatids if they are still bound by centromeric Cohesin. During the metaphase-to-anaphase transition and following the activation of the APC/C, Securin is destroyed, releasing its binding partner Separase. Separase can now cleave centromeric Cohesin, relieving sister chromatids from each other<sup>13,14</sup>. Although polar ejection forces can provide some contribution, it is microtubule depolymerisation pulling forces that are the main factor causing poleward movement of chromosomes in anaphase<sup>48,49</sup>. The pulling of chromosomes to poles is not the only mechanism occurring in anaphase. In fact, the elongation of interpolar microtubules (termed anaphase B) similarly contributes to chromosome movement<sup>18,50,51</sup>. This mechanism elongates the cell and aids the separation of sister chromatids. As anaphase completes and sister chromatids reach their respective spindle poles, the most error-prone stage of mitosis is complete. Cells must now reform their nuclear

envelopes and decondense chromosomes. The cytoplasm is divided into two and finally one mother cell has now become two identical daughter cells, with equal copies of each chromosome.

#### **1.2.4 The mitotic checkpoint and error correction**

As the process of chromosome segregation is crucial to produce healthy daughter cells, multiple mechanisms are in place to reduce the chance of errors occurring. Cell cycle checkpoints act as a control mechanism to halt progression through the cell cycle if necessary. The G1/S, intra-S and G2/M checkpoints are those active during interphase to assess cell size (G1/S, G2/M), DNA damage (G1/S, Intra-S, G2/M) and DNA replication (Intra-S, G2/M)<sup>52-54</sup>. The mitotic cell cycle checkpoint is known as the Spindle Assembly Checkpoint (SAC). The role of the SAC is to ensure proper chromosome segregation occurs. The SAC acts at kinetochores to determine if microtubules are attached. By sensing the absence of attachments, the SAC is able to halt mitotic progression, giving the cell time to form correct attachments at all kinetochores, therefore promoting accurate segregation. The KMN network has been reported as the scaffold for SAC signalling<sup>55</sup>. As this super-complex of proteins is the functional site for microtubule binding, this places it nicely to assess microtubule-kinetochore attachment state.

Though multiple proteins play a role in the SAC, the major effector kinase is MPS1. MPS1 acts to phosphorylate multiple sites in the KMN network, recruiting checkpoint proteins to initiate and maintain an active checkpoint<sup>56-59</sup>. Cooperatively, proteins involved in the SAC act to monitor the attachment status of kinetochores. An unattached kinetochore will cause inactivation and destruction of the APC/C activator, CDC20<sup>60</sup>. The SAC allows formation of a CDC20 inhibitory complex known as the Mitotic Checkpoint Complex (MCC); consisting of BUB3, BUBR1, CDC20, and MAD2<sup>61,62</sup>. By inhibiting CDC20 (BUBR1 binding blocks destruction-box recognition sites) and promoting its destruction (CDC20 incorporation into the MCC causes ubiquitylation by the APC/C) the activity of the APC/C is inhibited<sup>63,64</sup>. An inactive APC/C will therefore be unable to destroy Cyclin B to promote anaphase initiation or destroy Securin to promote Cohesin cleavage and sister chromatid separation. This inactivation will therefore cause a halt in mitosis; until the SAC is fully satisfied the cell will not proceed passed metaphase.

Some evidence suggests that, once a kinetochore has formed stable end-on attachments, the initiating kinase MPS1 is outcompeted for overlapping binding sites with the microtubules<sup>65,66</sup>. Specifically end-on and not lateral attachments satisfy the SAC<sup>67,68</sup>. A reduction in MPS1 at a

given kinetochore causes reduced phosphorylation of its targets, hence reducing SAC protein recruitment and, in turn, reducing MCC formation and liberating CDC20 to activate the APC/C. Upon microtubule-kinetochore attachment dependent SAC silencing at all kinetochores, the SAC is satisfied. Now the APC/C will facilitate anaphase progression through its roles in Cyclin B destruction and Securin destruction.

Along with the SAC, anaphase error correction mechanisms act to promote faithful chromosome segregation and prevent erroneous microtubule-kinetochore attachments. Mis-attachments of microtubules are common in prometaphase and early metaphase but are often resolved in order to prevent lagging chromosomes in anaphase<sup>69,70</sup>. Figure 1.3 shows the possible microtubule-kinetochore attachment types on a monocentric chromosome. The amphitelic attachment is the most optimal state for accurate chromosome segregation. While a monotelic attachment would be recognised by the SAC (due to presence of an unattached kinetochore), all other mis-attachments involve end-on microtubule-kinetochore attachments at both kinetochores and thus would satisfy the SAC, allowing anaphase progression. However, merotelic attachments (here split into subtypes: balanced-merotelic, mero-amphitelic and mero-syntelic) would cause a lagging chromosome between spindle poles in anaphase if left to persist. Error correction mechanisms exist to resolve these mis-attachments in two ways. Firstly, by detaching incorrect microtubule-kinetochore attachments it allows another attempt at forming correct attachments. Secondly, during the process of microtubule detachment, a kinetochore becomes unattached, triggering the SAC. This error correction mechanism allows cycles of trial and error until accurate microtubule-kinetochore attachments are formed.

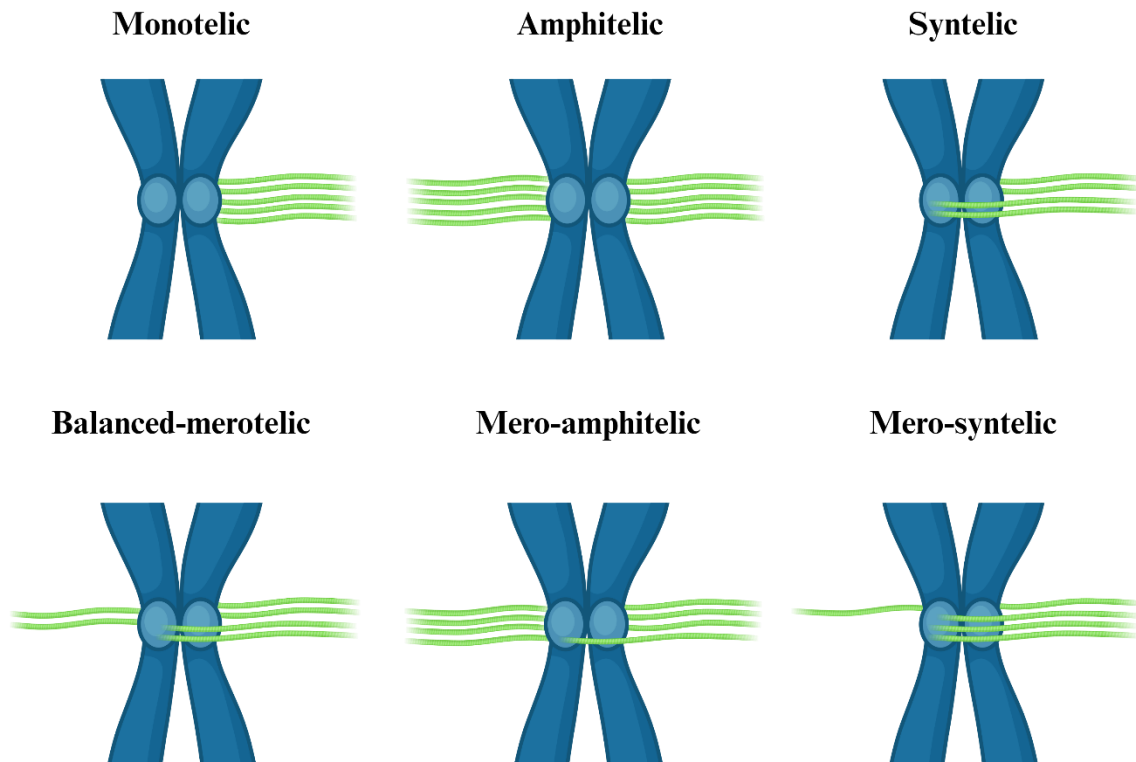


**Figure 1.3. Kinetochores-Microtubule attachment types.** Types of kinetochores-microtubule attachments on a monocentric chromosome. Correctly bi-oriented (Amphitelic), erroneously mono-oriented (Monotelic and Syntelic) and erroneously bi-oriented (Balanced-merotelic, Mero-amphitelic and Mero-syntelic) attachments are represented. Chromosomes in blue and microtubules in green. Adapted from Gregan *et al.*<sup>71</sup>.

The Chromosomal Passenger Complex (CPC) is a set of four proteins that act together at various locations and times in mitosis; INCENP, Survivin, Borealin and the enzymatic subunit Aurora B make up the CPC. While the proteins Survivin, Borealin and INCENP play more structural roles in the CPC, it is the kinase function of Aurora B which drives the mitotic regulatory function of the CPC. By phosphorylating target proteins, Aurora B contributes toward many different mitotic functions. During early mitosis, Aurora B (acting as part of the CPC) is required for the removal and repair of erroneous microtubule-kinetochores attachments<sup>72,73</sup>. Depletion of Aurora B (or Borealin) causes an increased number of syntelic and merotelic microtubule-kinetochores attachments<sup>74-76</sup>. Aurora B acts by phosphorylating Ndc80 on multiple sites, weakening its affinity for microtubule binding and promoting destabilisation of incorrect attachments<sup>77-79</sup>. By this mechanism, Aurora B creates unattached kinetochores, in turn activating the SAC<sup>80</sup>. While throughout these described process in early mitosis the CPC has been localised on the inner centromere, during the metaphase to anaphase transition, the CPC is moved to the spindle midzone and then also to the parts of the cortex at

the cell equator<sup>81-83</sup>. It is at these locations that Aurora B has functions in regulating contractile ring function and abscission<sup>84</sup>.

Few to no new microtubule-kinetochore attachments form during anaphase and so newly formed erroneous attachments are unlikely<sup>85,86</sup>, though persisting mis-attachments must be resolved in a timely manner. Although Aurora B plays an important role in error correction during early mitosis through its centromeric location, at anaphase Aurora B is at the midzone. Through experiments that acutely inhibit Aurora B function at anaphase or prevent midzone relocation, newer models suggest that the phosphorylation gradient that is set up by midzone Aurora B acts to influence microtubule-kinetochore interactions in anaphase<sup>87-90</sup>. These studies have shown that, despite leaving kinetochores during the metaphase to anaphase transition, the Aurora B midzone gradient can still act on kinetochore substrates in anaphase (to either play a role in error correction or to promote the stabilisation of microtubule attachments)<sup>89,90</sup>.

Evidently both the SAC and the error correction pathways are vital for accurate chromosome segregation. However, they are not fully independent; many proteins involved in these pathways are shared (e.g. Aurora B and MPS1). The SAC and error correction are intertwined, working together to facilitate accurate microtubule-kinetochore attachments and therefore faithful chromosome segregation. While these processes are well regulated and the vast majority of mitosis end correctly with two complete and identical daughter cells, this is not always the case.

### **1.2.5 Chromosome mis-segregation**

Data from primary cells, organoids and non-transformed cells predict that a mis-segregation event occurs in every 100-1,000 mitotic divisions in healthy tissue, with the rate in cancer cells sometimes being significantly higher<sup>91-95</sup>. Although these numbers may be elevated due to artifacts induced by cell culture, it is still evident that the risk of aneuploidy for human cells is significant, and the consequences can be drastic (cancer development).

Mis-segregation rates are not equal for all chromosomes. Multiple intrinsic chromosome attributes can affect their mis-segregation rate, causing non-random mis-segregation. It has been reported that larger chromosomes, particularly chromosomes 1 and 2 are more likely to mis-segregate than their smaller counterparts due to an increased susceptibility to cohesion fatigue<sup>95</sup>. In 2002 it was shown that there is a bias in chromosome segregation in female mouse meiosis that correlates with centromere size<sup>96</sup>. However, a more recent study has highlighted

how the non-random mis-segregation of chromosomes is dependent on both the size of the chromosome, the size of the centromere and the relationship between them; a small chromosome with a big centromere is least likely to mis-segregate and a big chromosome with a small centromere is most likely to mis-segregate<sup>97</sup>. A further property that may influence a chromosome's mis-segregation rate is its nuclear location during interphase and as the nuclear envelope breaks down. Chromosomes which are close to the cell periphery and behind the spindle poles (i.e. between the spindle pole and cell cortex) are more likely to mis-segregate than midzone chromosomes<sup>98</sup>. This undesirable location may lead to more frequent erroneous microtubule-kinetochore attachments<sup>99</sup>. As large chromosomes are often located near the cortex in interphase, this may be one reason adding to the effect of more frequent mis-segregation of these chromosomes<sup>100-102</sup>.

Recent live-imaging studies have shown that more chromosomes lag/mis-segregate during anaphase than previously expected<sup>87,88</sup>. However, most of these laggings are transient and are resolved before aneuploidy occurs. As described in section 1.2.4 most erroneous attachments are resolved by the SAC halting mitosis until end-on attachments are formed and by the error correction machinery resolving incorrect attachments. Work in mouse oocytes has shown that not all merotelic attachments necessarily lead to mis-segregation. More than 20% of microtubule-kinetochore attachments in metaphase II are merotelic, however <1% of chromosomes at anaphase II lag and <10% of laggings become aneuploid<sup>103</sup>. It is clear now that mis-attachments, and mis-segregations, are somewhat common, however cells can robustly resolve erroneous attachments and allow faithful segregation in the majority of cases.

If mis-segregating/lagging chromosomes are not resolved by error correction machinery and are not detected by the SAC, then it is likely that the mis-segregating chromosome will enter a chromosome bridge or a micronucleus. Chromosome bridges occur when a chromosome is stuck between spindle poles during anaphase and the microtubules forces cause stretching of the centromeric and inter-centromeric DNA. Micronuclei are also a common outcome for a mis-segregating chromosome. A micronucleus is a nucleus-like structure that occurs when a nuclear envelope forms around DNA (often a lagging or fragmented chromosome) that is not part of the primary nucleus. There are at least four possible outcomes for chromosome-containing micronuclei: persistence as stable independent structures, reintegration into the primary nucleus, micronucleus degradation and micronucleus extrusion<sup>104</sup>. The most common of these phenotypes is for a micronucleus to remain as its own independent structure, at least

until the next mitosis. Those that do persist are frequently subject to rupture and DNA damage<sup>105</sup>. This process is discussed in further detail in section 1.4.2.

Although mis-segregations are commonly resolved, if one persists such that daughter cells are subject to whole chromosome loss or gain, then these are cells are termed aneuploid. Aneuploidy is heavily associated with cancer; however, these events are not always a direct promoter of tumourigenesis. Due to the difficulty to untangle the processes of Chromosomal Instability (CIN) from the state of aneuploidy, these processes have been difficult to study independently. Recent findings have shown that aneuploidy can both promote or suppress tumour formation depending on the context<sup>106</sup>. Generally, whole chromosome gain or loss is detrimental to cell survival. However, in some circumstances aneuploidy can give survival advantages. In cancer, whether aneuploidy is detrimental or advantageous is dependent on multiple factors including tumour stage, cell type, tumour microenvironment and immune system interactions<sup>106</sup>.

Mis-segregation is a frequent process that is most often resolved. Even with the appropriate chromosome structure and centromeric proteins, errors can occur. So far, I have only discussed the segregation of ‘normal’ monocentric chromosomes. Aberrations in chromosome structure can further elevate the risk of mis-segregation. In particular, some chromosomes are dicentric in nature, creating further problems when it comes to accurate chromosome segregation.

### 1.3 **Dicentric chromosomes**

Centromeres play two important roles in mitosis. Firstly, they are necessary to hold sister chromatids together. While arm Cohesin is removed early in mitosis, during prophase, Cohesin at the centromere is protected by Shugoshin and therefore sister chromatids remain together until cleavage of Cohesin in a Separase-dependent manner at the metaphase to anaphase transition. Secondly, centromeres provide the site for kinetochore assembly. Centromeres, through interactions with the histone variant CENP-A and DNA binding protein CENP-B, facilitate the assembly of the kinetochore. Proper microtubule-kinetochore attachments then ensure faithful chromosome segregation.

Although most chromosomes are monocentric, with one centromere per sister chromatid, various forms of dicentric chromosomes exist in nature (two centromeres per sister chromatid). Dicentric chromosomes can be formed through various mechanisms. DNA breakage followed by chromosome fusion, telomere loss followed by fusion, and neocentromere formation have

all shown to be ways that these abnormal chromosomes occur<sup>107</sup>. While some dicentric chromosomes cause genomic instability, others persist and are stably inherited and passed on through multiple generations of offspring.

Throughout this thesis the term “dicentric” is used to describe a chromosome that has two separate regions of centromeric DNA. An “active” dicentric chromosome is used to describe one in which both centromeres have assembled proteins associated with the kinetochore (e.g. CCAN or KMN components). A “functional” dicentric chromosome is defined as one in which both centromeres have the ability to bind microtubules (via their kinetochores).

### **1.3.1 Robertsonian chromosomes**

Robertsonian translocations involve the fusion of two acrocentric chromosomes (chromosomes 13, 14, 15, 21 and 22). This fusion involves loss of p-arm DNA and often the creation of a dicentric chromosome (example shown in Figure 1.4 by fusion of chromosome 15 and chromosome 21 to produce rob(15;21)c). Robertsonian chromosomes are the most common translocation in humans with around 1 in 800 people carrying one of these chromosomes<sup>108-110</sup>. As acrocentric p-arms are not very gene rich (mostly containing ribosomal rDNA), most Robertsonian translocations are well tolerated.

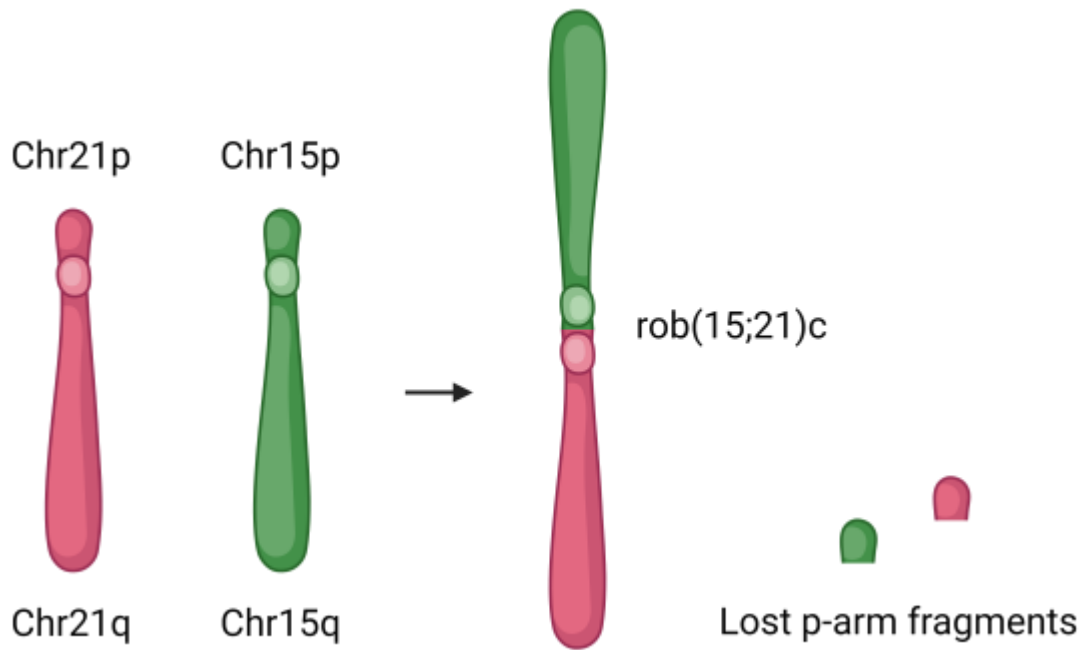
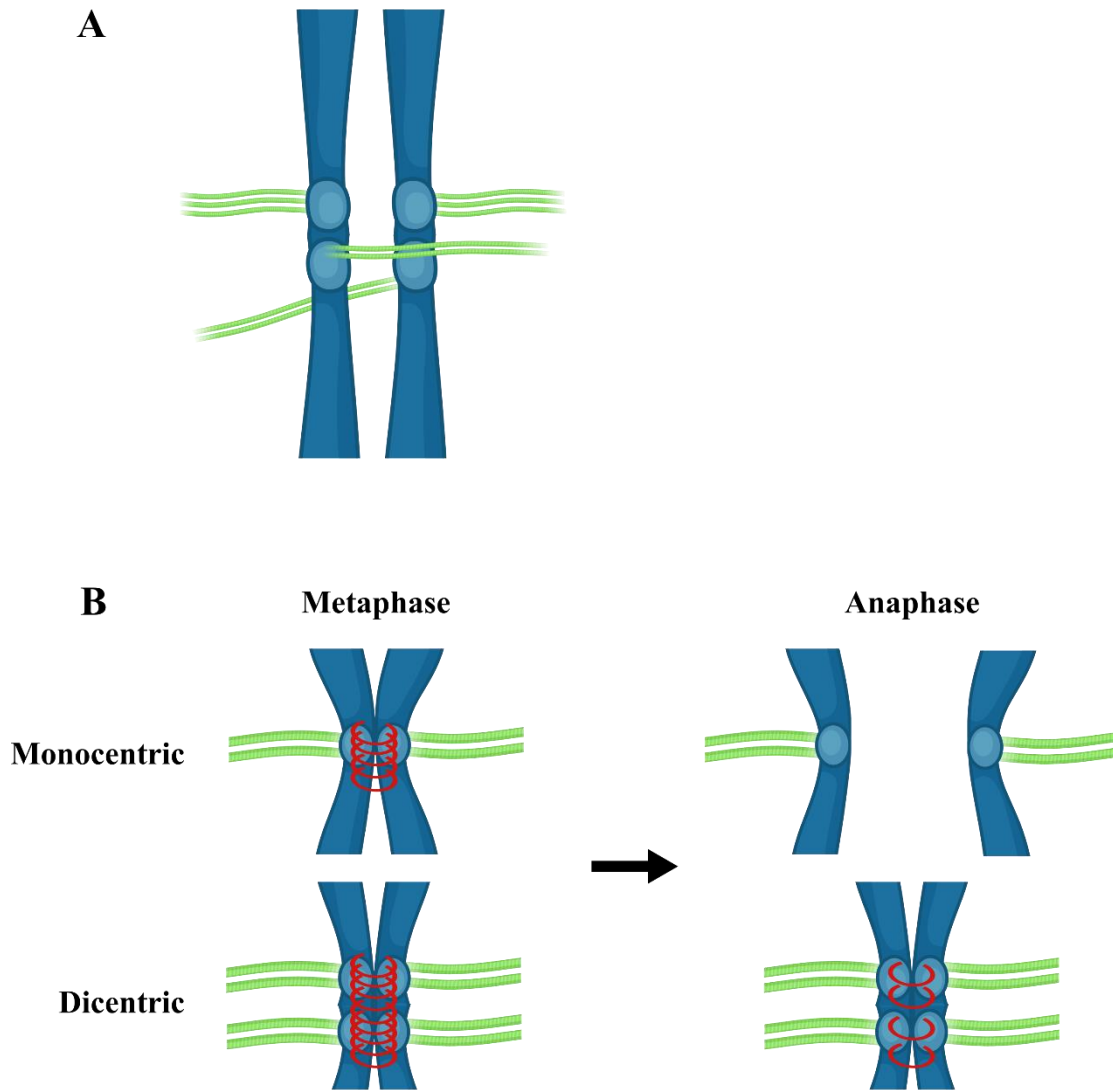


**Figure 1.4. Formation of rob(15;21)c from the acrocentric chromosomes 15 and 21.** Chromosome 15 is represented in green and chromosome 21 in magenta. The rob(15;21)c chromosome is indicated by the joining of the p-arms to create a dicentric chromosome with loss of p-arm fragments.

Robertsonian chromosomes can be classified into one of two groups. Class I Robertsonians (rob(13;14)c and rob(14;21)c) are both commonly occurring and have similar breakpoints, whereas class II Robertsonians (all other possible acrocentric formations) are rare and have more random breakpoints<sup>111</sup>. It is thought that these classes form through different mechanisms. While both classes are thought to form during oogenesis, Class I Robertsonians likely form through nonallelic homologous recombination on repetitive p-arm sequences, whereas Class II Robertsonians likely involve some form of telomere crisis that creates a different breakpoint in each case<sup>111-114</sup>. Rob(13;14)c accounts for 59-69% of all Robertsonian translocations, rob(14;21)c for 15-20% and all other Robertsonian translocations 0-5% each. These numbers differ depending on the study, though it is difficult to get an accurate number for Class II Robertsonians as they are much rarer<sup>115</sup>.

### **1.3.2 Causes and consequences of dicentric chromosome mis-segregation**

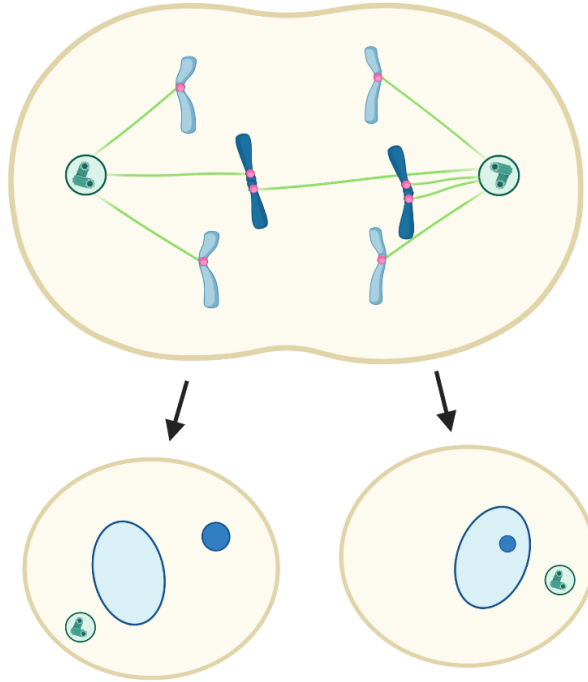
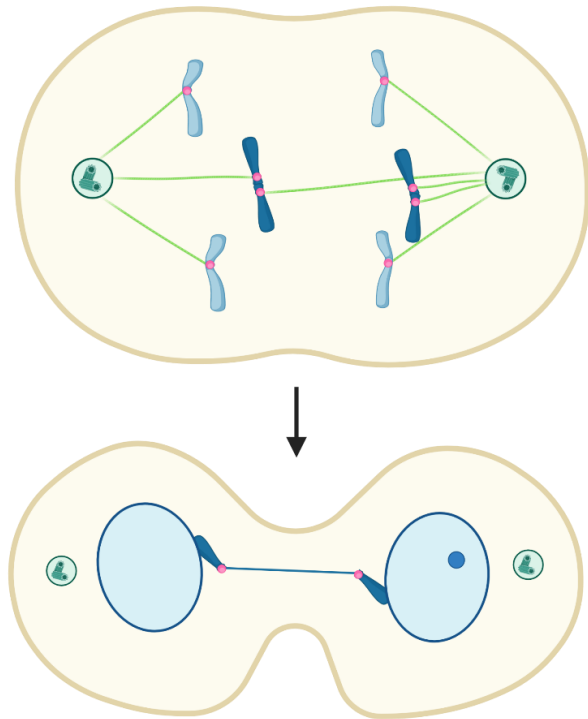
Dicentric chromosomes pose a threat to mitotic fidelity. The presence of an extra centromere on each sister chromatid potentially allows the assembly of another kinetochore and thus another site for microtubule interactions or increased cohesion. Dicentric chromosomes may promote chromosome mis-segregation by multiple mechanisms. Figure 1.5 highlights two means by which this could occur. If both centromeres of a dicentric chromosome are active, forming two kinetochores, then the two centromeres of one sister are able to bind microtubules emanating from opposite spindle poles (shown in Figure 1.5A). These aberrant attachments are similar to merotelic attachments on a monocentric chromosome. They may cause chromosome lagging during anaphase when other chromosomes are being pulled to spindle poles. Figure 1.5B then gives an example of a further mechanism by which dicentric chromosomes may cause chromosome mis-segregation. The second centromere may be a source of extra centromeric Cohesin that a monocentric chromosome would not have. If this additional Cohesin cannot be cleaved before the onset of anaphase, then it is again possible that this dicentric chromosome may become a lagger.



**Figure 1.5. Causes of dicentric chromosome mis-segregation.** (A) Aberrant microtubule attachments on a dicentric chromosome may cause chromosome lagging. (B) The increased amount of Cohesin at dicentric centromeres may, if not cleaved in time, physically hold sister chromatids together and cause chromosome lagging. Chromosome in blue. Microtubules in green. Cohesin rings in red.

If chromosome mis-segregations persist then the consequences can be severe (discussed in terms of monocentric chromosome mis-segregation in section 1.2.5). Like lagging monocentric chromosomes, if dicentric laggings are not resolved before the reformation of the nuclear envelope, then it is likely that this chromosome will enter a micronucleus (shown in Figure 1.6A). Micronuclei are known to be sites that are susceptible to extensive DNA damage (discussed further in section 1.4.2). As a dicentric chromosome may have increased susceptibility to erroneous microtubule attachments, it is plausible that when lagging, these chromosomes are less likely to be resolved in time and may appear more frequently in

micronuclei. An alternative consequence of dicentric chromosome mis-segregation is a chromosome bridge. The aberrant microtubule attachments frequently formed on actively dicentric chromosomes allow for the formation of chromosome bridges. These bridges involve the two centromeres of a single sister chromatid being pulled to opposite spindle poles, stretching out centromeric and inter-centromeric DNA (shown in Figure 1.6B). It has been well documented that these bridges are susceptible to breakage and further rounds of aberrant attachment and DNA damage (discussed further in section 1.4.3)<sup>114,116-118</sup>.

**A****B**

**Figure 1.6. Consequences of dicentric chromosome mis-segregation.** (A) Lagging dicentric chromosomes, if not resolved, can enter micronuclei. (B) Dicentric chromosomes can form chromosome bridges that are susceptible to breakage and further rounds of DNA damage. Chromosomes in blue. Centromeres in magenta. Microtubules in green.

The potential consequences shown in Figure 1.6 are possible for all forms of dicentric chromosome. However, Robertsonian chromosomes also have the potential to cause various downstream phenotypic effects. Robertsonian translocation carriers have frequent fertility problems; an increased risk of miscarriage, still birth, and offspring with an increased risk of congenital malformations and chromosomal aberrations<sup>119–121</sup>. This increased rate of fertility challenges likely occur due to the production of unbalanced gametes<sup>122</sup>.

Dicentric chromosomes broadly are found to be a driver of genomic instability, particularly in cancer<sup>123,124</sup>.

### **1.3.3 Promoting dicentric chromosome stability**

Dicentric chromosomes become more stable and have a reduced chance of undergoing the errors described in section 1.3.2 when they inactivate one of their centromeres; becoming pseudodicentric (or actively monocentric). Early studies discovered how dicentric chromosomes can act as actively monocentric or dicentric. Initial experiments showed that dicentric chromosomes that have two primary centromeric constrictions sometimes only have one active centromere, as revealed by C- and Cd- banding<sup>125</sup>. This was also backed up by staining of centromere proteins that showed CENP-B was present at both centromeres of a dicentric but when the chromosome was acting actively monocentric, CENP-C was only present at the active centromere and not the inactive<sup>126</sup>.

Interestingly, the distance between centromeres on a single dicentric sister chromatid appears to influence the centromeric state of these dicentrics. A study of dicentric X chromosomes highlighted how these chromosomes can sometimes have two active kinetochores but sometimes have only one; and this correlated with their inter-centromeric distance<sup>127</sup>. As the inter-centromeric distance increased, it became more likely that these chromosomes were actively monocentric. It has been proposed that dicentric chromosomes with short inter-centromeric distances can have cooperative centromeres. These short inter-centromeric distances may prevent chromosome twisting and therefore make it more likely that the two kinetochores of one sister bind microtubules from the same pole. This would therefore create a more stable chromosome when compared with a dicentric with a large inter-centromeric distance that was free to twist and allow sister centromeres to bind microtubules from opposite poles.

The mechanisms for centromere inactivation are not well understood. However, various mechanisms have been proposed that could influence centromere activity. The two primary hypotheses are that centromere inactivation occurs through DNA loss<sup>128</sup>, or via an epigenetic mechanism that causes loss of centromeric proteins<sup>126</sup>. Higgins *et al.* showed that although centromeric state is usually clonal, in some cell lines this state can change (switching from actively dicentric to actively monocentric)<sup>129</sup>. In this study they observed no change to DNA at the inactivated centromeres and therefore proposed that these switches must be epigenetic (though it is unlikely that small changes in repetitive centromeric DNA could accurately be observed in 2005). At that time, it was proposed that one possible epigenetic mechanism that could influence centromeric activity is the acetylation status of the centromeric histones. It had previously been demonstrated that centromeric heterochromatin is hypoacetylated<sup>130,131</sup>. Although the hyperacetylation of inactive centromeres has not yet been reported, it remains a plausible mechanism. Another epigenetic mechanism for centromere inactivation has been observed in plants. Koo *et al.* studied the B chromosome in maize and observed that a normal B centromere is hypomethylated but inactive centromeres exhibit hypermethylation<sup>132</sup>. DNA methylation therefore could be impacting the transition from an active to inactive centromere<sup>133</sup>. This idea is supported by the recent findings on the telomere-to-telomere human genome assembly that suggests CENP-A binding regions of the centromeric DNA of active centromeres are hypomethylated<sup>134</sup>.

While most often centromere inactivation in constitutional dicentric chromosomes is likely epigenetic, this may differ from dicentric chromosomes formed in cancer. Dicentric chromosomes often cause genomic instability, therefore it is no surprise that they are associated with cancer progression. These dicentrics are often stabilised by centromere inactivation, inversion (therefore reducing centromere distance), inter-centromeric deletion (also reducing inter-centromeric distance) or centromere excision into a ring chromosome<sup>135</sup>.

It is evident from the work discussed above that dicentric chromosomes with large inter-centromeric distances are problematic in mitosis. One example where this is evident in nature is with Robertsonian translocations. Similar to other types of dicentric chromosome, Robertsonians often undergo centromere inactivation, promoting stability<sup>136</sup>. The cases in which Robertsonian chromosomes are actively dicentric also involve a short inter-centromeric distance<sup>137</sup>. This supports the hypothesis that two centromeres with a short distance can act cooperatively as if monocentric. An interesting phenomenon that appears to occur in Robertsonian chromosomes that become functionally monocentric is preferential centromere

dominance. In 1994 Sullivan *et al.* studied patient derived Robertsonian chromosomes and proposed a hierarchy of acrocentric centromere dominance. The rate of this dominance varies between individuals and between cells (e.g. while most rob(13;14)c chromosomes have an active chromosome 14 centromere and an inactive 13 centromere in most cells (~75%), in ~25% of their cells the chromosome 13 centromere is active and 14 inactive). Whilst numbers were low for the class II Robertsonian chromosomes, the principal conclusion was that the chromosome 14 centromere is most often active, and the chromosome 15 centromere is least often active.

Although there has been some evidence for the epigenetic inactivation of dicentric centromeres<sup>126,129</sup>, 50% of *de novo* experimentally-induced Robertsonian chromosomes remain functionally dicentric and the other half appear to be frequently inactivated by loss of centromeric DNA. Centromere inactivation was frequently seen in conjunction with the temporary appearance of small chromosome fragments that contained centromeric proteins and alpha-satellite DNA of the inactive centromere<sup>138</sup>. The DNA of the inactivated centromere in the dicentric chromosome was also shown to be reduced in size. Therefore, whilst centromere inactivation occurs mostly epigenetically in non-Robertsonian dicentrics, in Robertsonian chromosomes (at least in *de novo* induced Robertsonians) inactivation occurs primarily through DNA loss.

## 1.4 Chromothripsis

### 1.4.1 Complex chromosomal rearrangements

There is plentiful evidence of sequential genetic changes which transform a cell to malignancy<sup>139</sup>. Acquired somatic mutations over time produce subpopulations with increasing proliferative potential. The selection of these subpopulations is then guided by Darwinian evolution.

Somatic mutations include substitutions, deletions, copy number changes (amplification or reduction) and chromosomal rearrangement. These mutations can be separated into those which are drivers and those which are passengers. Driver mutations give a selective advantage to the cell; e.g. amplification of an oncogene or deletion of a tumour suppressor, whilst passenger mutations describe all other somatic mutations. These passenger mutations do not confer a growth advantage and are likely to have been acquired in a previous subpopulation along with a driver<sup>139</sup>.

Whilst the cumulative acquisition of driver mutations provides the dogma for canonical cancer development, other mechanisms can also produce a malignant phenotype. Chromoanagenesis is a term first used by Holland and Cleveland in 2012 to describe a complex set of genomic rearrangements that occur at one or few chromosomes due to a single catastrophic event<sup>140</sup>. More recently this has been discussed further by Pellestor and Gatinois; the term chromoanagenesis now encompasses three unique mechanisms of chromosomal rearrangement<sup>141–143</sup>.

The first (and most relevant to this thesis), described by Stephens *et al.* in 2011, is chromothripsis; an event in which there is a large number of double stranded DNA breaks on a limited number of chromosomal segments. This is followed by reassembly of DNA fragments in a random order; thus producing an aberrant derivative chromosome with complex genetic rearrangements<sup>142,144</sup>. These events characteristically have oscillating copy numbers between two (or sometimes three) copy number states on the affected chromosome due to gains and or losses of multiple regions<sup>144–146</sup>. Chromothripsis is represented in Figure 1.7 in which a single chromosome undergoes many dsDNA breaks, followed by random fragment reassembly to produce a derivative chromosome with some fragments lost to the cell.

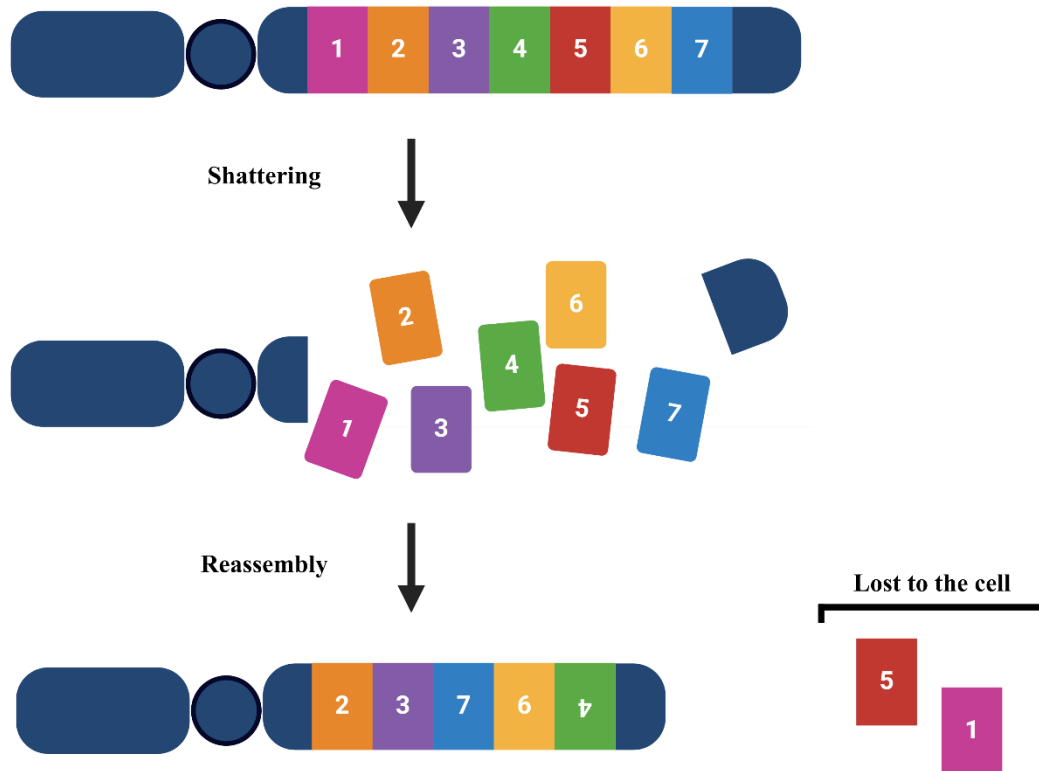


**Figure 1.7. Schematic of chromothripsis.** Chromosome fragments represented as coloured blocks become shattered during a catastrophic breakage event and then randomly reassembled to produce a derivative chromosome with some fragments being lost to the cell.

The second class of complex chromosomal rearrangements is chromoanasythesis, as described by Liu *et al.* later in 2011<sup>147</sup>. Chromoanasythesis, driven by defects in DNA replication, produces highly rearranged chromosomes; as in chromothripsis. Copy number changes, particularly duplications, triplications and deletions are seen in chromosomes that have undergone a chromoanasythesis event. These are caused by replication fork stalling and template switching (FoSTeS) or by microhomology-mediated break-induced replication (MMBIR). The copy number changes observed in chromoanasythesis cannot be explained by chromosome shattering, as seen in chromothripsis<sup>141</sup>. Replication stress due to endogenous or exogenous factors can lead to fork stalling followed by aberrant replication and repair due to these error prone pathways (FoSTeS and MMBIR)<sup>141–143</sup>. This is likely an event that occurs ‘all-at-once’ due to the rearrangements most often being at a distinct region of a single chromosome homologue and due to the clustering of breakpoints. Further, no mosaicism of chromosome rearrangement patterns is seen as cells proliferate, rather just lineages where the chromoanasythesis event has and has not occurred<sup>147</sup>.

The third class of complex chromosome rearrangement to be associated with chromoanagenesis is that of chromoplexy. Berger *et al.* discussed this type of catastrophic chromosomal rearrangement seen in prostate cancer in 2011<sup>148</sup>. But it was not until the group used further computational modelling in 2013 that it would be deemed as an all-at-once event<sup>149</sup>. It was then that the term chromoplexy was coined and that it started to be considered as a chromothripsis-like event. Chromoplexy is characterised by chains of inter- and intra-chromosomal translocations and deletions. Double stranded breaks have been observed in up to 8 chromosomes at a time, these are then re-assembled through non-homologous end joining (NHEJ); often with deletions seen at breakpoint junctions<sup>141–143,150</sup>.

These all-at-once events termed chromoanagenesis are most likely to have a negative effect on cell survival. However, some rearrangements will produce cell lineages that can not only survive, but that have a selective advantage, and in turn may cause a malignant phenotype. As opposed to the prolonged sequential mutations normally seen in cancer, chromoanagenesis can produce cells with the appropriate properties for cancer growth in a single event<sup>143,151</sup>.

Whilst all three mechanisms of chromoanagenesis produce complex chromosomal rearrangements and in turn complex phenotypes, chromothripsis is by far the most studied and clinically relevant, particularly in cancer<sup>152,153</sup>. Though chromothripsis has been seen in many different subtypes of cancer at varying rates, the mechanism of initiation and the events which lead to the reassembled chromosome are not entirely understood. Multiple models for chromothripsis initiation have been discussed, each with *in vitro* evidence to support them<sup>114,150,154,155</sup>. Originally there were two distinct proposed mechanisms (the micronucleus model and BFB model) but, more recently, it has been proposed that chromothriptic events involve components of both these models. In addition, chromothripsis may not truly occur all-at-once, but rather a few catastrophic processes are required in a short period of time<sup>156</sup>.

#### **1.4.2 Micronucleus model**

Micronuclei are small DNA containing structures that are separate from the primary nucleus. These are between 1/40th and 1/3rd the size of the primary nucleus<sup>157</sup>. Micronuclei have been found in disease (e.g. cancers and autoimmune diseases), with their presence being a marker for genomic instability<sup>158,159</sup>.

Micronucleus formation can be caused by many endogenous and exogenous factors. Double stranded DNA breaks cause fragmented DNA which can be moved to the membrane of the

primary nucleus; membrane blebbing will then produce micronuclei containing the chromosome fragments. This process can be induced by exogenous clastogens (e.g. anthracyclines) that promote DNA damage and disruption of DNA break repair<sup>160</sup>. However, more frequently, micronuclei are formed due to errors in mitosis, particularly in chromosome segregation. As discussed in 1.2.5, mis-segregation events can cause micronucleus formation from mis-segregating chromosomes if they remain separate from the main nucleus.

It has been shown that DNA replication, transcription and DNA break repair can occur in some, but not all micronuclei<sup>160-162</sup>. Replication of DNA in micronuclei is controversial, with some studies showing micronuclei with replicative ability, some showing micronuclei without and some with erroneous replication that is delayed from that in the primary nucleus<sup>94,163</sup>. In 2010, Terradas *et al.* showed that a single cell can have one micronuclei that is replicating DNA and one that is not, during the same S phase<sup>163</sup>. This highlights the heterogenous activity of DNA replication in micronuclei. These replication defects in micronuclei can in turn lead to chromoanaysynthesis<sup>147</sup>.

The occurrence of DNA damage in micronuclei is undoubtable, with the presence of  $\gamma$ H2AX (a phosphorylation event on histone H2AX that is used as a marker for double stranded DNA breaks) in micronuclei being reported in many studies<sup>94,164</sup>. However, the localisation to micronuclei of proteins associated with the DNA damage response is not as clear. Medvedeva *et al.* showed that proteins associated with early stages of double stranded break detection, ATM and MDC1 colocalise with  $\gamma$ H2AX in micronuclei<sup>164</sup>. Both ATM and MDC1 can be recruited to mitotic chromosomes for roles in the DNA damage response (DDR) and SAC regulation<sup>165</sup>. Therefore, it is possible that these proteins were already on DNA before they entered micronuclei. However, this study also found that MRE11 and Rad, members of the MRN complex colocalise with  $\gamma$ H2AX in the primary nucleus but not in micronuclei. The same could be found for TP53 binding protein 53BP1<sup>163,164</sup>. The lack of localisation of MRE11, Rad50 and 53BP1 to micronuclei, led Medvedeva *et al.* to propose that downstream double stranded break repair in micronuclei is likely defective. X-ray irradiation was used in a study by Yoshikawa *et al.* to induce micronuclei<sup>162</sup>. They found that 53BP1 did not colocalise with  $\gamma$ H2AX in these micronuclei. However, contrary to work from Medvedeva *et al.*, Yoshikawa *et al.* found that phosphorylated ATM also did not colocalise with micronuclear  $\gamma$ H2AX foci. Nevertheless, although mechanisms have not been thoroughly elucidated, it is clear that micronuclei have some defects in DNA damage repair and recruitment of associated proteins.

An explanation for the aberrant transcription, replication and repair sometimes seen in micronuclei is through defects in nuclear envelope organisation. It appears that functional micronuclei which can transcribe, replicate and repair DNA have an intact nuclear envelope, whereas those without these capabilities have defects in the micronuclei envelope<sup>166–168</sup>. It was first argued in 1987 by Labidi *et al.* that some micronuclei have incomplete envelopes that may contain gaps and have heterogeneity in their nuclear pore proteins<sup>167</sup>. Géraud *et al.* built on this in 1989 by identifying regions in micronuclei without nuclear lamina and by showing that it was only smaller micronuclei that were likely to have incomplete nuclear envelopes<sup>161</sup>. However, it was not until more recently that the understanding of the micronuclear envelope has been further developed. During chromosome decondensation in telophase the nuclear envelope forms two pools of proteins around chromosomes. The core proteins which bind at central regions, close to the mitotic spindle (e.g. membrane protein – Emerin) and non-core proteins which assemble on the chromosome periphery (including nuclear pore complexes and lamin B receptor)<sup>169,170</sup>. These non-core proteins are temporarily excluded from the core regions. Liu *et al.* have demonstrated how only the core proteins are able to efficiently assemble to lagging chromosomes that form micronuclei<sup>171</sup>. Further work has shown that once a nuclear envelope has formed lacking nuclear pore complexes (NPC) they will not be assembled and incorporated into the nuclear envelope as long as it is intact<sup>172</sup>. Therefore, micronuclei which have envelopes lacking NPCs will likely have defective translocation of proteins required for transcription, replication, and DNA break repair.

Mis-segregating chromosomes that sit between daughter nuclei often have micronuclear envelopes that lack non-core proteins. These midzone micronuclei are densely surrounded by microtubules and this may be the reason preventing assembly of non-core nuclear envelope proteins<sup>171,173,174</sup>. Evidence for this model comes from the work of Liu *et al.*, who observed that micronuclei forming away from the midzone are able to assemble both core and non-core nuclear envelope proteins<sup>171</sup>. An alternative model for failure to incorporate non-core proteins into midzone micronuclear membranes involves Aurora B. Afonso *et al.* discovered that experimental inactivation of Aurora B at anaphase onset allows nuclear pore complex formation on lagging chromosomes<sup>175,176</sup>. It was hypothesised that the presence of Aurora B at the midzone normally facilitates the condensation of lagging chromosomes and inhibits the formation of nuclear pore complexes<sup>88,177,178</sup>. However, it has also been suggested that Aurora B may be acting indirectly, through its mitotic spindle regulatory role<sup>171,179,180</sup>. This model combining both Aurora B regulation and microtubule obstruction may explain the lack of non-

core nuclear envelope protein recruitment to the membranes of micronuclei formed around midzone lagging chromosomes.

That chromothripsis occurs in micronuclei was first hypothesised by David Pellman's group (Dana-Farber Cancer Institute) in 2012. Crasta *et al.* found that micronuclei can persist through several cell cycles and the DNA replication that occurs in micronuclei is often defective and asynchronous<sup>94</sup>. As cells enter mitosis, DNA in micronuclei can fragment as it may still be replicating when chromosome condensation commences. A lagging chromosome that is isolated in a micronucleus provides an explanation for how only one chromosome can undergo severe chromosomal damage and rearrangement (chromothripsis). A further mechanism by which micronuclei could promote chromothripsis is through collapse of the nuclear envelope; seen in over 60% of micronuclei as shown by Hatch *et al.*<sup>105</sup>. Work from the Pellman laboratory aimed to demonstrate directly how a chromothriptic event could occur to a single mis-segregated chromatid<sup>154</sup>. A method which combines live-cell imaging and single-cell sequencing was developed. This novel technique, named Look-Seq was used to identify and sequence the DNA of daughter cells without micronuclei that were derived from cells which had micronuclei. These cells were presumed to have re-incorporated micronuclear DNA into the main nucleus following mitosis. This study showed that the chromosome that mis-segregated into a micronucleus had extensive localised chromosome rearrangements, characteristic of the oscillating copy number changes seen in chromothripsis. Ly *et al.* have recently built on this idea by using a centromere-specific inactivation technique, termed CEN-SELECT to produce mis-segregating chromosomes<sup>181</sup>. Using this, they show how chromosomes that mis-segregated into micronuclei have a largely increased vulnerability to an array of genomic rearrangements, including chromothripsis. Therefore, whilst being a marker for chromosomal instability (CIN), micronuclei can also facilitate further rearrangements.

The work described above provides strong evidence for a chromothripsis model involving extensive DNA damage and rearrangement occurring to a single chromosome or chromatid in a micronucleus. However, this does not have to be the only model; it is likely that more than one mechanism can cause chromothripsis *in vivo*.

### **1.4.3 Breakage-fusion-bridge model**

The phenomenon of breakage-fusion-bridge (BFB) cycles was first described by Barbara McClintock in 1941<sup>116</sup>. Excessive telomere shortening would usually cause senescence through DNA damage signalling pathways. However, upon loss of tumour suppressor proteins p53 and

retinoblastoma protein (Rb), senescence is bypassed<sup>114</sup>. Continuous telomere attrition may cause a crisis, during which ends of sister chromatids fuse together by non-homologous end joining (NHEJ), creating a dicentric chromosome. These dicentric chromosomes have been shown to drive genomic instability in multiple cancers<sup>123,124,145</sup>. Dicentric chromosomes will likely form microtubule attachments at both centromeres, producing an anaphase bridge. Mechanisms including nuclease activity on bridge DNA can cause breakage at any part of the DNA between the centromeres<sup>114,116</sup>. Daughter nuclei will therefore contain a chromosome with one centromere but with a broken end, lacking a telomere. After S phase DNA replication, a sister chromatid is synthesised that will likely fuse by fold-back inversion, again creating a dicentric chromosome likely to form an anaphase bridge. Continuous cycles of this breakage-fusion-bridge mechanism can promote chromosomal instability and localised amplification often seen in the karyotypes of malignant tumours.

Upon characterising chromothripsis, Stephens *et al.* stated that it is possible that these BFB cycles could induce the DNA damage seen in chromothripsis<sup>144</sup>. However, it was an influential paper from Maciejowski *et al.* in 2015 that provided clear evidence for this<sup>114</sup>. This study used in vitro models with Rb and p53 pathways knocked down, combined with expression of TRF2-DN, a dox-inducible dominant negative allele of TRF2 (telomeric repeat binding factor 2) to induce BFB cycles. Chromatin bridges had weak staining for histones, suggesting nucleosome loss due to stretching. Bridges remained intact for 3-20 hours before being resolved through exonuclease activity<sup>114</sup>. The major cytoplasmic 3' exonuclease TREX1 was present at chromatin bridges formed due to telomere dysfunction and at those formed due to lagging chromosomes. Cells containing chromatin bridges underwent transient nuclear envelope rupture during interphase (NERDI), allowing the dissociation of RPA from primary nuclei to the cytoplasm, where they bound single stranded DNA (ssDNA). It has been suggested that bridge resolution occurs when two TREX1 exonucleases meet each other<sup>114</sup>. The timely rupture of chromatin bridges following TREX1 appearance and RPA accumulation suggests it is this exonuclease activity which causes bridge resolution.

Karyotyping and sequencing of subclones that have undergone telomere crisis show that many of these have experienced rearrangement events that exhibit the characteristics of chromothripsis. Half of the sub clones analysed by Maciejowski *et al.* showed rearrangements that exhibited an oscillation in copy number states, random orientation of fragments and spatial clustering<sup>114</sup>. These examples showed patterns implying that two copies of the affected regions were involved, suggesting a fold-back inversion of sister chromatids, as seen in BFB cycles.

Kataegis was also seen near regions associated with chromothripsis. The presence of kataegis in cancer is well documented<sup>182,183</sup>, as is the high frequency of BFB cycles in cancers with unspecific chromosome aberrations<sup>184</sup>. However, this work by Maciejowski *et al.* demonstrated the association between these clustered mutations (kataegis) and chromothripsis<sup>114</sup>. Thus, both chromothripsis and kataegis can be consequences of telomere crisis through the formation of chromatin bridges and potentially numerous BFB cycles.

Whilst Maciejowski *et al.* show kataegis occurring in an *in vitro* model system, Cortés-Ciriano *et al.* sequenced 2,658 tumours from 38 types of cancer and found the co-occurrence of chromothripsis and kataegis to be relatively low<sup>114,153</sup>. Although chromothripsis and kataegis can co-occur, only 9.3% of tumours with chromothripsis (n=734) have greater than 20 clustered APOBEC-induced mutations, suggesting that the co-occurrence of chromothripsis may not actually be very common<sup>153</sup>.

#### **1.4.4 Intertwined micronucleus and chromosome bridge model**

It is not necessary that the breakage-fusion-bridge model is independent from the micronuclei model. Indeed, although none of the chromatin bridges gave rise to micronuclei in the Maciejowski BFB study, Hoffelder *et al.* found that, of the chromatin bridges which are ruptured during mitosis in oral squamous cell carcinoma lines, 70% give rise to a micronucleus<sup>166</sup>. This illustrated that the micronuclei and BFB models may not in all circumstances be independent of one another. Recent work from the Pellman lab gives an explanation for how BFB cycles and micronuclei may be interwoven with chromothriptic events and in turn can cause complex genome evolution<sup>156</sup>. Their novel model suggests that defective replication at chromosome bridges produce stalled replication forks. These bridges are broken through mechanical force caused by the actin cytoskeleton (not dependent on TREX1 as suggested by Maciejowski *et al.*)<sup>114</sup>. Bridge breakage can cause simple fragmentation, which is resolved by end joining or erroneous replicative repair (e.g. MMBIR). These events cause early, low frequency chromothripsis. DNA damage then further occurs at the mitosis following bridge breakage; the ends of broken bridge chromosomes undergo a burst of aberrant DNA replication – similar to that seen for chromosomes in micronuclei<sup>94</sup>. Finally, these damaged chromosomes have a high propensity to mis-segregate into micronuclei due to their compromised centromere function. As previously described these micronuclei may provide an environment for further chromothripsis to occur. This model not only suggests how both BFB cycles and micronuclei are important for chromothripsis, but also how a single chromosome bridge breakage event can lead to complex cancer genomes.

Regardless of the mechanism of chromothripsis initiation, the extensive DNA damage caused by this event must be repaired and DNA must be reintegrated into the primary nucleus for propagation into daughter cells.

#### 1.4.5 DNA damage, re-integration and repair

Mass DNA damage must occur in a catastrophic event during chromothripsis. The mechanism of DNA damage may be dictated by the chromosomal environment caused by an initiating event. As previously discussed, chromosomes which have entered a micronucleus are subject to events unique to a micronuclear environment. Particularly, delayed DNA replication can cause replicative stress. Premature chromosome condensation before replication is complete can in turn promote dsDNA breaks<sup>150,185</sup>. These are likely to occur most abundantly at fragile sites<sup>186</sup>. However it is probable, given the many underlying defects in micronuclei, that more than one source of DNA damage exists. Similarly, DNA damage promoting chromothripsis may arise at chromatin bridges via multiple mechanisms. These are not well understood, however Stephens *et al.* theorise that stretching of the chromatin bridge and the pinching of the cleavage furrow during cytokinesis may cause catastrophic DNA damage<sup>144</sup>. Additionally, chromosome bridges are known to be attacked by exonucleases, causing DNA damage and creating ssDNA which is more vulnerable to become double stranded breaks through further damage<sup>114</sup>. Other sources of chromothripsis driving mutagenesis have also been discussed. Stephens *et al.* make another prediction; ionising radiation (IR) would be able to penetrate a cell during mitosis and inflict dsDNA breaks on a region of or a whole chromosome. However, few natural sources of IR can provide strong enough energy to cause a substantial amount of dsDNA breaks<sup>187</sup>. Tubio and Estivill further propose that programmed cell death may be halted in a small number of cells<sup>188</sup>. By aborting apoptosis these cells could have the extensive DNA damage seen in chromothripsis.

Interestingly, two recent studies from Lin *et al.* and Trivedi *et al.* discovered that shattered chromosome fragments from chromothripsis are tethered together and inherited by one daughter cell<sup>189,190</sup>. In parallel, these groups uncovered that a complex containing CIP2A and TOPBP1 proteins hold together chromosome fragments to facilitate the inheritance to one daughter nucleus. Instead of being randomly segregated into the two daughter nuclei (as would be expected for acentric fragments), collective inheritance allows for fragment re-assembly into a chromosome without the complex copy number oscillations classically seen in chromothripsis. It has been proposed that the prevalence of canonical chromothripsis copy number patterns is due to strong selection pressure from tumour suppressor loss and that

chromosomes that have undergone chromothripsis often are reassembled without catastrophic rearrangements<sup>189</sup>.

Double stranded DNA damage can be repaired via two main mechanisms: non-homologous end joining (NHEJ) and homologous recombination (HR). The former is an error prone repair mechanism that ligates double stranded breaks with little or no homology. The latter is only available during late S and G2 phase as it requires a sister chromatid to use as a template for repair<sup>187,191</sup>. Sequencing done by Stephens *et al.* predicts erroneous repair to have occurred either side of breakpoint junctions. A lack of overlap between breakpoint sequences suggests that either NHEJ (classical-NHEJ) or microhomology mediated end joining (MMEJ or alt-NHEJ) is the major repair mechanism associated with chromothripsis<sup>144</sup>.

Ly *et al.* model chromosome mis-segregation by selectively inactivating the centromere of one chromosome<sup>181</sup>. Through this method they produce micronuclei enriched with the chromosome containing the inactivated centromere (chromosome Y). By inducing premature condensation (with the addition of calyculin A), the micronucleated chromosome could be fragmented. However, micronuclei of cells in G1 did not fragment (whilst those in G2 did) when induced, highlighting the requirement for an S phase replication defect as a priming event for mitotic fragmentation. Sequencing of purified micronuclei fractions show that ligation of chromosome fragments mostly occurs in the primary nucleus following fragment re-incorporation; as previously proposed by Zhang *et al.*<sup>150,181</sup>. Then after characterising the consequences of knocking down components of DNA damage repair pathways, Ly *et al.* proposed that classical-NHEJ is the predominant method for repair following micronuclear shattering and fragment re-incorporation<sup>181</sup>. This DNA ligase IV (LIG4) dependent classical-NHEJ caused structural rearrangements to the chromosome that was mis-segregated two cell cycles earlier. Additionally, the pan-cancer sequencing analysis by Cortés-Ciriano *et al.* identifies classical-NHEJ as the principal repair mechanism in chromothriptic events, with some stretches of breakpoint microhomology that predict contribution from microhomology-mediated break-induced replication (MMBIR) or alt-NHEJ<sup>153</sup>. This data was further supported by a recent preprint that showed inactivating various NHEJ components led to reduced complex rearrangements following the fragmentation of micronuclear chromosomes<sup>192</sup>.

#### **1.4.6 Chromothripsis in disease**

The increase in capability of high throughput sequencing technologies has allowed for the detection of chromothriptic events in many diseases. Whilst the most obvious environment for

a chromothriptic event to occur is in cancer, these complex structural rearrangements are by no means limited to malignant cells. Chromothripsis can occur in germlines and during early embryonic development as shown by Chiang *et al.* and discussed further by Pellestor *et al.*<sup>193,194</sup>. However, chromothripsis seen in congenital disorders is less catastrophic than that seen in cancer. Congenital chromothripsis often has fewer breakpoints and either has only deletions or is copy neutral; therefore there is no obvious amplification in these cases<sup>193,195,196</sup>. Additionally, chromothripsis can be identified in healthy individuals, often passed down from their mother. A study from de Pagter *et al.* shows a complex rearrangement event in several mothers, creating a stable derivative chromosome which is inherited by offspring<sup>197</sup>.

Chromothripsis has been strongly linked with mutation of the TP53 gene and thus dysfunction of the tumour suppressor protein p53. It is likely that chromothripsis can be tolerated better in cells with an inactive or poor p53 checkpoint. TP53 mutants have been linked with chromothripsis in multiple paediatric tumours<sup>198,199</sup>, with a striking study from Rausch *et al.* highlighting that 100% of Sonic-Hedgehog medulloblastoma cases with a TP53 mutation underwent chromothripsis<sup>200</sup>. However, though TP53 mutation is associated with chromothripsis, a recent pan-cancer analysis showed that 60% of cases with chromothripsis show no mutation in either TP53 or MDM2 (regulator of TP53), indicating that this catastrophic DNA damage event can still occur with an intact p53 response<sup>201</sup>.

The prevalence of chromothripsis in cancer varies greatly between cancer types; ranging from 100% in liposarcoma and 77% in osteosarcoma to 1.2% in chronic lymphocytic leukaemia and 0% in pilocytic astrocytomas<sup>153</sup>. Our increasing ability to detect chromothriptic events by high throughput sequencing methods means that the prevalence of chromothripsis in cancer is now known to be higher than originally thought<sup>202,203</sup>. When Cortés-Ciriano *et al.* analysed 2,658 human cancers, they reported that 29% of them had undergone a chromothriptic event with high confidence<sup>153</sup>. When low confidence events were included, the prevalence increases to 40%. It is not obvious which of these were initiating events that caused transformation, and which are a consequence of the genomic instability in a pre-existing cancer. Nevertheless, chromothripsis is clearly more abundant in cancer than was once thought and it is therefore vital to understand how it arises and its consequences.

One subtype of cancer, iAMP21-ALL, with particular relevance to this thesis, has been strongly associated with chromothripsis<sup>145</sup>.

## 1.5 iAMP21-ALL

Acute lymphoblastic leukaemia (ALL) is a form of blood cancer that originates in the lymphoid development pathway. While ALL occurs in adults, it is much more common in children. ALL is the most frequent form of childhood cancer, with an annual incidence of 35/million for 0-14 years of age and particularly high at 63/million for 1-4 years of age<sup>204</sup>. Many genetic subtypes of ALL exist with differing prognoses although, in general, childhood ALL has a good outcome. Childhood ALL has a remission rate of ~98% after treatment and >90% of patients are alive at 5 years<sup>205-207</sup>.

One particular ALL subtype of interest is iAMP21-ALL. This cancer was discovered in 2003 and involves a unique chromosomal abnormality that causes a distinct subtype of B-cell precursor ALL (BCP-ALL)<sup>208,209</sup>. Common characteristics in patients with iAMP21-ALL were originally described by Rand *et al.*, including a common region of amplification spanning 5.1 Mb of chromosome 21, from 32.8 to 37.9 Mb<sup>210</sup>. This region includes the *RUNX1* gene, one of the most commonly mutated and mis-regulated genes in cancer; particularly in haematological malignancies<sup>211,212</sup>. However, more recently, Hormann *et al.* further narrowed this common region of amplification to 1.57 Mb between 36.07 and 37.64 Mb<sup>213</sup>. Interestingly, this narrowed common amplification region does not contain the *RUNX1* gene. Therefore, although *RUNX1* amplification is present in most iAMP21-ALL cases, it appears not to be the target gene driving this subtype of cancer. iAMP21-ALL is typically characterised by the presence of five or more total copies of the *RUNX1* gene on a single chromosome and is most often identified by Fluorescence In-Situ Hybridisation (FISH). However, recent studies have suggested that FISH is insufficient at identifying all iAMP21-ALL cases, particularly those where *RUNX1* is not contained in the most amplified region<sup>214,215</sup>. It has been suggested that FISH should be backed up with copy number profiling by SNP array or whole genome sequencing for iAMP21-ALL identification<sup>214</sup>.

iAMP21-ALL accounts for 2% of childhood BCP-ALL cases and has prognostic relevance<sup>216</sup>. Patients with iAMP21-ALL are often older, have a low white blood cell count and have low 5-year event-free survival compared to other BCP-ALL cases, when treated on standard therapy<sup>217,218</sup>. Studies in the UK and US respectively from Moorman *et al.* and Heerema *et al.* demonstrated that intensive treatment of these patients greatly improved their 5-year event-free and overall survival. Now, iAMP21-ALL patients are treated on intensive treatment arms in most protocols worldwide<sup>219,220</sup>.

The seminal work in 2014 from Li *et al.* described two subtypes of iAMP21-ALL and how they are both associated with chromothripsis<sup>145</sup>. The first subtype is sporadic in nature, likely initiated by BFB cycles and later influenced by chromothripsis. The second subtype (that is most relevant to this study) occurs in individuals with constitutional rob(15;21)c translocations which undergo a chromothriptic event in order to initiate amplification. In both cases the derivative chromosome is rearranged in a manner optimal for leukaemic growth. It is likely that the presence of a dicentric chromosome (either constitutionally for rob(15;21)c or generated somatically by BFB cycles) is necessary for a downstream chromothriptic event. The inherent increased rate of microtubule mis-attachments on dicentric chromosomes may allow chromosome mis-segregation, placing the chromosome in an environment susceptible to chromothripsis (a micronucleus). The research from Li *et al.* was done on patient samples; however, sequencing analysis and model prediction was done *in silico*. Although this work makes predictions on the mechanism of iAMP21-ALL formation, little has been done to understand the basic cell biology driving these cancers, with multiple questions still left unanswered (e.g. how two copies of rob(15;21)c are present in the chromothriptic event).

### **1.5.1 sporadic iAMP21-ALL**

All non-rob(15;21)c dependent iAMP21-ALL cases examined have been sporadic cases whose chromothriptic events are predicted to be preceded by BFB cycles<sup>221</sup>. As described in 1.4.3, BFB cycles are induced by an initiating event causing a dsDNA break (e.g. telomere loss)<sup>222,223</sup>. After the following S phase, when the broken chromosome has been replicated, two sister chromatids will have a dsDNA break, promoting their fusion in G2. During anaphase, a bridge will form as the dicentric chromosome is pulled by microtubules from both poles. The bridge is then broken, leaving two more broken chromosomes with dsDNA breaks, thus allowing a further BFB cycle to occur<sup>114</sup>. These BFB cycles can produce fold-back inversions and altered copy numbers. All of the sporadic iAMP21 cases sequenced by Li *et al.* showed at least one fold-back inversion on the derivative chromosome 21, thus predicting a minimum of one round of BFB in each case<sup>145</sup>. In the majority of sporadic iAMP21 cases the derivative chromosome possessed clusters of back-and-forth rearrangements that are characteristic of chromothripsis. Copy number patterns suggest that the chromothriptic event has happened after BFB cycles. The BFB cycles will produce a dicentric chromosome that is likely to play a vital role in the initiation of chromothripsis. The derivative 21 chromosome then often undergoes large scale duplication after rearrangement<sup>145,216</sup>. These complex rearranged chromosomes may then possess the ability to drive tumourigenesis.

### 1.5.2 rob(15;21)c dependent iAMP21-ALL

Li *et al.* discovered the massive yet specific predisposition of constitutional rob(15;21)c carriers for developing iAMP21-ALL. The rob(15;21)c translocation accounts for only 0.5-1.0% of all Robertsonian translocations<sup>108,224</sup>. However, carriers are predisposed to ~2700x risk of developing iAMP21-ALL. The rob(15;21)c chromosome has been proposed to encourage iAMP21-ALL development due to a propensity to undergo chromothripsis. *In silico* work has suggested that two copies of rob(15;21)c are present in a chromothriptic event, producing one derivative chromosome, der(15;21), but the molecular mechanisms underlying this feature are unknown. This process causes copy number gain and copy number loss of some regions on the derivative chromosome. As discussed in 1.4.1, these copy number oscillations are characteristic of chromothripsis. In rob(15;21)c dependent iAMP21-ALL the chromothriptic event is often followed by further rearrangements, including whole chromosome duplication. Interestingly, both FISH and sequencing data have shown that der(15;21) consistently loses the centromere of chromosome 15, presumably providing stability for mitosis<sup>145</sup>. Both sporadic and rob(15;21)c dependent iAMP21-ALL are evidently influenced by chromothripsis; the association is undoubtable but the mechanism causing susceptibility of these chromosomes is not well understood.

### 1.6 Aims of this project

This project aims to understand the rob(15;21)c chromosome and why carriers are predisposed to chromothripsis and leukaemia. This study makes use of a unique set of resources: EBV-transformed lymphoblastoid cell lines derived from monozygotic twin carriers of rob(15;21)c; one of whom developed iAMP21-ALL whilst the other did not. These cell lines were used to study the structure and segregation of the rob(15;21)c chromosome, and to observe any possible differences between a carrier that developed cancer and a genetically identical one that did not.

The dicentric nature of the Robertsonian chromosome rob(15;21)c is thought to be the explanation for the predisposition of carriers to iAMP21-ALL. However, little is known about the centromeres of this chromosome and why they may be the cause of such catastrophic downstream effects. By studying the activity of the dicentric centromeres we will gain insight into potential mis-segregation mechanisms which drive a chromothriptic event.

Specific aims include:

- 1) Establish lymphoblastoid cell lines as a model to study rob(15;21)c.
- 2) Characterise the rob(15;21)c chromosome; particularly the activity of the dicentric centromeres.
- 3) Characterise how rob(15;21)c behaves through mitosis and how the abnormal centromeres influence chromosome segregation.

Ultimately, this project aims to understand why carriers of the rob(15;21)c chromosome are predisposed to chromothripsis and the development of iAMP21-ALL. In doing so, further insights will also be gained on Robertsonian chromosomes, chromosome mis-segregation and how a dicentric chromosome can play a role in cancer development.

## Chapter 2: Methods

---

### 2.1 Genetic testing

SNP arrays were performed on DNA extracted from bone marrow aspirates taken at diagnosis and blood samples taken at remission, and the lymphoblastoid cell lines, L995 and L996, using the SNP 6.0 Affymetrix array or the Illumina Infinium CytoSNP-850k beadchip array. The SNP 6.0 Affymetrix array was performed by AROS Applied Biotechnology (Denmark) as previously described<sup>225</sup>, and the Illumina Infinium CytoSNP-850k beadchip array was carried out by the Northern Genetics Service, Newcastle-upon-Tyne Hospitals NHS Foundation Trust. Processing of Illumina SNP array data was done in GenomeStudio 2.0. Both Illumina and SNP 6.0 data was then analysed using Nexus Copy Number 10 as described in Creasey *et al*<sup>226</sup>.

### 2.2 Cell culture

Suspension L995 and L996 lymphoblastoid cell lines were grown in Roswell Park Memorial Institute (RPMI) 1640 media with L-glutamine. Medium was supplemented with 20% foetal bovine serum (FBS), 100 U/ml penicillin, 100 µg/ml streptomycin and 2 mM L-glutamine. Lentivirally transduced cell lines were grown in selection media containing 5-10 µg/ml Blasticidin. HEK293FT cells were grown in Dulbecco's Modified Eagle Medium (DMEM) – high glucose (Sigma-Aldrich). DMEM was supplemented with 10% FBS, 100 U/ml penicillin, 100µg/ml streptomycin and 2mM L-glutamine. Cells were grown with 5% CO<sub>2</sub> at 37°C in a humidified incubator.

### 2.3 Cloning

The U6 promoter, CCDB gene and 2xBoxB region were cut out of pLH-sgRNA1-2XboxB (Addgene #75391), the U6 promoter, CCDB gene and 2xPP7 region were cut out of pLH-sgRNA1-2XPP7 (Addgene #75390) and the Blasticidin resistance gene was cut from pLenti6-CENP-A-mCherry (Addgene #89767); cutting and amplification were done using a KOD hot start PCR kit (Merck). Target plasmids pHAGE-EFS-N22p-3XRFPnls (Addgene #75387), pHAGE-EFS-PCP-3XGFPnls (Addgene #75385) and pHAGE-TO-dCas9 (Addgene #75381) were all linearised also using KOD hot start PCR. Part of the PCR products were run on an agarose gel to determine if their size was correct. The remaining PCR product was then purified using a Thermo Fisher Scientific GeneJET PCR purification kit. Concentrations of the purified PCR products were determined by Nanodrop.

The NEBuilder HiFi DNA assembly cloning kit was used to clone the inserts from #75391, #75390 and #89767 respectively into the linearised backbones from #75387, #75385 and #75381. Recombinant plasmids without the CCDB gene were transformed into NEB 5-alpha competent cells and those with the CCDB gene were transformed into One Shot™ ccdB Survival™ 2 T1R Competent Cells. Transformed bacteria were grown on LB (Luria Broth) agar plates with ampicillin resistance, colonies picked and grown up in liquid LB media. Plasmid DNA was isolated from liquid cultures using either a QIAGEN QIAprep Spin Miniprep Kit or a QIAGEN EndoFree Plasmid Maxi Kit. Isolated DNA was sent to Plasmidsaurus for whole-plasmid long-read sequencing. These recombinant plasmids are the lentiviral transfer plasmids used for lentiviral transformation in section 2.9.

#### **2.4 Flow cytometry**

L995 and L996 cell suspensions were pelleted at 300g for 5 minutes. The supernatant was removed, leaving 500 µl. The pellet was re-suspended and 4.5 ml ice cold 70% ethanol was added dropwise whilst vortexing. Cells were fixed in ethanol and stored overnight at 4°C. The following day, cells were spun down and washed in PBS. Cells were then pelleted, supernatant removed and re-suspended in 50 µl RNase at 100 µg/ml. Propidium Iodide (PI) solution containing 0.1% Triton X-100 and 300 µl of 50 µg/ml PI was added to cell suspension before it was transferred to FACS tubes and stored in the dark for 30-60 minutes. Flow cytometry was performed on BD Fortessa X20 or BD Symphony A5 using DIVAv8 and data was analysed using FCS Express 7.

#### **2.5 Metaphase and Anaphase enrichment**

Cells were incubated in 1 µM nocodazole in the well of a 6 well plate for 4 hours at 37°C. These blocked cells were then spun down and washed three times with pre-warmed RPMI media followed by being spun down at 300 g x 5 minutes. Pelleted cells were re-suspended in 1 ml of fresh media and seeded onto a poly-L-lysine coated coverslip (Corning™ 354085) in a 12-well plate. Whilst adhering to the coverslips, cells were allowed to progress through mitosis and enriched in metaphase by fixing 30 minutes post-washout with Carnoy's fixative (if doing FISH) or 4% PFA (if doing immunostaining) and enriched in ana/telophase by fixing 45-60 minutes post-washout.

## 2.6 Immunostaining

Following PFA fixation, coverslips were washed in PBS, permeabilised for 5 minutes in 0.15% Triton X-100 and washed again in PBS. Coverslips were then blocked in 1% BSA (bovine serum albumin) in PBS for 45 minutes at room temperature, then incubated in a humid chamber at 37°C for 1 hour with primary antibodies diluted in 1% BSA/PBS. Coverslips were washed for 5 minutes, three times with PBS and then incubated in a humid chamber at 37°C for 45 minutes with secondary antibodies diluted in 1% BSA/PBS. Finally, coverslips were washed a further three times with PBS, air-dried and mounted with ProLong Glass Antifade Mountant with NucBlue.

## 2.7 Fluorescence In-Situ Hybridisation

Coverslips or slides with attached cells or chromosome spreads were fixed for 10 minutes in Carnoy's fixative and allowed to air dry. Cytocell  $\alpha$ -satellite enumeration probes were prepared with hybridisation buffer and added to slides according to the data sheet (3-4  $\mu$ l total volume). For chromosome painting, 1.5  $\mu$ l each of Metasystems XCP 15 and XCP 21 probes were added to slides (3  $\mu$ l total volume). Coverslips were sealed on to slides using rubber cement. DNA was denatured at 75°C for 5 minutes and hybridised at 37°C overnight. The following day, slides were washed in 2X SSC and coverslips removed, then a 2 minute wash at 72°C in wash solution 1 (2% 20X SSC, 0.3% NP40, DI water) and a 2 minute wash at room temperature in wash solution 2 (10% 20X SSC, 0.1% IGEPAL-CA-630, DI water). Slides were dried and mounted with ProLong<sup>TM</sup> Glass Antifade Mountant with NucBlue<sup>TM</sup>.

## 2.8 Chromosome spreads

L995 and L996 cell suspensions were incubated with 0.1  $\mu$ g/ml KaryoMAX<sup>TM</sup> Colcemid<sup>TM</sup> (Gibco) for 3 hours. Cells were washed in PBS then re-suspended in the appropriate volume of 0.075 M KCl + 0.1% Tween-20 to make up 75-150,000 cells/ml. This hypotonic solution was incubated at room temperature for 15 minutes and 250  $\mu$ l was loaded to each cytofunnel in a Cytospin 3 (Shandon). The Cytospin was run at 1500 rpm for 5 minutes; attaching cells to glass slides.

Depending on the antibodies used and whether FISH was also to be performed, one of the following methods was used to stain chromosome spreads:

- A) Slides were fixed in 4% PFA for 10 minutes at room temperature, washed three times in PBS, blocked for 45 minutes in 1% BSA, stained with primary antibodies (diluted in 1% BSA) for 1h at 37°C, washed three times in PBS, stained with secondary antibodies (diluted in 1% BSA), washed a further three times in PBS and mounted with ProLong™ Glass Antifade Mountant with NucBlue™.
- B) Slides were incubated for 10 minutes at room temperature with KCM buffer (10 mM Tris pH8.0, 120 mM KCl, 20 mM NaCl, 0.5 mM EDTA, 0.1% Triton X-100). Primary antibody incubation was then done in a humid chamber at 4°C for 1 hour, followed by two 5 minute washes with KCM. Secondary antibody incubation was then done in a humid chamber at 4 °C for 1 hour, followed by another two 5 minute KCM washes. Slides were fixed with 4% PFA/KCM for 10 minutes at room temperature and if doing only IF then slides were mounted to coverslips using ProLong™ Glass Antifade Mountant with NucBlue™. If slides were to be stained for FISH after IF then they were incubated with Carnoy's fixative for 10 minutes at room temperature and labelled using the FISH protocol above.

## 2.9 Lentiviral transformation

Lentivirus was produced by transfecting HEK293FT cells with 11 µg of pMD2.G VSV-G envelope plasmid, 12 µg pCMV-dR8.91 packaging plasmid and 14 µg of lentiviral transfer plasmid containing gene of interest. The transfer, envelope and packaging plasmids were added to a microcentrifuge tube with 360 µl of pre-warmed Opti-MEM reduced serum media (Gibco) and vortexed on low speed. A solution containing 360 µl of pre-warmed Opti-MEM and 27 µl of EndoFectin Max transfection reagent (GeneCopoeia) were added dropwise to the vortexing plasmid solution. The solution was incubated at room temperature for 15 minutes before being added dropwise to a 10 cm dish containing HEK293FT cells. 10 µl of 25 mM Chloroquine was added to the 10 cm dish before incubating at room temperature for 15 minutes and then placing in a 37°C, 5% CO<sub>2</sub> incubator. After 7h of incubation, cells were washed and re-suspended in fresh RPMI 1640 media. 72h after the initial transfection virus containing supernatant was filtered through a 0.45 µm filter and aliquoted into 1ml microcentrifuge tubes, then frozen down at -80°C.

L995 and L996 cells were transduced by spinfection with lentivirus produced using the transfer plasmids pLenti6-CENP-A-mCherry (Addgene #89767) or pHAGE-TO-dCas9 (Addgene

#75381). Cells were seeded into wells of a 6-well plate at 500,000 cells/ml in virus supernatant. Protamine sulphate was added at a final concentration of 50 µg/ml and plates spun at 1000g for 90 minutes at 37°C. Plates were then incubated for 24h in a 37°C, 5% CO<sub>2</sub> incubator then cells washed with PBS and re-suspended in fresh RPMI 1640 media. Cells were allowed to grow up and then put into selection media containing Blasticidin (10 µg/ml).

## 2.10 Western blotting

Cells were counted using a haemocytometer and  $2 \times 10^6$  cells were pelleted by centrifugation and resuspended in 250 µl lysis buffer (140 µl RIPA buffer – 150 mM NaCl, 50 mM Tris pH 7.5, 0.1% SDS, 1% Triton X-100, 0.5% sodium deoxycholate, phosphatase inhibitors 10 µl/ml, 10 µl protease inhibitors. 100 µl SDS loading dye - 50 mM Tris-Cl pH 6.8, 100 mM dithiothreitol, 10% SDS, 0.1% bromophenol blue, 50% glycerol). Cell lysates were frozen down at -20°C overnight. The next day samples were boiled at 95°C for 10 minutes, loaded into precast BIO-RAD mini-PROTEAN TGX 4-15% gels and separated at 180V for 45-60 minutes using BIO-RAD tank with BIO-RAD Tris/Glycine/SDS buffer. Thermo Fisher Scientific Spectra multicolour broad range protein ladder was also loaded as a size marker.

Following SDS-PAGE, a BIO-RAD tank with BIO-RAD Tris/Glycine buffer and 20% methanol was run at 100V for 1 hour to transfer proteins onto Amersham Protran Premium 0.2 µm nitrocellulose blotting membrane.

Using the ladder as a marker, the nitrocellulose membrane was cut at an appropriate level so that proteins of different sizes could be stained separately. Membranes were blocked in 5% milk in TBST (Tris-buffered saline with 0.1% Tween 20) for 1 hour at room temperature. Following blocking, membranes were incubated with primary antibodies diluted in blocking buffer in a 50 ml falcon tube on a roller at 4°C overnight. The next day, membranes were washed three times in TBST and incubated in secondary antibodies diluted in blocking buffer for 1 hour at room temperature. Finally, membranes were washed twice in TBST and once in TBS before being incubated in ECL (Pierce) for 5 minutes, then imaged on an Invitrogen iBright™ FL1500 Imaging System.

## 2.11 Expansion microscopy

The protocol used for expansion microscopy was altered from the Ultrastructure-Expansion Microscopy (U-ExM) protocol for *Plasmodium falciparum* in Liffner *et al.*<sup>227</sup>. This involved

enriching cells in anaphase as in section 2.5, fixing in PFA, protein crosslinking prevention in formaldehyde and acrylamide, and gelation in a solution containing TEMED and APS. The gel was then denatured at 95°C, expanded in water, stained with antibodies, DNA dyes and NHS-esters, expanded again and prepared for imaging in a glass bottomed 35mm dish (Ibidi).

## 2.12 Correlative Light and Electron Microscopy (CLEM)

L995 and L996 cells were enriched in anaphase as in section 2.5. Cells were allowed to progress into anaphase and stick down onto Mattek 35 mm dishes with gridded coverslips that had been coated in poly-L-lysine. Medium was removed and cells fixed with 4% glutaraldehyde in PBS containing 1 µg/ml DAPI for 45 minutes at room temperature. Dishes were washed for 5 minutes, three times in PBS then stored at 4°C in PBS until light microscopy was done. A Zeiss LSM800 Airyscan microscope was used to acquire high resolution images of DAPI and a low magnification tiled brightfield image of cells of interest such that the grid on the coverslip could be seen.

Following light microscopy, dishes were prepared for electron microscopy with heavy metal staining and resin embedding. PBS was removed from dishes and replaced with reduced osmium stain (2% osmium, 1.5% potassium ferrocyanide, 0.1 M sodium cacodylate in deionised water) and incubated for 1 h at room temperature. Osmium stain was removed, and dishes were washed for five minutes, three times in deionised (DI) water. Tannic acid was used as a mordant and was added at 1% in DI water for 20 minutes at room temperature. Three DI water washes were done as above followed by a second osmium staining (2% osmium in DI water for 40 minutes at room temperature). Three more DI water washes were done and then dishes were stained with 1% uranyl acetate in DI water overnight at 4°C. The following day, uranyl acetate was washed out of the dish with three more DI water washes and then dishes were stained with filtered Walton's lead aspartate (0.00399g/ml L-aspartic acid, 0.00066g/ml lead nitrate at pH 3.8 in DI water) at 60°C for 30 minutes. Walton's lead aspartate was removed and cells were dehydrated with a graded ethanol series (5 minutes 30% ethanol, 5 minutes 50% ethanol, 5 minutes 70% ethanol, 5 minutes 90% ethanol, 2 x 5 minutes 100% ethanol). The final ethanol solution was removed and the dish was infiltrated with resin with the use of a graded hard resin series (30 minutes 1:2 resin:ethanol, 30 minutes 1:1 resin:ethanol, 30 minutes 2:1 resin:ethanol, 2 x 30 minutes pure resin). Resin embedding was done by filling the dish 1/3 full with fresh 100% hard-setting resin and allowed to cure at 60°C for 24-48 h.

Cells were now embedded in resin but surrounded by the plastic of the dish and glass coverslip. Stubs required for EM were now prepared by cutting away all plastic and glass with the use of cable cutters and a razor blade. A stereoscope was used to find the negative impression in the resin of grid coordinates of interest, these were marked and cut down using a junior hacksaw. These stubs were trimmed further and gold coated by Newcastle University's electron microscopy research facility. Imaging was done on either a Zeiss Sigma scanning electron microscope with Gatan 3view system (serial block face-scanning electron microscope), or Hitachi H T7800 120 kV TEM (transmission electron microscope) at Newcastle University's electron microscopy research services facility.

### **2.13 Correlative immunofluorescence and Fluorescence IN-Situ Hybridisation**

As the fixative required for FISH has a negative effect on immunostaining of some proteins, it was not possible to do both IF and FISH at the same time. A protocol was developed to correlate IF and FISH on the same cell. Firstly, cells were prepared on coverslips and stained as in 2.6. Then coverslips were mounted using Invitrogen™ SlowFade™ glass soft-set antifade mountant, with DAPI and sealed using nail polish. When imaging a cell of interest, wider snapshots of the cells location were taken and the glass marked with a diamond scribing pen. After imaging, coverslips were removed by cutting the nail polish and incubating the slide in a Coplin jar with PBS at 4°C overnight. Coverslips were washed a further two times in PBS before fixing in Carnoy's fixative and undergoing FISH as in section 2.6. After FISH, coverslips were re-mounted onto slides using ProLong™ Glass Antifade Mountant with NucBlue™. The marks on the glass and the wide snapshot images were used to re-locate cells of interest for imaging of the FISH staining. Original images of the IF and the images of FISH staining could be correlated to determine which chromosome was Chr15, Chr21 and rob(15;21)c.

### **2.14 Fluorescence microscopy**

#### **2.14.1 Confocal microscopy**

Images were acquired on a Leica SP8 point scanning confocal microscope with a Leica HC PL APO CS2 63x 1.4 NA oil objective. Fluorophores were excited with a Leica white light laser. Images were captured with optimal Nyquist sampling, ensuring optical sections every 0.13µm and zoom set so that each pixel covers an area equal to or less than 43 x 43 nm. 1024 x 1024 pixels (or larger in order to satisfy Nyquist sampling) images were captured using Leica HyD hybrid detectors. Acquisition parameters for each fluorophore were changed from experiment to experiment depending on fluorophores used (narrowing detection gates when multiple

fluorophores were used to limit bleedthrough) and brightness of each fluorophore (to prevent saturation). However, parameters were kept the same within each experiment (and repeats of each experiment).

Confocal microscopy for correlative light and electron microscopy (CLEM) was done on a Zeiss LSM800 AiryScan microscope using Plan-Apochromat 63x 1.4 NA oil DIC M27 objective lens. Confocal microscopy for expansion microscopy gels was done on a Zeiss LSM880 microscope using AiryScan fast and a Plan-Apochromat 63x 1.4 NA oil DIC M27 objective lens.

#### **2.14.2 Stimulated emission depletion microscopy**

Stimulated emission depletion (STED) images were acquired on a Leica SP8 point scanning confocal microscope as above. However, a Leica HC PL APO 100x 1.4 NA oil objective was used to capture all STED images. A 775 nm STED laser was used at 100% laser power and with 20% 3D STED (to improve Z resolution) to deplete Alexa Fluor 594, Abberior STAR 635P and Abberior STAR 460L. Optimal Nyquist sampling was done to maximise information captured.

#### **2.14.3 High throughput microscopy**

Large images were made up of hundreds of tiled images stitched together for visualisation of all cells on an entire coverslip. These images were acquired on a Zeiss CD7 microscope using a 20x/0.7 NA Plan-Apochromat air lens. Dapi, FITC and TRITC were excited respectively by the 365 nm, 470 nm and 567 nm LED-modules from the Zeiss Colibri 7 light source and detected by a Monochrome sCMOS Hamamatsu Fusion camera.

Some high throughput images were instead taken on a Zeiss Axioscan 7 microscope with a 40x/0.95 NA lens. Dapi, FITC and TRITC were excited respectively by the 385 nm, 475 nm and 567 nm LED-modules from the X-cite Xylis LED illumination system and detected by a Zeiss AxioCam 712 Mono camera.

#### **2.14.4 Live cell imaging**

L995 and L996 cells were seeded on a poly-L-lysine coated 35mm glass bottomed dish (Ibidi) or 10-well glass bottom cell view slides (Greiner). One hour before the start of live imaging, cells were incubated with 250 nM Sir-Hoechst (Spirochrome). Imaging was done on a VisiTech

iSIM array scanning confocal microscope using a Nikon TiE body and a plan apo VC 60x/1.4NA oil DIC N2 objective lens. Images were taken every 5 minutes for 18 hours.

## 2.15 Image analysis

### 2.15.1 Image deconvolution

All STED images were deconvolved to further resolve closely located signals. Huygens Essential software was used with either a classic MLE or Good's MLE algorithm depending on what the software recommended as the best algorithm for each experiment. When deconvolved images were to be later quantified (e.g. CENP-C staining of chromosome spreads for centromere dominance studies), initial tests were done to determine the optimal algorithm, absolute background number and number of iterations required to best deconvolve the image without artificially creating structures from over-deconvolution. Once optimal settings were determined then a deconvolution template was created, and this was used on all images within an experiment.

### 2.15.2 Analysis of centromeric foci

Foci of CENP-C from deconvolved STED images of chromosome spreads + IF + FISH experiments were analysed using Fiji (ImageJ)<sup>228</sup>. A self-made ImageJ macro was run to create a sum slices Z project and threshold each image (thresholding adjusted manually for each cell) to best identify all centromeres and create regions of interest from them. The macro then ran the 'analyse particles' function. The output of this macro was a table of measurements with information on area and integrated density of each CENP-C focus. These data were compared with the original image which contained FISH probes labelling Chr15 and Chr21 and therefore each CENP-C focus could be assigned to either Chr15, Chr21, rob15 or rob21 (if they belonged to the Chr15 arm or the Chr21 arm of rob(15;21)c), or other (if not labelled by any FISH probe).

### 2.15.3 Mis-segregation analysis

Large, tiled images obtained as in section 2.14.3 were analysed using Qupath<sup>229</sup>. The automatic cell detection feature was used for total cell counts. Parameters used for this were as follows: Requested pixel size – 1  $\mu\text{m}$ , Background radius – 15  $\mu\text{m}$ , median filter radius – 0  $\mu\text{m}$ , Sigma – 2.5  $\mu\text{m}$ , Minimum area – 35  $\mu\text{m}^2$ , Maximum area – 500  $\mu\text{m}$ , Threshold – 2000, Cell expansion – 5  $\mu\text{m}$ .

Each image was manually analysed to count cells in anaphase/telophase and then those with actively mis-segregating chromosomes. Analysis of cell stage and whether there were mis-segregating chromosomes was done without Chr15 and Chr21 FISH channels. Once a mis-segregate was determined, the FISH channels were turned on and the mis-segregating chromosome then labelled as Chr15, Chr21, rob(15;21)c or other (if the mis-segregate had no FISH probes co-localising with it). The number of each FISH probe in the mis-segregate and in the daughter primary nuclei were used to determine if one or both sister chromatids were present in the mis-segregation.

#### **2.15.4 Metaphase analysis**

Large, tiled images obtained as in section 2.14.3 were analysed using the '20240126\_Nuclear\_Segmentation' macro in FIJI. This macro split the large, tiled images into smaller, more manageable images and nuclear ROIs identified by the plugin StarDist<sup>230</sup>. The morphology of the nucleus was analysed and only images of those cells with a metaphase-like shape were kept (cells deleted if median < 4000, major < 12, minor > 10, Aspect ratio > 3, roundness > 0.7 or circularity > 0.9). The remaining metaphase-like images were manually analysed to remove incorrectly identified metaphases (e.g. cellular debris of a similar shape to a metaphase cell). Remaining real metaphases were now manually analysed to count chromosomes that were late-aligning/off the plate. FISH channels were then switched on to see if the late-aligning chromosome was Chr15, Chr21, rob(15;21)c or another chromosome.

#### **2.15.5 Chromosome nuclear location analysis**

Large, tiled images obtained as in section 2.14.3 were analysed using the 'Identify\_Nuclei\_Spots\_And\_NND' macro in FIJI. The distance of each FISH focus from the centre of each interphase nucleus was determined. Nearest neighbour distance was used to determine which of the Chr15 and Chr21 FISH focus belonged to rob(15;21)c (The Chr15 focus with the closest distance to a Chr21 focus, and vice-versa, was labelled rob(15;21)c and the middle of these two foci was labelled the centre of the rob(15;21)c chromatin. The distance of this centre from the nucleus centre was then measured). These distances were plotted in RStudio using visualisation package ggplot2 to compare the distance of Chr15 chromatin, Chr21 chromatin and rob(15;21)c chromatin from the centre of the nucleus<sup>231</sup>.

### 2.15.6 Macros used for image analysis

The FIJI macros used for image analysis can be found on GitHub ([https://github.com/NCL-ImageAnalysis/Nuclear\\_Segmentation\\_and\\_Cell\\_Cycle\\_Investigation](https://github.com/NCL-ImageAnalysis/Nuclear_Segmentation_and_Cell_Cycle_Investigation)). These macros were written by George Merces from the Newcastle University Image analysis Unit and BioImaging Unit.

### 2.16 Data visualisation

The analysis and quantification done in section 2.15 were plotted in RStudio using visualisation package ggplot2 or in Graphpad Prism v9.5.0 and then figures were assembled in Inkscape<sup>231</sup>.

### 2.17 Antibodies

**Table 2.1. List of primary antibodies**

Target	Species	Source	Dilution
CENP-A	Mouse	Invitrogen (MA1-20832)	1/100
CENP-B	Rabbit	Abcam (ab25734)	1/500
CENP-C	Guinea pig	MBL (PD030)	1/500 - 1/1000
NUF2	Rabbit	Abcam (ab122962)	1/500
Hec1	Mouse	Gift from Jennifer DeLuca	1/500
Hec1S44ph	Rabbit	Gift from Jennifer DeLuca	1/500
Aurora B	Mouse	BD Biosciences (611083)	1/500
Survivin	Rabbit	Novus (NB500-201)	1/500
INCENP	Rabbit	Sigma (I5283)	1/500

Cas9	Mouse	Cambridge Bioscience (CAS9-AB-2)	1/500
Cohesin (SA2)	Rabbit	Bethyl (A300-158A)	1/100 – 1/500
PICH (ERCC6L)	Mouse	Abnova (H00054821-B01P)	1/500
Emerin	Mouse	Abcam (ab204987)	1/100
Nup358	Rabbit	Atlas Antibodies (HPA018437)	1/100
Nup107	Mouse	Invitrogen (MA1-10031)	1/100
Lap2 $\alpha$	Rabbit	Abcam (ab5162)	1/100
UNC84B	Rabbit	Invitrogen (PA5-51539)	1/100
$\alpha$ -tubulin	Rat	Abcam (ab6160)	1/500 – 1/1000

**Table 2.2. List of secondary antibodies**

<b>Target</b>	<b>Source</b>	<b>Dilution</b>
Mouse (Alexa Fluor 488)	Invitrogen (A32766)	1/500 – 1/1000
Mouse (Alexa Fluor 594)	Invitrogen (A32744)	1/500 – 1/1000
Mouse (Alexa Fluor 647)	Invitrogen (A-21235)	1/500 – 1/1000
Rabbit (Alexa Fluor 488)	Invitrogen (A32790)	1/500 – 1/1000
Rabbit (Alexa Fluor 594)	Invitrogen (A32754)	1/500 – 1/1000
Rabbit (Alexa Fluor 647)	Invitrogen (A-21245)	1/500 – 1/1000
Rabbit (Atto 647N)	Active Motif (15048)	1/500 – 1/1000
Rat (Alexa Fluor 488)	Invitrogen (A-11006)	1/500 – 1/1000
Rat (Alexa Fluor 594)	Invitrogen (A-21209)	1/500 – 1/1000
Rat (Alexa Fluor 647)	Invitrogen (A-21247)	1/500 – 1/1000
Rat (Abberior STAR 635P)	Abberior (ST635P-1007)	1/500 – 1/1000
Guinea pig (Alexa Fluor 594)	Invitrogen (A-11076)	1/500 – 1/1000
Guinea pig (Alexa Fluor 647)	Invitrogen (A-21450)	1/500 – 1/1000
Guinea pig (Abberior STAR 460L)	Abberior (ST460L-1006)	1/500 – 1/1000

## 2.18 Primers

**Table 2.3. List of primers**

<b>Name</b>	<b>Sequence</b>	<b>Use</b>
dCas9 linearisation fwd	GGACTAGCGATGCTAGCTGATGCGG	Linearising Addgene plasmid #75381 to insert the BlastR gene
dCas9 linearisation rev	AAACTGGATCTCTGCTGTCCCT	Linearising Addgene plasmid #75381 to insert the BlastR gene
GFP linearisation fwd	ACTAGCGATGCTAGCTGATGCGGG	Linearising Addgene plasmid #75385 to insert the U6 promoter, CCDB gene and 2x PP7 sequences
GFP linearisation rev	CCAAACTGGATCTCTGCTGTCCC	Linearising Addgene plasmid #75385 to insert the U6 promoter, CCDB gene and 2x PP7 sequences
mCherry linearisation fwd	ACTAGCGATGCTAGCTGATGCGG	Linearising Addgene plasmid #75387 to insert the U6 promoter, CCDB gene and 2x BoxB sequences
mCherry linearisation rev	CCAAACTGGATCTCTGCTGTCCCTGT	Linearising Addgene plasmid #75387 to insert the U6 promoter, CCDB gene and 2x BoxB sequences

mCherry-3 linearisation 1	GTTTCGTCCTTTCCACAAG	Paired with mCherry-3 primer 2 for linearisation of mCherry-3 to remove CCDB gene and insert target sequence
mCherry-3 linearisation 2	GAGAGCTAGGGCCCTGAAG	Paired with mCherry-3 primer 1 for linearisation of mCherry-3 to remove CCDB gene and insert target sequence
mCherry-3 linearisation 3	CGGTGTTTCGTCCTTTCC	Paired with mCherry-3 primer 4 for linearisation of mCherry-3 to remove CCDB gene and insert target sequence
mCherry-3 linearisation 4	GTTTGAGAGCTAGGGCCCTG	Paired with mCherry-3 primer 3 for linearisation of mCherry-3 to remove CCDB gene and insert target sequence
GFP-1 linearisation 3	CGGTGTTTCGTCCTTTCC	Paired with GFP-1 primer 4 for linearisation of GFP-1 to remove CCDB gene and insert target sequence
GFP-1 linearisation 4	GTTTGAGAGCTACCGGAGC	Paired with GFP-1 primer 3 for linearisation of GFP-1 to remove CCDB gene and insert target sequence

mCherry-3/GFP-1 linearisation 5	CCGGTGTTTCGTCCTTCCAC	Paired with mCherry-3 primer 4 or GFP-1 primer 4 for linearisation of mCherry-3 or GFP-1 to remove CCDB gene and insert target sequence
------------------------------------	----------------------	---

## Chapter 3: Characterising rob(15;21)c

---

### 3.1 Introduction

Robertsonian chromosomes involve the fusion of the short arms of two acrocentric chromosomes to create a translocated chromosome that often contains one centromere from each of the original chromosomes. Robertsonian chromosomes are the most common form of chromosomal rearrangement. Approximately 1 in 800 newborns have a Robertsonian translocation, with most of them being regarded as phenotypically neutral<sup>115,232,233</sup>. However, Li *et al.* in 2014 reported that carriers of the Robertsonian chromosome rob(15;21)c had a massive 2700x increased risk of developing iAMP21-ALL<sup>145</sup>. This rare subtype of acute lymphoblastic leukaemia involves the rearrangement of a dicentric chromosome. The two subtypes of iAMP21-ALL are sporadic iAMP21-ALL, in which a dicentric chromosome is formed by breakage-fusion-bridge cycles, or rob(15;21)c dependent iAMP21-ALL in which the dicentric chromosome is constitutional. Both subtypes involve an event in which a dicentric chromosome undergoes chromothripsis, producing a derivative chromosome that drives cancer progression.

The presence of the chromosome rob(15;21)c is linked with a drastic increased risk of developing iAMP21-ALL. Only two other known cases exist that involve iAMP21-ALL development in a patient with a Robertsonian chromosome that is not rob(15;21)c. Gao *et al.* reported one case from a rob(21:22) carrier and unpublished work from a co-supervisors lab has observed one case with rob(14;21)<sup>234</sup>. A model was proposed in section 1.5 that suggested rob(15;21)c is prone to chromothripsis due to its dicentricity promoting mis-segregation and in turn placing rob(15;21)c in an environment susceptible to chromothripsis. However, this model is based on sequencing analysis and needs to be confirmed experimentally with cell biological evidence. Therefore, we reasoned that studying rob(15;21)c and its dynamics through cell division would provide insight into multiple topics of interest, including dicentric chromosomes, the mechanisms leading to chromothripsis, and ultimately possible targetable axes for cancer treatment.

As dicentric chromosomes are discussed frequently in this work, it is of importance to define words of interest relating to centromeres. In this thesis, “dicentric” is used to define a chromosome which has two separate regions of centromeric DNA, often shown in this chapter

by  $\alpha$ -satellite FISH staining. “Active” is used in reference to a centromere that has staining for proteins that have been shown to be a marker of a centromere which can assemble a kinetochore, in this chapter particularly CENP-C. “functional” refers to the ability of a kinetochore to bind microtubules; a centromere can also be labelled functional if its kinetochore is functional.

In order to study this Robertsonian chromosome, EBV transformed lymphoblastoid cell lines were produced (L995 and L996) from blood samples taken from an identical twin pair that carried rob(15;21)c and of which one twin developed iAMP21-ALL and the other did not. The iAMP21-ALL affected patient was 11 years old at diagnosis. Blood samples for EBV transformation were taken from both twins 6 years and 1 month after diagnosis of the affected twin. When these samples were taken, the patient who had iAMP21-ALL was in remission and thus these were non-cancerous cells that were EBV transformed. Blood samples were lymphoprepped and sent to Public Health England (PHE) at Porton Down for EBV transformation. In both samples, transformation was successful and the two stable lymphoblastoid cell lines were produced; named L995 (from the iAMP21-ALL patient, reg ID 23299) and L996 (from the identical twin who did not develop cancer, reg ID 27405). These provided us with a highly useful tool to not only study the rob(15;21)c chromosome but also to provide initial insight into possible differences between carriers who develop leukaemia and those who do not. In all experiments in this thesis the researcher was blind to the identity of each cell line, not knowing which had come from the patient that developed iAMP21-ALL and which was the control, therefore minimising bias. The researcher was unblinded at the end of this study so to appropriately interpret the data and discuss results in this thesis.

In this chapter, I first set out to show that the cell lines L995 and L996 are good models to study the chromosome rob(15;21)c. I illustrate that these lines are genetically and karyotypically similar to the patients from which they were derived and that they are tractable for experiments (as shown by the stability of their ploidy across passages). The remainder of this chapter then focuses on better understanding the centromere of rob(15;21)c as we hypothesised that the dicentric nature of this chromosome may be causing aberrant microtubule attachment events that in turn could be initiating chromothripsis. I study inner and outer kinetochore proteins, how the centromeres of rob(15;21)c change over cell passages, relative centromeric strength within the dicentric and the propensity for these kinetochores to bind microtubules.

## 3.2 Results

### 3.2.1 SNP arrays show the differences between diagnostic and remission samples of the iAMP21-ALL patient.

Cancer genomes are often complex; containing a spectrum of events, from gross chromosomal changes such as aneuploidy and whole genome duplication, to single nucleotide mutations<sup>235</sup>. More recently, with advancements in sequencing technologies, complex mutational events have become better understood. Stephens *et al.* described chromothripsis, a catastrophic phenomenon that involves many rearrangements acquired in a single event<sup>144</sup>.

To characterise the structure of chromosomes in the twin patient who developed iAMP21-ALL (23299), single nucleotide polymorphism (SNP) analysis was carried out. A bone marrow aspirate was taken at diagnosis and a blood sample was taken when the patient was in remission. SNP array data were collected at both time points and a remission sample was used to develop the L995 cell line. Figure 3.1 assesses copy number variants (CNVs) in the above samples when compared to the reference genome GRCh37. Figure 3.1A shows the diagnostic and remission samples separately, indicating the vast differences between them. In the diagnostic sample the complexity of the genome is evident; the oscillating copy number on chromosome 15 and chromosome 21 is consistent with chromothripsis on rob(15;21)c and further dramatic events have occurred, including loss of the majority of chromosome 9p, loss of a large amount of chromosome 11q, gain of chromosome 20p and loss of chromosome 20q. The SNP array data from the patient when in remission is much quieter, there are few large or small CNVs, many of which will be germline variation with no pathogenicity<sup>236</sup>. Figure 3.1B is an aggregate plot for the two samples, though as the remission sample is quiet, this visual representation is largely showing the diagnostic sample copy number changes.

As with all copy number analysis plots shown in this thesis, there appears to be complete loss of one copy of the X chromosome. However, this is simply due to the samples being from male patients. The Nexus software used to analyse these data is not gender specific and therefore visualises samples with only one copy of chromosome X as having copy number loss.

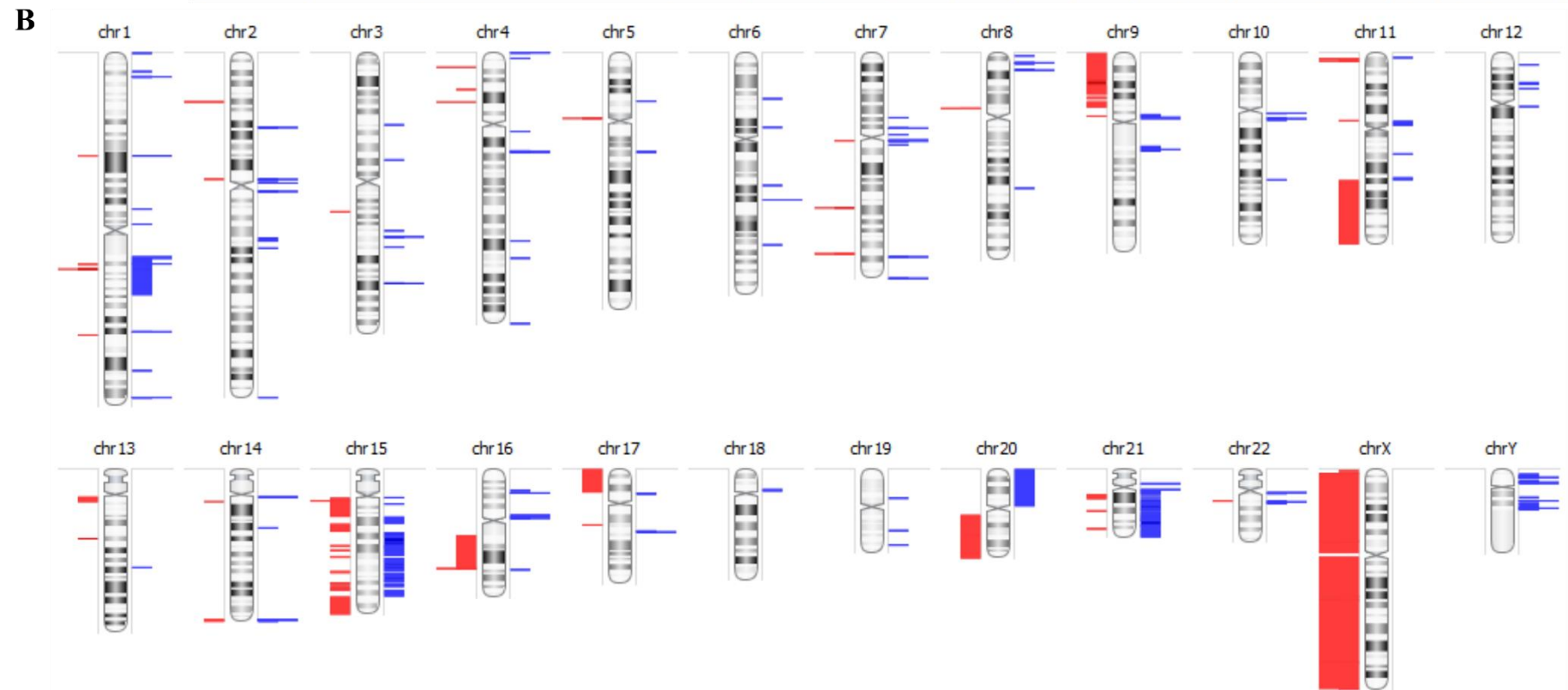
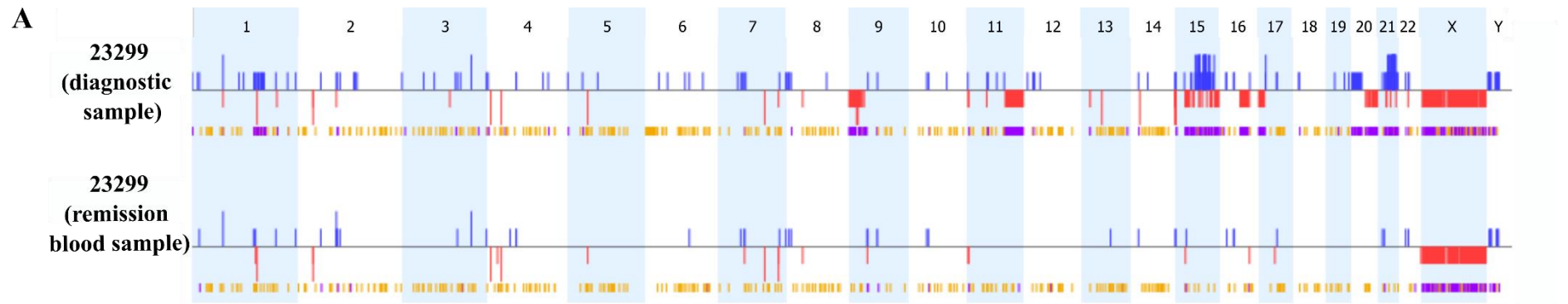


**Figure 3.1. The diagnostic sample of patient 23299 shows a chromothriptic der(15;21).** Copy number variation analysis comparing SNP array data for patient 23299 diagnostic bone marrow aspirate and remission blood sample to the GRCh37 reference genome. This copy number analysis is shown in a whole genome view (**A**) and in a chromosome summary view (**B**). Blue represents copy number gain. Red represents copy number loss. Purple shows allelic imbalance. Yellow shows Loss Of Heterozygosity (LOH). DNA from both the diagnostic and remission blood samples were run on an Affymetrix SNP 6.0 array.

### **3.2.2 L995 and L996 cell lines have no obvious genetic differences from the blood samples from which they were derived.**

As the lymphoblastoid cell lines were to be used to study the Robertsonian chromosome rob(15;21)c, it was important to show that they were representative of the cells from which they were derived. The method used to transform B lymphocytes into lymphoblastoid cells (Epstein-Barr virus transformation) has the possibility to cause genomic instability<sup>237-239</sup>. In order to confirm that no gross chromosomal changes had occurred in the process of EBV transformation, SNP arrays were done on DNA from the L995 and L996 cell lines, and from the blood samples of the twins. Figure 3.2 shows a summary of these SNP array data to highlight that there are no evident large differences between the L995 cell line (iAMP21-ALL patient) and the remission blood sample of the same twin (23299). Figure 3.2A shows the CNV data from these two samples separated, and Figure 3.2B shows an aggregated plot of the CNV data along with their locations on each chromosome. There appears to be no substantial gains or losses in copy number seen in the L995 cell line when compared with the 23299 blood sample. Figure 3.3 shows the same when comparing the L996 cell line (unaffected twin) to the blood sample from which it was derived (27405). Again, there are no obvious gross differences in copy number between L996 and this patient's blood sample.

The data in Figure 3.2 and Figure 3.3 show that there are no gross karyotypic changes between the L995 and L996 cell lines and the blood samples from which they were derived. Later, in Figure 3.8 and Figure 3.9, I show that L995 and L996 cells have a stable ploidy across passages and therefore this cell line appears tractable and a useful model to study the rob(15;21)c chromosome.

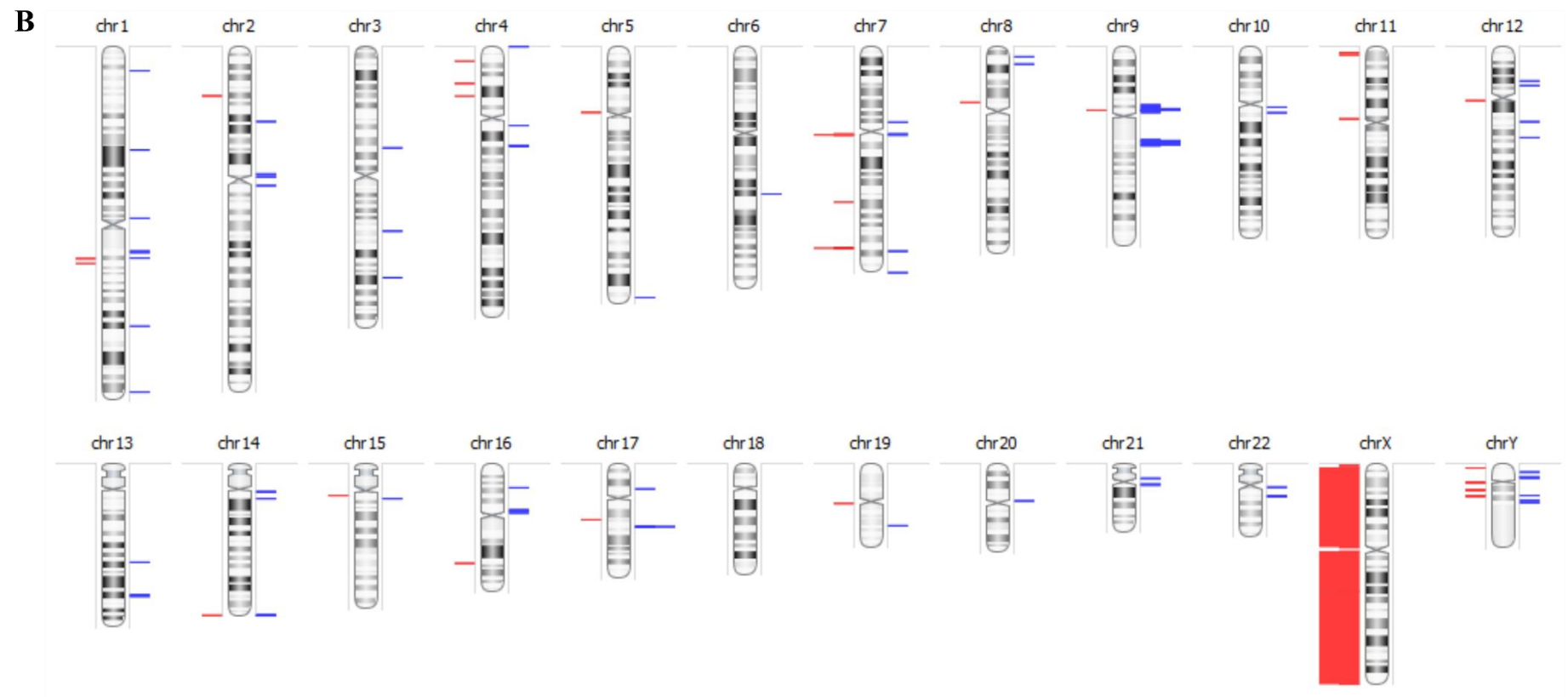
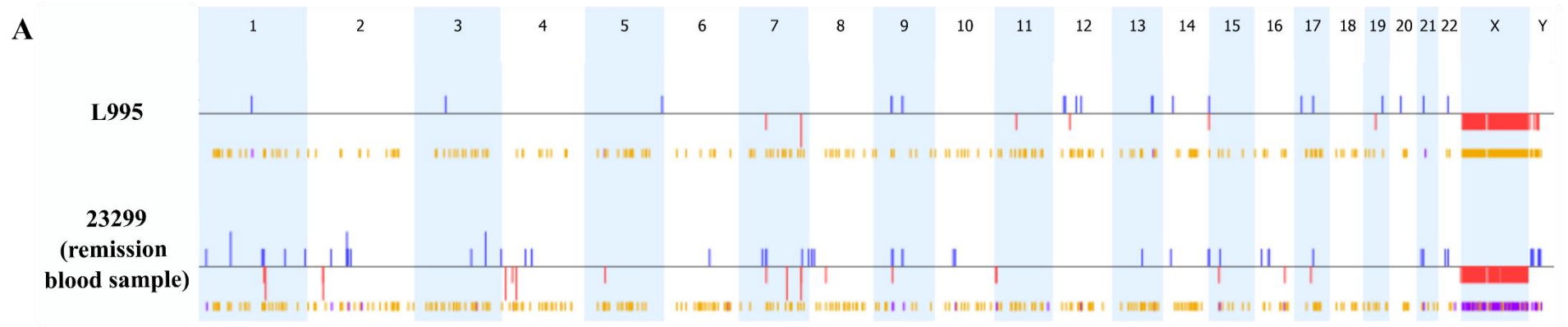


**Figure 3.2. L995 cell line is representative of the blood sample from which it was derived.** Copy number variation analysis comparing SNP array data for patient 23299 remission blood sample and the L995 cell line that it was EBV transformed into, compared to the GRCh37 reference genome. This copy number analysis is visualised in a whole genome view (**A**) and in a chromosome summary view (**B**), showing an aggregated plot of the gains and losses from both the blood sample and the L995 cell line when compared with GRCh37. Blue represents copy number gain. Red represents copy number loss. Purple shows allelic imbalance. Yellow shows Loss Of Heterozygosity (LOH). DNA from the 23299 remission blood sample was run on an Affymetrix SNP 6.0 array but due to the discontinuation of SNP 6.0 the L995 cell line DNA was run on an Illumina 850k array.

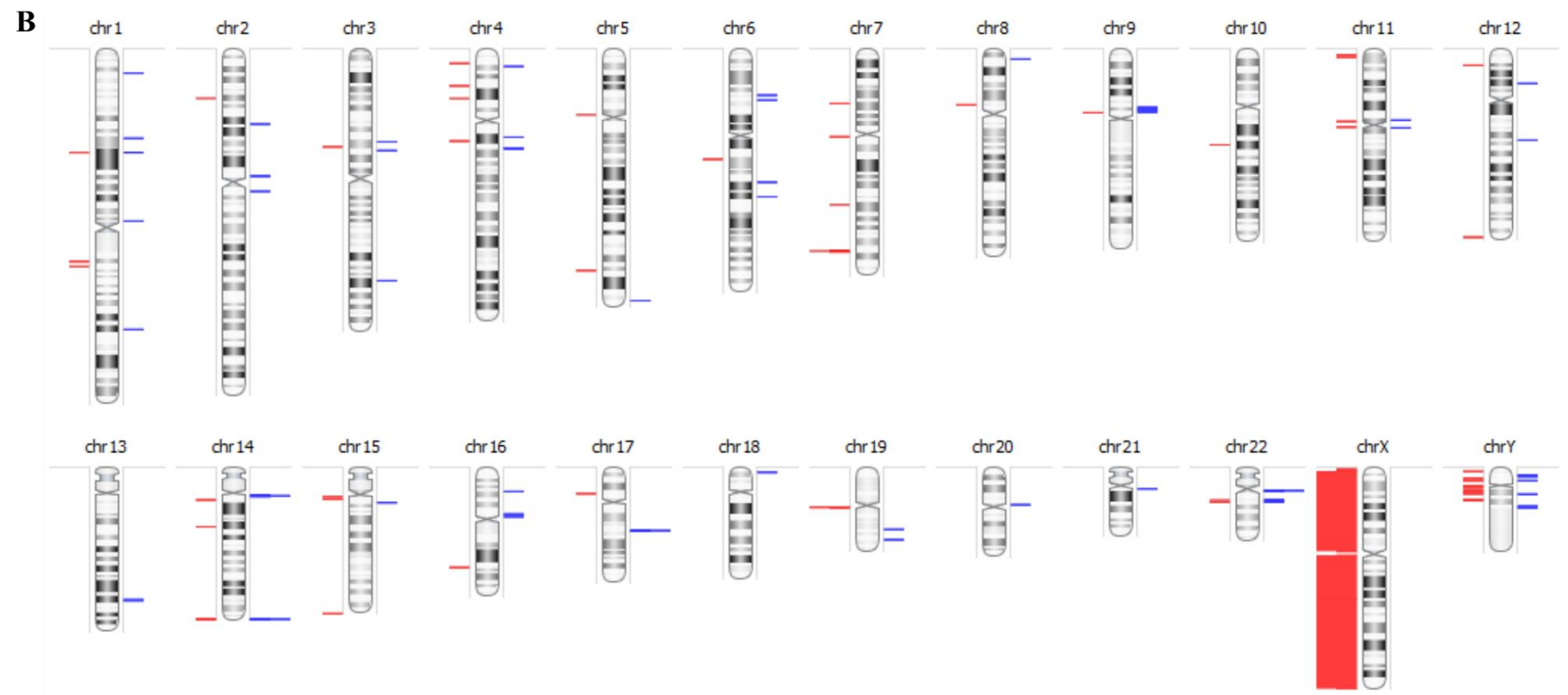
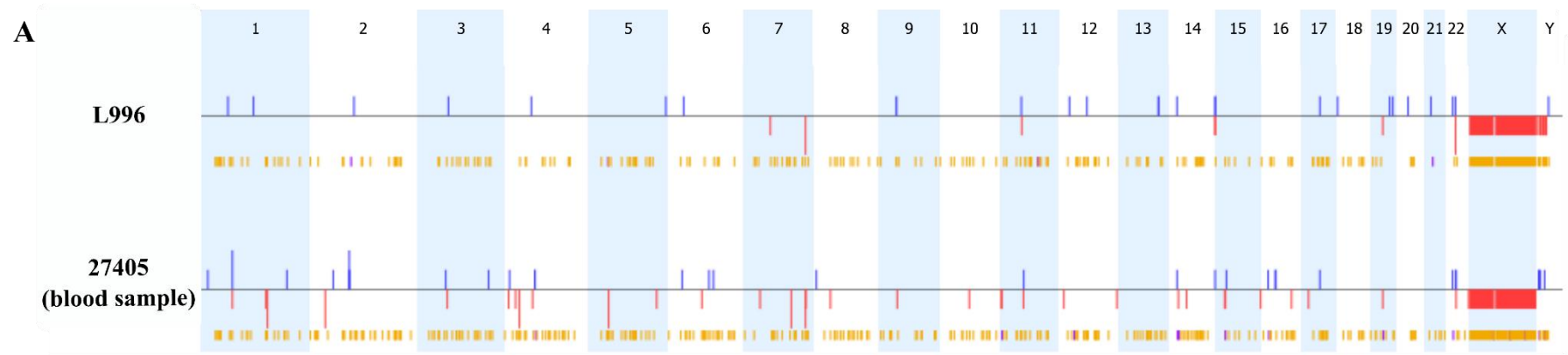


**Figure 3.3. L996 cell line is representative of the blood sample from which it was derived.** Copy number variation analysis comparing SNP array data for patient 23299 remission blood sample and the L995 cell line that it was EBV transformed into, compared to the GRCh37 reference genome. This copy number analysis is shown in a whole genome view (A) and in a chromosome summary view (B) showing an aggregated plot of the gains and losses from both the blood sample and the L996 cell line when compared with GRCh37. Blue represents copy number gain. Red represents copy number loss. Purple shows allelic imbalance. Yellow shows Loss Of Heterozygosity (LOH). DNA from the 27405 blood sample was run on an Affymetrix SNP 6.0 array but due to the discontinuation of SNP 6.0 the L996 cell line DNA was run on an Illumina 850k array.

### **3.2.3 iAMP21-ALL patient derived cell line has no obvious genetic differences to the unaffected twin derived cell line**

In this thesis, the cell lines L995 (derived from cells from the iAMP21-ALL patient) and L996 (derived from cells from the unaffected, identical twin of this iAMP21-ALL patient) are used to study the chromosome rob(15;21)c. We know from Li *et al.* that carriers of this chromosome have a ~2700x increased risk of developing iAMP21-ALL<sup>145</sup>. The aim of using cell lines derived from twin carriers of rob(15;21)c is to assess cellular mechanisms that may lead to chromothripsis and in turn tumourigenesis in these carriers, whilst minimising any other genetic differences that may be having an effect. To confirm that there are no cancer predisposing genetic differences between the affected patient cell line and the unaffected patient cell line, SNP array data from the two cell lines were compared and visualised as copy number variations when compared with the reference genome GRCh37 (Figure 3.4). Figure 3.4A shows L995 and L996 data separated and Figure 3.4B shows an aggregated view of these two samples and the location of the CNVs on each chromosome. These data show no gross chromosomal changes on either L995 or L996 and most CNVs are the same for both samples, with only minor differences between them. Further, ultra-long whole genome sequencing (WGS) was done on L995 and L996 cells. Data from this sequencing supported that shown in Figure 3.4, showing no obvious Structural Variants (SV) or Single Nucleotide Variants (SNV) of interest in L995 and L996. Therefore, both SNP array data and WGS data suggest that there are no obvious cancer-predisposing abnormalities in germline cells of 23299 (affected twin) or 27405 (unaffected twin).

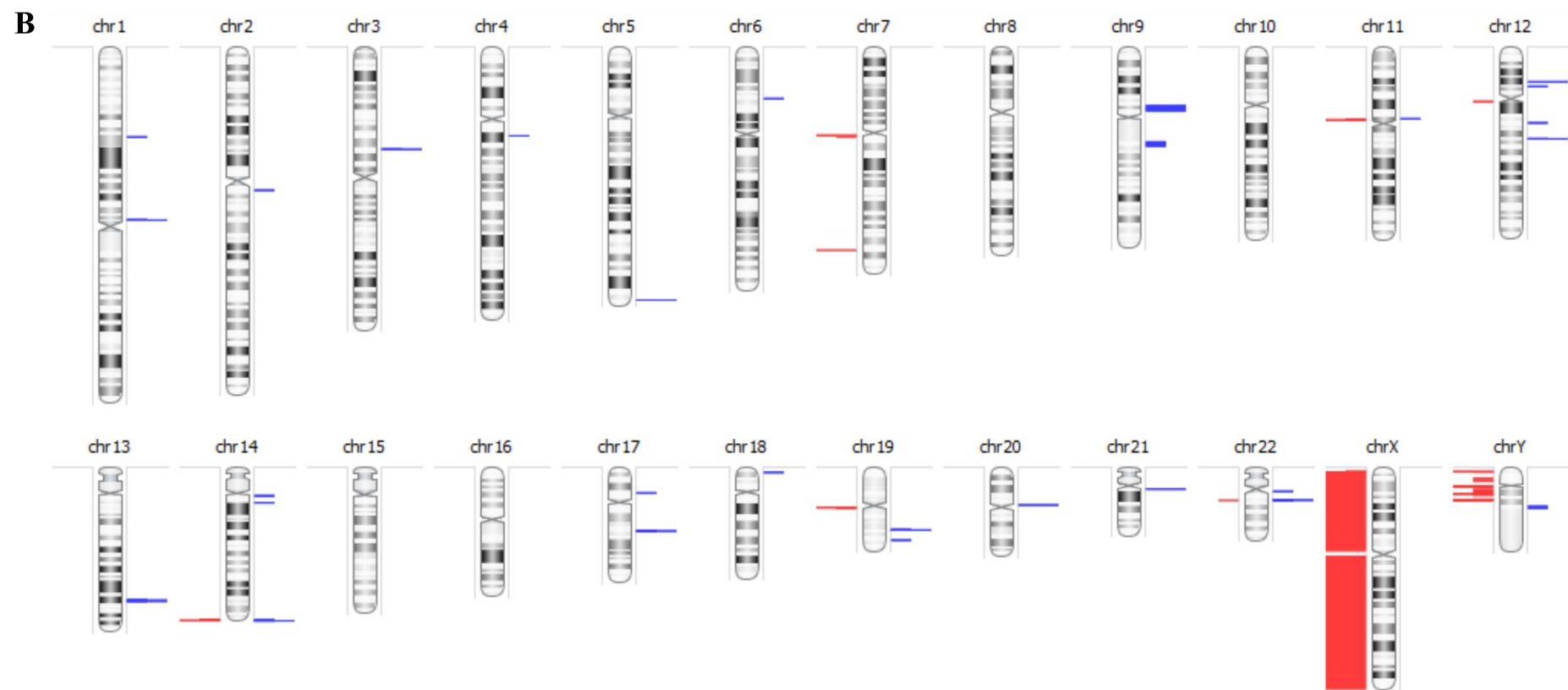
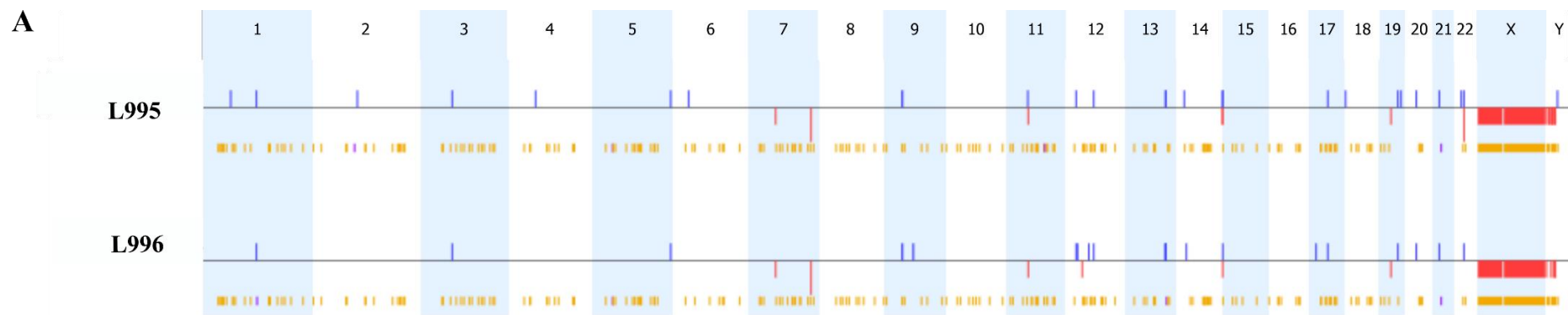


**Figure 3.4. Cell lines derived from the iAMP21-ALL twin patient and the unaffected twin patient have no gross chromosomal differences.** Copy number variation analysis comparing SNP array data for L995 and L996 cell lines compared to the GRCh37 reference genome. This copy number analysis is shown in a whole genome view (A) and in a chromosome summary view (B). Blue represents copy number gain. Red represents copy number loss. Purple shows allelic imbalance. Yellow shows Loss Of Heterozygosity (LOH). DNA from both the L995 and L996 cell lines were run on an Illumina 850k array.

To test for loss or gain of any specific genes of interest in L995 and L996, the CNV data from L995 and L996 in Figure 3.4 were first compared against the COSMIC cancer gene census database of known cancer-causing genes. CNV data were analysed in Nexus software which produced a table of the CNVs that overlapped with known genes. This gene list was filtered such that genes were only retained if the CNV overlapped with >50% of the gene. This gene list was compared against the COSMIC database gene list in R to produce the data in Table 3.1. Although there are a number of CNVs in genes associated with cancer, most were present in both samples. The only gene that had a CNV in L995 (cell line derived from twin patient affected by iAMP21-ALL) and not in L996 was CIC. 66% of the CIC gene showed Loss of Heterozygosity (LOH) in L995. This gene encodes an HMG-box-containing protein that is a component of the EGFR signalling pathway and is associated with multiple forms of brain tumour<sup>240,241</sup>. There has only been one report of the loss of CIC being involved in leukaemia<sup>242</sup>. We believe it unlikely that this partial LOH of CIC in the patient who developed iAMP21-ALL to be the reason why they developed this cancer, and their identical twin did not.

Chromosome segregation was of interest as it has been associated with chromothripsis, and the rob(15;21)c chromosome is dicentric, possibly leading to elevated mis-segregation. To test if the L995 and L996 cell lines have loss or gain of any genes known to have a role in chromosome segregation, the CNV data from these cell lines (Figure 3.4) was compared against known chromosome segregation genes (database from Gene Ontology). As above, the gene list was filtered such that genes were only retained if >50% of the CNV overlapped with the gene. Table 3.2 shows the genes in which there was a CNV in L995 and/or L996. Only 5 genes associated with chromosome segregation contained CNVs in L995 and L996. All of these CNVs were present in both samples. One gene of interest is NUMA1; this appears in both the COSMIC gene list (Table 3.1) and the chromosome segregation gene list (Table 3.2). NUMA1 plays a role in mitotic spindle formation and has been associated with Acute Promyelocytic Leukaemia (APL). However, the function of NUMA1 in APL development is usually through the production of a fusion gene. The CNV that is present in both L995 and L996 is LOH; it is unlikely that this NUMA1 fusion gene exists in these cells.

**Table 3.1. L995 and L996 CNVs compared against the COSMIC database of known cancer genes.**

Gene Symbol	Event	Chromosome Region	% of CNV/Gene overlap	Present in L995	Present in L996	Associated Tumour Type
AXIN1	LOH	chr16:218,783-765,779	54.7	Yes	Yes	colorectal, endometrial, prostate, hepatocellular carcinoma, hepatoblastoma, sporadic medulloblastoma
CIC	LOH	chr19:42,799,231-43,504,242	66.3	Yes	No	oligodendroglioma, soft tissue sarcoma
DCTN1	LOH	chr2:74,370,238-74,971,153	51.5	Yes	Yes	inflammatory myofibroblastic tumour, Spitzoid tumour
FKBP9	LOH	chr7:33,005,568-33,592,998	100.0	Yes	Yes	glioma
GPC5	CN Gain	chr13:93,299,682-93,331,639	100.0	Yes	Yes	lung adenocarcinoma
GPHN	LOH	chr14:66,908,573-67,889,484	77.5	Yes	Yes	AL
HIP1	LOH	chr7:75,218,473-77,045,752	66.9	Yes	Yes	CMML, NSCLC
MAX	LOH	chr14:65,272,718-65,878,325	100.0	Yes	Yes	pheochromocytoma, endometrioid carcinoma, colon carcinoma
NOTCH2	CN Gain	chr1:120,531,096-121,045,858	100.0	Yes	Yes	marginal zone lymphoma, DLBCL, bladder
NUMA1	LOH	chr11:71,299,610-71,910,723	59.5	Yes	Yes	APL
SETD2	LOH	chr3:46,738,472-48,377,520	73.4	Yes	Yes	clear cell renal carcinoma
ZMYM2	LOH	chr13:20,151,204-20,687,519	67.1	Yes	Yes	MPN, NHL

**Table 3.2. L995 and L996 CNVs compared against a database of known chromosome segregation genes from Gene Ontology.**

Gene Symbol	Event	Chromosome Region	% of CNV/Gene overlap	Present in L995	Present in L996	Role
STAG3	LOH	chr7:99,808,966-100,522,632	100.0	Yes	Yes	Cohesin subunit
ZCWPW1	LOH	chr7:99,808,966-100,522,632	100.0	Yes	Yes	Homologous chromosome pairing at meiosis I
NUMA1	LOH	chr11:71,299,610-71,910,723	59.5	Yes	Yes	Function and organisation of mitotic spindle
M1AP	LOH	chr2:74,370,238-74,971,153	51.5	Yes	Yes	Meiosis progression
TUBGCP5	LOH	chr15:20,071,673-22,866,986	100.0	Yes	Yes	Microtubule nucleation

In conclusion, there appear to be no obvious cancer-predisposing abnormalities that were linked to leukaemia development in patient 23299 that were not present in their identical twin, 27405. Importantly for this study, the cell lines derived from these patients' cells showed no gross chromosomal changes and appeared to be a good representative model of the cells from which they were derived.

#### **3.2.4 rob(15;21)c translocation is confirmed in L995 and L996 cell lines**

Analysis of SNP array data showed no gross changes to copy number in L995 and L996 cell lines when compared to the non-cancerous blood samples. However, to confirm that the rob(15;21)c chromosome was retained in these lines after EBV transformation,  $\alpha$ -satellite FISH was done. Figure 3.5 and Figure 3.6 show examples of chromosome spreads from these experiments respectively in L995 and L996. The  $\alpha$ -satellites of chromosome 15 (green) and chromosomes 21/13 (magenta) were stained. Due to the homology of the  $\alpha$ -satellite DNA of chromosomes 21 and 13, FISH probes could not be designed to differentiate them. However, in a chromosome spread they can frequently be distinguished by chromosome size. Chromosome 21 is significantly smaller than chromosome 13.

The Robertsonian translocation can be seen in the far-right insets of Figure 3.5 and Figure 3.6. Colocalisation of the  $\alpha$ -satellites of chromosome 15 and 21/13 on one chromosome suggests that this chromosome was retained in both cell lines post EBV transformation. It is also of note that the  $\alpha$ -satellite of chromosome 21 within the rob(15;21)c chromosome frequently appears smaller and less brightly stained than that on the normal chromosome 21.

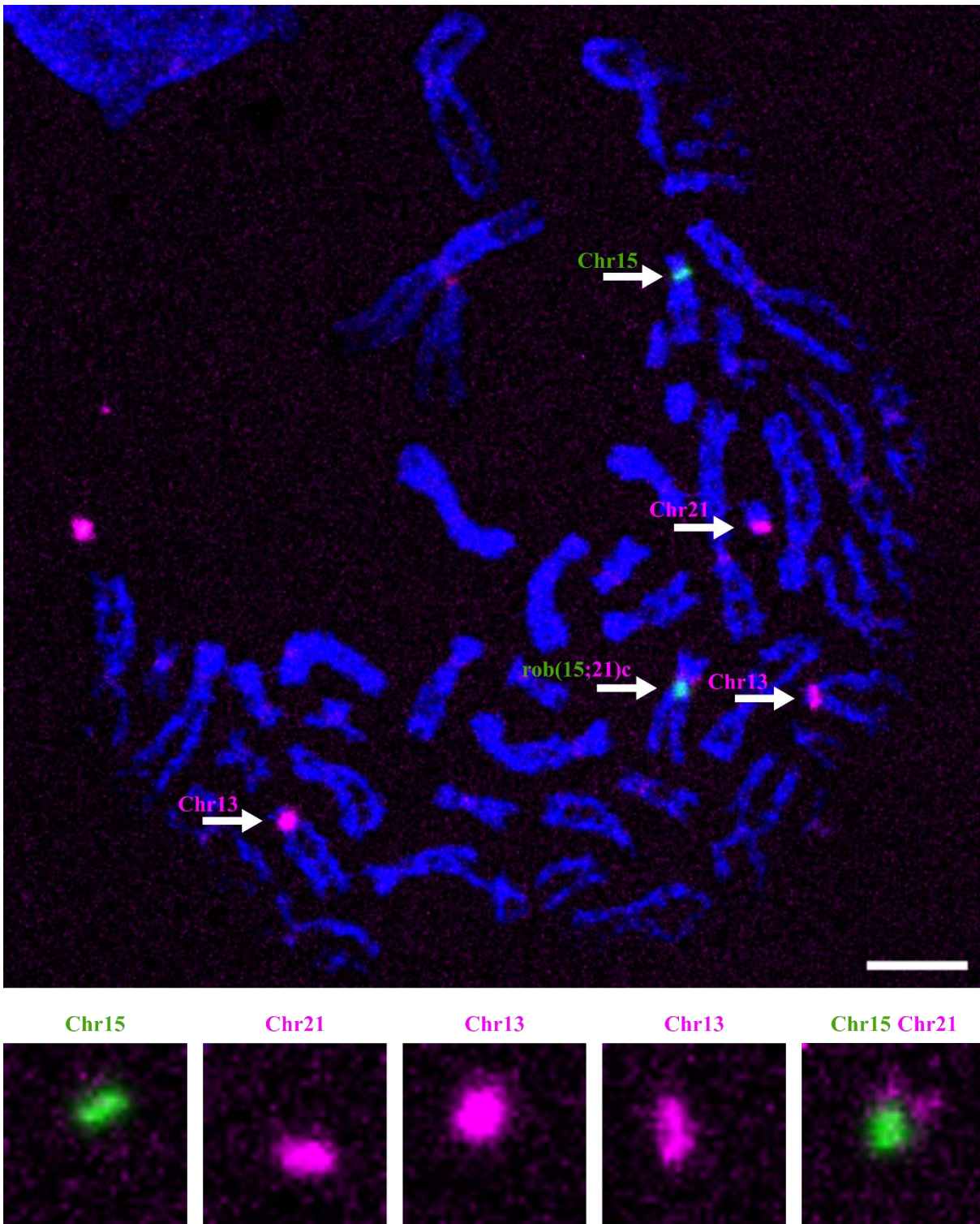


**Figure 3.5. *rob(15;21)c* is confirmed in L995.** Example chromosome spread from an L995 cell with  $\alpha$ -satellites of chromosome 15 (green) and chromosomes 21/13 (magenta) stained by FISH. Insets show zoomed in regions of interest to highlight all FISH-stained chromosomes. Scale bar = 5  $\mu$ m.

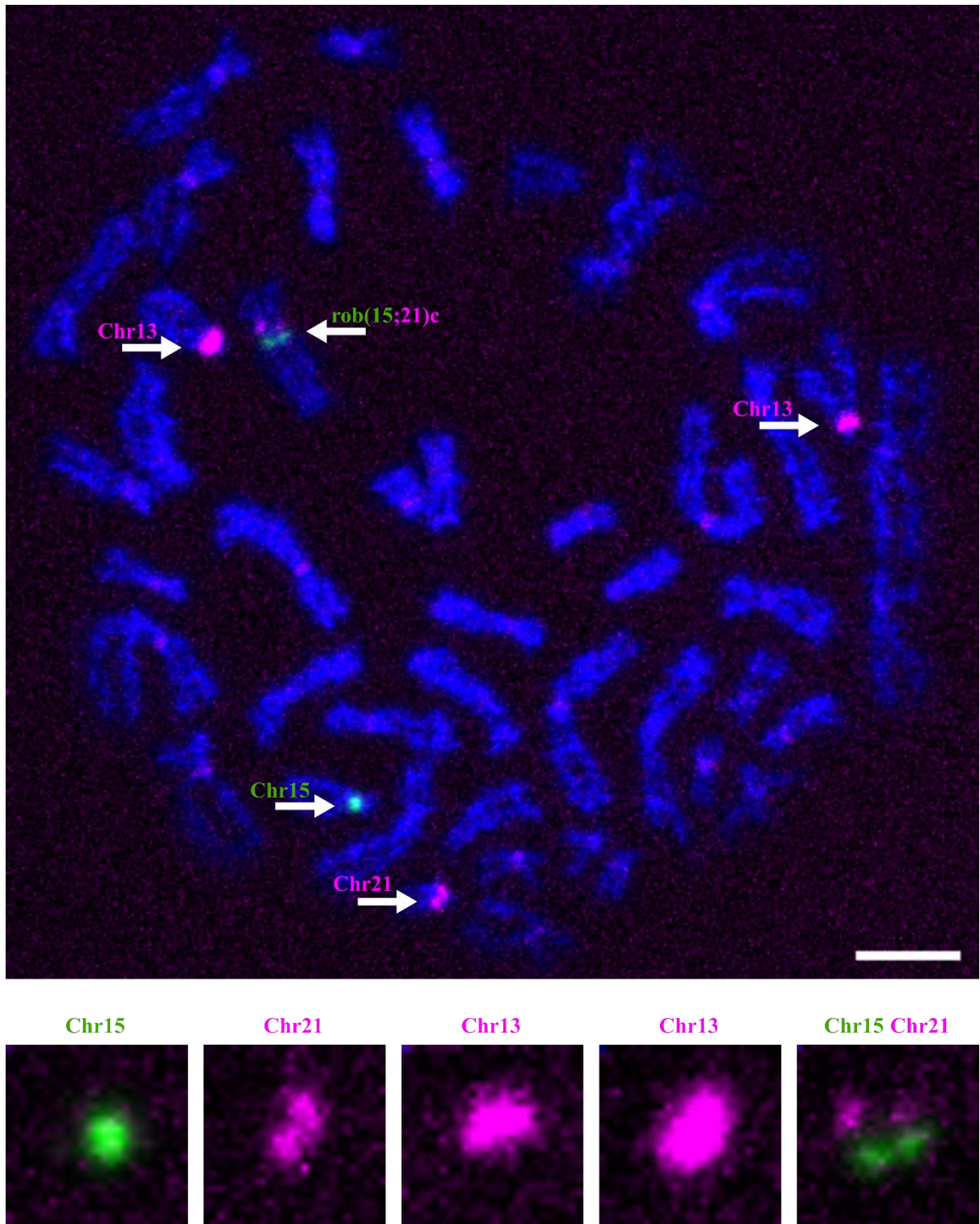


**Figure 3.6. *rob(15;21)c* is confirmed in L996.** Example chromosome spread from an L996 cell with  $\alpha$ -satellites of chromosome 15 and chromosomes 21/13 stained by FISH. Insets show zoomed in regions of interest to highlight all FISH-stained chromosomes. Scale bar = 5  $\mu$ m.

### **3.2.5 L995 and L996 cell lines are predominantly diploid**

EBV transformed lymphoblastoid cell lines can have compromised genomic stability<sup>237-239</sup>. Early fluorescence in-situ hybridisation (FISH) experiments raised concerns regarding ploidy of both L995 and L996 lines. As represented by centromere 15 of L995 in Figure 3.7, it appeared that a considerable subpopulation of these cells may have become tetraploid. A diploid cell would have two foci for each respective centromere per cell (during G1). As seen in Figure 3.7, a considerable number of cells appear to have 4 foci of centromere 15. The number of cells which appear to be tetraploid was noticeably greater than would be expected for late stage S phase and G2 phase cells; thus observation of four chromosome 15 centromeres led to the suspicion of aneuploidy.

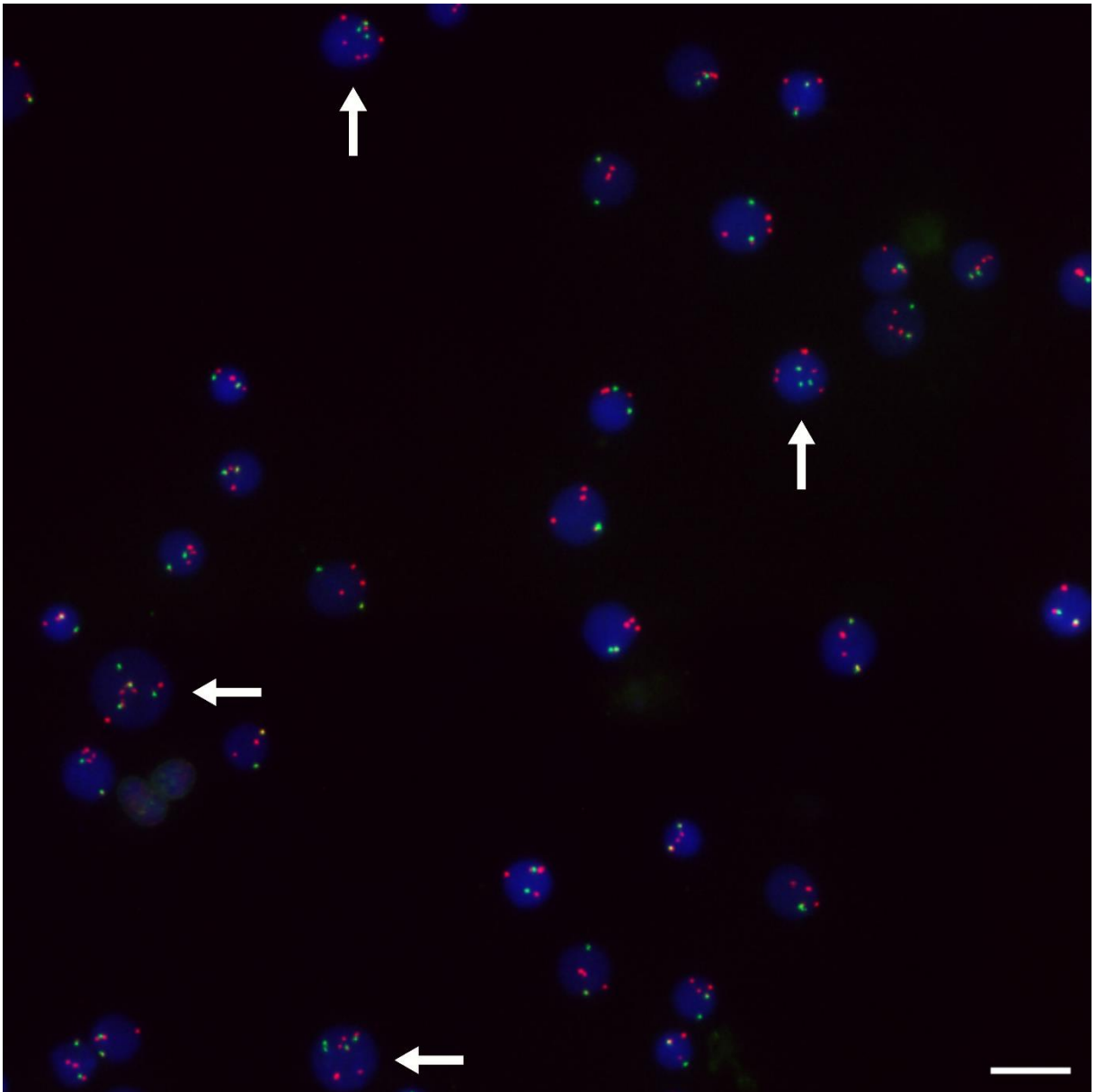


**Figure 3.7. FISH shows possible tetraploid population in L996 cells.** L996 cells stained with FISH probes for the centromeres of chromosome 15 (green) and chromosomes 13/21 (red). Arrows showing possible tetraploid cells. Scale bar = 20  $\mu\text{m}$ .

By manual analysis of FISH across L995 and L996 it appeared that tetraploidy decreased over passages; occurring earlier in the faster growing line. This suggested that tetraploid populations were being outgrown by diploid populations, leading to an apparent increase in stability over time. This process of lymphoblastoid lines turning from tetraploid to diploid and becoming more genomically stable over time has been previously seen (table 2, LCL1-18 and LCL2-15 from Lacoste *et al*)<sup>243</sup>.

This hypothesis was from manual observation and lacked quantification. To address this, cell cycle analysis by flow cytometry was used, measuring DNA content with propidium iodide (PI) (Figure 3.8 and Figure 3.9). Multiple passages of L995 and L996 were fixed, stained with PI, and analysed by cytometry to assess ploidy by overall DNA content per cell/event. Gating was used to exclude doublets, multiplets and dead cells/debris from the analysis.

Figure 3.8A of early passage L995 cells shows the characteristic cell cycle distribution expected from a diploid cell line, exhibiting a large peak for 2n (G1) events, a smaller peak for 4n (G2) events and a number of events with varying intensity between these (S phase). Figure 3.8A also shows a dot plot for these same events; occurring from early passage L995 cells. This highlights the obvious peaks at 2n and 4n but shows a lack of events greater than 4n (>4n). This is emphasised by the red box showing all events >4n, where S phase and G2 phase of a tetraploid population would lie. Particularly, there is no obvious cluster of events at 8n, where G2 tetraploid cells would be expected. Figure 3.8B and Figure 3.8C then show cell cycle distribution for L995 cells at a mid and late passage respectively. No distinctive difference between these figures and Figure 3.8A provide evidence to suggest that our hypothesis was incorrect. It appears that neither early nor late passage L995 cells have significant tetraploid populations. Events >4n account for only 1.43% of total events for early passage cells, 2.12% for mid passage cells and 1.80% for late passage cells. Possible tetraploid cells observed in early FISH experiments were presumably predominantly diploid cells in G2.

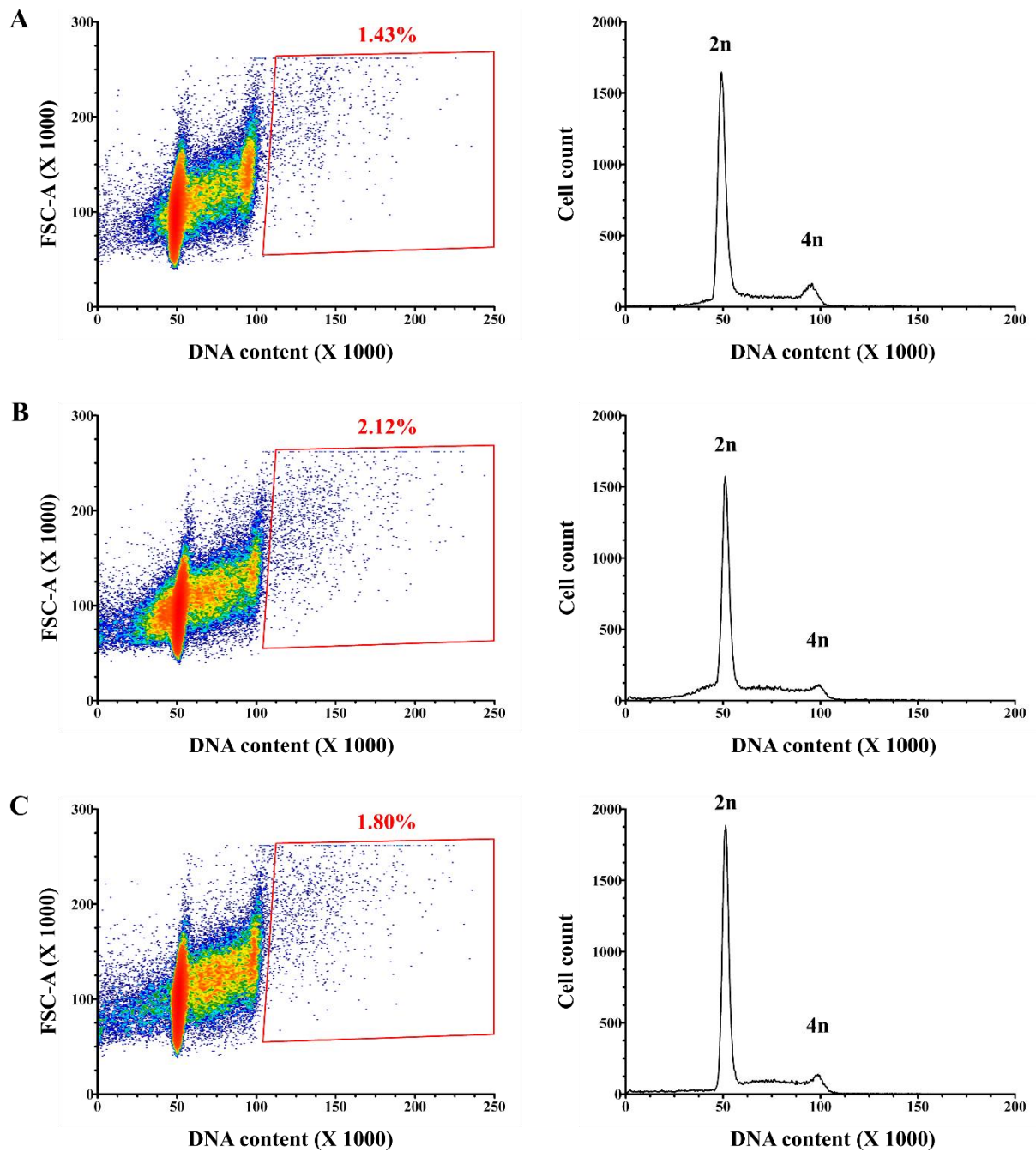


**Figure 3.8. L995 does not have a large tetraploid population.** (A) Density dot plot and DNA content histogram of early passage L995 cells. (B) Density dot plot and DNA content histogram of mid passage L995 cells. (C) Density dot plot and DNA content histogram of late passage L995 cells.

Figure 3.9A, Figure 3.9B and Figure 3.9C respectively represent events from early passage, mid passage and late passage L996 cells. As with L995, L996 appear to have the characteristic cell cycle distribution of a diploid population, with a lack of events  $>4n$ . Approximately 2.1-2.4% of total L996 events (at early, mid and late passage) are  $>4n$ , thus demonstrating that L996 also don't show significant tetraploid populations at any passage. The ploidy of both L995 and L996 cell lines therefore appears to not be fluctuating largely; with the majority of the cell population being stably diploid.

Neither L995 nor L996 lymphoblastoid cell lines appear to have substantial aneuploid populations. However, there are still some events (~2%) that have DNA content  $>4n$ . This can be explained by events that have slipped through the gating workflow used. Many of these events may be due to doublets, large cellular debris, or very small populations of aneuploid cells which are not of great significance.

The outcome of these cell cycle analysis experiments was favourable; showing that these unique resources still cytogenetically resemble the cells from which they were derived. Nevertheless, it is important to continue monitoring the ploidy of these cell lines in case they have potential for outgrowth of aneuploid populations.

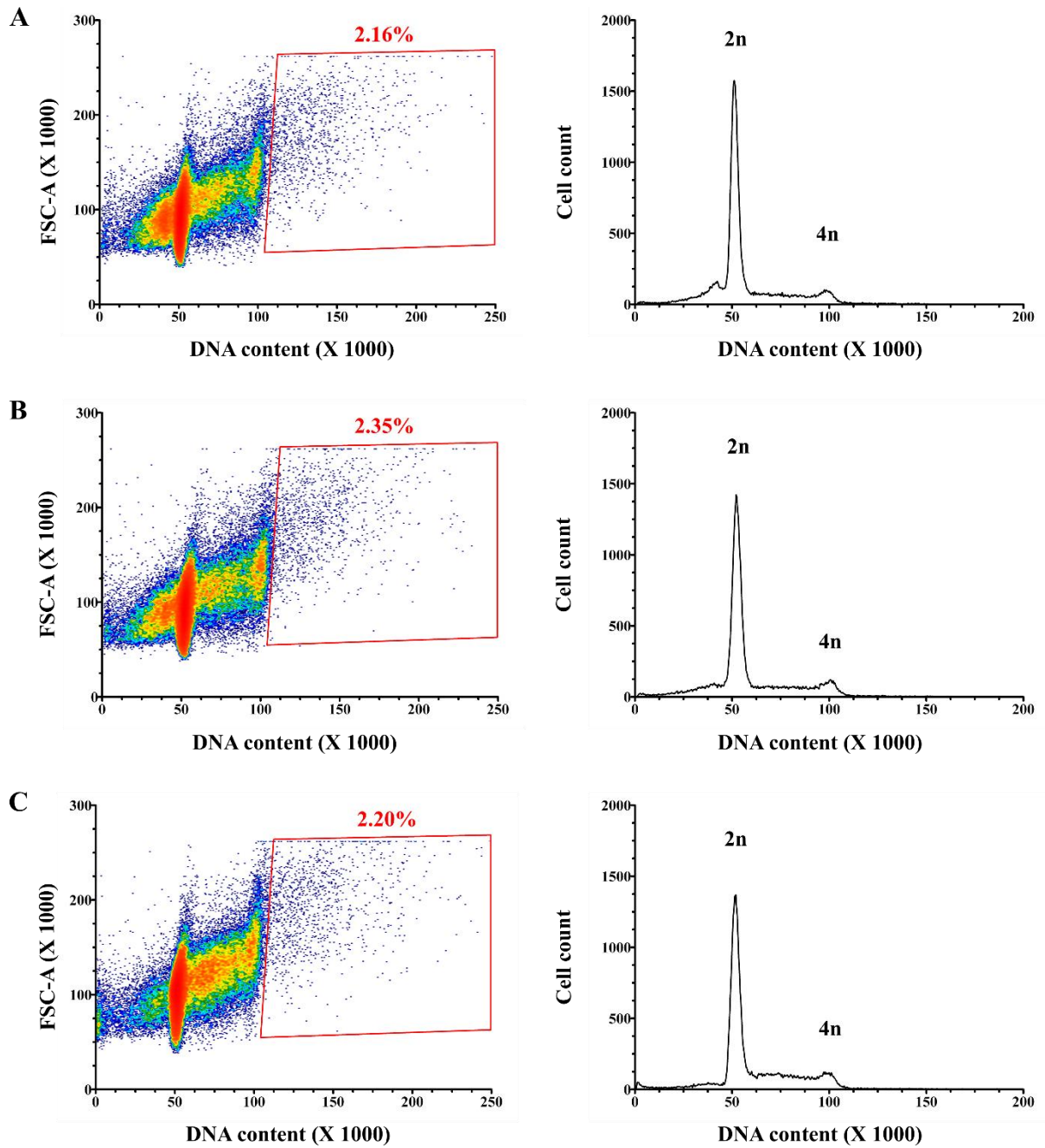


**Figure 3.9. L996 does not have a large tetraploid population.** (A) Density dot plot and DNA content histogram of early passage L996 cells. (B) Density dot plot and DNA content histogram of mid passage L996 cells. (C) Density dot plot and DNA content histogram of late passage L996 cells.

### **3.2.6 The dicentric chromosome rob(15;21)c has heterogeneity in its ability to assemble kinetochores**

Alpha-satellite FISH in Figure 3.5 and Figure 3.6 has shown that rob(15;21)c in L995 and L996 cells is dicentric in its centromeric DNA content. We set out to show that this chromosome is also an active dicentric in the proteins which assemble onto the centromere; creating the outer centromere and the kinetochore at both centromeres on each sister chromatid of rob(15;21)c. Possession of kinetochores on both centromeres of the dicentric would indicate that rob(15;21)c has the potential to be functionally dicentric.

A protocol was designed to integrate chromosome spreads, Immunofluorescence (IF) and Fluorescence In-Situ Hybridisation (FISH). This allowed for the identification of rob(15;21)c through the use of specific fluorophore-labelled FISH probes for chromosome 15 and chromosome 21. Incorporating IF into this protocol allowed for the staining of Centromere Protein-C (CENP-C), an inner kinetochore protein that is a good marker of an active centromere<sup>244,245</sup>.

In a mitotic cell, chromosomes sit spatially very close to each other and when imaging; the signals of each chromosome overlap and identifying specific chromosomes can be difficult. Creating chromosome spreads with the use of Colcemid allowed for the separation of each condensed chromosome without microtubule attachments. Colcemid has the ability to bind tubulins, inhibiting microtubule elongation and promoting microtubule depolymerisation. Cells arrested using Colcemid are arrested in a prometaphase like state, with condensed chromosomes but without functioning microtubules they lack the ability to form a proper metaphase plate and segregate chromosomes appropriately. With the use of a hypotonic buffer to swell cells and centrifugation using a Cytospin to spatter cells onto slides, chromosome spreads can easily be produced from the Colcemid arrested cells. As can be seen in Figure 3.10 and Figure 3.11, in a chromosome spread with FISH staining, chromosome 15, chromosome 21 and the Robertsonian chromosome rob(15;21)c all from the same cell can be easily identified.

We know from alpha satellite FISH experiments that the CEN15 and CEN21 centromeres of rob(15;21)c in L995 and L996 have a short inter-centromeric distance. While making preliminary chromosome spreads + IF + FISH experiments we noticed that the staining of centromeric proteins often overlapped on these closely located centromeres, creating a staining pattern that looked like there was only one active centromere. This brought up the question whether rob(15;21)c was truly functionally dicentric. To answer this question, future

experiments were optimised for Stimulated Emission Depletion (STED) super-resolution microscopy. Whilst standard confocal microscopy has a resolution limit dictated by the diffraction limit of light (~200nm) STED microscopy is able to overcome that diffraction limit and reach resolutions  $<50 \text{ nm}^{246,247}$ . Therefore, the incorporation of STED microscopy, followed by image deconvolution would provide us with images with the best resolution possible to determine if rob(15;21)c was actively dicentric or not.

We found that there appeared to be cell-to-cell heterogeneity in the CENP-C staining of rob(15;21)c chromosomes. Figure 3.10 shows how, regardless of the imaging modality, rob(15;21)c still has a monocentric phenotype in some cells. Figure 3.10A and Figure 3.10B show normal chromosome 15 and chromosome 21 from L995 cells as a reference for a monocentric chromosome and what the staining of CENP-C looks like with confocal microscopy, STED microscopy and then a STED microscopy image that has been further improved with deconvolution. When comparing rob(15;21)c from the same cell (Figure 3.10C) it is clear that this chromosome has no detectable second centromere in at least some cells. CENP-C is a vital part of the kinetochore and without it on the second centromere of the dicentric it is unlikely that a second functional kinetochore could be assembled<sup>248,249</sup>. Figure 3.11 provides an example of a rob(15;21)c chromosome that appears dicentric clearly, due to a large inter-centromeric distance. The example chromosome in Figure 3.11C is a particularly obvious example of an actively dicentric rob(15;21)c and therefore it could already be resolved by confocal microscopy, though the improved resolution from STED and deconvolution further confirm how truly distinct these two kinetochores can be on rob(15;21)c. Figure 3.11A and Figure 3.11B are respectively chromosome 15 and chromosome 21 from the same cell and therefore give examples of control monocentric chromosomes.

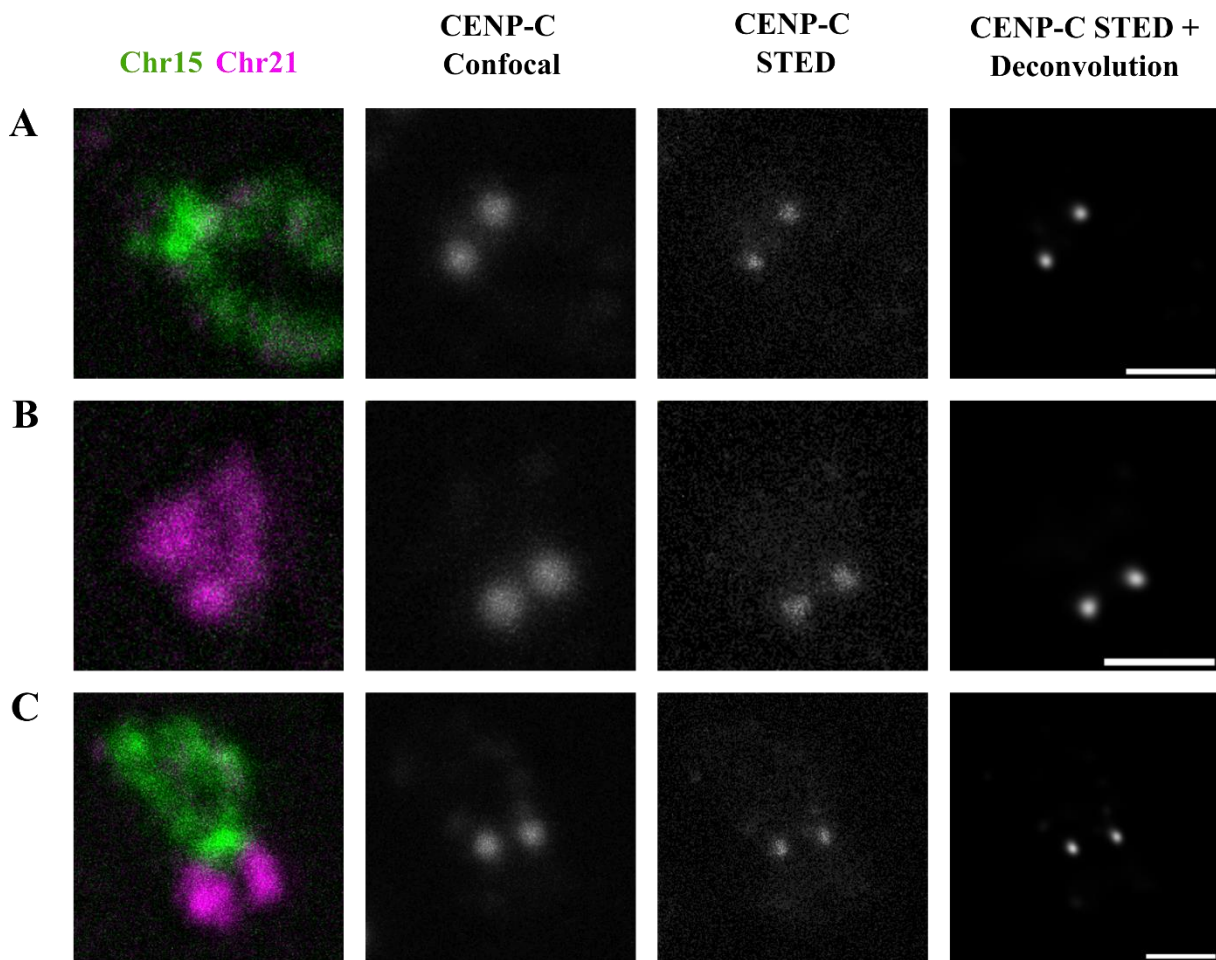


**Figure 3.10. rob(15;21)c sometimes appears actively monocentric.** Chromosomes 15 (A), 21 (B) and rob(15;21)c (C) from the chromosome spread of one cell stained with FISH probes for Chr15q (green) and Chr21q (magenta) and immunostaining for CENP-C. The same samples were imaged with standard confocal microscopy then with STED super-resolution microscopy to improve resolution of CENP-C foci. STED images were deconvolved to further improve resolution. Scale bars = 1 $\mu$ m.

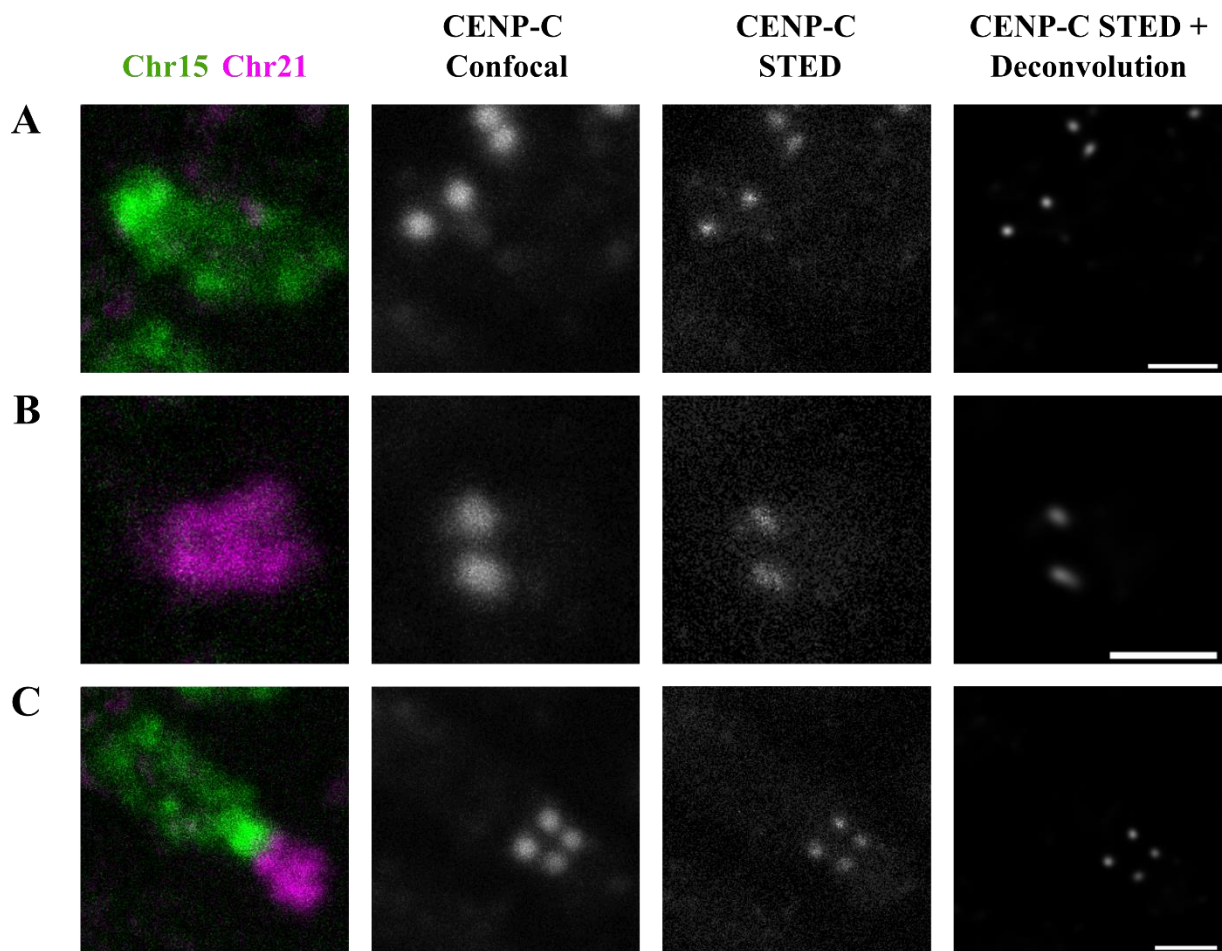


**Figure 3.11. rob(15;21)c sometimes appears actively dicentric.** Chromosomes 15 (A), 21 (B) and rob(15;21)c (C) from the chromosome spread of one cell stained with FISH probes for Chr15q (green) and Chr21q (magenta) and immunostaining for CENP-C. The same samples were imaged with standard confocal microscopy then with STED super-resolution microscopy to improve resolution of CENP-C foci. STED images were deconvolved to further improve resolution. Scale bars = 1 $\mu$ m.

Through imaging experiments of rob(15;21)c chromosomes it is clear that the apparent inter-centromeric distance varies greatly. However, we believe that this is due to the variability in chromosome spreads rather than a real difference in amount of centromeric DNA between one centromere and the other on a dicentric sister chromatid of rob(15;21)c. Generally, rob(15;21)c chromosomes that have spread more are elongated and have greater inter-centromeric distances (e.g. Figure 3.11C). Those which appear to have overlapping CENP-C foci are shorter as they have spread less (e.g. Figure 3.12C).

Figure 3.12C is an example of an image where rob(15;21)c appears to have overlapping, close CENP-C foci. By standard confocal microscopy these could easily be mistakenly identified as only one CENP-C focus per sister chromatid. However, with the improvements in resolution that STED microscopy and image deconvolution brings, rob(15;21)c in this cell can be properly

identified as actively dicentric. These data are backed up by the line graphs in Figure 3.13. The graph in Figure 3.13A correlating with the confocal image shows that quantification of the intensity of CENP-C along the yellow line would characterise this chromosome as being monocentric (due to the presence of a singular peak). However the line graphs in Figure 3.13B and Figure 3.13C clearly identify the two peaks once the resolution has been improved by STED microscopy and STED microscopy + deconvolution respectively; thus characterising this rob(15;21)c image as actively dicentric.

Whilst the visualised inter-centromeric distance can change and rob(15;21)c can sometimes be mis-characterised as monocentric when CENP-C foci are close, we believe that there is still a real population of cells with a monocentric rob(15;21)c chromosome. Images such as those in Figure 3.10C where CENP-C foci are extremely punctate, even after STED imaging and deconvolution, provide us with sufficient evidence to confirm this phenotype. However, it is fair to say that the quantification of the two vs four CENP-C phenotype as done in Figure 3.15 and Figure 3.16 will likely make an underestimation of the actively dicentric phenotype (i.e. 4 centromere puncta per mitotic chromosome) and an overestimation of the monocentric phenotype due to the occasional mis-characterisation.

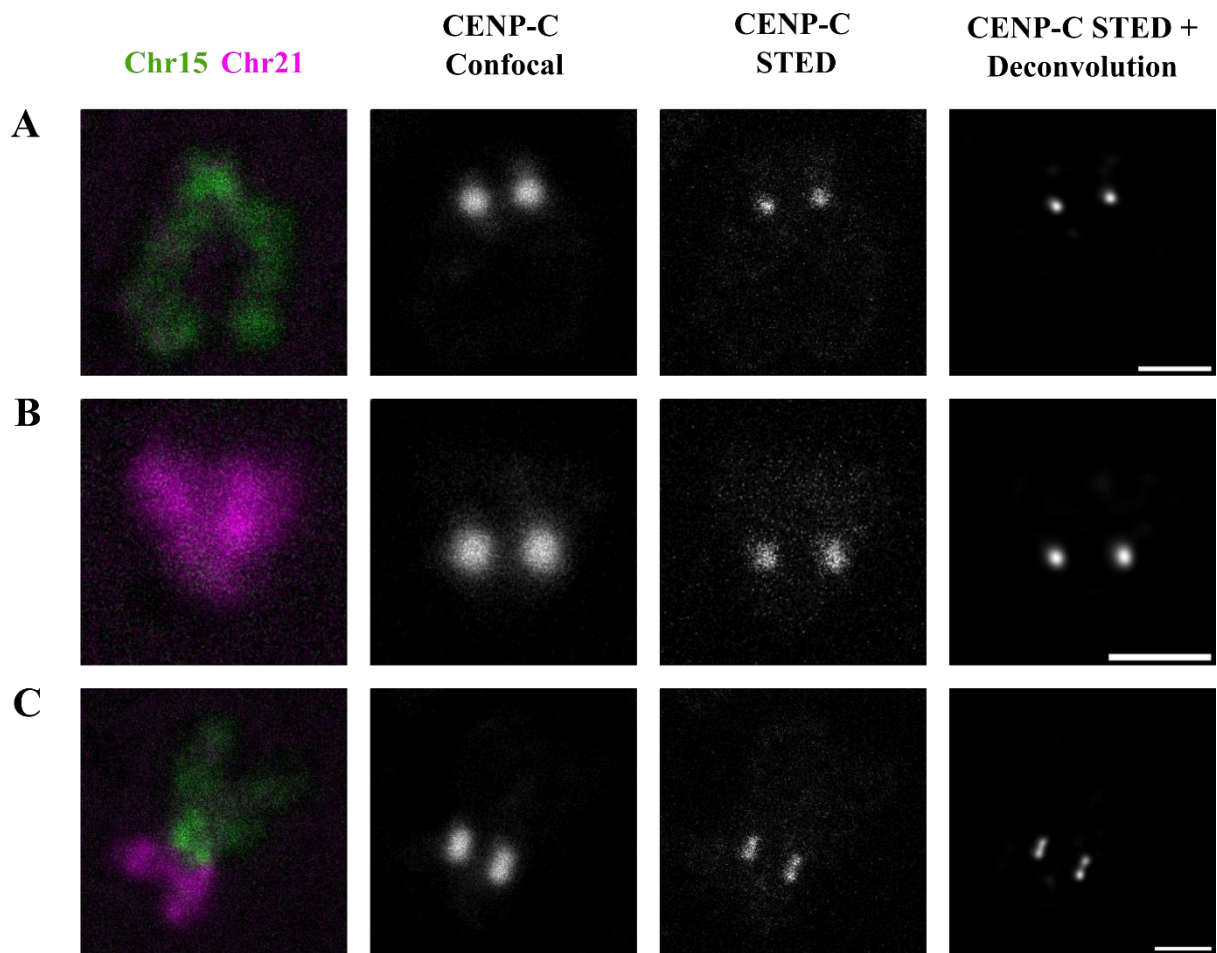


**Figure 3.12. Actively dicentric rob(15;21)c inter-centromeric distance can appear short due to chromosome spread variation.** Chromosomes 15 (A), 21 (B) and rob(15;21)c (C) from the chromosome spread of one cell stained with FISH probes for Chr15q (green) and Chr21q (magenta) and immunostaining for CENP-C. The same samples were imaged with standard confocal microscopy then with STED super-resolution microscopy to improve resolution of CENP-C foci. STED images were deconvolved to further improve resolution. Scale bars = 1 $\mu$ m.

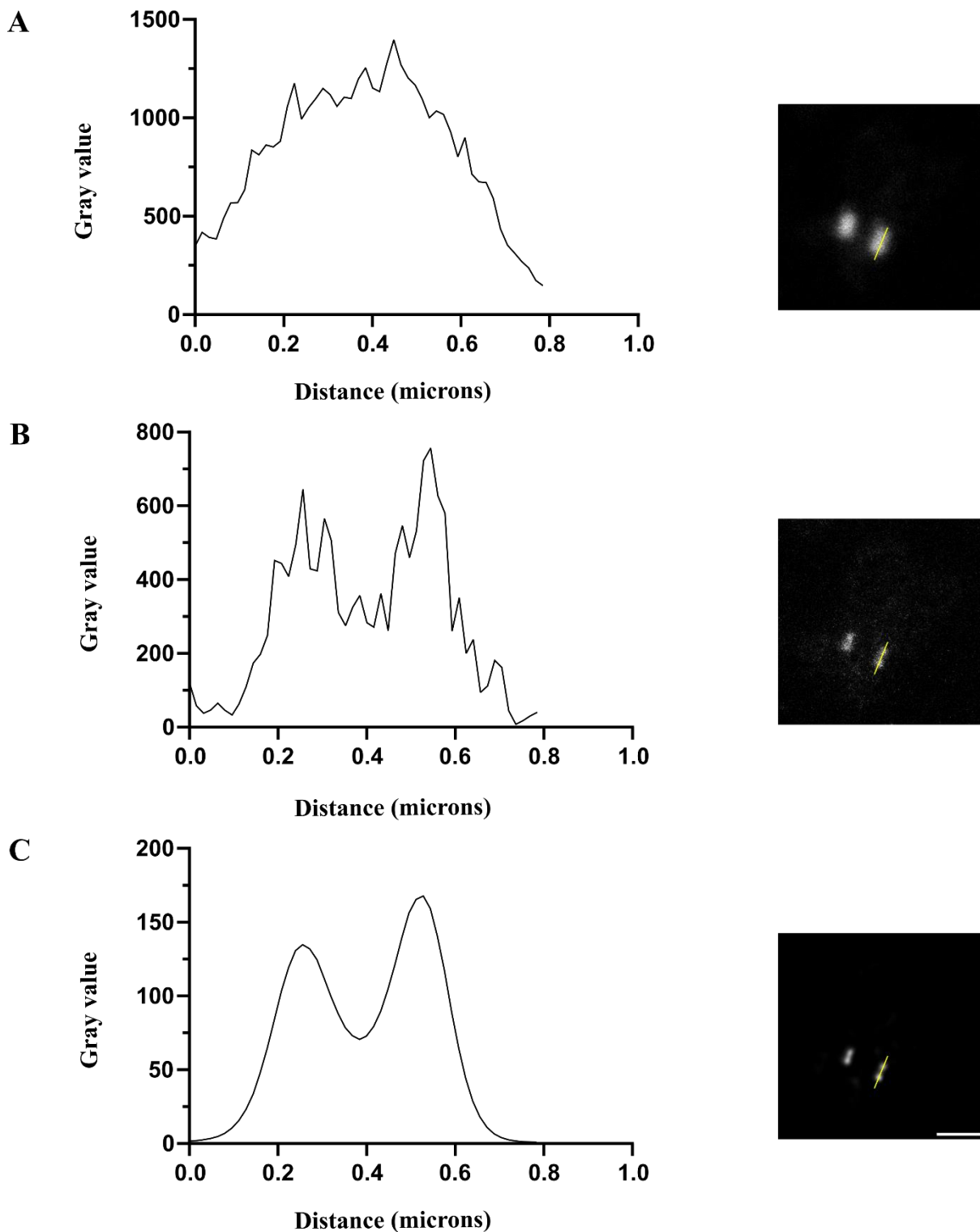


**Figure 3.13. Line graphs showing the resolution of CENP-C foci with small inter-centromeric distance.** Line graphs of the rob(15;21)c CENP-C foci shown in Figure 3.12C. **(A)** Line graph and respective image from the rob(15;21)c CENP-C foci imaged by confocal microscopy. **(B)** Line graph and respective image from the rob(15;21)c CENP-C foci imaged by STED microscopy. **(C)** Line graph and respective image from the rob(15;21)c CENP-C foci imaged by STED microscopy and deconvolved for further resolution improvements. Yellow line indicates the pixels quantified for the line graphs. Scale bars = 1 $\mu$ m.

Studies show that CENP-C is a marker for an active kinetochore and therefore it could be presumed that rob(15;21)c chromosomes with four CENP-C dots (e.g. Figure 3.11C) have two fully functioning kinetochores per sister chromatid<sup>244,245</sup>. CENP-C is part of the Constitutive Centromere Associated Network (CCAN), an inner kinetochore complex that plays a role in coupling nucleosomes and outer kinetochore microtubule-binding proteins in the KNL-1/Mis12 complex/Ndc80 complex (KMN) network<sup>250-253</sup>. Unlike the CCAN which is present at the centromere throughout the cell cycle, the KMN network is recruited during mitosis. Due to the possible mitotic problems that having two functional kinetochores could cause and the short inter-centromeric distance seen in rob(15;21)c, we thought to further stain more outer kinetochore proteins; in particular those which directly bind microtubules, to better understand the possible functionality of these centromeres.

Hec1 (also known as NDC80) and NUF2 are core components of the outer kinetochore plate<sup>254</sup>. These two proteins form essential parts of the Ndc80 complex and are pivotal for the organisation and binding of plus-end microtubules to kinetochores. The Ndc80 complex directly binds microtubules and without these proteins, microtubules do not successfully bind to kinetochores<sup>254</sup>.

Figure 3.14 shows three examples of an actively dicentric rob(15;21)c in a chromosome spread with outer kinetochore proteins also stained. Similar to that in Figure 3.12 and Figure 3.13, the chromosomes in Figure 3.14 have relatively short inter-centromeric distances but were not set up for STED imaging. Despite this, it can still be seen that, when rob(15;21)c is dicentric by CENP-C staining other outer kinetochore proteins also assemble to both centromeres. Figure 3.14A shows an example where the close dicentric CENP-C foci overlap and are not fully resolvable from one another, however, the staining of the more punctate, outer proteins Hec1 and NUF2 start to resolve these distinct centromeres. Figure 3.14B shows an example of a rob(15;21)c where the orientation of the chromosome is such that one arm has spread/opened up more than the other. This causes the appearance of one sister chromatid with two CENP-C foci and one with only one, albeit brighter (due to there being two overlapping foci), CENP-C focus. This phenotype translates onto the outer kinetochore protein Hec1 also with clear staining of two independent foci that colocalise with CENP-C on the sister chromatid that is more open. Figure 3.14C is of a rob(15;21)c chromosome in which both sister chromatids have two distinct CENP-C foci, each with a colocalising focus of NUF2.

Due to what is already known about the proteins required to build a microtubule-binding kinetochore, the presence of both Hec1 and NUF2 on both centromeres when rob(15;21)c appears actively dicentric is further evidence to suggest that both centromeres are functional.

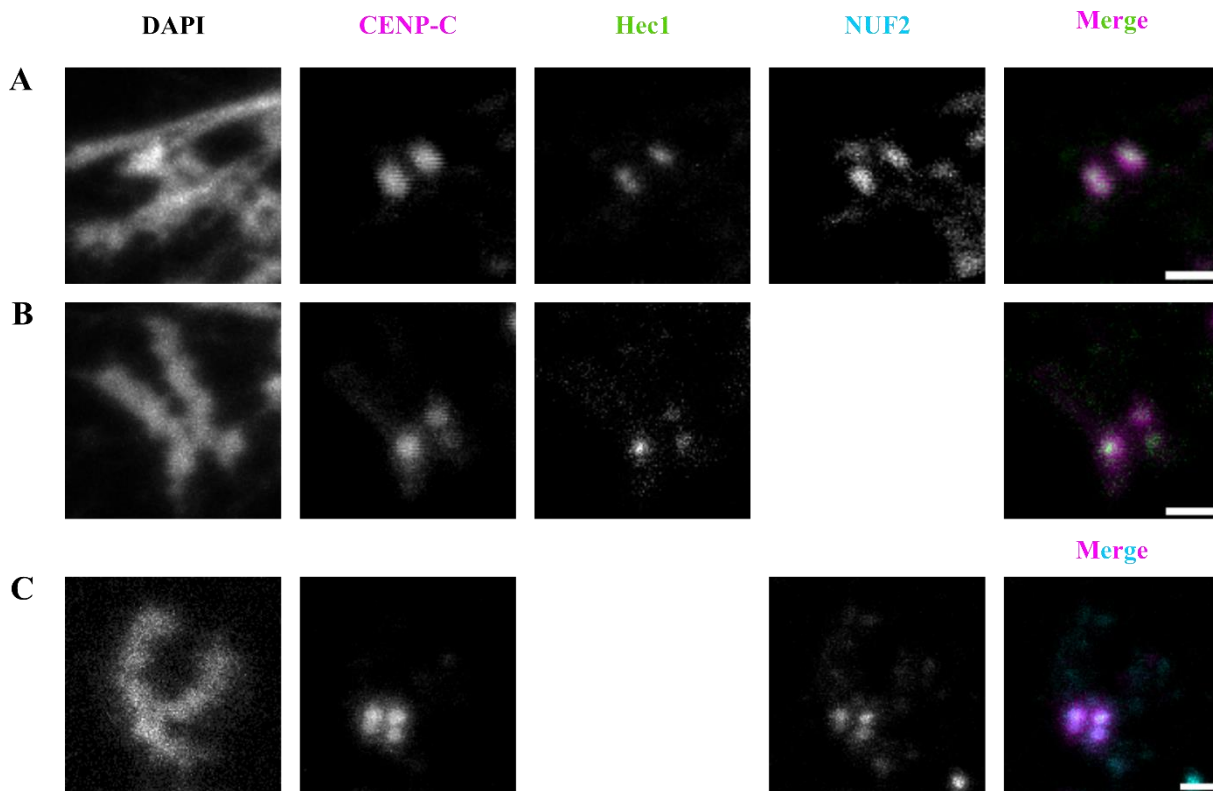


**Figure 3.14. rob(15;21)c assembles a full outer kinetochore at both centromeres.** (A) Dicentric rob(15;21)c with Hec1 and NUF2 assembling at both centromeres. (B) Dicentric rob(15;21)c with Hec1 assembling at both centromeres (NUF2 not stained). (C). Dicentric rob(15;21)c with Hec1 assembling at both centromeres (Hec1 not stained). Scale bars = 1  $\mu$ m.

### 3.2.7 The rob(15;21)c centromeric heterogeneity does not change across passages

We hypothesised that the actively monocentric and dicentric phenotypes shown in 3.2.6 were changing across passages. Dicentric chromosomes have mechanisms to reduce/remove their dicentricity in order to become more stable<sup>136,255</sup>. Preliminary results from CENP-C staining of rob(15;21)c chromosomes suggested that the actively dicentric phenotype may be seen mostly in early passages and the monocentric mostly in later passages. Our hypothesis was that dicentric rob(15;21)c chromosomes had a mechanism for deleting centromeric DNA or epigenetically silencing one of the centromeres to promote a chromosome that could be more stably inherited throughout mitosis. This mechanism would produce a monocentric rob(15;21)c chromosome that should be more faithful in segregation, and therefore those with an actively monocentric rob(15;21)c would outgrow those with an actively dicentric rob(15;21)c. The

model stated above would lead to a cell population with mostly dicentric rob(15;21)c chromosomes becoming a cell population with mostly monocentric rob(15;21)c chromosomes.

To test the hypothesis that the mono/dicentricity of rob(15;21)c is changing as cells divide, chromosome spreads + immunofluorescence + FISH experiments (as described in 2.13) were done on L995 and L996 cells from early (P6-8), middle (P17-19) and late (P32-34) passages. Chromosome spreads from these experiments were imaged by STED microscopy and images were deconvolved for the best possible resolution. The CENP-C staining of rob(15;21)c chromosomes was manually analysed to characterise each chromosome as having two or four CENP-C foci. Raw counts of rob(15;21)c chromosomes with each phenotype in three repeat experiments across passages is shown in Table 3.3.

**Table 3.3. Counts of rob(15;21)c with actively monocentric (2 CENP-C) or actively dicentric (4 CENP-C) phenotypes across passages.**

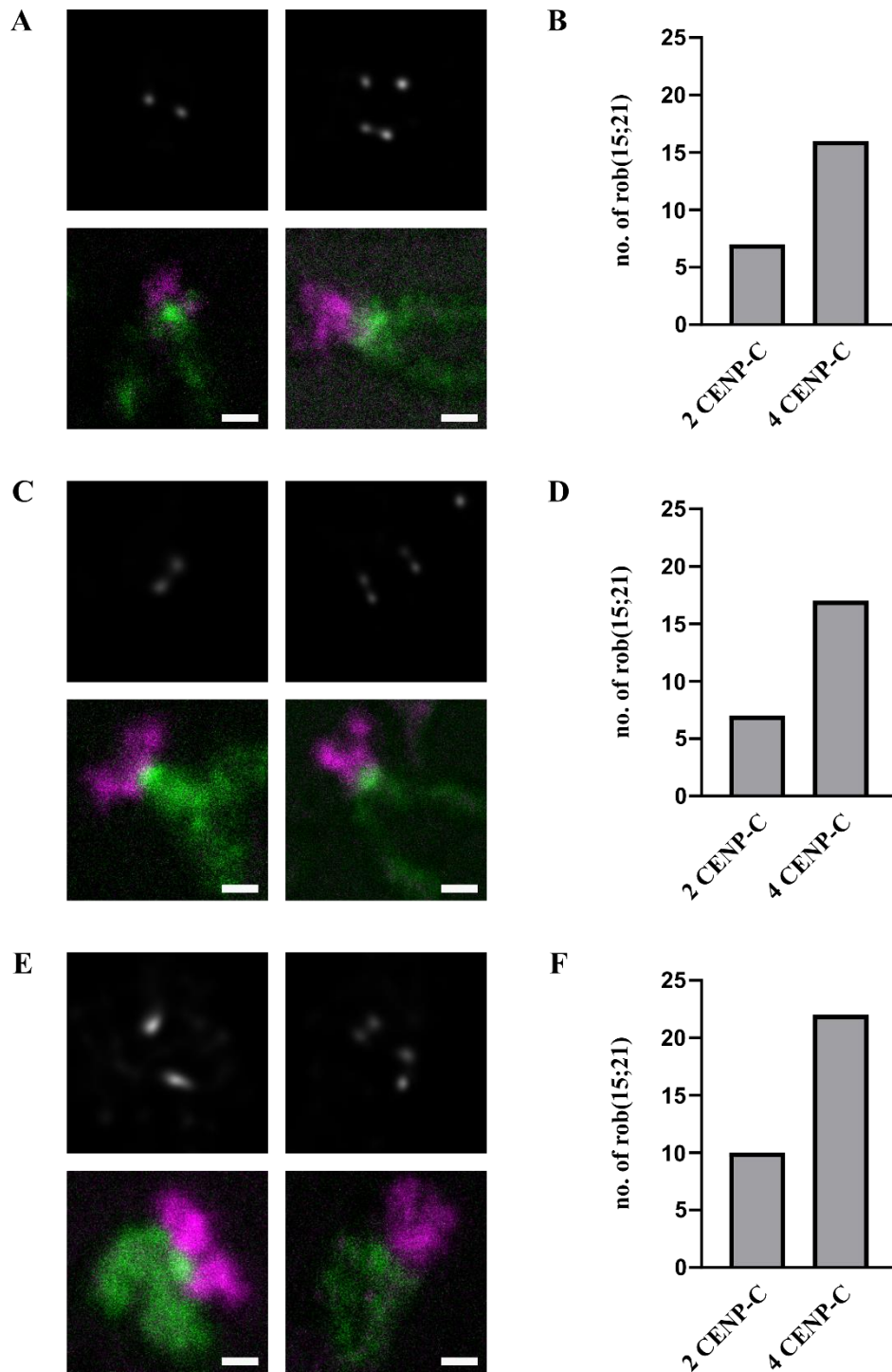
		Early			Mid			Late			Total	Ratio (%)
		Expt. 1	Expt. 2	Expt. 3	Expt. 1	Expt. 2	Expt. 3	Expt. 1	Expt. 2	Expt. 3		
L995	2 CENP-C	3	4	0	4	2	1	6	3	1	24	30.4
	4 CENP-C	8	6	2	10	6	1	7	6	9	55	69.6
L996	2 CENP-C	0	2	1	8	3	0	12	4	2	32	40.5
	4 CENP-C	0	11	3	8	9	2	1	4	9	47	59.5

Figure 3.15A shows rob(15;21)c chromosomes from early passage L995 cells with examples of both the actively monocentric and dicentric phenotype. Figure 3.15B is the quantification of the monocentric and dicentric phenotypes in early passage L995 cells. The numbers in Figure 3.15B are how many rob(15;21)c chromosomes with the respective phenotype were seen across three repeat experiments with early passage L995 cells. Examples of each phenotype in middle passage L995 cells are shown in Figure 3.15C with their quantification in Figure 3.15D and examples of each phenotype in late passage L995 cells are shown in Figure 3.15E with their quantification in Figure 3.15F. Whilst the total number of chromosomes counted in each passage group differs, it can be seen that the ratio of rob(15;21)c chromosomes with two CENP-C foci to those with four CENP-C foci remains similar across all passages. The major outcome from these experiments is that rob(15;21)c appears to most often have four CENP-C and that this is not changing across passages (from passage 6 to passage 34).

Figure 3.16 is the equivalent Figure 3.15 though for L996 cells. Figure 3.16A, Figure 3.16C, Figure 3.16E show that both the actively monocentric and dicentric phenotypes exist in early,

middle and late passage L996 cells. The quantification of these phenotypes in early (Figure 3.16B), middle (Figure 3.16D) and late (Figure 3.16F) L996 cells seems different to those in L995. Whilst the rob(15;21)c chromosomes from early L996 cells are predominantly actively dicentric (as in L995), the middle passages have more monocentric rob(15;21)c chromosomes in relation to the number of dicentrics; and in the late passages a monocentric rob(15;21)c appears to be the more common phenotype.

Whilst the quantification appears to tell a different story for rob(15;21)c chromosomes in L995 cells versus those in L996 cells, this may be misleading. A large number of the quantified chromosomes for late passage L996 cells (Figure 3.16F) comes from one experiment and contradicts that of the other repeats (as shown in Table 3.3), skewing the results. These results will be discussed further in 3.3.



**Figure 3.15. L995 rob(15;21)c centromeric heterogeneity does not change across passages.**

(A) Images of example rob(15;21)c chromosomes with 2 and 4 CENP-C foci from early passage L995 cells.

(B) Raw counts of rob(15;21)c chromosomes with 2 and 4 CENP-C foci from early passage L995 cells (N=3).

(C) Images of example rob(15;21)c chromosomes with 2 and 4 CENP-C foci from mid passage L995 cells.

(D) Raw counts of rob(15;21)c chromosomes with 2 and 4 CENP-C foci from mid passage L995 cells (N=3).

(E) Images of example rob(15;21)c chromosomes with 2 and 4 CENP-C foci from late passage L995 cells.

(F) Raw counts of rob(15;21)c chromosomes with 2 and 4 CENP-C foci from late passage L995 cells (N=3). Scale bars = 1  $\mu$ m.

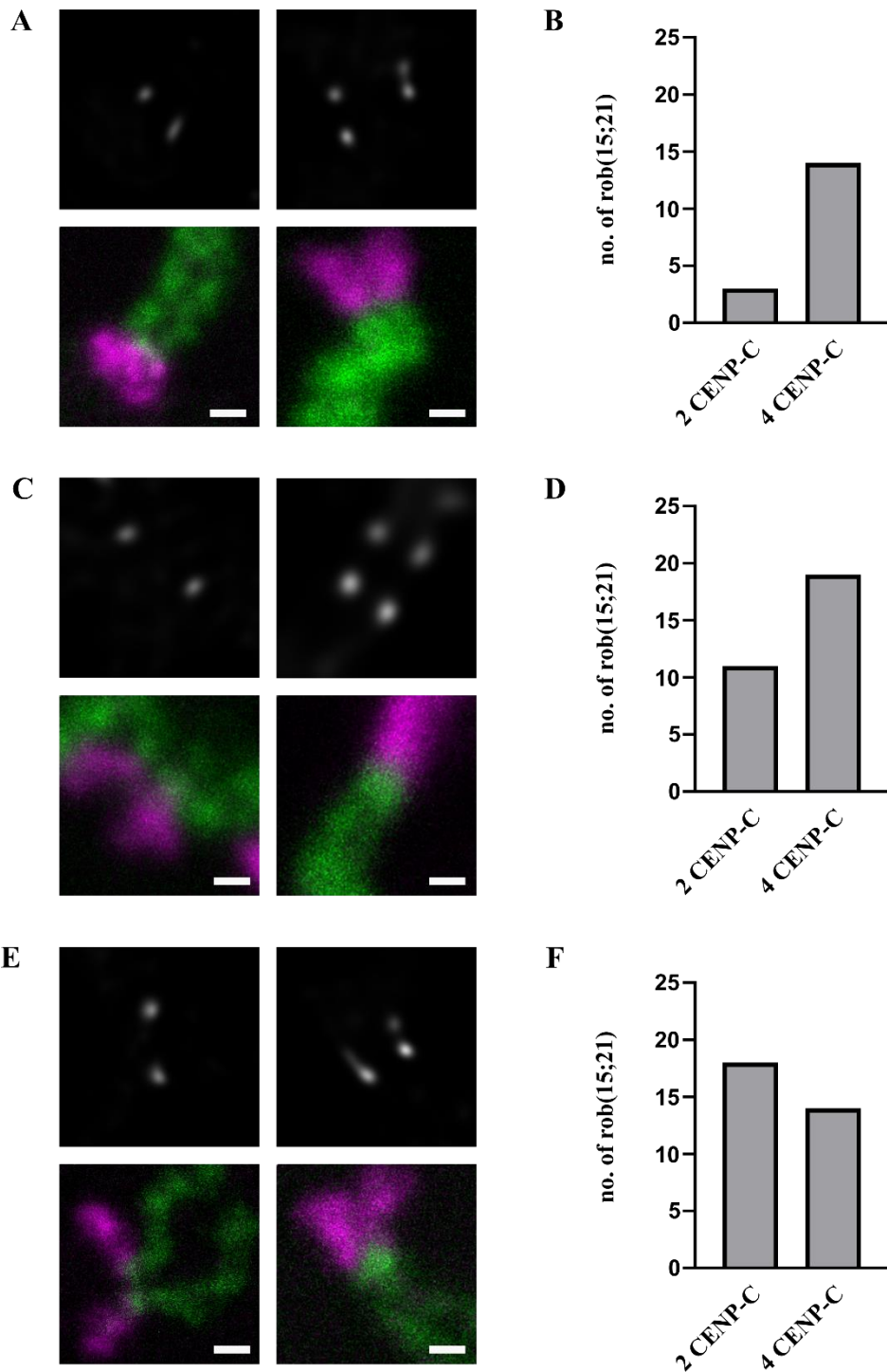


**Figure 3.16. L996 rob(15;21)c centromeric heterogeneity does not change across passages.** (A) Images of example rob(15;21)c chromosomes with 2 and 4 CENP-C foci from early passage L996 cells. (B) Raw counts of rob(15;21)c chromosomes with 2 and 4 CENP-C foci from early passage L996 cells (N=3). (C) Images of example rob(15;21)c chromosomes with 2 and 4 CENP-C foci from mid passage L996 cells. (D) Raw counts of rob(15;21)c chromosomes with 2 and 4 CENP-C foci from mid passage L996 cells (N=3). (E) Images of example rob(15;21)c chromosomes with 2 and 4 CENP-C foci from late passage L996 cells. (F) Raw counts of rob(15;21)c chromosomes with 2 and 4 CENP-C foci from late passage L996 cells (N=3). Scale bars = 1  $\mu$ m.

### 3.2.8 The rob(15;21)c chromosome has one dominant and one weaker centromere

During manual analysis of CENP-C foci on rob(15;21)c the observation was made that when rob(15;21)c had an actively dicentric phenotype it appeared that one pair of the centromeres were often brighter and larger than the other. Examples of this from four rob(15;21)c chromosomes in L995 cells are shown in Figure 3.17A and examples for four rob(15;21)c in L996 cells are shown in Figure 3.17B. After analysing these dicentric rob(15;21)c chromosomes it became clear that not only was there centromere dominance, but also that this dominance seemed to be centromere specific, with the brighter and larger CENP-C foci always belonging to the Chr15 centromere (rob 15) within the dicentric and the weaker always being Chr21 centromere (rob 21).

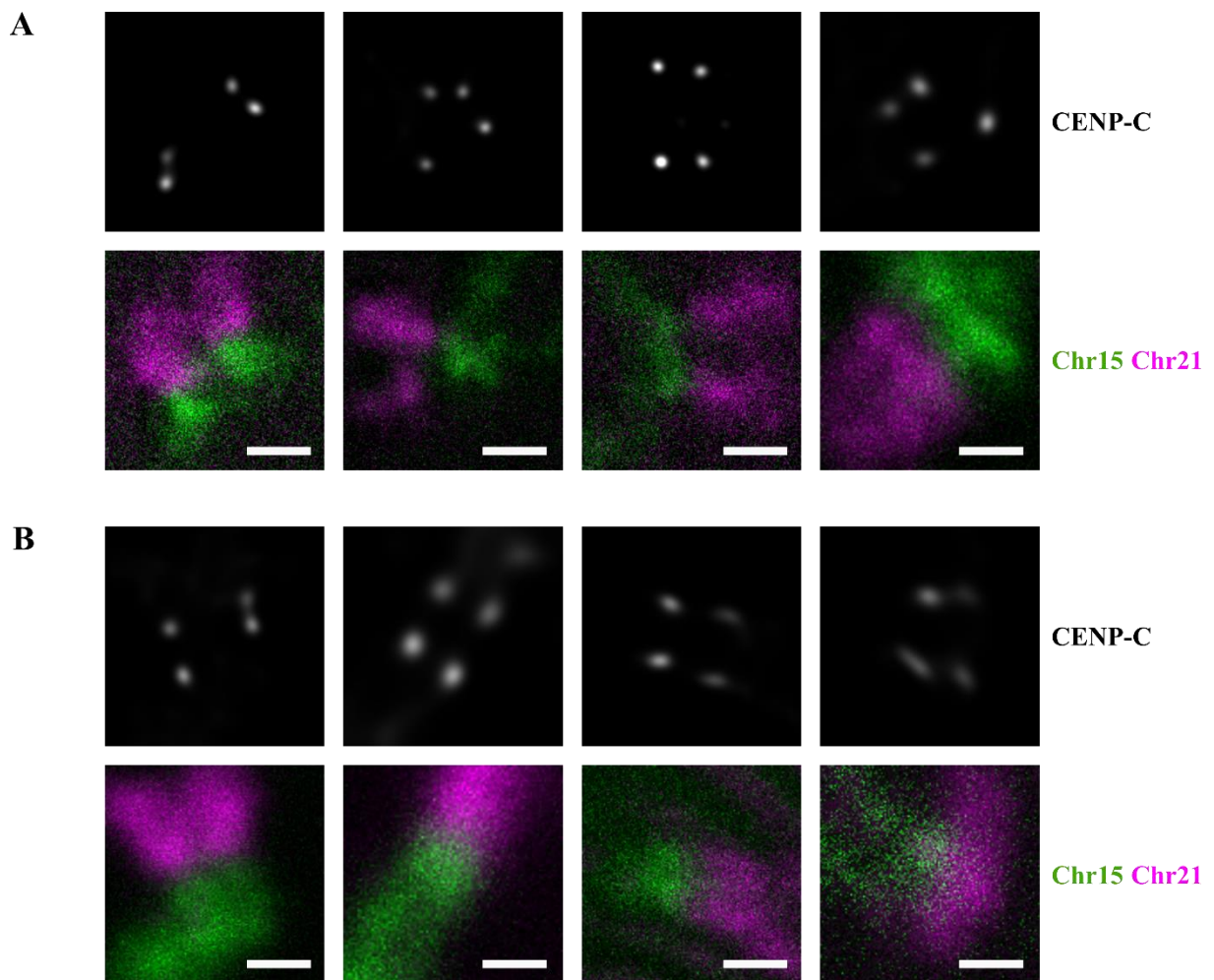


**Figure 3.17. Actively dicentric rob(15;21)c chromosomes have one stronger and one weaker centromere.** (A) STED images of four example rob(15;21)c chromosomes from L995 cells with dicentric centromeres with dominance. (B) STED images of four example rob(15;21)c chromosomes from L996 cells with dicentric centromeres with dominance. Scale bars = 1  $\mu$ m.

To quantify the centromere dominance phenotype, all images obtained for spreads across passages experiments in Figure 3.15 and Figure 3.16 were run through a Fiji analysis pipeline described in section 2.15.2. The output from this was data on the intensity and size of CENP-C foci on normal chromosome 15 (n = 101 in L995 and n = 81 in L996), normal chromosome 21 (n = 103 in L995 and n = 82 in L996), the chromosome 15 centromere of rob(15;21)c (n = 106 in L995 and n = 80 in L996), the chromosome 21 centromere of rob(15;21)c (n = 64 in L995 and n = 19 in L996) and all other chromosomes in a given chromosome spread (n = 4959 in L995 and n = 3858 in L996).

Figure 3.18 shows these quantifications of CENP-C data. Figure 3.18A and Figure 3.18B are respectively the intensities and areas of CENP-C foci in L995 cells normalised to that of all chromosomes. These data show that CENP-C foci on normal chromosome 15 are both larger and more intense than the average CENP-C focus. Also, whilst the size of CENP-C on rob 15 is not significantly different to that on normal 15, the intensity is, with the intensity on rob 15 being slightly less than that on normal chromosome 15. However, the most striking result in these data is that the CENP-C foci on rob 21 are far less intense and far smaller than that on normal chromosome 21. This result provides quantification to support the images in Figure 3.17 that suggests dicentric rob(15;21)c exhibits centromere dominance; with rob 15 always being dominant over rob 21 when dominance at rob(15;21)c occurs.

Figure 3.18C and Figure 3.18D provide similar results to that shown in Figure 3.18A and Figure 3.18B, though in L996 cells. CENP-C on normal chromosome 15 and normal chromosome 21 are larger (Figure 3.18D) and more intense (Figure 3.18C) than the average CENP-C focus. The CENP-C on rob 15 is not significantly different, if at all, to that on normal chromosome 15. Again, the striking result is that rob 21 is clearly weaker in both size and intensity than normal chromosome 21.

Our data suggest that dicentric rob(15;21)c chromosomes have a regular centromere 15 and a somehow altered, weaker centromere 21.

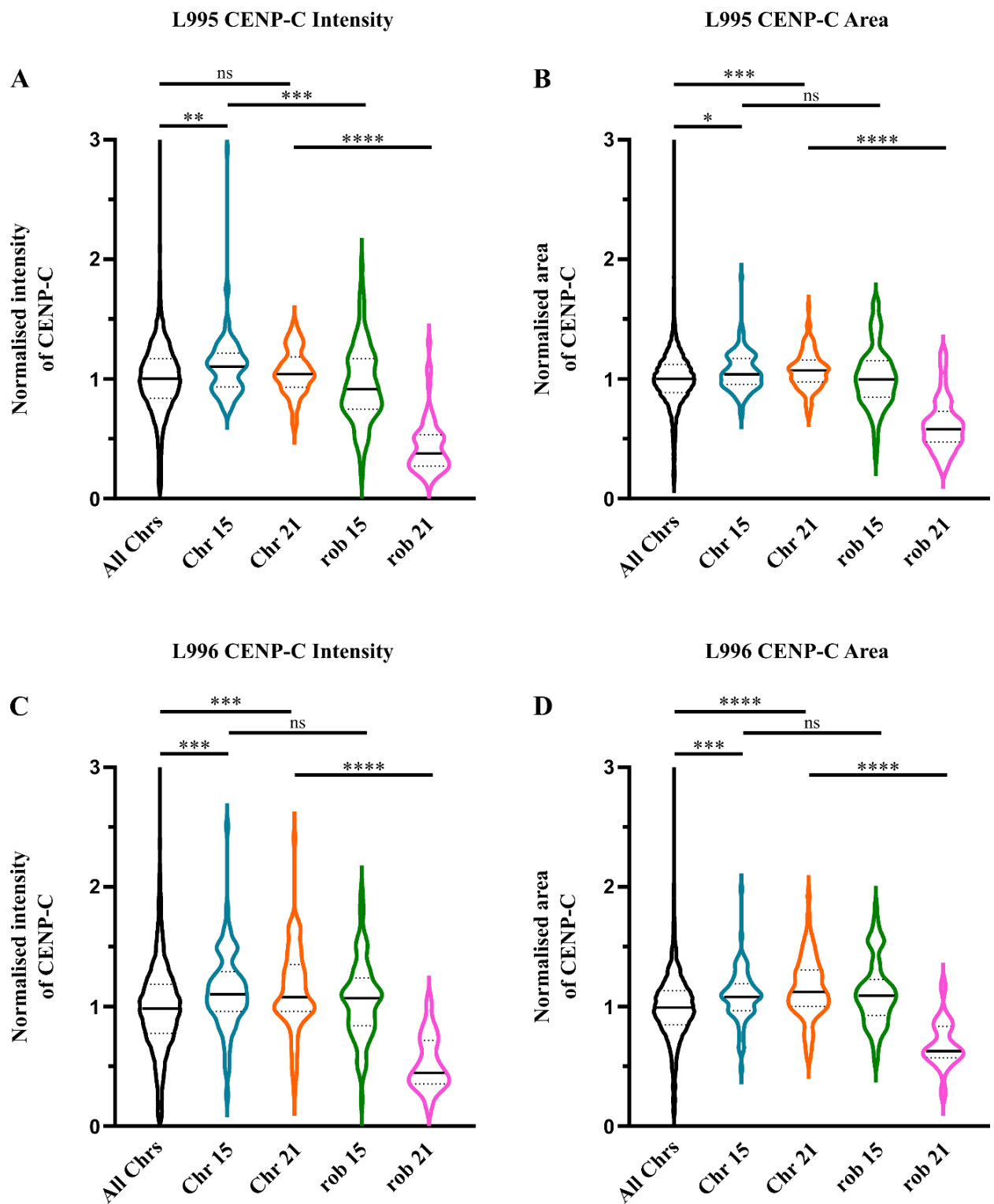


**Figure 3.18. CEN 21 of rob(15;21)c is significantly weaker than other centromeres.** (A) Intensity of CENP-C foci on L995 chromosome spreads with intensities normalised to the mean intensity of CENP-C foci across all chromosomes in a given cell. (B) Area of CENP-C foci on L995 chromosome spreads with areas normalised to the mean area of CENP-C foci across all chromosomes in a given cell. (C) Intensity of CENP-C foci on L996 chromosome spreads with intensities normalised to the mean intensity of CENP-C foci across all chromosomes in a given cell. (D) Area of CENP-C foci on L996 chromosome spreads with areas normalised to the mean area of CENP-C foci across all chromosomes in a given cell. Statistical analysis done by Kruskal-Wallis test. ns = not significant. \* = p-value  $\leq 0.05$ , \*\* = p-value  $\leq 0.01$ , \*\*\* = p-value  $\leq 0.001$ , \*\*\*\* = p-value  $\leq 0.0001$ .

The Robertsonian chromosome rob(15;21)c has a stronger centromere (stronger than the other centromere in rob(15;21)c but similar to normal centromere 15), centromere 15 and a weaker centromere, centromere 21 as shown in Figure 3.17 and Figure 3.18. However, this chromosome was also found to have a monocentric phenotype and so it was logical to image and analyse location of the CENP-C from these monocentric versions of rob(15;21)c. Images in Figure 3.19A show three example monocentric rob(15;21)c chromosomes from L995 cells and Figure 3.19B shows three examples from L996 cells. It is obvious from these images that the CENP-C dots are colocalising with the green arms labelled by the FISH probes for chromosome 15 and not with those for chromosome 21.

The data in Figure 3.19 highlights that in both L995 and L996 when rob(15;21)c is monocentric it appears to retain the centromere of rob 15 and lose the centromere of rob 21. Therefore, from these data in actively monocentric rob(15;21)c, that in Figure 3.17 of actively dicentric rob(15;21)c and quantification in Figure 3.18 it seems that the centromere belonging to the chromosome 15 arm of rob(15;21)c is more dominant than the centromere belonging to the chromosome 21 arm of rob(15;21)c.

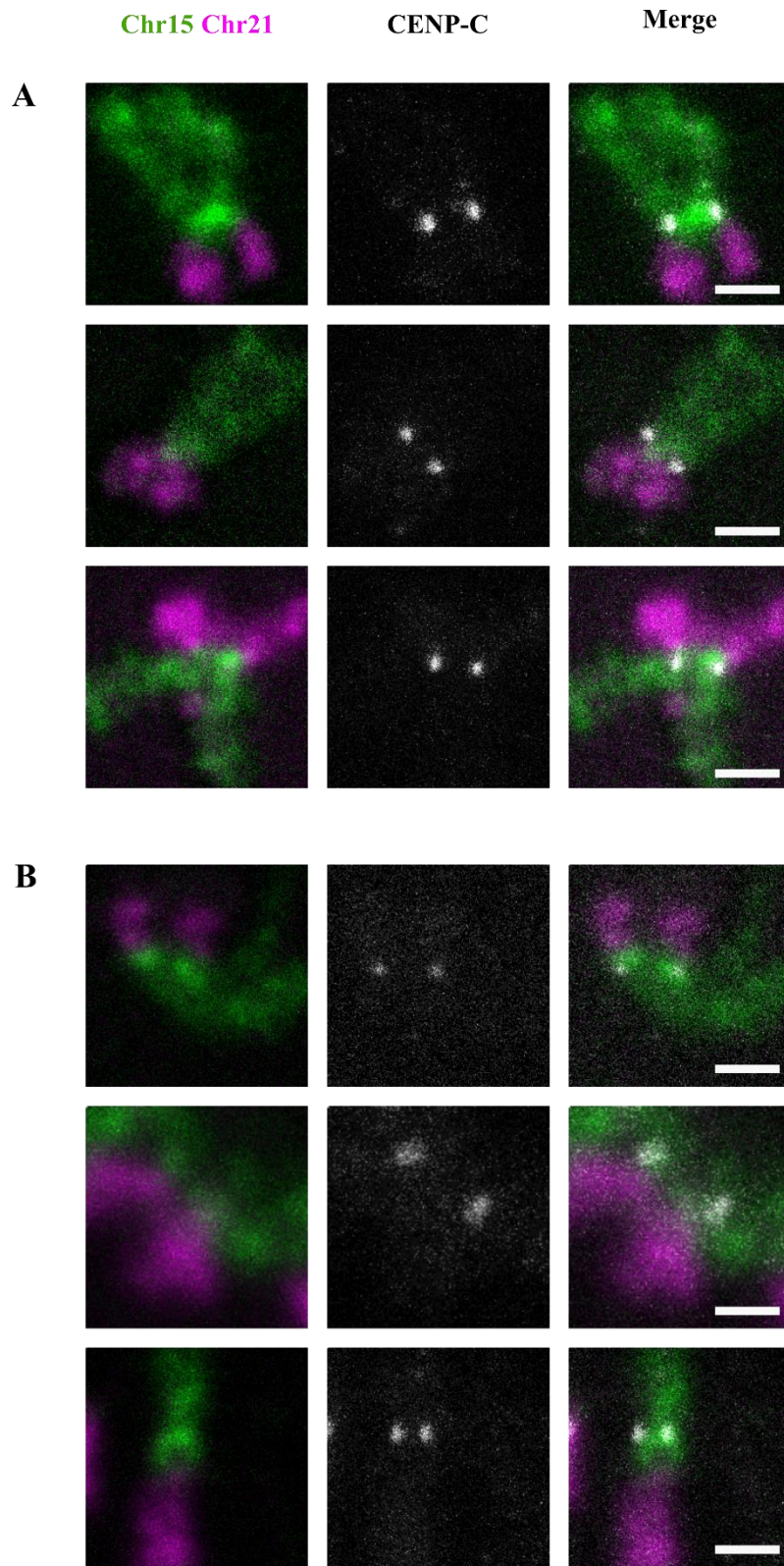


**Figure 3.19. Monocentric rob(15;21)c chromosomes specifically retain CEN15.** (A) STED images of three example L995 rob(15;21)c chromosomes with monocentricity retaining only the CEN15 centromere. (B) STED images of three example L996 rob(15;21)c chromosomes with monocentricity retaining only the CEN15 centromere. Scale bars = 1  $\mu$ m.

### **3.2.9 Both rob(15;21)c kinetochores have the ability to bind microtubules**

As rob(15;21)c is often actively dicentric, an obvious mitotic outcome for these chromosomes would be mis-segregation due to aberrant MT attachments; in turn causing a lagging chromosome. A lagging rob(15;21)c could be a driver for chromothripsis involving this chromosome. Therefore, we wanted to determine whether both centromeres/kinetochores on a dicentric rob(15;21)c chromosome have the ability to bind microtubules and if this causes aberrant attachments during mitosis.

Many techniques were attempted in order to image microtubule-kinetochore binding at rob(15;21)c centromeres, though this proved to be difficult. Upon immunofluorescence microscopy of whole cells (not in a chromosome spread) the dicentric centromeres (stained by CENP-C staining) appear very close together and are often difficult to distinguish. Further, it is more difficult to use both FISH probes and immunostaining in whole cells than it is in chromosome spreads as it appears both IF and FISH staining are poorer when combined in whole cells, likely hindered by the protocol adaptations made to allow both staining methods simultaneously on one sample. Therefore it was not possible in our hands to have a chromosome marker for rob(15;21)c and simultaneously stain kinetochores and microtubules by IF and so any images of microtubule binding at what looks like a dicentric chromosome are with the presumption that the chromosome being imaged is rob(15;21)c and not the colocalisation of two monocentric chromosomes.

In an attempt to resolve the dicentric centromeres and the microtubules binding to them both, STED microscopy and Ultrastructure-Expansion Microscopy (ExM) were done. Figure 3.20A shows one Z-slice through a mitotic cell focusing on the microtubule binding at a dicentric chromosome. Whilst all microtubule attachments are not fully formed it does appear that both kinetochores on one sister chromatid of this dicentric chromosome are binding microtubules. The pattern of tubulin staining comes from one pole and shows one tubulin bundle splitting and colocalising with two CENP-C foci, presumably the two kinetochores from one sister of rob(15;21)c. This can be seen more clearly in Figure 3.20B; images as in Figure 3.20A though with zoomed in regions on the dicentric kinetochores.

Imaging microtubule binding events on rob(15;21)c proved difficult in whole cells due to short inter-centromeric distance, therefore making it difficult to resolve the kinetochores of rob(15;21)c from each other. In order to overcome the resolution limit, I optimised an Ultrastructure-Expansion Microscopy (U-ExM) protocol for my cells of interest. By embedding

mitotic cells in a swellable hydrogel, samples can be expanded isotropically  $\sim 4.5\times$  in X, Y and Z; creating a volume increase of  $\sim 90\times$ . This sample preparation technique allowed for imaging at much higher resolution whilst still using standard confocal microscopy.

Figure 3.20C is a single Z-slice through a metaphase cell that has been expanded using an Ultrastructure-Expansion Microscopy protocol as in section 2.11. The zoomed in region of interest (ROI) highlights a dicentric chromosome which is presumably *rob(15;21)c*. Microtubules emanating from one pole appear to be binding to both kinetochores on one sister chromatid. Whilst this does not show what microtubule binding is like at all kinetochores on the dicentric and does not show what these microtubule-kinetochore attachments look like when *rob(15;21)c* is mis-segregating, it does further reinforce the STED data to suggest that both kinetochores on *rob(15;21)c* have the ability to bind microtubules.

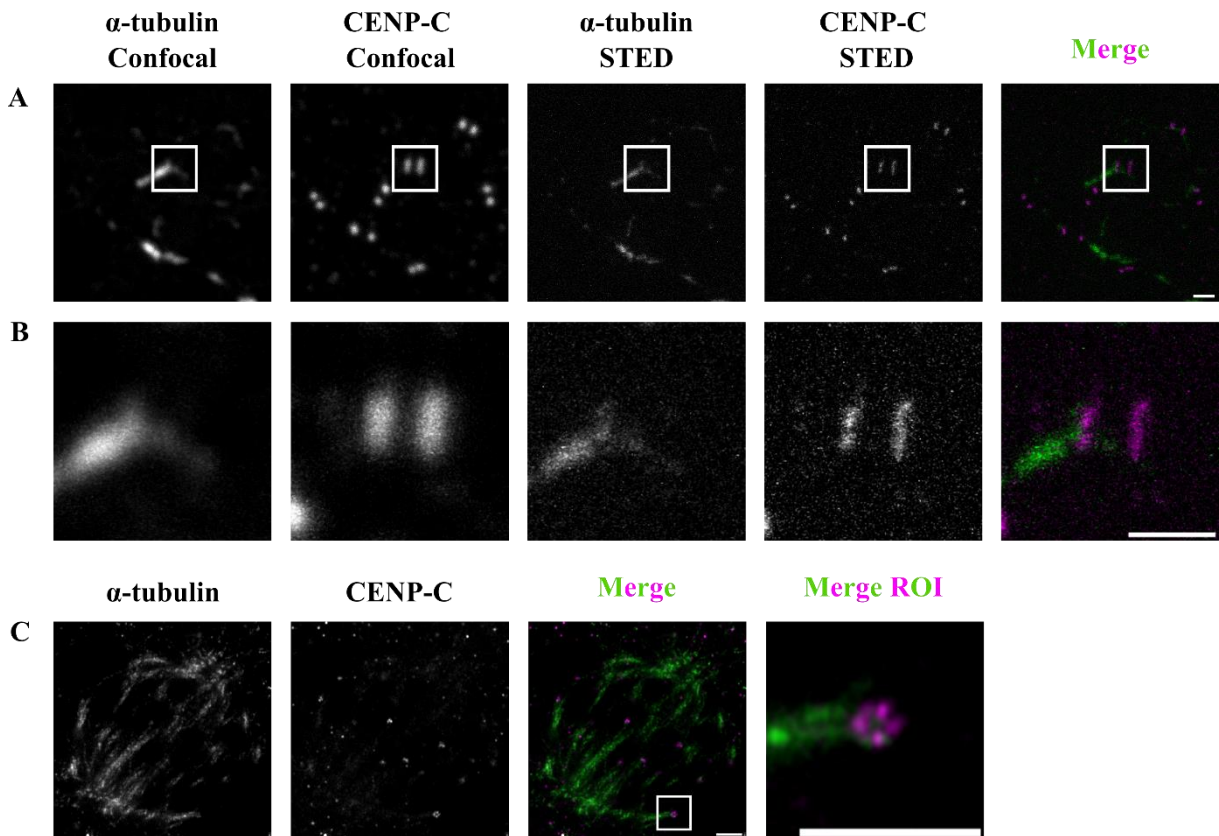


**Figure 3.20. Both kinetochores of *rob(15;21)c* have the ability to bind microtubules.** (A) dicentric chromosome (presumably *rob(15;21)c*) as shown by CENP-C staining with one sister chromatid binding microtubules at both kinetochores. (B) zoomed in regions of interest (ROIs) from A. (C) Expansion microscopy image showing a dicentric chromosome with all kinetochores binding microtubules. Scale bars in A and B =  $1\mu\text{m}$ , Scale bars in C =  $4\mu\text{m}$

### 3.3 Discussion

In this chapter I have described the production and characterisation of lymphoblastoid cell lines L995 and L996 as a model system to study the Robertsonian chromosome rob(15;21)c. Carriers of the chromosome rob(15;21)c have a huge increased risk of developing iAMP21-ALL by a process which involves the rob(15;21)c chromosome undergoing a chromothriptic event. The work in this chapter starts to characterise rob(15;21)c, in particular the dicentric centromere, in order to try and understand why this chromosome has a high predisposition to chromothripsis.

Analysis of SNP arrays in 3.2.2 and 3.2.3 confirmed that there are no gross chromosomal differences between the cells of the patient who developed iAMP21-ALL (23299) and their identical twin who did not develop iAMP21-ALL (27405). Data in this section also checked for any obvious differences between the L995 and L996 cell lines and the blood samples from which they were derived. Figure 3.2 and Figure 3.3 highlighted that there were no gross differences and in fact the cell lines look extremely quiet, even more so than the blood samples. However, this could be for several reasons. SNP arrays on the blood samples were done on an Affymetrix SNP 6.0 array, whereas due to the discontinuation of SNP 6.0, the data for cell lines L995 and L996 was from Illumina 850k arrays. This technical difference could cause the quietness seen in L995 and L996 samples. It is possible that SNP 6.0 had better resolution and therefore detected more CNVs than in the Illumina data. Alternatively, it is possible that the quality of DNA in the blood samples were poorer than that from the cell lines, thus causing the busier CNV profiles seen in blood samples when compared with L995 and L996. Ultimately though, there are no gross chromosomal changes seen between L995 and L996 and the cells from which they were derived, making these cells a good model to study the rob(15;21)c chromosome in an environment that is near-physiological but also tractable for experimental use.

Preliminary FISH experiments of asynchronous L995 and L996 cells validated the presence of rob(15;21)c in these cell lines (Figure 3.5 and Figure 3.6). However, these initial results also brought to light a potential problem (Figure 3.7). Across a cell population there appeared to be significant number of cells with four foci for the centromere of chromosome 15 and eight foci for the centromere of chromosomes 21/13 (the alpha satellites of Chr21 and Chr13 are not different enough to design unique FISH probes that distinguish them). Lymphoblastoid cell lines are known to have some genomic instability, and these preliminary FISH images highlighted the possibility that there was a tetraploid population amongst these cells<sup>237-239</sup>. This

would have been problematic for subsequent experiments. Fortunately, flow cytometry experiments done to quantify this problem indicated that in fact there was no significant aneuploid population across multiple passages of L995 or L996 cells (Figure 3.8 and Figure 3.9). Any cells that had ploidy greater than the normal diploid population would appear as events greater than  $4n$  (S phase, G2 and M phase cells tetraploid cells). Whilst the presence of the two peaks labelled  $2n$  and  $4n$  do not provide the exact number of chromosomes in each cell, the presence of them in combination with the absence of a peak  $>4n$  and the absence of a peak  $<2n$  does suggest a near pure population; not one that is heterogeneous with diploid and tetraploid cells. As a pure tetraploid and pure diploid population would look the same by simple flow cytometry, FISH experiments were used to confirm that L995 and L996 cells were mostly diploid and not mostly tetraploid. Throughout early, middle and late passages of L995 and L996 the population of cells that were greater than  $4n$  was between 1.4% and 2.4%. These small percentage of events greater than  $4n$  are likely to also include doublets that have slipped through the gating workflow and large cellular debris. Therefore, we can be confident that there is no significant tetraploid population in L995 or L996 cells ( $<2\%$ ).

The results obtained above show that L995 and L996 are good model systems in which to study rob(15;21)c. The remaining experiments in this chapter from 3.2.6 onwards make use of L995 and L996 to study this chromosome of interest, and focus on characterising the centromeres of rob(15;21)c. Having a single centromere on each sister chromatid allows biorientation during mitosis. However, having two functional centromeres on each sister chromatid may cause erroneous attachments. FISH experiments to label the alpha-satellite DNA of chromosome 15 and chromosome 21 showed that rob(15;21)c in the L995 and L996 cell lines had the DNA of two centromeres. Having centromeric DNA though is not enough to consider a centromere as active. Further experiments to stain inner kinetochore proteins (Figure 3.11), outer kinetochore proteins (Figure 3.14) and microtubule-kinetochore binding (Figure 3.20) all provide support for the case of rob(15;21)c often having two fully functioning kinetochores.

Early work on dicentric chromosomes found that one centromere was often inactivated to form a functionally monocentric chromosome that was more stable through mitosis and meiosis. This work was done by analysis of primary constrictions, C- and Cd-banding and immunostaining to show a lack of CENP-A, CENP-C and CENP-E at the inactive centromere<sup>125,126,249,256-258</sup>. Particularly of interest, this was also shown for patient-derived Robertsonian chromosomes<sup>136,255</sup>. Work from Sullivan *et al.* demonstrated that centromere inactivation occurred preferentially at a particular centromere in most cases<sup>255</sup>. As rob(15;21)c is somewhat

rare compared to other Robertsonian chromosomes, this study only had samples from two rob(15;21)c patients. Cells from one rob(15;21)c carrier had preference for an active chromosome 21 centromere and the other was split somewhat evenly, with some cells containing a rob(15;21)c with an active 15 centromere and some with an active 21 centromere. However, this study looked at many other patient derived Robertsonian chromosomes and concluded that the centromere of chromosome 15 within a Robertsonian is rarely the preferentially active centromere. Contrary to this finding, we see that in L995 and L996 cells the chromosome 15 centromere is more dominant in a dicentric rob(15;21)c (Figure 3.17 and Figure 3.18) and is often the only centromere with markers of an active kinetochore (i.e. in rob(15;21)c that may be monocentric, Figure 3.19). This finding is of particular interest as FISH staining of leukaemic cells from iAMP21-ALL patients with rob(15;21)c has shown that the derivative chromosome that is rearranged after a chromothriptic event is monocentric, specifically retaining the 21 centromere and not the 15 centromere<sup>145</sup>. Therefore, in combination with our results, this suggest that the 15 centromere in rob(15;21)c is dominant pre-chromothripsis but selected against post-chromothripsis. Interestingly, this also indicates that those chromosomes that undergo chromothripsis to drive iAMP21-ALL must be dicentric rob(15;21)c and not a monocentric.

The mechanism for the inactivation and/or reduction in strength of centromere 21 in rob(15;21)c is not well understood. In *de novo* induced Robertsonian dicentrics it has been shown that inactive centromeres have smaller alpha satellite arrays, suggesting partial DNA deletion as a mechanism for centromeric inactivation<sup>138</sup>. As the  $\alpha$ -satellite of chromosome 21 within rob(15;21)c often appears smaller than that on normal chromosome 21 in L995 and L996 cells, it is possible that partial DNA deletion has happened at this dicentric to produce a more stable chromosome. However, when centromere state changes in a growing population, Higgins *et al.* showed that there were no obvious changes to DNA, hence suggesting a possible epigenetic mechanism for centromere inactivation<sup>129</sup>.

Whilst it is common for dicentric chromosomes to act as if actively monocentric in order to promote chromosomal stability, we have seen that across passages, rob(15;21)c in L995 and L996 more often remains actively dicentric (Figure 3.15 and Figure 3.16). There was no shift in centromeric phenotype across the passages of L995 and L996 cells in this study and actively dicentric remained the more prominent phenotype. These results suggest that there is no strong selection pressure on rob(15;21)c to be monocentric and that the dicentric phenotype must be at least somewhat stable. A similar finding was seen in dicentric X chromosomes and

Robertsonian chromosomes with a short inter-centromeric distance<sup>127,137</sup>. As the distance between dicentric centromeres increases the likelihood of that chromosome acting as actively monocentric also increases<sup>127</sup>. Dicentric chromosomes with a larger inter-centromeric distance may allow for problematic microtubule attachments that would cause lagging. However, when inter-centromeric distance is short, the two centromeres may act cooperatively and more similarly to a regular monocentric chromosome, despite possessing two formed kinetochores. It has been hypothesised that closely located centromeres on a dicentric would limit twisting in the region between the centromeres, therefore promoting both kinetochores to face the same direction and thus bind microtubules from the same pole<sup>137,259</sup>. A potential example of this can be seen in Figure 3.20B and Figure 3.20C. As the inter-centromeric distance in rob(15;21)c in L995 and L996 cells is short and our results show an actively dicentric phenotype frequently, our work supports the hypothesis that a small inter-centromeric distance will more likely lead to two functional kinetochores on each sister. However, how these two kinetochores may be functioning together is less well understood.

Though it has not been possible to show that aberrant attachments on rob(15;21)c drive mis-segregation, I have shown images in Figure 3.20 that suggest both kinetochores on rob(15;21)c can bind microtubules. It is a real possibility that simultaneous attachments at all rob(15;21)c kinetochores would cause a mis-segregating chromosome during mitosis.

Identification of rob(15;21)c whilst imaging microtubule-kinetochore attachments was a large problem and so we hoped to use a fluorescent dCas9 labelling system to create cell lines with a fluorescent rob(15;21)c (as described later in Chapter 5). These cell lines would then be used for Correlative Light and Electron Microscopy (CLEM). In these experiments we would be able to identify rob(15;21)c by the fluorescent dCas9 system and then image the same cell with the resolution of electron microscopy. Electron microscopy would show the number of microtubules bound to each kinetochore and whether there were any aberrant attachments when rob(15;21)c was mis-segregating (as identified in the same cell by light microscopy). However as discussed later, the development of these cell lines was more difficult than anticipated.

Higgins *et al.* in 2005 provided evidence to suggest that whilst centromere activity in a dicentric is usually clonal, some cell lines can switch the centromere state in a growing population (from actively dicentric to actively monocentric). Our experiments in Figure 3.15 and Figure 3.16 to determine if the centromere state of rob(15;21)c was changing across passages highlighted that this state was stable in L995 cells (the majority of cells had actively dicentric rob(15;21)c with

a small proportion having actively monocentric rob(15;21)c). However, in L996 cells the results were less clear (Figure 3.16). At first glance it appeared that centromere state may be changing from mostly dicentric to mostly monocentric. However, the results in Figure 3.16F came from three technical replicates that are difficult to interpret. The three repeats do not provide consistent results (as shown in Table 3.3). One experiment shows the majority of rob(15;21)c chromosomes with an actively monocentric phenotype (experiment 1), one with a predominantly active dicentric phenotype (experiment 3) and one with equal amounts of monocentric and dicentric (experiment 2). Ultimately, there are limited n numbers within each individual repeat of this experiment and therefore more should be done to produce data with greater statistical significance. Nevertheless, many further experiments were done on the centromeres of rob(15;21)c in various passages of L995 and L996 cells throughout the work described in this thesis, and there were no noticeable changes to centromere state that appeared obvious; both the actively dicentric and actively monocentric phenotype were seen at all passages.

In summary, the work in this chapter characterised the rob(15;21)c centromeres; showing that this chromosome is often actively dicentric, with the ability to assemble outer kinetochore proteins that suggest functional dicentricity; and this predominantly dicentric phenotype likely does not change across passages. Also, the dicentric centromeres of rob(15;21)c do not seem to be equal. The rob 15 centromere appears stronger as defined by the amount of kinetochore proteins which assemble to it and the rob 21 centromere is more likely to be inactivated.

Previous work from Li *et al.* highlighted a massive 2700x increased risk for carriers of rob(15;21)c to develop iAMP21-ALL by undergoing chromothripsis. An obvious mechanism would be that the actively dicentric centromere of rob(15;21)c is causing unfaithful segregation and in turn subjecting this chromosome to an environment that has shown to be susceptible to events such as chromothripsis (e.g. a micronucleus). In Chapter 4, the segregation tendencies of rob(15;21)c will be assessed to further understand the mechanism causing such predisposition to cancer.

## Chapter 4: Characterising how rob(15;21)c behaves

---

### 4.1 Introduction

In Chapter 3, I showed that the Robertsonian chromosome rob(15;21)c appears to be frequently, actively dicentric. The pivotal paper from Li *et al.* in 2014 highlighted how carriers of the rob(15;21)c chromosome have a dramatically increased risk of developing iAMP21-ALL through a mechanism that involves rob(15;21)c undergoing chromothripsis<sup>145</sup>. This chapter aims to find the links between this chromosome's centromeric structural irregularity and its predisposition to chromothripsis.

Active dicentricity of rob(15;21)c may lead to aberrant microtubule-kinetochore attachments. If not properly resolved, then these mis-attachments may cause segregation defects in mitosis. Chromosome mis-segregation has been shown to be the initiating event that drives chromothripsis<sup>156</sup>. Micronuclear environments have the ability to facilitate the mis-segregation-to-chromothripsis mechanism due to their aberrant nuclear envelopes, leading to rupture and cytosolic DNA damage<sup>94,154,156,181,260,261</sup>.

Many different mechanisms can cause a chromosome to mis-segregate<sup>262</sup>. Aberrant microtubule-kinetochore attachments (e.g. merotelic attachments) can cause a chromosome to lag during anaphase and enter a micronucleus. Defects in the Spindle Assembly Checkpoint (SAC) may allow premature anaphase onset before appropriate attachments are formed, in turn causing mis-segregation. Defects in cohesion can cause premature or delayed sister chromatid separation, depending on the specific defect. Problematic cell cycle regulation can also disrupt multiple aspects of mitosis and promote chromosomal instability. Inherent characteristics within chromosomes can cause non-random mis-segregation. Both the size of a chromosome and the size of its centromere (and the relationship between them) have the ability to influence specific mis-segregations<sup>97</sup>. More recently, it has also been shown that chromosomes which have an interphase nuclear location close to the cell periphery are more likely to mis-segregate due to their position relative to the spindle poles in mitosis<sup>98,99</sup>. These mechanisms that cause chromosome mis-segregation are not necessarily mutually exclusive, it is possible that multiple problems act together to cause nondisjunction.

In this chapter, I aim to determine if the dicentric nature of rob(15;21)c is driving mis-segregation, and if so, what mechanism is driving it. To assess this, I have used a mixture of low throughput (for high resolution imaging) and high throughput (for quantification of large

numbers of cells) fixed imaging and imaging analysis methods. As in Chapter 3, I made use of the lymphoblastoid cell lines L995 and L996 derived from twin carriers of rob(15;21)c to study this chromosome of interest. I stained the Robertsonian chromosome and internal control chromosomes with FISH probes for Chr15q and Chr21q and, in some cases where smaller fluorescent foci were required, probes for CEN15 and CEN21/13. I also stained multiple proteins of interest by immunofluorescence at various stages of the cell cycle to better understand how the behaviour of rob(15;21)c may be leading to chromothripsis.

As data from Li *et al.* suggested that a chromothriptic event involved just rob(15;21)c (and often two copies of this chromosome), we focussed on studying mis-segregation mechanisms that could occur on only one chromosome (e.g. erroneous microtubule-kinetochore attachments but not defective cell cycle regulation).

In summary, this chapter characterises the behaviour of rob(15;21)c. Firstly, I study the propensity for rob(15;21)c to mis-segregate, whether one or both sister chromatids are seen in mis-segregations and the micronuclear environment of cells containing rob(15;21)c. The rest of this chapter then studies potential mechanisms that may drive aberrant segregation of rob(15;21)c, including error correction, cohesion, nuclear location and metaphase plate alignment.

## 4.2 Results

### 4.2.1 rob(15;21)c frequently mis-segregates during mitosis

The Robertsonian chromosome rob(15;21)c is often dicentric. We have shown that in the patient derived cell lines L995 and L996 containing rob(15;21)c, this chromosome often appears actively dicentric with the potential to be functionally dicentric. In chapter 3 it was shown that both centromeres of dicentric rob(15;21)c chromosomes have the ability to assemble outer kinetochore proteins and bind microtubules. The presence of multiple active kinetochores on each sister chromatid may promote aberrant microtubule attachments such as merotelic attachments; if not appropriately resolved before anaphase these could cause mis-segregation of the attached chromosome.

Previous work from Li *et al.* highlighted that rob(15;21)c frequently undergoes chromothripsis to drive iAMP21-ALL. Either this chromosome has a huge predisposition to chromothripsis or presence of this chromosome in a chromothriptic event causes a selective advantage for cancer

cell growth. We also know from multiple studies that both micronuclei and chromosome bridges are environments that facilitate a chromothriptic event<sup>114,154,156</sup>. We hypothesised that the dicentric nature of rob(15;21)c causes a high rate of chromosome mis-segregation in this chromosome, therefore placing this chromosome in an environment that has been shown to be susceptible to chromothripsis.

To study the nature of rob(15;21)c chromosome segregation, we enriched populations of L995 and L996 cells into anaphase and telophase with the use of a nocodazole block for prometaphase enrichment followed by nocodazole washout and then allowing cells to progress for 1h before fixation. FISH probes were used to stain chromosome 15q and chromosome 21q in these ana/telophase enriched cells so that chromosome 15, chromosome 21 and rob(15;21)c could be identified. These were particularly of interest if they were present in a mis-segregation event.

As asynchronous cell populations did not contain many mitotic cells (due to a low mitotic index and the tendency for mitotic cells to struggle to stick down), nocodazole was used to both synchronise cells in mitosis and induce a higher rate of chromosome mis-segregation. It has been shown that nocodazole will elevate mis-segregation rates in a non-random manner, specifically affecting chromosome 1 and chromosome 2 more strongly than other chromosomes. However, this non-random elevation of mis-segregation has not shown to be preferential for either chromosome 15 or chromosome 21 and therefore presumably will not have preference for rob(15;21)c either<sup>95,97</sup>.

Figure 4.1 is a confocal microscopy image of an ana/telophase cell from an initial such experiment in which both sister chromatids of rob(15;21)c are clearly lagging/mis-segregating between the daughter nuclei. One copy of the normal chromosome 15 (green) and the normal chromosome 21 (magenta) can also be seen in each daughter nucleus, segregating as expected. This image highlighted that studying rob(15;21)c mis-segregation rates further would be a good idea.

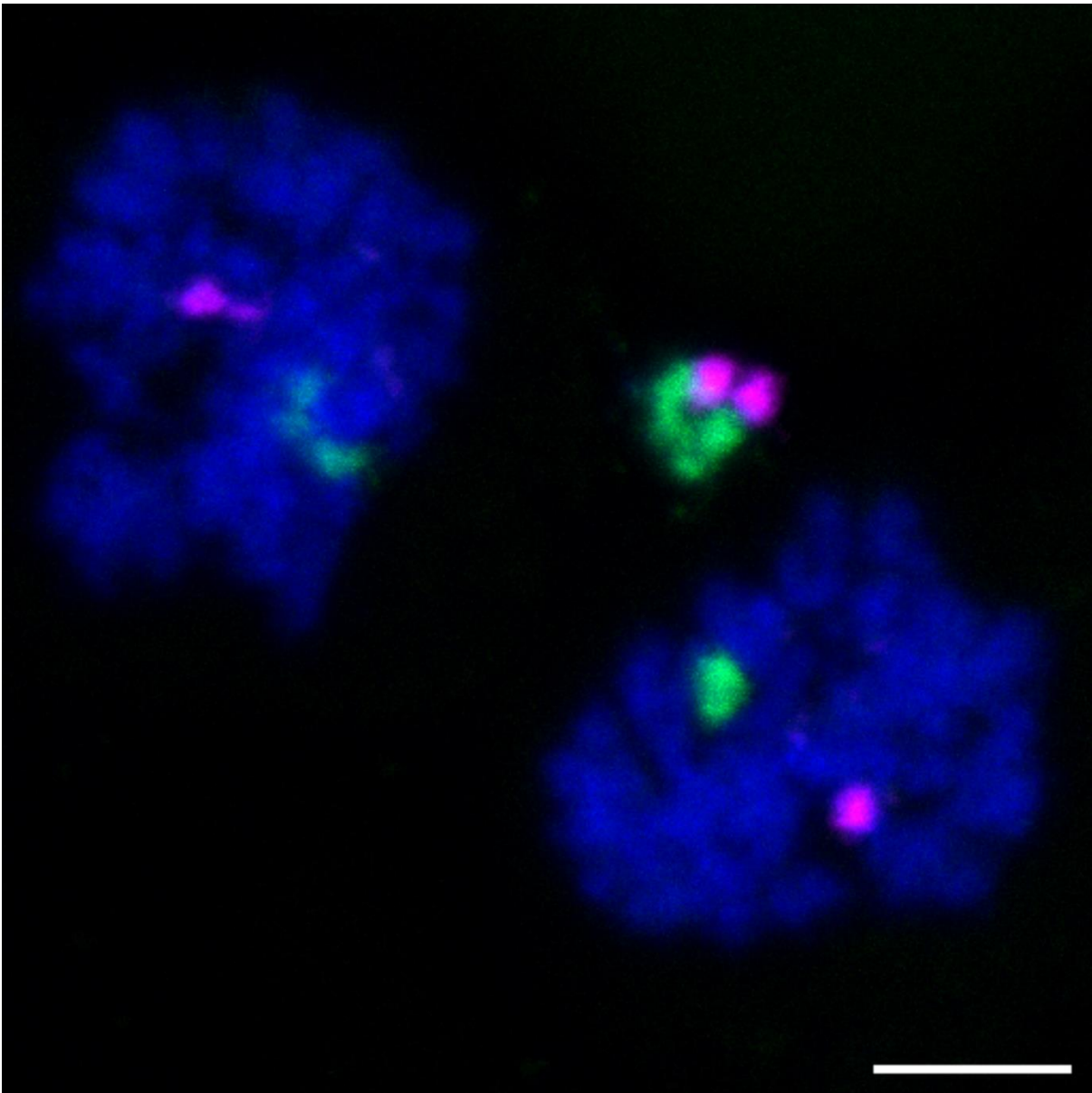


**Figure 4.1. Anaphase cell with mis-segregating rob(15;21)c.** Confocal image of an L996 anaphase cell with both sister chromatids of rob(15;21)c mis-segregating. FISH probes stained chromosome 15q (green) and chromosome 21q (magenta) and dapi stained DNA (blue). Scale bar = 5  $\mu$ m.

To better understand if rob(15;21)c was truly mis-segregating frequently, the throughput of these imaging experiments needed to be much higher. This required resolution to be sacrificed as a trade off for throughput, but preliminary experiments showed that the decreased resolution was still sufficient to observe actively mis-segregating chromosomes and to identify if these contained chromosome 15, chromosome 21 or rob(15;21)c. Many experimental coverslips were set up as above to enrich ana/telophase cells with FISH-stained chromosomes 15 and 21. However, each full coverslip was imaged by tiling together hundreds of images. Figure 4.2A is an example of a full coverslip worth of tiled images with tens to hundreds of thousands of cells. Analysis of these large images was done in a semi-automated manner. Thresholding was done

on the Dapi channel in ZEN software to produce an automated cell count and then further analysis was done manually. This analysis involved counting all ana/telophases and those with an actively mis-segregating chromosome on the Dapi channel without reference to the presence or absence of FISH probes. All cells counted with a mis-segregation were then assessed to see if they contained the chromosome 15q FISH probe, the chromosome 21q FISH probe or both (presumably rob(15;21)c). Figure 4.2B and Figure 4.2C are examples from the image in Figure 4.2A showing respectively one and then two rob(15;21)c sister chromatids mis-segregating. The quantification of this mis-segregation data is provided in Figure 4.3.

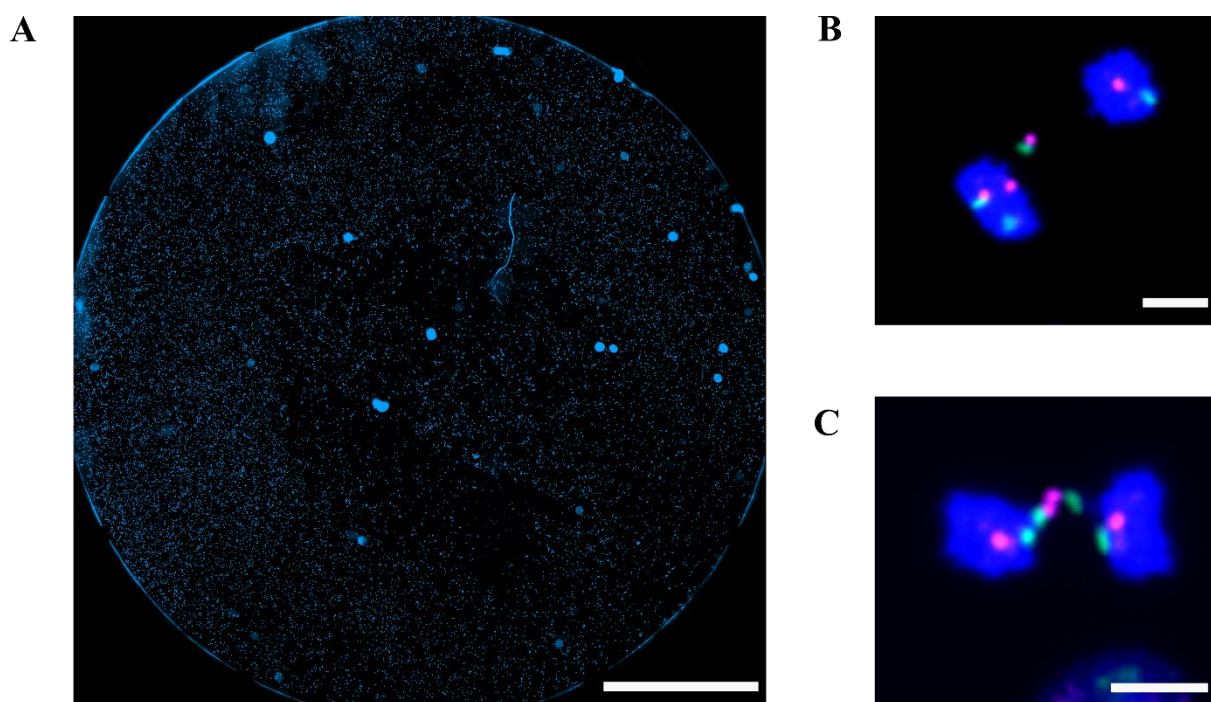


**Figure 4.2. High throughput analysis of rob(15;21)c mis-segregation.** (A) Tiled image of entire coverslip of cells induced into anaphase and telophase. (B) Example of a cell with one rob(15;21)c sister chromatid mis-segregating. (C) Example of a cell with both rob(15;21)c sister chromatids mis-segregating. Scale bar in (A) = 4 mm. Scale bars in (B) and (C) = 10  $\mu$ m.

Whilst cells were enriched in ana/telophase, there were still proportionally not a large number of these cells, though being able to analyse such a large number of total cells (2.36 million total cells) meant that the smaller populations of cells were still significant. 11,520 cells (0.5%) were identified as being in ana/telophase and of those 1,368 had an actively occurring mis-segregation (12% of anaphase/telophase cells).

If mis-segregation is random and each chromosome has an equal chance of mis-segregating, then in L995 and L996 cells the chance of chromosome 15, chromosome 21 or rob(15;21)c mis-

segregating would each be 2.2%. These cells have 45 chromosomes with one copy of normal 15, one copy of normal 21 and one rob(15;21)c, therefore 1 in 45 times we would expect to see each of these chromosomes mis-segregating. In practice, the results in Figure 4.3A for L995 and in Figure 4.3B for L996 show that the real mis-segregation rate for rob(15;21)c is far from the expected 2.2%. In both L995 and L996 cells the rate of mis-segregation for chromosome 15 and chromosome 21 is still relatively low. The chance of a mis-segregating chromosome being chromosome 15 is 1.8% (15/852 total mis-segregations) in L995 and 3.9% (20/516 total mis-segregations) in L996 and the chance of it being chromosome 21 is 0.9% (8/852 total mis-segregations) in L995 and 2.7% (14/516 total mis-segregations) in L996. However, contrary to the low mis-segregation rates of normal chromosomes 15 and 21, the rate of rob(15;21)c mis-segregation is significantly higher than expected. The chance of a mis-segregating chromosome being rob(15;21)c is 17.3% (147/852 total mis-segregations) in L995 and 16.1% (83/516 total mis-segregations) in L996. Statistical analysis was done by one-way ANOVA with Holm-Šídák's multiple comparisons test and shows that the difference between rob(15;21)c mis-segregation rate and that of chromosome 15 and chromosome 21 is significant. In L995, the P value of rob(15;21)c versus chromosome 15 is 0.0033 and that of rob(15;21)c versus chromosome 21 is 0.0031. In L996, the P value of rob(15;21)c versus chromosome 15 is 0.0001 and that of rob(15;21)c versus chromosome 21 is 0.0002. These results provide strong support for the hypothesis of frequent mis-segregation driving rob(15;21)c into an environment that is susceptible to chromothripsis.

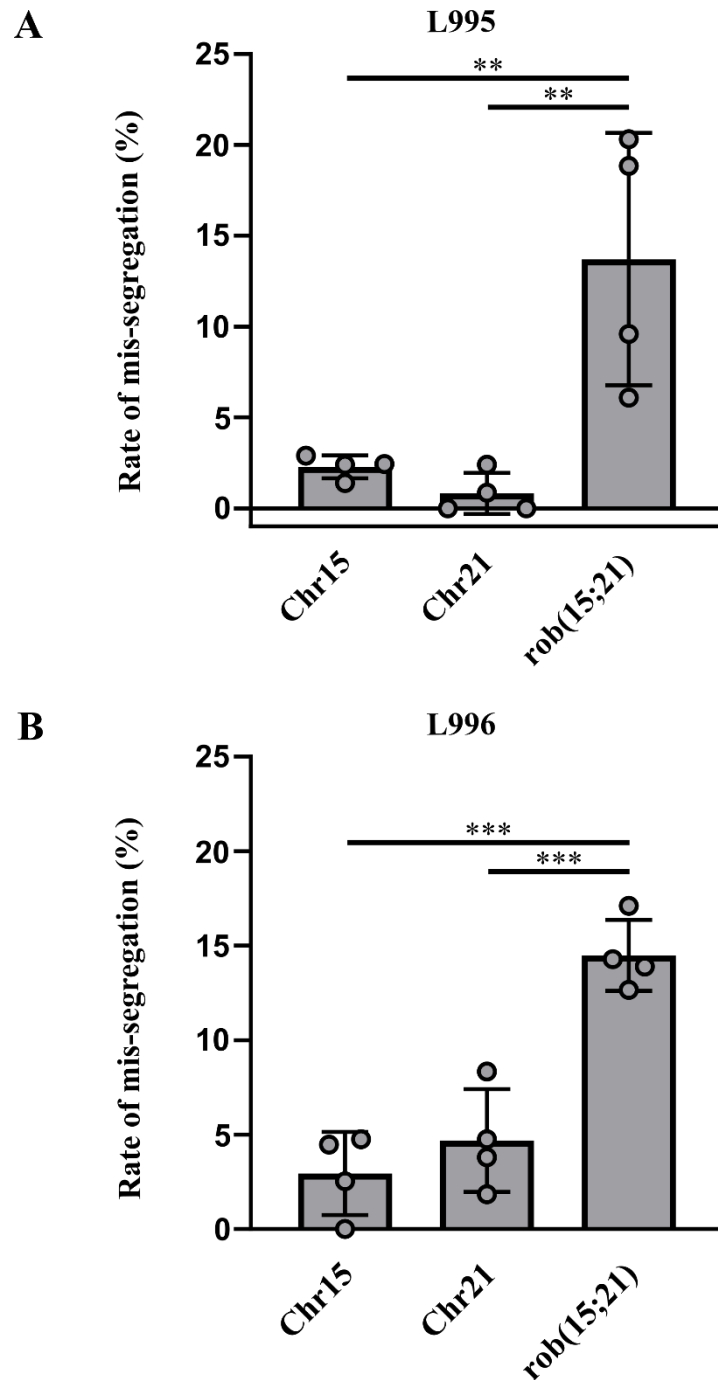


**Figure 4.3. rob(15;21)c mis-segregates frequently.** (A) Rate of chromosome 15, chromosome 21 and rob(15;21)c mis-segregation rates in L995 cells. (B) Rate of chromosome 15, chromosome 21 and rob(15;21)c mis-segregation rates in L996 cells. Statistical analysis done by one-way ANOVA with Holm-Šídák's multiple comparisons test. \*\* = p-value  $\leq 0.01$ , \*\*\* = p-value  $\leq 0.001$ . n = 4 where n is experimental repeats from early, mid, late and unknown passage cells.

Sequencing from Li *et al.* in 2014 predicted that two copies of rob(15;21)c are present during the chromothriptic event which produces one derivative chromosome and ultimately drives iAMP21-ALL<sup>145</sup>. This is contrary to most chromothripsis models which only involve the presence of one copy of the affected chromosome<sup>154,156</sup>. Although it is conceivable that the

involvement of two sister chromatids in events causing iAMP21-ALL is entirely because they might enhance a post-chromothripsis cell growth advantage, we hypothesised that there is a mechanism that allows or specifically drives both sister chromatids of rob(15;21)c to be in an environment susceptible to chromothripsis. One hypothesis is that two rob(15;21)c sisters mis-segregate together during mitosis due to their dicentric nature. This could result in them being together in a micronucleus or in a chromatin bridge, two cellular environments that have shown to be susceptible to a chromothriptic event<sup>114,154,156</sup>.

It is difficult to predict the expected rate of one sister chromatid mis-segregating vs. both sisters mis-segregating together due to the many factors that may play a role in this. However, unless the mis-segregation rate of a single chromatid is extremely high, then it is rational to presume that it would be much more common to see one sister mis-segregating than two. Despite a high rob(15;21)c mis-segregation rate, the most common outcome is still for accurate segregation; 2.2% (147/6581) of anaphases involve rob(15;21)c mis-segregation in L995 and 1.7% (83/4939) in L996. Whilst analysing the high-throughput imaging data of mis-segregations in Figure 4.2 we also counted how many rob(15;21)c containing mis-segregations involved one sister chromatid versus both sisters. This was determined largely by the presence/form of FISH probes in the actual mis-segregation but also by the number of chromosome 15q and chromosome 21q probes counted in the daughter nuclei of the cell with the mis-segregating rob(15;21)c. Figure 4.4 shows the plots of these counts. Of the 230 rob(15;21)c containing mis-segregations, we observed 120 with just one sister chromatid but, strikingly, we observed 110 with both sister chromatids present. In both L995 (Figure 4.4A) and L996 (Figure 4.4B) cells we see that roughly half of the time a mis-segregation event involves rob(15;21)c, it involves both sisters. This rate of co-mis-segregation of rob(15;21)c sisters is considerably higher than we would expect. This suggests a mechanistic reason driving both sister chromatids to be together in a chromothriptic event and not just that selection during cancer evolution requires two copies for tumourigenesis.

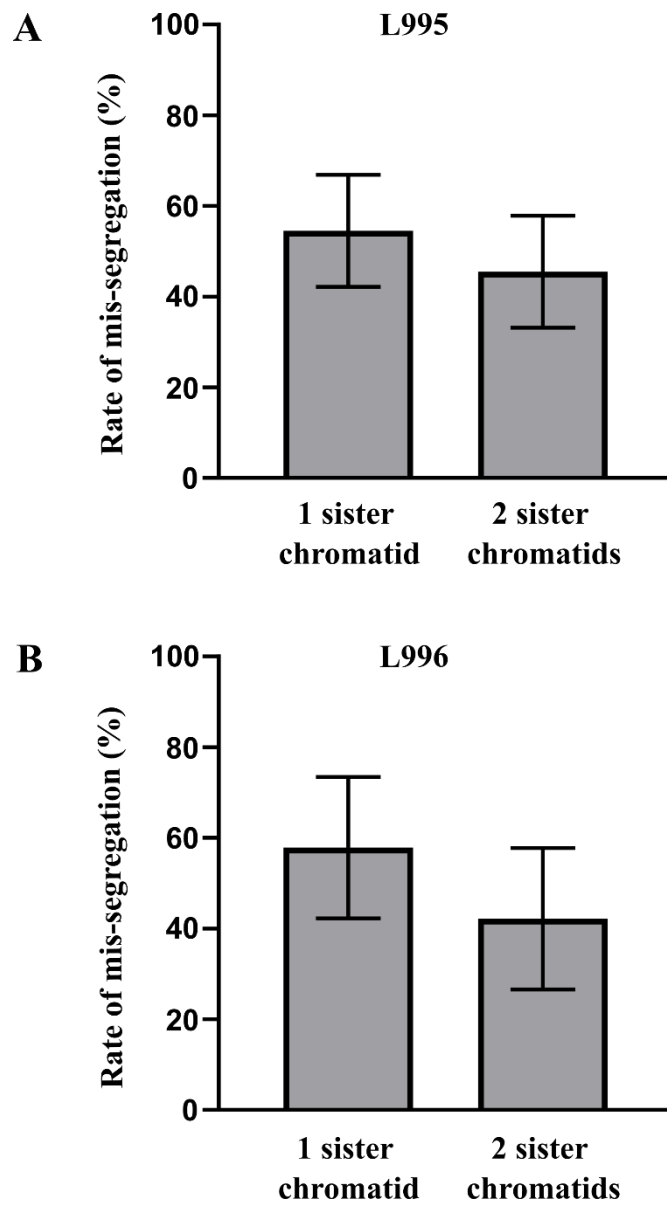


**Figure 4.4. rob(15;21)c sister chromatids often mis-segregate together.** (A) Rate of one sister and two sister rob(15;21)c mis-segregation in L995 cells. (B) Rate of one sister and two sister rob(15;21)c mis-segregation in L996 cells. n = 4 where n is experimental repeats from early, mid, late and unknown passage cells.

#### **4.2.2 rob(15;21)c mis-segregation rates across passages**

As we hypothesised that centromeric heterogeneity may have been changing across passages in section 3.2.7, we also sought to assess how this may affect the mis-segregation rate of rob(15;21)c. We hypothesised that if a population of cells tended towards having actively monocentric rob(15;21)c then the mis-segregation rate of this chromosome would decrease and be more similar to that of the internal control chromosomes, chromosome 15 and chromosome 21.

High throughput mis-segregation experiments as in Figure 4.2 were done in parallel with experiments in Figure 3.15 and Figure 3.16 using the same flasks of cells to study rates of mis-segregation in early (P6-8), middle (P17-19) and late passage (P32-34) L995 and L996 lines.

Figure 4.5 is the quantification of high-throughput mis-segregation across passages analysis. Figure 4.5A and Figure 4.5B show that respectively in L995 and L996 there was no evident differences in rob(15;21)c mis-segregation rate in early, middle or late passage cells. Although the mean rob(15;21)c mis-segregation rate remained high across all passages in both L995 and L996 cells, there appeared to be high variance in this rate within each passage (across repeats). Similar to the experiments in 3.2.7 to assess centromeric changes as L995 and L996 cells age, the results in Figure 4.5 also show that the segregation tendencies of rob(15;21)c remain consistent but aberrant. However, as there was no passage of cells with a predominantly actively monocentric phenotype for rob(15;21)c in Figure 3.15 and Figure 3.16 it was not possible to test if the mis-segregation rate changed with centromeric phenotype.

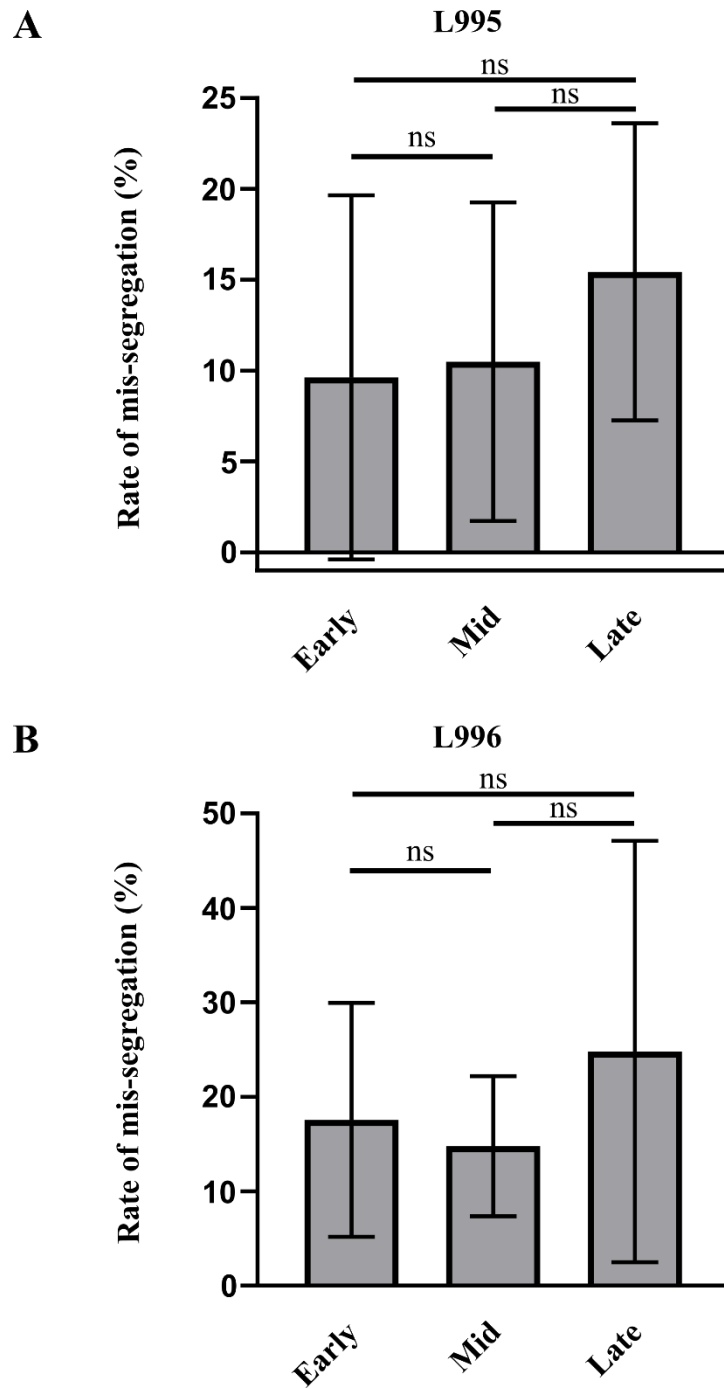


**Figure 4.5. *rob(15;21)c* mis-segregation rates do not change across passages. (A)** Rate of *rob(15;21)c* mis-segregation in early, middle and late passage L995 cells. **(B)** Rate of *rob(15;21)c* mis-segregation in early, middle and late passage L996 cells. Statistical analysis done by one-way ANOVA with Holm-Šidák's multiple comparisons test. ns = not significant. n = 3 where n is technical repeats.

### 4.2.3 rob(15;21)c mis-segregates into environments that are susceptible to chromothripsis

The suggestion that rob(15;21)c mis-segregates now has much data to support it. Published data indicates that micronuclei are a precursor for chromothripsis<sup>94,154,156,181</sup>. The next logical step to better understand the process of rob(15;21)c becoming chromothriptic was to see if the frequently mis-segregating chromosome entered micronuclei and if so what this environment looked like.

Figure 4.6 shows widefield images of cells from blood samples of the iAMP21-ALL patient whose cells were transformed into L995. These samples were taken when the patient was in remission and therefore they were non-cancerous cells. The cells in Figure 4.6 were stained with FISH probes for the alpha satellites of chromosome 15 (green) and chromosome 21/13 (magenta). Both images showed three magenta foci in the primary nucleus (presumably normal chromosome 21 and both copies of chromosome 13) and one green foci (normal chromosome 15). The micronucleus in each image shows one green focus colocalising with a small magenta focus. Due to the close location and the infrequency of normal 15 and 21 chromosomes to mis-segregate it is a fair presumption that it is rob(15;21)c in these micronuclei and not both normal 15 alongside normal 21 or 13. The presence of a particularly smaller focus for the 21 alpha satellite within rob(15;21)c is not surprising. Figure 3.17 and Figure 3.18 in Chapter 3 are images and quantified data indicating that the 21 centromere is likely less active than the 15 centromere within rob(15;21)c. Partial DNA deletion has been suggested previously as a mechanism for centromere inactivation in Robertsonian chromosomes<sup>138</sup>.

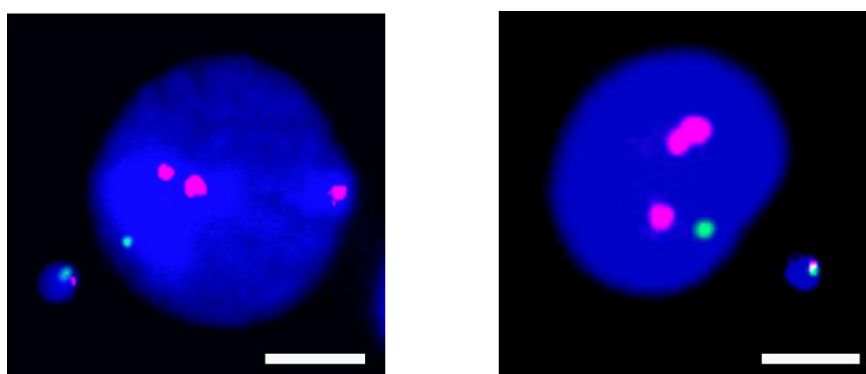


**Figure 4.6. rob(15;21)c in micronuclei.** Two example images of FISH staining for the centromere of chromosome 15 (green) and the centromeres of chromosome 21/13 (magenta) showing rob(15;21)c in micronuclei. Images provided by Claire Schwab. Scale bars = 5  $\mu$ m.

The spatiotemporal assembly of the nuclear membrane on mis-segregating chromosomes was not well understood until recently. Work from multiple groups in recent years has shown that the membrane formed around mis-segregating chromosomes (becoming micronuclei) is often aberrant<sup>94,114,171</sup>. Mis-segregating chromosomes that find themselves between daughter nuclei seem to lack non-core nuclear envelope proteins, including nuclear pore complexes (NPC). Miyazaki *et al.* define three types of micronuclear envelope<sup>263</sup>. 1) Those with a fully intact nuclear envelope, including both core and non-core proteins. 2) Those that have assembled core nuclear envelope proteins but without detectable non-core proteins. 3) Those that lack both core and non-core nuclear envelope proteins.

Mis-segregating chromosomes that are between daughter nuclei in the late stages of mitosis are densely surrounded by the spindle. It is likely that physical obstruction by the spindle prevents appropriate assembly of non-core nuclear envelope proteins to micronuclei in the midzone<sup>171,173,174</sup>. Liu *et al.* nicely demonstrated this by showing micronuclei that form peripherally to the spindle zone are able to form type 1 nuclear envelopes with both core and non-core proteins<sup>171</sup>. Although midzone micronuclei are released from the web of microtubules post-mitosis, they are unable to repair their membranes and recruit non-core nuclear envelope proteins during interphase<sup>94,114,171,173</sup>. An alternative model suggests that midzone Aurora B may play a role in promoting lagging chromosome condensation, which in turn inhibits NPC formation<sup>88,173,177,178</sup>. Aurora B inactivation at anaphase onset restored NPC formation on lagging chromosomes<sup>175,176</sup>. However, it is possible that Aurora B acts indirectly to prevent assembly of NPC proteins via its regulatory role on the mitotic spindle<sup>171,179,180</sup>. This hybrid model involving Aurora B regulation and spindle obstruction may explain how NPC proteins fail to assemble on midzone lagging chromosomes.

Micronuclei with aberrant nuclear envelopes have the propensity to rupture. The DNA within these micronuclei are often subject to erroneous DNA replication and extensive DNA damage<sup>105,171</sup>. These micronuclei have been shown to be a precursor to chromothripsis<sup>94,154,156,181</sup>.

Rob(15;21)c mis-segregates frequently (Figure 4.3) and enters micronuclei (Figure 4.6). The next logical step to assess on the pathway from dicentric chromosome to chromothripsis was to see if these micronuclei have atypical nuclear envelopes, therefore predisposing them to DNA damage.

Due to the number of different fluorophores that would be required and the poor quality of combined immunofluorescence and FISH in whole cells, it was not possible to stain rob(15;21)c in combination with nuclear envelope proteins. However, as rob(15;21)c mis-segregates frequently (16-17% of mis-segregations contain rob(15;21)c), I reason that the micronuclear phenotypes seen in L995 and L996 cells will sometimes contain other chromosomes, but will also frequently contain rob(15;21)c.

Figure 4.7 shows staining of multiple different core and non-core nuclear envelope proteins on daughter primary nuclei and on micronuclei. Core nuclear envelope proteins are all stained in green and non-core in yellow. Figure 4.7A is a cell that was not stained for any non-core proteins; however, the staining of the core protein Emerin is clear around the two micronuclei. The Emerin staining in Figure 4.7B is less clear, though it is seen in the vicinity of micronuclear DNA. Interestingly though, the primary nuclei here have clear staining of the non-core protein Nup358 whilst the micronuclei do not. This observation is backed up with staining of different core and non-core nuclear envelope proteins in Figure 4.7D. This figure shows strong staining of the core protein Lap2 $\alpha$  on micronuclear DNA, but only weak staining of the non-core protein Nup107 when compared to the primary nuclei. Of the non-core nuclear envelope proteins tested, the only one that has clear staining on micronuclei in L995 and L996 cells was UNC84B, as shown in Figure 4.7C.

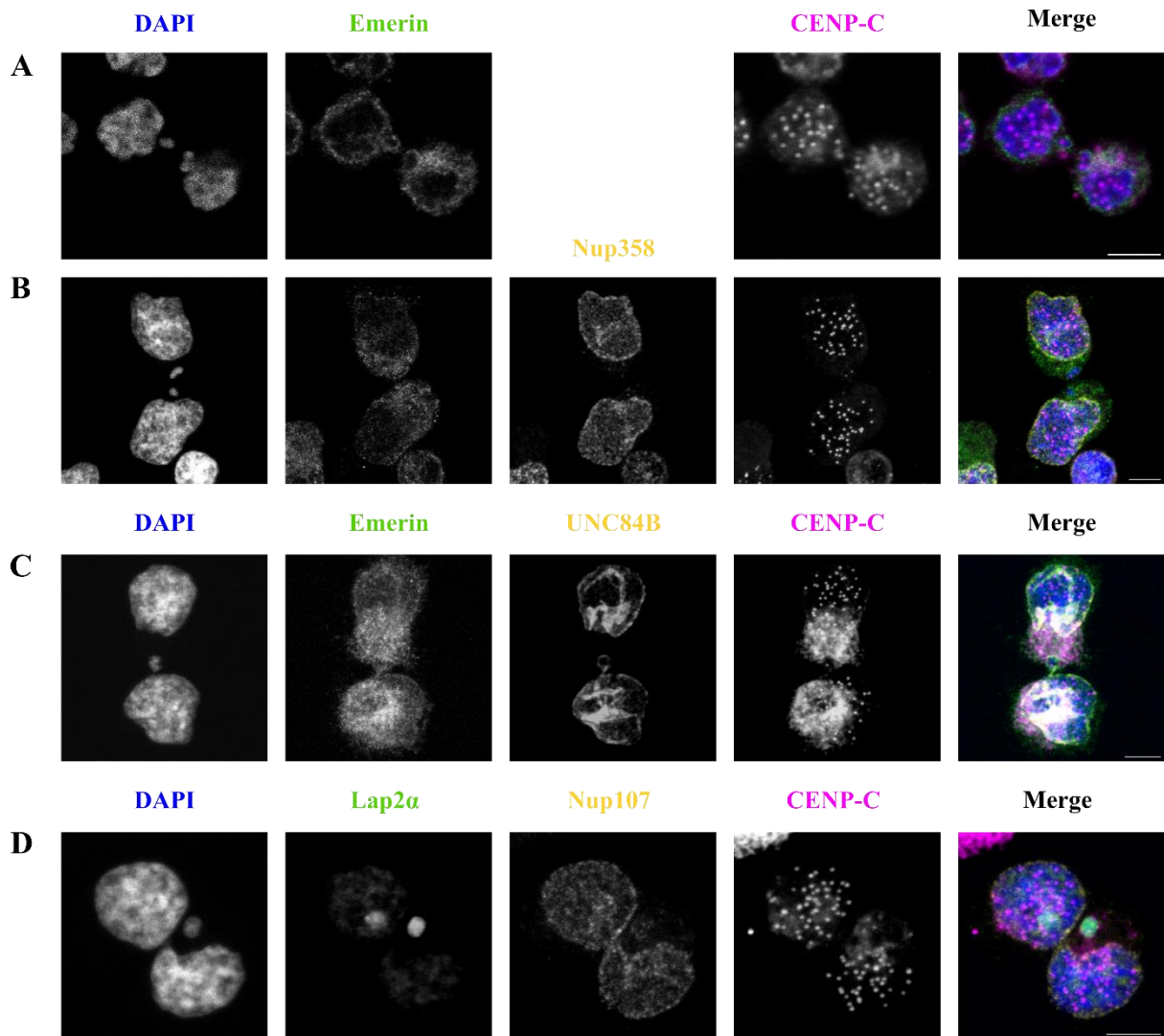


**Figure 4.7. Mis-segregating chromosomes in L995 and L996 cells enter micronuclei.** (A) Telophase cell with micronucleus stained with Emerin (core nuclear envelope protein) and CENP-C. (B) Telophase cell with micronucleus stained with Emerin, Nup358 (non-core nuclear envelope protein) and CENP-C. (C) Telophase cell with micronucleus stained with Emerin, UNC84B (non-core nuclear envelope protein) and CENP-C. (D) Telophase cell with micronucleus stained with Lap2 $\alpha$ , Nup107 (non-core nuclear envelope protein) and CENP-C. Scale bars = 5  $\mu$ m

The results in Figure 4.7 highlight that mis-segregating chromosomes in L995 and L996 cells do enter micronuclei. When these micronuclei are in the midzone of daughter nuclei they are able to assemble core nuclear envelope proteins but often fail to incorporate normal levels of non-core proteins (with the possible exception of UNC84B). As rob(15;21)c frequently mis-segregates in these cells, some of these micronuclei are likely to contain this chromosome. This result supports the hypothesis that a dicentric rob(15;21)c (and likely both sister chromatids) frequently mis-segregating into an environment that is susceptible to chromothripsis as the mechanism for high predisposition of rob(15;21)c carriers to iAMP21-ALL.

#### 4.2.4 Why does rob(15;21)c frequently mis-segregate?

Clearly rob(15;21)c mis-segregates at a higher rate than expected by chance; particularly as the mis-segregations often involve both sister chromatids. This implies that there is a mechanistic reason driving the frequent co-mis-segregation of rob(15;21)c sister chromatids. Understanding the mechanism causing frequent mis-segregation, in particular that causing co-sister mis-segregation, may help to uncover the reason that carriers of rob(15;21)c have an increased risk of developing iAMP21-ALL.

##### 4.2.4.1 Location of rob(15;21)c in the nucleus

It has been well reported that chromosome mis-segregation is non-random. Larger chromosomes have frequently been shown to mis-segregate at a higher rate than smaller chromosomes in mitosis; in particular chromosomes 1 and 2 have a high mis-segregation rate<sup>95</sup>. Multiple models have been supposed, with data to suggest that the reason for a non-random chromosomes mis-segregation rate is multi-factorial. Cohesion fatigue, centromere size and nuclear location all seem to affect mis-segregation<sup>95,97,264,265</sup>. Klaasen *et al.* described how the location of chromosomes within interphase nuclei influenced mis-segregation rates<sup>98</sup>. Chromatin that is more peripheral is more likely to be behind the centrosomes (in relation to the spindle) upon chromosome condensation and in the early stages of mitosis. These peripherally located chromosomes are then more difficult to biorient and line up on the metaphase plate. Delayed biorientation and congression causes a higher mis-segregation rate for peripherally located chromosomes.

Usually it is larger chromosomes that sit most peripherally in the interphase nucleus, with acrocentric chromosomes being quite central as the Nucleolar Organiser Regions (NORs) on acrocentric short arms interact with the nucleolus<sup>266</sup>. As the chromosome rob(15;21)c has not been well studied, we wished to assess if its interphase nuclear location was more peripheral than that of chromosome 15 and chromosome 21; therefore causing a high mis-segregation rate. We hypothesised this may be happening due to the loss of short arm DNA in the constitutional translocation that created the Robertsonian chromosome. A loss of some or all of the NOR DNA would mean that rob(15;21)c might not interact with the nucleolus, unlike normal acrocentric chromosomes 15 and 21.

Figure 4.8 shows results from experiments done to analyse the location of rob(15;21)c in interphase nuclei. Entire coverslips of fixed cells were stained with FISH probes for the  $\alpha$ -satellites of chromosome 15 and chromosome 21/13 and imaged by tiling together hundreds of

images (as in Figure 4.2). Whilst it would have been better to have FISH probes that stained just chromosome 21 and not chromosome 13, as in Figure 4.1 and Figure 4.2, the chromosome paint arm probes were not punctate enough for interphase analysis; fluorescence was dispersed and it was not possible to achieve a consistent measurable position. Therefore  $\alpha$ -satellite probes were used as these were much more punctate, although this meant not being able to distinguish chromosome 21 and chromosome 13 (due to similarities in their  $\alpha$ -satellite array). Large images as in Figure 4.2 were run through a FIJI macro as described in section 2.15.5. This macro splits images into individual cells; examples are shown in Figure 4.8A. Then the rob(15;21)c chromosome was defined as the chromosome 15 focus and chromosome 21/13 focus with the smallest nearest-neighbour distance. We then determined the distance from the centre of each chromosome 15, chromosome 21/13 and rob(15;21)c focus to the centre of the nucleus, defined as the centroid of nuclear Dapi staining. Finally, the radial positions of the centromeres are reported as the distance from the centre of the nucleus as a proportion of the length of the radius of the specific nucleus in which they reside. Figure 4.8B is the plotted data of L995 cells. The mean distances of chromosome 15 (0.29), chromosome 21/13 (0.28) and rob(15;21)c (0.26) differed only slightly, though as this automated analysis allowed for such high n numbers (13,479 chromosome 15 foci, 20,866 chromosome 21/13 foci and 12,296 rob(15;21)c foci) the differences are extremely statistically significant. The results from L996 cells are shown in Figure 4.8C and they tell a similar story. The mean distances for L996 are 0.26 for chromosome 15, 0.25 for chromosomes 21/13 and 0.24 for rob(15;21)c. N numbers for L996 cells were 19,327 chromosome 15 foci, 30,928 chromosome 21/13 foci and 18,751 rob(15;21)c foci.

Whilst there appears to be a significant difference between how peripherally located rob(15;21)c is compared with normal chromosome 15 and normal chromosomes 21/13, this does not immediately suggest that interphase nuclear location is an underlying factor in rob(15;21)c mis-segregation. The results in Figure 4.8 show how the average distance of rob(15;21)c from the centre of the nucleus is shorter than that of chromosome 15 and chromosome 21/13. This result is contrary to the hypothesis that rob(15;21)c has a higher distance from the nucleus centre and therefore would increase the likelihood of a polar chromosome location during mitosis and, in turn, aberrant microtubule attachments and mis-segregation. We therefore did not obtain any evidence that changes in nuclear location contribute to the mis-segregation of rob(15;21)c.

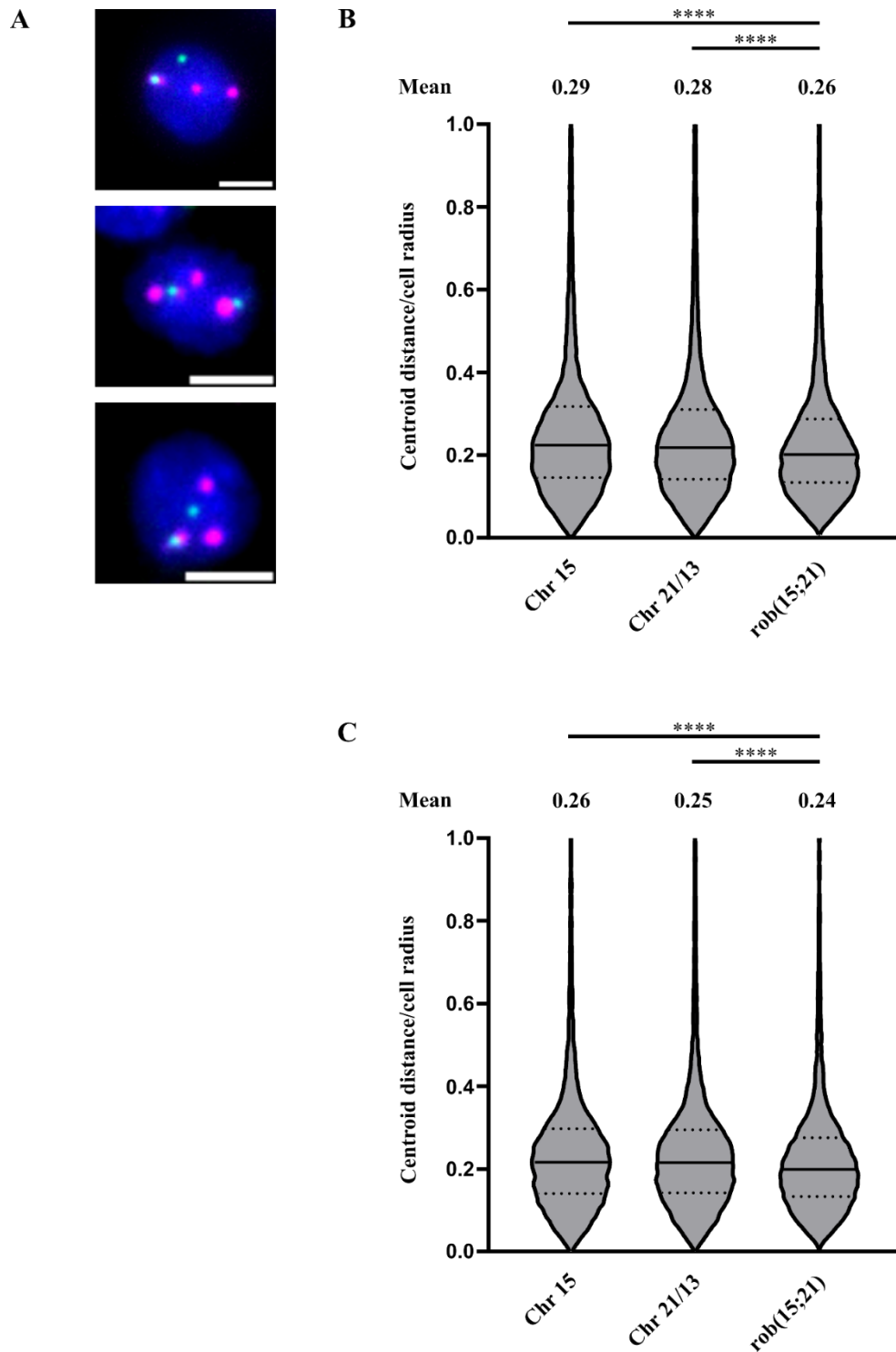


**Figure 4.8. The interphase location of rob(15;21)c likely does not promote mis-segregation (A)**

Three example images from high-throughput analysis of chromosome 15, chromosome 21 and rob(15;21)c nuclear location. Scale bars = 10 $\mu$ m. **(B)** Plots of data from L995 cells showing the distance of chromosome 15, chromosome 21 and rob(15;21)c centromeres from the centre of each nucleus (centroid distance), relative to the radius of each nucleus. **(C)** Plots of data from L996 cells showing the distance of chromosome 15, chromosome 21 and rob(15;21)c centromeres from the centre of each nucleus (centroid distance), relative to the radius of each nucleus. Statistical analysis done by one-way ANOVA with Šídák's multiple comparison test. \*\*\*\* = p-value  $\leq$  0.0001. n = 12,000-31,000 foci (depending on the chromosome and the cell line – further detail in text).

#### 4.2.4.2 *rob(15;21)c centromeric cohesion*

Appropriate regulation of cohesion is required for mitotic fidelity. Whilst the cohesin complex has roles throughout the cell cycle, those of most interest to this thesis are its roles during mitosis. From S phase until anaphase onset, cohesin maintains sister chromatid interactions<sup>267</sup>. Timely removal of cohesin in a two-step process is essential for accurate chromosome segregation. As a vertebrate cell enters mitosis, sister chromatids are bound together at both their centromeres and along their arms by cohesin complexes. The first step of removal is known as the prophase pathway and involves removing arm cohesin in a cleavage-independent manner<sup>9</sup>. Centromeric and pericentromeric cohesin though is protected from the prophase pathway due to the action of Shugoshin<sup>10</sup>. This protection persists until microtubule-kinetochore attachments have satisfied the SAC. The remaining centromeric cohesin can then be removed in the second removal step. This involves cleavage of cohesin rings by Separase, which is liberated from its inactivating partner Securin upon destruction of Securin by APC/C-mediated proteosomal degradation<sup>13,14</sup>.

Cells that are delayed or arrested in metaphase can undergo cohesion fatigue; a process that involves asynchronous sister chromatid separation due to the loss of cohesin (usually starting at the centromere), caused by prolonged spindle pulling forces<sup>268</sup>.

I hypothesised that there could be atypical cohesin staining at the dicentric centromeres of *rob(15;21)c*. In principle, this could be caused by two opposing mechanisms. Firstly, an increased level of cohesin could result in problems cleaving centromeric cohesion in time and therefore causing co-mis-segregation of *rob(15;21)c* sister chromatids. Alternatively, reduced cohesin that allows for cohesion fatigue will prematurely separate sister chromatids. This would normally cause each sister to be pulled to opposing poles. However the presence of a functionally dicentric chromosome may allow more frequent single chromatid biorientation, where the two centromeres on one sister chromatid are attached to microtubules from opposing poles. If this single chromatid biorientation was common, then midzone laggings may often end up in the same daughter cell if not resolved in a timely manner.

Because the majority of cohesin is released rapidly from chromosome in mitosis, staining for residual centromeric cohesin is notoriously difficult<sup>269-271</sup>. Whilst I did not manage to produce enough data for quantifiable analysis, the images in Figure 4.9 shed light onto the state of cohesion at *rob(15;21)c*.

Figure 4.9A is an example chromosome spread from an L995 cell in which CENP-C and cohesin (SA2 subunit) have been stained by IF and imaged by standard confocal microscopy. Slides were marked, un-mounted and re-stained with FISH probes for chromosome 15q and chromosome 21q arms. After FISH staining, the same chromosome spreads were found and re-imaged to determine which chromosome was rob(15;21)c and to identify the internal control chromosomes, chromosome 15 and chromosome 21. As the fixation required for FISH often hindered IF staining, to have chromosome validating FISH and IF for cohesin (a protein that is already difficult to stain) this staining and imaging had to be done in a two-step manner. Figure 4.9B is a similar example to Figure 4.9A but from an L996 cell. These images show how the cohesin staining on rob(15;21)c does not appear greatly different from that on chromosome 15 or chromosome 21.

Whilst it is difficult to draw strong conclusions from a small number of images and without quantification, we did not obtain evidence for the hypothesis that there is aberrant cohesion at the rob(15;21)c centromeres; any strong phenotype would likely have been seen in the number of cells imaged. Although in these experiments we only observed the quantity of cohesin, it is still possible that cohesion on rob(15;21)c is persistent into anaphase and causing mis-segregation in this manner.

Unfortunately, due to the small number of chromosome spreads that could be effectively stained, the examples of cohesin staining on rob(15;21)c were not of chromosomes where there was an obvious second centromere (the example in Figure 4.9B may have a weak rob 21 centromere but this is not conclusive).

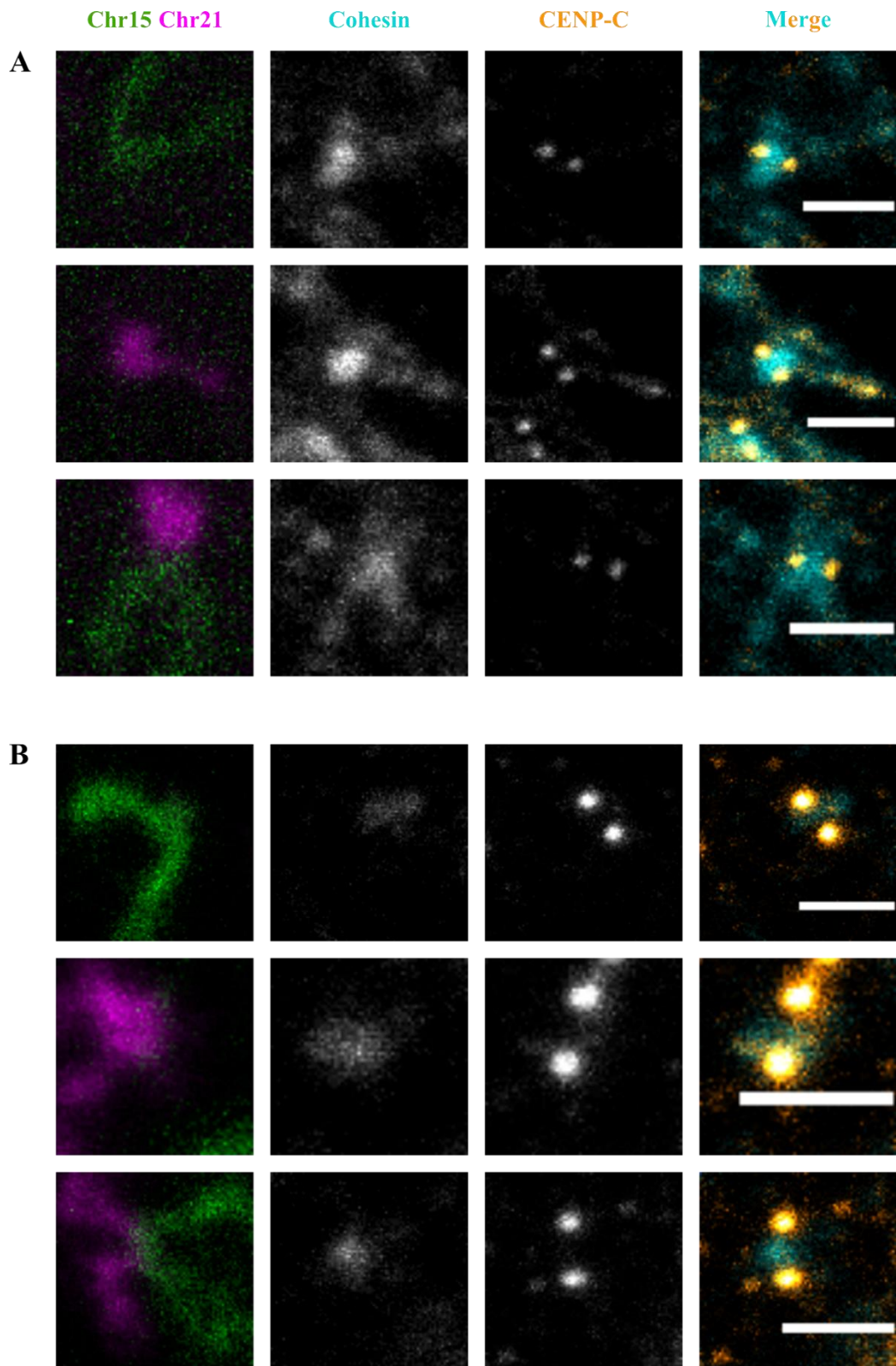


**Figure 4.9. Cohesin staining at rob(15;21)c is not aberrant.** (A) Chromosome 15, Chromosome 21 and rob(15;21)c from a chromosome spread of an L995 cell. Staining for Cohesin (SA2) and CENP-C were done by immunofluorescence and then correlative FISH on the same chromosome spreads was done to label chromosomes 15 and 21. (B) Chromosome 15, Chromosome 21 and rob(15;21)c from a chromosome spread of an L996 cell. Staining for Cohesin (SA2) and CENP-C were done by immunofluorescence and then correlative FISH on the same chromosome spreads was done to label chromosomes 15 and 21. Scale bars = 2  $\mu$ m.

#### 4.2.4.3 CPC activity at *rob(15;21)*

Appropriate chromosome segregation in human cells is largely coordinated by two processes; the error correction pathway that acts to fix incorrect microtubule-kinetochore attachments and the Spindle Assembly Checkpoint (SAC) that acts as a surveillance mechanism to prevent the segregation of chromosomes with unattached kinetochores<sup>67,272–275</sup>.

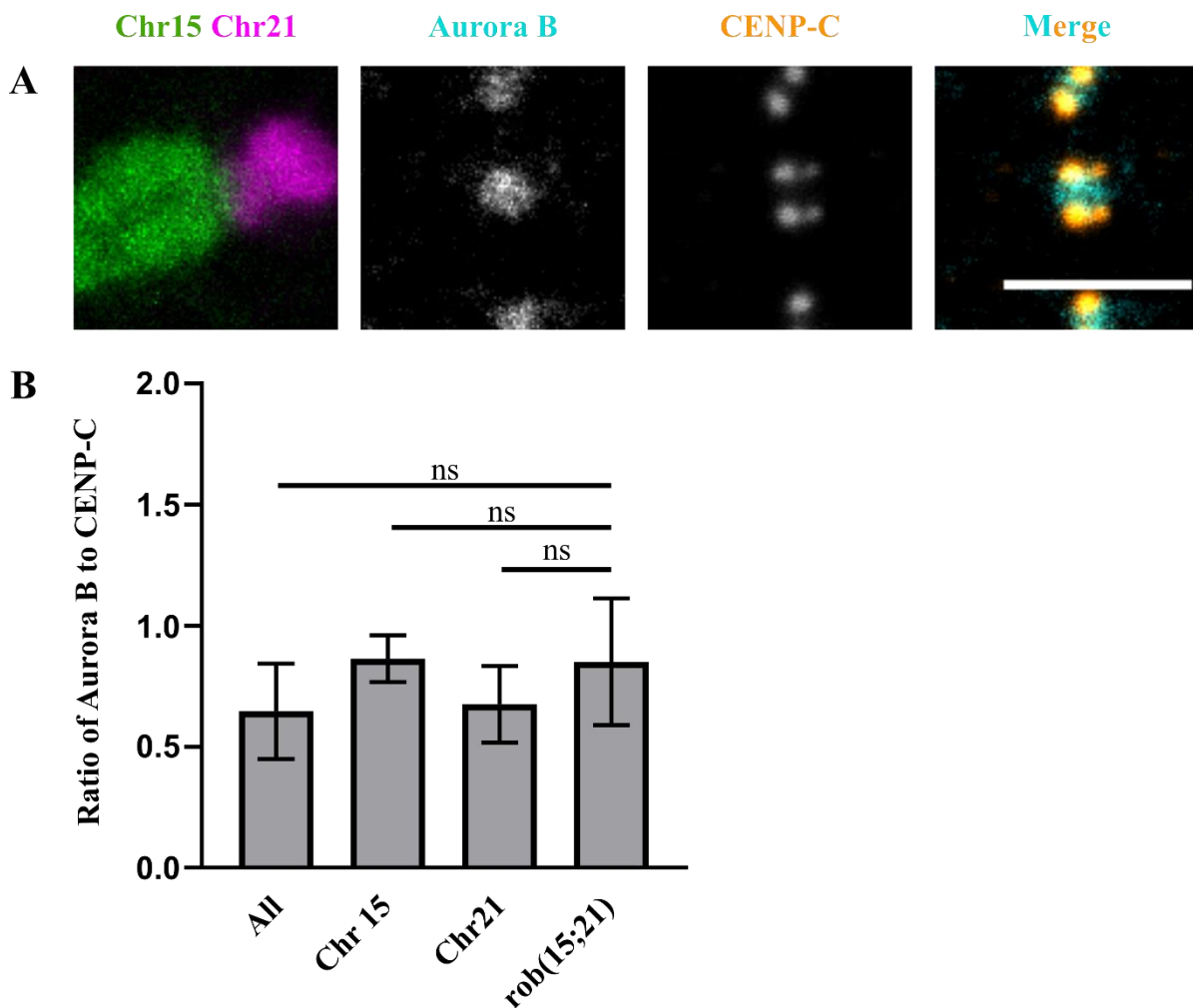
There are two possible mechanisms relating to microtubule attachments and error correction on the dicentric chromosome *rob(15;21)c* and how they may induce mis-segregation. Firstly, if *rob(15;21)c* is functionally dicentric then it is possible that merotelic attachments frequently occur, causing the chromosome to lag during anaphase. With functioning error correction, *rob(15;21)c* may still lag due to the increased amount of mis-attachments (caused by the presence of active dicentric centromeres) that cannot be resolved by a regular amount of CPC (Chromosomal Passenger Complex) activity. Alternatively, the dicentric centromeres of *rob(15;21)c* may have little problem in forming appropriate bioriented attachments, however, if error correction is faulty at this chromosome then the normal level of mis-attachments seen on a monocentric chromosome may not be resolved on *rob(15;21)c*. It is also possible that the reality is somewhere between these two hypotheses. The dicentric *rob(15;21)c* may have a small increased number of mis-attached microtubules and have slightly flawed error correction that together cause an increased rate of *rob(15;21)c* mis-segregation.

The Chromosomal Passenger Complex (CPC) is a key regulator of mitosis that is composed of the proteins Aurora B, INCENP, Survivin and Borealin. The location of the CPC changes throughout mitosis as it facilitates the regulation of different mitotic events<sup>84,90,276</sup>. One key role for the CPC is to correct erroneous kinetochore-microtubule attachments. During early mitosis the CPC is localised to the inner centromere; here it plays a role in regulating erroneous microtubule-kinetochore attachments in response to a lack of tension. This task is largely facilitated by the kinase Aurora B<sup>84,276,277</sup>.

The histone kinases Bub1 and Haspin are required for the localisation of the CPC at the inner centromere<sup>276</sup>. As *rob(15;21)c* appears to be frequently actively dicentric and with a short inter-centromeric distance, I hypothesised that these closely located dicentric centromeres/kinetochores were affecting proper CPC recruitment to the *rob(15;21)c* inner centromere. This would in turn prevent the resolution of erroneous microtubule-kinetochore attachments and enable mis-segregation of *rob(15;21)c* chromatids.

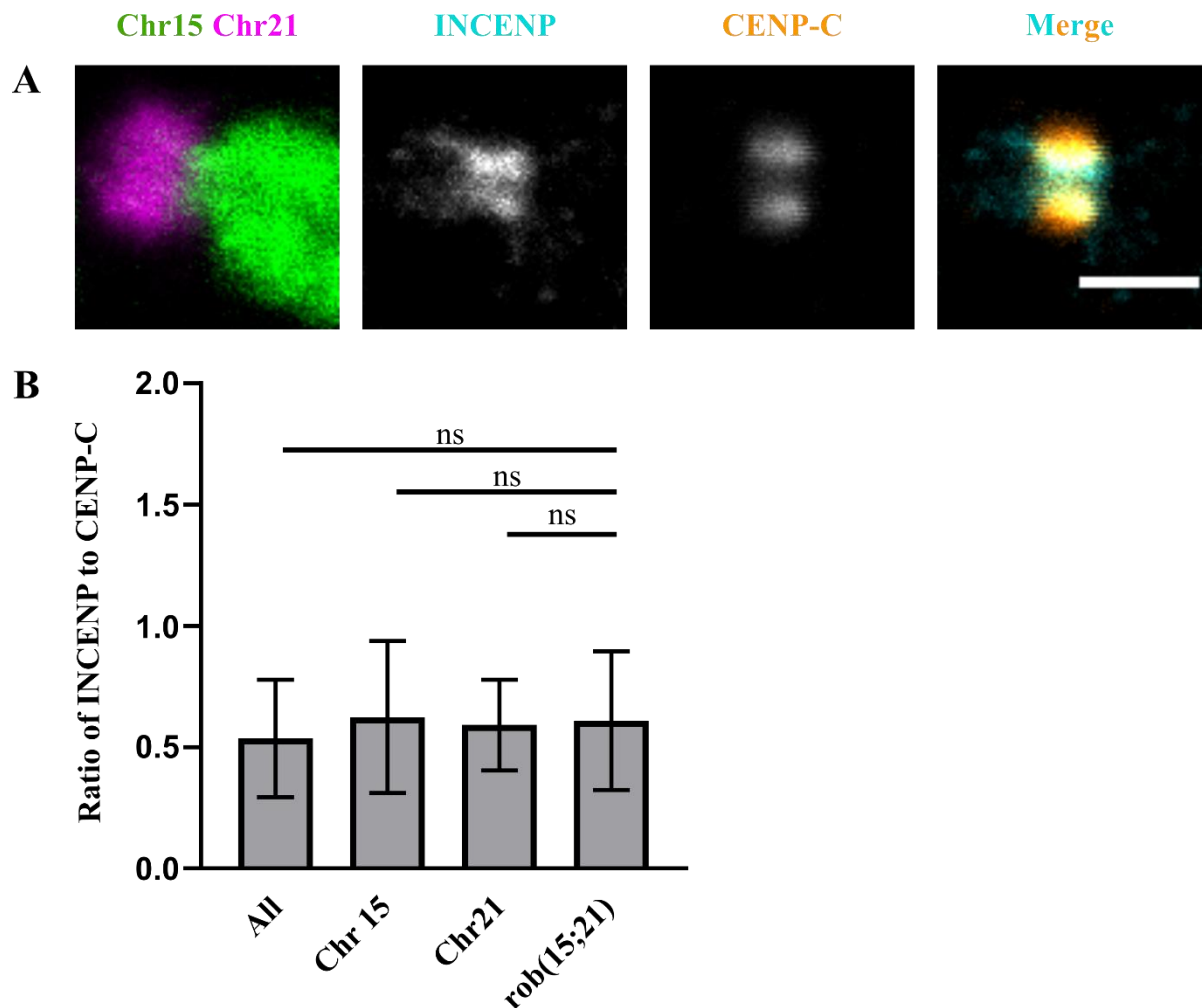
In order to test this hypothesis, chromosome spreads from L995 and L996 cells were stained with immunofluorescence and then correlative FISH as described in section 2.13. Preparation of chromosome spreads involved prometaphase synchronisation with colcemid and so the CPC should be localised to the inner centromere. Components of the CPC and the centromeric protein CENP-C were stained by IF and correlative FISH marked chromosome 15q, chromosome 21q and rob(15;21)c. Image analysis was done in FIJI to compare ratios of each CPC protein to CENP-C on chromosome 15, chromosome 21, rob(15;21)c and all other chromosomes from the same cell.

Multiple proteins of interest were stained, although the most obvious to test our hypothesis was Aurora B. Figure 4.10A shows an example rob(15;21)c chromosome with inner centromere Aurora B and inner kinetochore CENP-C staining. Quantification of multiple chromosome spreads was done (as shown in Figure 4.10B) to determine an average ratio of Aurora B to CENP-C. Chromosome 15 (n = 6), chromosome 21 (n = 6) and rob(15;21)c (n = 6) were identified by FISH staining and all other chromosomes (n = 239) were classified by a lack of FISH staining. This analysis highlighted that there is no significant difference in the ratio of Aurora B to CENP-C on rob(15;21)c when compared with internal control chromosomes 15 and 21 or with all other chromosomes in a given cell.



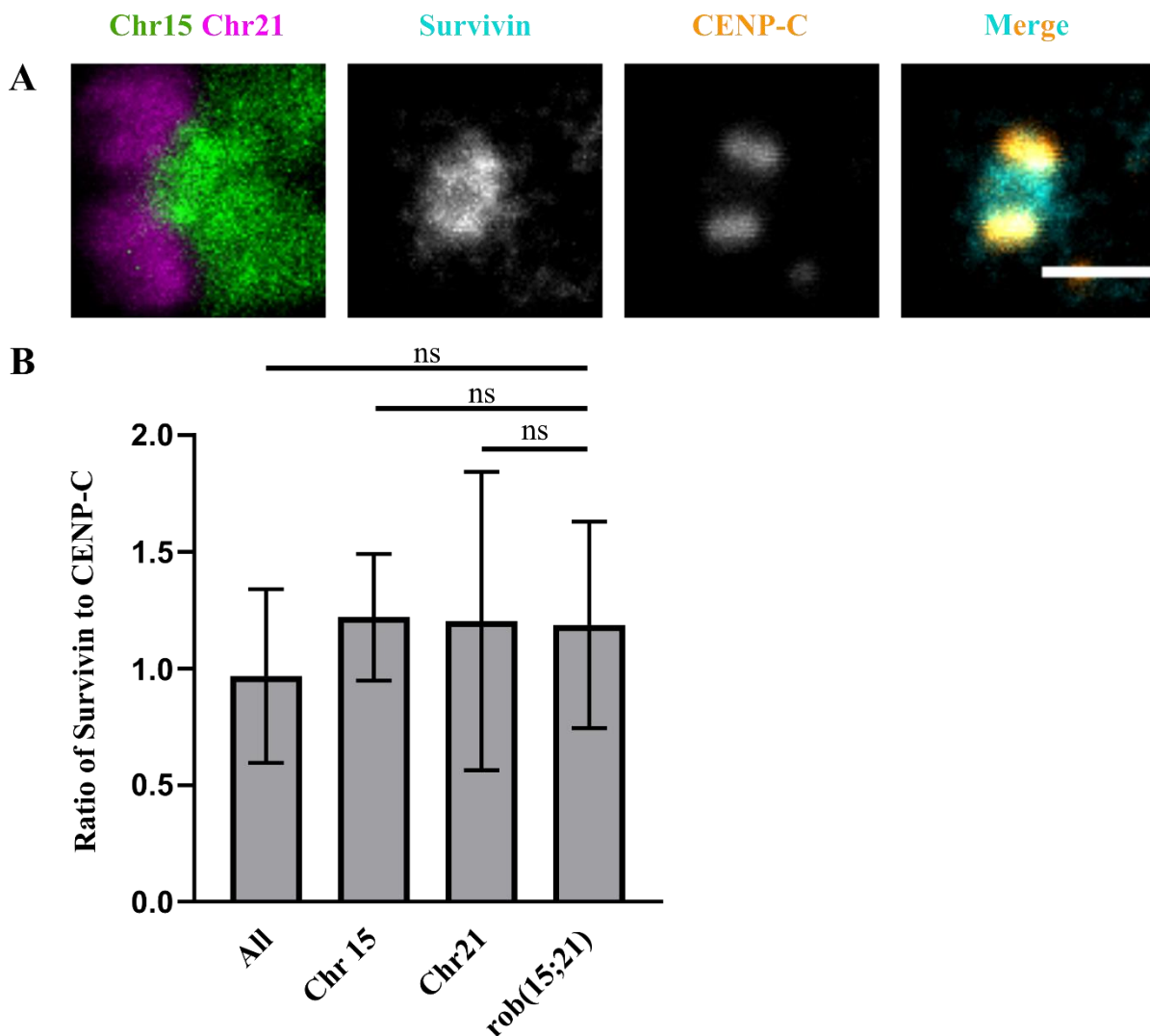
**Figure 4.10. Aurora B staining on rob(15;21)c is not aberrant.** (A) Example rob(15;21)c chromosome with Aurora B and CENP-C staining. Scale bar = 5  $\mu$ m. (B) Quantification of the ratio of Aurora B intensity to CENP-C intensity on all chromosomes, chromosome 15, chromosome 21 and rob(15;21)c. Statistical analysis done by one-way ANOVA with Tukey's multiple comparisons test. ns = not significant. n = 239 chromosomes for All, n = 6 chromosomes for Chr 15, n = 6 chromosomes for Chr 21, n = 6 chromosomes for rob(15;21)c.

Although results in Figure 4.10 do not support the hypothesis, I thought to confirm this finding with other CPC components at the inner centromere in prometaphase-like chromosome spreads. Figure 4.11A shows an example of INCENP staining on rob(15;21)c and the quantification of these images in Figure 4.11B show no significant difference between rob(15;21)c (n = 4) Aurora B to CENP-C ratio and that of chromosome 15 (n = 3), chromosome 21 (n = 4) and all other chromosomes (n = 153) (supporting the findings in Figure 4.10B).



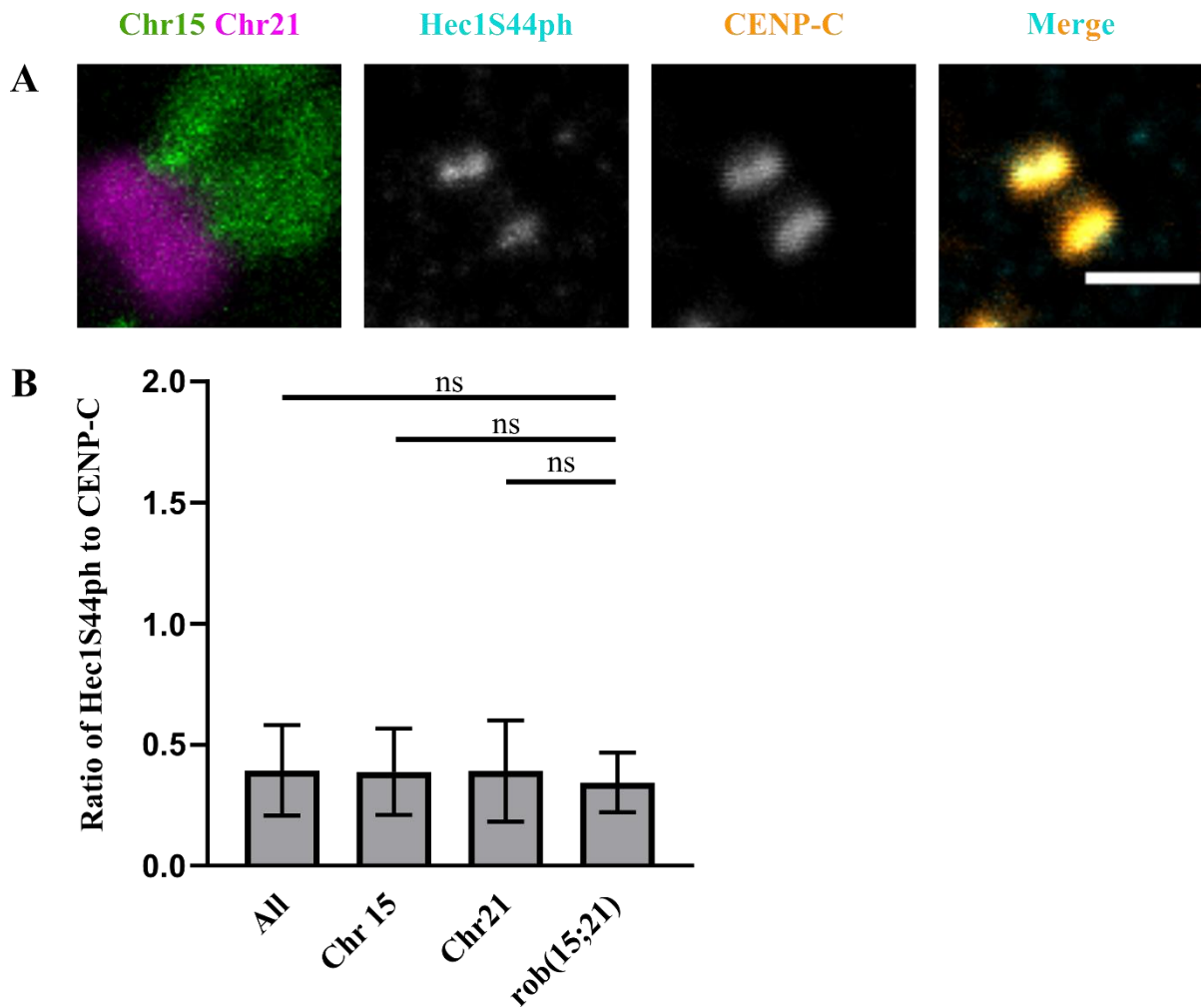
**Figure 4.11. INCENP staining on rob(15;21)c is not aberrant.** (A) Example rob(15;21)c chromosome with INCENP and CENP-C staining. Scale bar = 2  $\mu$ m. (B) Quantification of the ratio of INCENP intensity to CENP-C intensity on all chromosomes, chromosome 15, chromosome 21 and rob(15;21)c. Statistical analysis done by one-way ANOVA with Tukey's multiple comparisons test. ns = not significant. n = 153 chromosomes for All, n = 3 chromosomes for Chr 15, n = 4 chromosomes for Chr 21, n = 4 chromosomes for rob(15;21)c.

Figure 4.12 shows staining of a further component of the CPC. Figure 4.12A shows an example image of Survivin staining at rob(15;21)c and Figure 4.12B provides the quantification to go alongside. Supporting the results in Figure 4.10B and Figure 4.11B, Figure 4.12B highlights that there is no significant difference between the Survivin to CENP-C ratio on rob(15;21)c (n = 7) when compared to chromosome 15 (n = 7), chromosome 21 (n = 7) or all other chromosomes (n = 272).



**Figure 4.12. Survivin staining on rob(15;21)c is not aberrant.** (A) Example rob(15;21)c chromosome with Survivin and CENP-C staining. Scale bar = 2  $\mu$ m. (B) Quantification of the ratio of Survivin intensity to CENP-C intensity on all chromosomes, chromosome 15, chromosome 21 and rob(15;21)c. Statistical analysis done by one-way ANOVA with Tukey's multiple comparisons test. ns = not significant. n = 272 chromosomes for All, n = 7 chromosomes for Chr 15, n = 7 chromosomes for Chr 21, n = 7 chromosomes for rob(15;21)c.

Figure 4.10 highlighted how the levels of Aurora B were similar on rob(15;21)c compared with other chromosomes. However, to test if the activity of Aurora B was different on rob(15;21)c, I also stained for a downstream Aurora B phosphorylation site on the outer kinetochore protein Hec1. Multiple sites on Hec1 are phosphorylated by Aurora B to help destabilise microtubule-kinetochore attachments<sup>79,278</sup>. One known modification is the phosphorylation of serine 44 on Hec1 (Hec1S44ph). In Figure 4.14 I stained this phosphorylation site; an example rob(15;21)c image is shown in Figure 4.14A and quantification shown in Figure 4.14B. These data indicate that the ratio of Hec1S44ph to CENP-C on rob(15;21)c (n = 7) is not significantly different to that on chromosome 15 (n = 8), chromosome 21 (n = 8) or all other chromosomes (n = 329).



**Figure 4.13. Hec1S44ph staining on rob(15;21)c is not aberrant.** (A) Example rob(15;21)c chromosome with Hec1S44ph and CENP-C staining. Scale bar = 2  $\mu$ m. (B) Quantification of the ratio of Hec1S44ph intensity to CENP-C intensity on all chromosomes, chromosome 15, chromosome 21 and rob(15;21)c. Statistical analysis done by one-way ANOVA with Tukey's multiple comparisons test. ns = not significant. n = 329 chromosomes for All, n = 8 chromosomes for Chr 15, n = 8 chromosomes for Chr 21, n = 7 chromosomes for rob(15;21)c.

Figure 4.10, Figure 4.11, Figure 4.12 and Figure 4.13 do not support the hypothesis that aberrant CPC activity on rob(15;21)c is a driver behind its high mis-segregation rate. Evidently, all tested CPC components are found at the inner centromere of rob(15;21)c at normal levels. By using Hec1S44ph as a proxy for the activity of Aurora B, I show that not only is the CPC localised correctly, but it is also likely functioning as expected.

#### 4.2.4.4 *Metaphase plate alignment of rob(15;21)c*

In order to promote mitotic fidelity, chromosomes align on the cell equator during the transition from prometaphase to metaphase, this is termed congression<sup>47</sup>. Chromosomes must start poleward movement during anaphase from the same starting position to prevent dispersion and uneven distribution of chromosomes. Two different mechanisms exist to move chromosomes to the equator<sup>279–281</sup>. If the chromosome sits between the newly formed spindle poles in prometaphase then it quickly establishes biorientation through end-on microtubule attachments and congression occurs through growth and shrinkage of microtubules. If the chromosome is located closer to the spindle poles then lateral microtubule attachments form between microtubules and kinetochores. Lateral attachments allow movement of chromosomes toward the equator (driven by chromokinesins and CENP-E), where the chromosome will bi-orient, converting lateral attachments to end-on attachments<sup>39</sup>.

When a chromosome is closely located to one spindle pole then kinetochores are more prone to attach to microtubules emanating from the closer pole (as there is a higher microtubule density). This results in erroneous microtubule-kinetochore attachments. With the help of Aurora B, the kinase Aurora A (which is concentrated at spindle poles) prevents the persistence of these erroneous attachments by destabilising kinetochore-microtubule attachments<sup>282</sup>. Peripheral chromosomes can then travel along the microtubules toward the equator through lateral attachments.

Chromosomes that align late to the equator may not have time to properly establish biorientation (through lateral to end-on conversion) before anaphase. It has been shown that these late aligners can mis-segregate due to their lack of biorientation, frequently entering micronuclei. Late alignment is therefore both a cause and consequence of aberrant biorientation<sup>39</sup>.

I hypothesise that the actively dicentric nature of rob(15;21)c would promote more frequent aberrant microtubule-kinetochore attachments and, even with a functioning error correction pathway (involving Aurora A and Aurora B), congression of rob(15;21)c would be delayed. Therefore, evidence that rob(15;21)c is aligned late on the metaphase plate compared to other chromosomes would support the idea that this dicentric chromosome is susceptible to incorrect microtubule-kinetochore attachment. In addition, if rob(15;21)c congression is delayed, it may have less time to resolve persisting erroneous attachments at the metaphase plate before the SAC is satisfied and anaphase can begin. Persistent erroneous attachments at rob(15;21)c would

increase the likelihood of this chromosome to mis-segregate into a micronucleus, and in turn facilitating chromothripsis.

To test the above hypothesis, L995 and L996 cells were synchronised into metaphase and stained with FISH probes for chromosome 15q and chromosome 21q as in section 2.7. Large tiled images were acquired in order to capture images of all metaphase-like cells. These images were analysed using a high-throughput analysis pipeline as described in section 2.15.6. This involved the use of a FIJI macro to identify cells that have Dapi staining characteristic of a metaphase cell (manual analysis confirmed that metaphase-like cells where a chromosome was off the plate were not preferentially excluded from this dataset). The output images were manually analysed to count metaphase-like cells with chromosomes that were off the plate (defined by a dapi-stained chromosome that was either separate from the plate or attached to the plate but protruding significantly compared with the majority of chromosomes in that metaphase), and of those, which were chromosome 15, chromosome 21 and rob(15;21)c.

Figure 4.14A shows a confocal image of an example metaphase-like cell with rob(15;21)c failing to align on the metaphase plate (as shown by the close apposition of the green chromosome 15q FISH probe and the magenta chromosome 21q FISH probe). Figure 4.14B is quantification from the previously described high-throughput analysis of metaphase-like cells. Despite observing 394 metaphase-like cells with 563 late aligning chromosomes, all chromosomes of interest were infrequently seen off the plate. As with mis-segregation rates, if the chance of any particular chromosome being off the plate was equal, then the expected rate of chromosome 15, chromosome 21 or rob(15;21)c aligning late would be 2.2% each (1 in 45). In practice, only 2/563 (0.36%) were chromosome 15, 0/563 were chromosome 21 and 10/563 (1.8%) were rob(15;21)c. Whilst all three chromosomes of interest were present in mis-alignments at lower rates than expected, rob(15;21)c was significantly higher than the internal controls, chromosome 15 and chromosome 21.

The results in Figure 4.14 provide some support for the hypothesis that erroneous microtubule-kinetochore attachments on dicentric rob(15;21)c may cause late-alignment or mis-alignment of the Robertsonian chromosome. In addition, this could be part of the process driving a high mis-segregation rate in this chromosome and therefore causing carriers to have a high predisposition to chromothripsis and iAMP21-ALL.

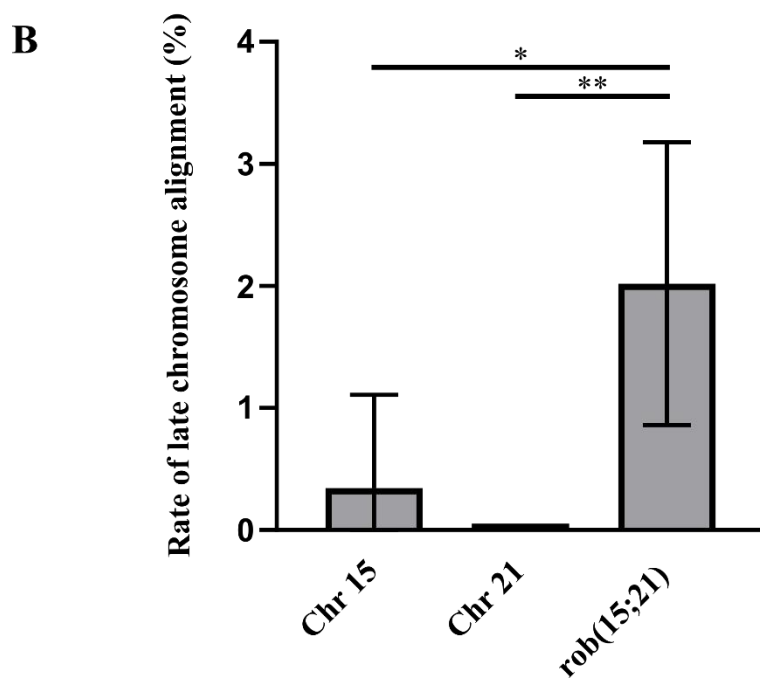
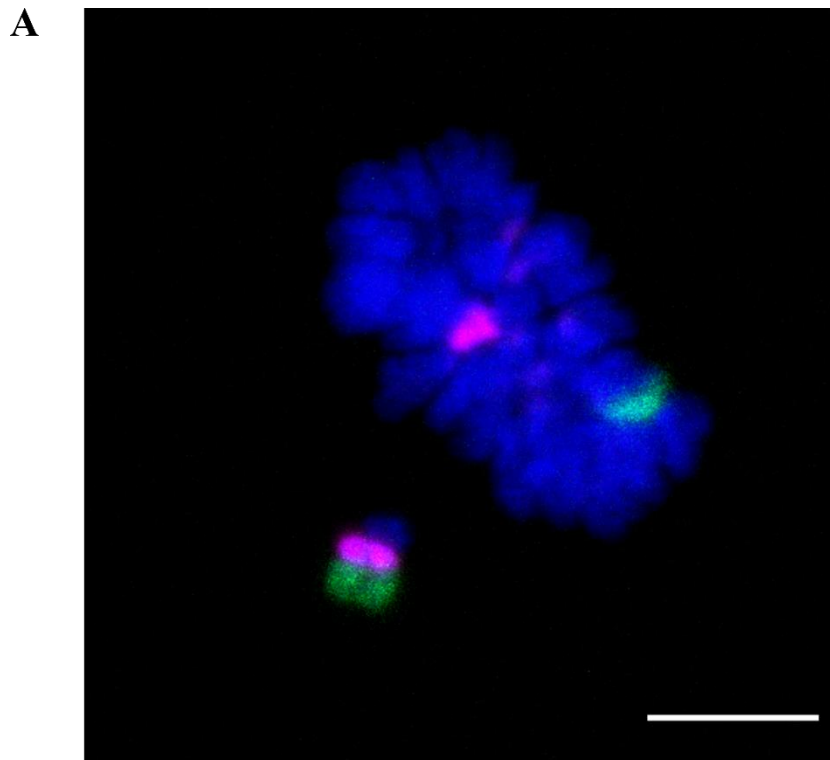


**Figure 4.14. rob(15;21)c mis-aligns on the metaphase plate.** (A) Example image of metaphase-like cell with rob(15;21)c off the plate. FISH probes stained for chromosome 15 (green) and chromosome 21 (magenta). Scale bar = 5  $\mu$ m. (B) Quantification of 2,270 metaphase-like cells plotted to show the chance of an off-plate chromosome to be chromosome 15, chromosome 21 or rob(15;21)c. Statistical analysis done by one-way ANOVA with Šídák's multiple comparison test. \* = p-value  $\leq$  0.05, \*\* = p-value  $\leq$  0.01.

### 4.3 Discussion

In this chapter I have characterised some of the behaviours of the Robertsonian chromosome rob(15;21)c in L995 and L996 cells. By studying rob(15;21)c containing lymphoblastoid cell lines through various mitotic processes, we fill in some of the gaps in knowledge in the mechanism giving a dicentric rob(15;21)c chromosome a large increased chance of undergoing chromothripsis.

In Chapter 3, it was shown that rob(15;21)c is often actively dicentric. These actively dicentric kinetochores may all have the ability to bind microtubules (as suggested in section 3.2.9). We hypothesised that the dicentric nature of rob(15;21)c would frequently allow aberrant microtubule attachments and in turn drive mis-segregation. This hypothesis was supported by the results in Figure 4.1 and Figure 4.3 which showed that rob(15;21)c is present in ~16-17% of mis-segregations. This is significantly high when compared with the expected rate (2.2%) and with internal control chromosome mis-segregation rate; chromosome 15 (~2-4%), chromosome 21 (~1-3%).

As the rate of rob(15;21)c mis-alignment on the metaphase plate was only ~1.8% (although significantly higher than chromosome 15 and chromosome 21) and the rate of rob(15;21)c mis-segregation is ~16-17% the mis-alignment of rob(15;21)c on the metaphase plate is not a prerequisite for mis-segregation. However, this statement assumes that our calculated rate (~1.8%) for mis-alignment is correct, though in practice there are multiple reasons why this may not be true. These results come from fixed cell experiments, for a more accurate determination of the true rate of mis-alignment, rob(15;21)c could be tracked through live-cell imaging. For mis-segregation experiments we used nocodazole followed by washout to enrich cells in anaphase and telophase. As nocodazole affects microtubule dynamics, and causes a mitotic delay, it is known to artificially increase the rate of chromosome mis-segregation. Whilst it has been shown that the mis-segregation induced by nocodazole is non-random in RPE-1, BJ, HUVEC and FNE1 cells, there is no clear evidence to suggest that either chromosome 15 or chromosome 21 mis-segregate at a higher rate than expected due to nocodazole<sup>95,97</sup>. This is confirmed in practice by our results that show low rates of chromosome 15 and chromosome 21 mis-segregation after nocodazole synchronisation (Figure 4.3). Although it cannot be ruled out that nocodazole is having some unknown effect on rob(15;21)c that causes chromosome specific mis-segregation, we deem it unlikely. Therefore, the observed mis-segregation rate may be higher than in an

unperturbed cell, but it is still significantly high compared to chromosome 15 and chromosome 21 in the same system.

Whilst it is difficult to predict an expected rate of one sister versus two sister mis-segregation, we would presume that the most likely outcome in a mis-segregation event would be for only one sister chromatid to be involved. Once centromeric cohesin is cleaved, it is fair to presume that sister chromatids act independently. Contrary to this, the findings in Figure 4.4 show how in approximately half of the events involving rob(15;21)c mis-segregation, both sister chromatids are involved. This suggests that there is a mechanism driving the co-mis-segregation of rob(15;21)c sister chromatids. This result is of high interest; sequencing from Li *et al.* predicted that two copies of rob(15;21)c are often present in the chromothriptic event that drives iAMP21-ALL<sup>145</sup>. Here we have evidence of a potential early step in the mechanism that facilitates this. Co-mis-segregation of rob(15;21)c sister chromatids may place two copies simultaneously into an environment that has previously shown to be vulnerable to chromothripsis (e.g. micronuclei or chromosome bridges)<sup>94,154,156,171</sup>.

As with all other results in this thesis that compare the cell lines L995 (from iAMP21-ALL patient) and L996 (from unaffected, identical twin patient), no obvious difference was seen between the mis-segregation rates of rob(15;21)c in cells derived from the patient that developed cancer and the twin that did not. The rob(15;21)c mis-segregation rate is clearly elevated in both twins and therefore it is likely that just the presence of this chromosome is enough to cause elevated mis-segregation and not some inherent genetic or other difference in the twin who developed cancer. It is very possible that there is no mechanistic reason why one identical twin carrier of rob(15;21)c developed cancer and the other did not, but rather it may be down to the stochastic nature of chromosomal rearrangements from chromothripsis. These rearrangements may often cause cell death, but infrequently confer a selective advantage that drives cancer progression.

The rate at which rob(15;21)c mis-segregates appears to be similar (and high) at all tested passages (Figure 4.5). We initially hypothesised that in a population of cells where rob(15;21)c had a predominantly active monocentric phenotype, the rate of rob(15;21)c mis-segregation would be low. However, results in section 3.2.7 showed that in L995 and L996 cells, rob(15;21)c is predominantly actively dicentric in all tested passages and thus our hypothesis could not be easily tested.

In Chapter 3, it was shown that the most frequent centromeric phenotype for rob(15;21)c is to be actively dicentric. Whilst the results in Figure 4.3 show that rob(15;21)c mis-segregates at a higher rate than expected, the most common segregation phenotype is still that rob(15;21)c segregates accurately; 2.2% (147/6581) of all anaphases involve rob(15;21)c mis-segregation in L995 and 1.7% (83/4939) in L996. Comparing the rate of mis-segregation vs. the rate of actively dicentric rob(15;21)c (~70% of rob(15;21)c are actively dicentric in L995 and ~60% in L996) would suggest that not all actively dicentric rob(15;21)c chromosomes lead to mis-segregation. Clearly it is not as simple as active dicentricity always leads to erroneous microtubule-kinetochore attachments which always leads to mis-segregation. The mechanism causing rob(15;21)c mis-segregation must be more complex.

Micronuclear environments have been reported as a precursor to chromothripsis<sup>154,181,260,283</sup>. We found that, in interphase FISH experiments from blood samples (affected twin in long term remission) of these rob(15;21)c carriers, micronuclei can be seen that contain rob(15;21)c (Figure 4.6). Recent work to better understand the components of the micronuclear membrane suggest that micronuclei in the midzone fail to incorporate non-core proteins (including nuclear pore complexes) due to physical obstruction from the spindle or by Aurora B dependent regulation<sup>173,178</sup>. In these micronuclei with imperfect nuclear envelopes, there is defective DNA replication coupled with DNA damage followed by further, extensive DNA damage upon re-entry into mitosis<sup>105,156,171</sup>. The results in Figure 4.7 indicate that, in cells that carry (and frequently mis-segregate) rob(15;21)c, micronuclei exist that assemble core but not the majority of non-core nuclear envelope proteins. It was not possible to stain all nuclear envelope proteins of interest simultaneously with FISH probes for rob(15;21)c detection. Therefore, the micronuclei in Figure 4.7 images do not necessarily contain rob(15;21)c, although these images represent midzone micronuclei in cells that we have shown frequently mis-segregate rob(15;21)c. From this, we propose that rob(15;21)c also enters these aberrant micronuclei. These data support our overarching hypothesis that the dicentric nature of rob(15;21)c leads to mis-segregation into an environment shown to be susceptible to chromothripsis (a micronucleus).

The rest of this chapter focused on trying to understand the reason for such elevated mis-segregation rates in rob(15;21)c compared to chromosome 15 and chromosome 21. In particular, trying to understand how both sisters are frequently mis-segregating together.

One mechanism for frequent mis-segregation we assessed was the possibility of aberrant error correction on rob(15;21)c. We hypothesised that the abnormal centromeric structure of rob(15;21)c caused atypical localisation of the CPC at the inner centromere. However, the results in Figure 4.10, Figure 4.11, Figure 4.12 and Figure 4.13 provide strong evidence to oppose this hypothesis. It appears that the amount of CPC components, Aurora B, INCENP and Survivin at rob(15;21)c inner centromere are not significantly different from that at chromosome 15 or chromosome 21. Also, by analysing a target phosphorylation site of Aurora B, Hec1S44ph, I showed that the activity of the CPC is also likely normal at rob(15;21)c.

Although CPC activity appears to be normal at rob(15;21)c, this does not necessarily imply that it is able to resolve all erroneous attachments. It is possible that, due to the two kinetochores on each sister chromatid of rob(15;21)c, more erroneous microtubule-kinetochore attachments are formed than on normal monocentric chromosomes. For these attachments to be resolved in a timely manner, rob(15;21)c may need an increased level of CPC activity. Therefore the ‘normal’ level of CPC activity that we observe on rob(15;21)c may not be enough to remove all mis-attachments and allow movement of rob(15;21)c to the metaphase plate before the SAC is satisfied and anaphase begins. Alternatively, the geometry of mis-attachments on dicentric chromosomes may prevent the error correction machinery from working effectively. Merotelic attachments cause chromosome twisting<sup>284,285</sup>. As it has been proposed that Aurora B activity is regulated by tension at the kinetochores<sup>286,287</sup>, it is possible that aberrant microtubule-kinetochore attachments at the dicentric rob(15;21)c chromosome cause an abnormal chromosome morphology, in turn compromising tension-dependent Aurora B regulation.

The results shown in Figure 4.14 support this hypothesis. Although n numbers are somewhat low, rob(15;21)c seems to be mis-aligned at a significantly higher rate than chromosome 15 or chromosome 21. In these experiments, the chance of a mis-aligning chromosome to be chromosome 15, chromosome 21 or rob(15;21)c were all lower than expected if all chromosomes have an equal chance of mis-segregating. It is possible that our method of metaphase synchronisation (Nocodazole washout) is inducing mis-alignment in a non-random manner. Worrall *et al.* reported that a similar Nocodazole washout protocol caused non-random lagging of chromosomes and ultimately non-random aneuploidy<sup>95</sup>. I propose that we observed a similar phenotype here. A large portion of the mis-aligned metaphase chromosomes that we saw may be from premature sister chromatid separation caused by cohesion fatigue on chromosomes 1 and 2 (caused by nocodazole arrest – as shown by Worrall *et al.*). Nevertheless, we have the benefit of having stained normal chromosome 15 and normal chromosome 21 as

internal controls. These helped us highlight how, comparatively, rob(15;21)c is mis-aligning significantly more frequently than its two homologous chromosomes. As these results come from fixed imaging experiments it is not possible to tell whether these events are late aligning chromosomes that will eventually reach the metaphase plate before anaphase, or whether anaphase can commence while rob(15;21)c remains off the plate. To answer this question we had hoped to do live cell imaging to study the dynamics of rob(15;21)c throughout mitosis. In Chapter 5 I will discuss why this has not yet been possible.

Aberrant cohesion on rob(15;21)c was another obvious mechanism that needed to be tested; particularly as cohesion is a factor that could be physically linking sister chromatids together and allowing co-mis-segregation of both rob(15;21)c sisters. We had two opposing cohesion hypotheses. 1) The two centromeres of rob(15;21)c were recruiting a high amount of centromeric cohesin which could not be cleaved in time for proper anaphase separation. 2) The two centromeres of rob(15;21)c prevent proper cohesin recruitment and therefore a reduced amount of cohesin at rob(15;21)c is vulnerable to cohesion fatigue. This would cause premature sister chromatid separation, but as these sister chromatids are dicentric they may still form incorrect biorientation after separation, therefore allowing single sister mis-segregation. If single sister mis-segregation rates were high enough, then the most likely outcome would be that both sisters mis-segregate (and sometimes into the same daughter cell). However, the mis-segregation rates that we observe in Figure 4.3 and Figure 4.4 (~98% of all segregations do not involve a mis-segregating rob(15;21)c, but those that do, contain one sister chromatid half of the time) do not support this hypothesis. It seems more likely that, if there is aberrant cohesion at rob(15;21)c, then it would be an increased amount, or persistence, of cohesin that forces sister chromatids to be stuck together too long, causing co-mis-segregation of sisters (hypothesis 1). As staining cohesin by immunofluorescence was difficult, only a small number of images could be captured of cohesin staining on rob(15;21); unfortunately not enough to accurately quantify. However, the images in Figure 4.9 suggest that the quantity and location of cohesin is broadly normal on rob(15;21)c when compared with chromosome 15 and chromosome 21 in the same cell. The next steps to confirm that cohesion is not the mechanism driving rob(15;21)c mis-segregation would be to assess Shugoshin staining (to check for enhanced protection of centromeric cohesin) and to check the timing of centromeric cohesin cleavage via live cell imaging.

One further mechanism that we hypothesised as potentially influencing rob(15;21)c mis-segregation was this chromosome's interphase nuclear location. Recent studies have shown

how a chromosome with a peripheral nuclear location in interphase can frequently end up behind the spindle poles during mitosis, creating a greater distance to travel to the metaphase plate, and in turn causing an increased mis-segregation rate<sup>98,99</sup>. Acrocentric chromosomes are usually located near to the centre of the nucleus due to interactions between the Nucleolus Organiser Regions (NORs) on acrocentric p-arms and the nucleolus. However, the Robertsonian chromosome rob(15;21)c has lost most of the chromosome 15 and chromosome 21 p-arms. We hypothesised that this p-arm loss gave rob(15;21)c a nuclear location that was much more peripheral than normal acrocentric chromosomes, and that this nuclear location promoted mis-segregation of rob(15;21)c.

High throughput imaging and analysis allowed for the study of thousands of interphase cells. Whilst there were small, but significant differences in the interphase nuclear location of chromosome 15, chromosome 21 and rob(15;21)c, they did not suggest that rob(15;21)c was more peripheral in the nucleus during interphase. In fact, rob(15;21)c was more central than chromosome 15 and chromosome 21. The large n numbers in this work provide strong evidence to oppose our hypothesis that a preferential peripheral nuclear location of rob(15;21)c facilitates mis-segregation. One disadvantage to this experiment is that centromeric FISH probes had to be used to produce more tight puncta in interphase (compared to arm FISH probes which were too disperse due to the decondensed nature of interphase chromatin). It is possible that the centromere of a chromosome does not represent its nuclear location very well and possibly using arm FISH probes with a shorter length may have given a different result. Another drawback of these experiments was that the experimental pipeline was not validated against known chromosomes with clearly different nuclear locations. These experiments were not done as it proved difficult to identify a control chromosome that would undoubtedly be very peripheral. Whilst the consensus is that larger chromosomes are more peripheral, multiple studies contradict each other on this point<sup>98,266,288–290</sup>. This is likely something which differs between cell lines and, as no work has previously been done on the L995 and L996, we thought that experiments in these cells with a chosen control chromosome may provide uncertain results.

In summary, the work in this chapter has helped to better understand why the Robertsonian chromosome rob(15;21)c has a high predisposition to undergoing chromothripsis. Evidently, rob(15;21)c has a high propensity to mis-segregate in mitosis. This chapter provides support to the model that these frequent mis-segregations place rob(15;21)c in a micronuclear environment that is susceptible to chromothripsis. The results suggest that both sisters of

rob(15;21)c mis-segregate together frequently. This provides a potential mechanistic reason why two copies of this chromosome are seen in chromothriptic events that lead to iAMP21-ALL (as opposed to, or in addition too, the possible requirement for two copies being driven by selection). The underlying mechanism that is driving frequent mis-segregation of both rob(15;21)c sister chromatids is not yet fully understood. This chapter has provided evidence that suggests against some possible mechanisms that could have been driving mis-segregation, including aberrant error correction/CPC recruitment to rob(15;21)c, aberrant cohesion at the rob(15;21)c centromeres, and a peripheral, mis-segregation enabling, nuclear rob(15;21)c location. Although results in this chapter showed normal recruitment to rob(15;21)c of proteins involved in error correction, this hypothesis for mis-segregation is not completely resolved. It has been highlighted in this chapter that rob(15;21)c may be aligning late onto the metaphase plate. I hypothesise that a 'normal' amount of error correction proteins are not enough to compensate for the increased number of erroneous microtubule-kinetochore attachments that are occurring at the dicentric centromeres of rob(15;21)c.

There is now evidence that highlights how rob(15;21)c is segregating defectively. However, all experiments thus far have been using fixed cells for imaging studies. In Chapter 5 I will describe attempts to use live cell imaging to study the dynamics of rob(15;21)c throughout the cell cycle, in order to gain more information on the process driving rob(15;21)c to chromothripsis.

## Chapter 5: Tagging rob(15;21)c and live imaging of L995 and L996 cells

---

### 5.1 Introduction

In Chapter 3 I showed that the Robertsonian chromosome rob(15;21)c is frequently actively dicentric and in Chapter 4 I showed that this led to a high rate of this chromosome mis-segregating. It is now obvious that rob(15;21)c segregates aberrantly, though all experiments described thus far have been in a fixed cell environment. To better understand what happens to this chromosome both before and after mis-segregation, we hoped that live cell imaging experiments with a marker for the rob(15;21)c chromosome would be informative.

Whilst developing the methods required to study rob(15;21)c in live L995 and L996 cells, it became apparent that multiple challenges stood in the way before these experiments could be successful. Using lymphoblastoid cell lines brought about two problems. These suspension cells move around a lot and do not adhere well to glass or plastic, as would be necessary for live imaging over a full cell cycle. This cell type is also notoriously difficult to transfect by most conventional methods<sup>291,292</sup> and alternative approaches would have to be optimised in order to express fluorescent proteins in L995 and L996 cells.

To fluorescently tag rob(15;21)c, we intended to use a technique that makes use of a catalytically dead Cas9 to target fluorescently tagged proteins to specific chromosomal loci (CRISPRainbow)<sup>293</sup>. However, the optimisation of this technique for use in my system also brought about challenges.

The aim of the work described in this chapter was to study the dynamics of rob(15;21)c throughout a cell cycle, specifically observing why this chromosome undergoes frequent mis-segregation and what happens to it after it has mis-segregated. To reach this aim, a variety of techniques to promote adherence of the lymphoblastoid cell lines L995 and L996 to imaging dishes were assessed. In addition, with use of the CRISPRainbow system optimised for lentiviral transduction, I aimed to fluorescently tag chromosome 15, chromosome 21 and rob(15;21)c. By tagging the centromere of chromosome 15 in green and the centromere of chromosome 21 in red, we would be able to distinguish the rob(15;21)c chromosome through the colocalisation of red and green foci at the dicentric centromere. However, many challenges arose that were difficult to resolve and as time was limited, only some problems could be addressed. This chapter shows the experiments used to troubleshoot these problems and

proposes some modifications that could be made in the future should these experiments be resumed.

## 5.2 Results

### 5.2.1 Problem 1 – L995/6 move around too much for live imaging

Lymphoblastoid cells are non-adherent and therefore usually move around in suspension. When unprovoked, these cells settle to the bottom of a dish. It was these settled cells that we attempted to image, however they still moved somewhat due to their lack of adhesion to the glass dish. Imaging these cells over time proved difficult due to this movement. To track a cell through an entire cell cycle it must stay in frame and in focus long enough for a cell to go through G1, S phase, G2 and mitosis. As can be seen in Figure 5.1, lymphoblastoid cells (in this case L995) move around considerably on an untreated glass surface. Ideally, to track chromosome movements in L995 and L996, cells should be imaged over 24 hours. However, Figure 5.1 shows that in just 3 hours these cells move so much that individual cells cannot be tracked.

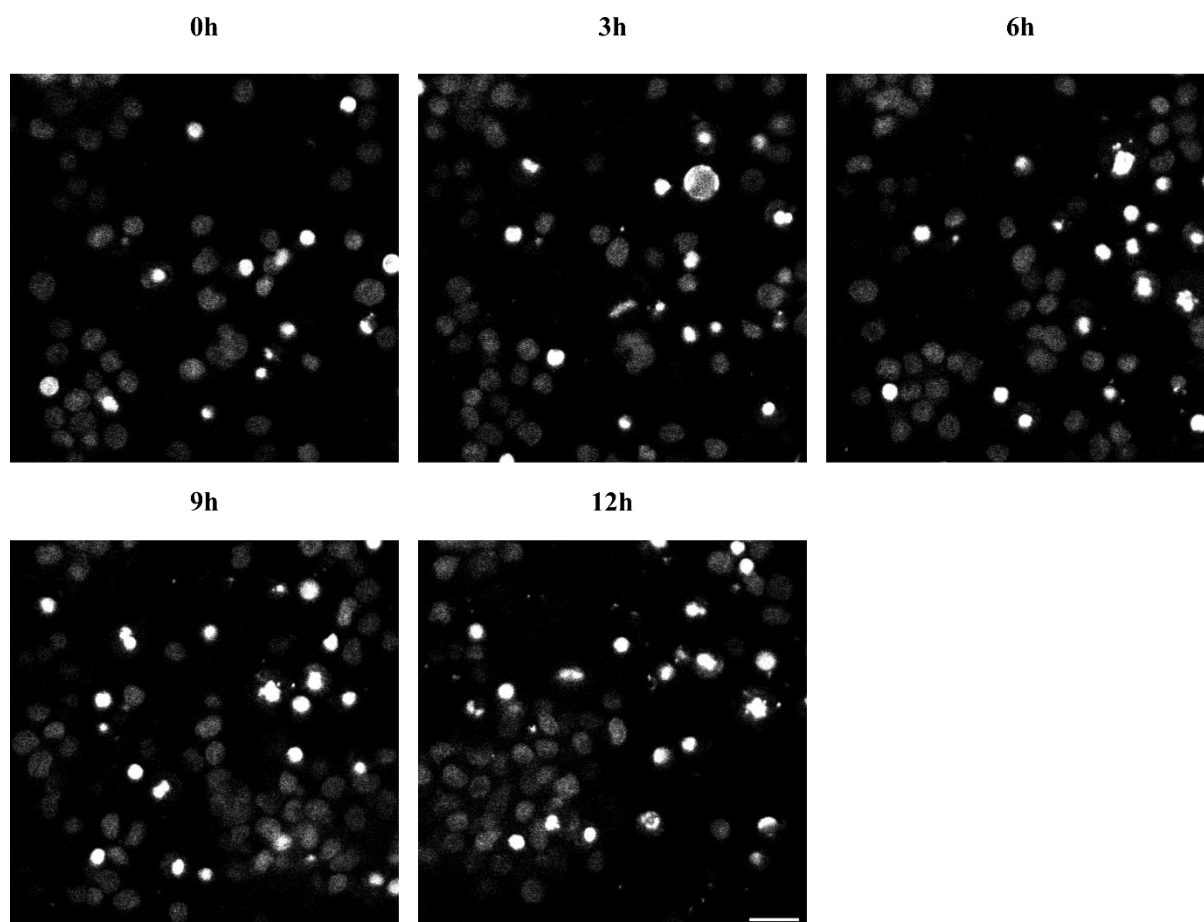


**Figure 5.1. Lymphoblastoid cells are difficult to live image due to their movement.** Live imaging of L995 cells stained with SiR-DNA. Images shown in 3-hour intervals over 12h. Scale bar = 20  $\mu\text{m}$

The amount of cell movement seen in Figure 5.1 is not compatible with studying chromosome dynamics throughout a cell cycle. Generally, for live-cell imaging, an alternative to hindering cell movement would be to track individual cells such that the imaging frame moves with the cell. However, as we are interested in mis-segregation events that are somewhat rare, choosing one cell to track in advance would be inefficient. Ideally, we would be able to have a wider field of view in order to image multiple cells in one frame, therefore increasing the chances of seeing an event of interest. Therefore to image the same population of cells over time, a method must be developed to inhibit or limit cell movement. Various methods currently exist for this purpose. In Figure 5.2, poly-L-lysine (Figure 5.2A) or Cell-Tak (Figure 5.2B) are used to create an adhesive surface on the dishes used for imaging lymphoblastoid cells, with the hope of physically sticking cells down onto the dish, in order to hinder movement.

Poly-L-lysine is an attachment factor that promotes cell adherence through the electrostatic interactions between the positively charged polymer and the negatively charged cell membrane. Cell-Tak is a protein solution taken from the marine mussel *Mytilus edulis* and is a component of the secretion that allows mussels to stick to solid structures<sup>294</sup>. We proposed that creating a layer of either poly-L-lysine or Cell-Tak on glass bottomed dishes used for imaging would allow greater cell adhesion and in turn reduced movement of lymphoblastoid cells.

In these experiments, other measures were simultaneously taken to further reduce cell movement. This included reducing volume of media in the culture dish and slowing the speed of stage movement such that there was less disruption between imaging points.

Figure 5.2 shows that neither poly-L-lysine nor Cell-Tak made an improvement in cell adherence. As with untreated dishes (Figure 5.1), Figure 5.2A (poly-L-lysine) and Figure 5.2B (Cell-Tak) show that cells have both moved out of frame and moved out of focus within the imaging time. Further, it appeared that both of these treatments caused prolific cell death. This is shown by the abnormal nuclear morphology represented by SiR-DNA staining at all time points. The timepoint 0 h was from the start of imaging and not from the seeding of the cells. The cells at time 0 h had been in contact with the poly-L-lysine coated or Cell-Tak coated surface for at least 1 hour before the time point 0 h, hence explaining the presence of dead cells even at this time point. It has previously been reported that poly-L-lysine mediated cell adhesion can cause pyroptosis<sup>295</sup>. It is possible that the increased cell death seen in Figure 5.2 has been caused by this mechanism. Ultimately, the use of poly-L-lysine or Cell-Tak are clearly not

efficient methods for reducing cell movement for long-term live cell imaging of lymphoblastoid cells.

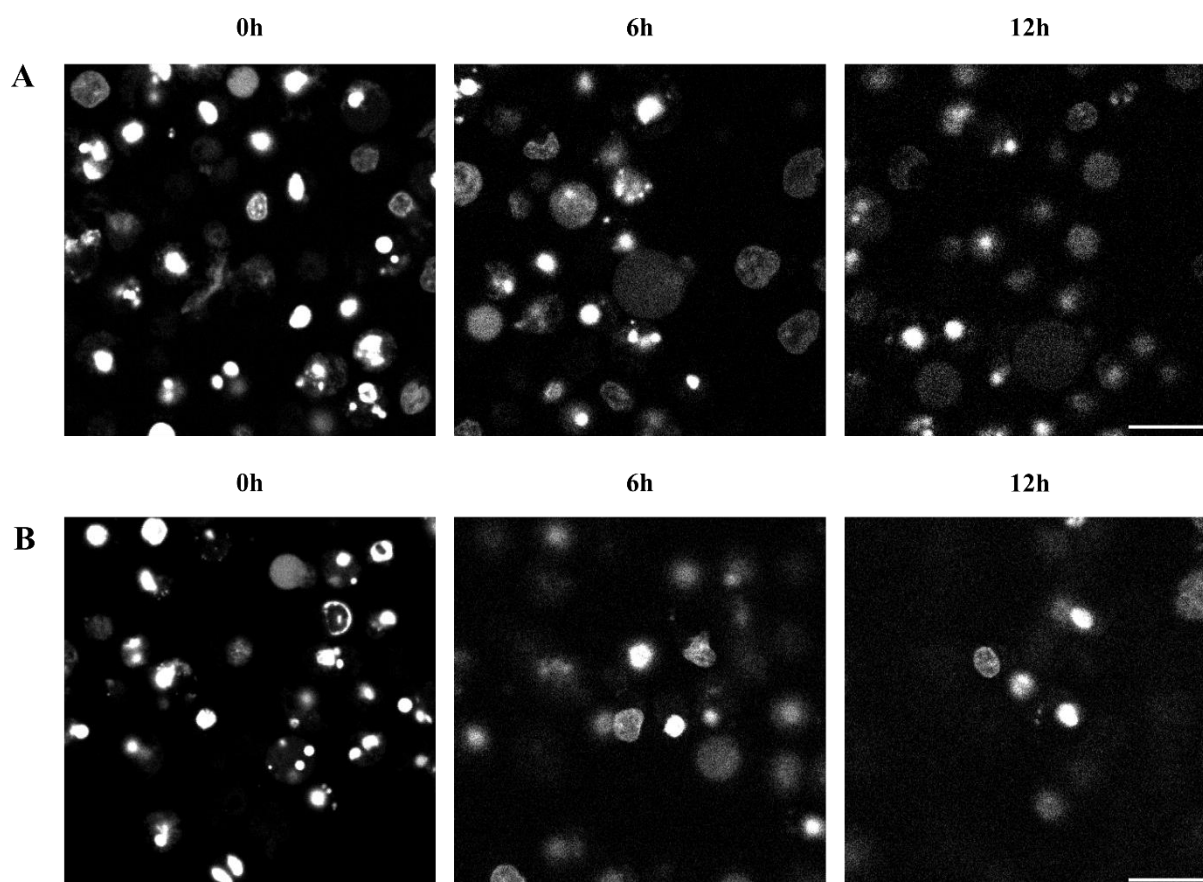


**Figure 5.2. Poly-L-Lysine and Cell-Tak do not efficiently stick down lymphoblastoid cells.** (A) Live imaging of L995 cells on a PLL treated dish. (B) Live imaging of L995 cells on a Cell-Tak treated dish. Images taken every 5 minutes but shown at every 6h to highlight death and movement over time. Scale bars = 20  $\mu\text{m}$ .

One alternative method that was also tested to improve cell adherence was the use of pre-coated imaging dishes. Thermo Scientific plates with CC2 surface coating were used to assess cell division over time. The CC2 surface modification was recommended by Thermo Fisher Scientific technical support and is stated to be similar to Poly-D-lysine and superior for cell adhesion (Thermo Fisher Scientific). Figure 5.3A shows how this method did not produce significant improvements over a long time (12 hours). However, Figure 5.3B shows that these plates did somewhat reduce cell movement over a shorter time (60 minutes). It can be seen that a single cell can be tracked going through mitosis when imaging with 15 minute intervals over 60 minutes. However, the daughter cells leave the frame as time increases, preventing the tracking of these cells for a full cell cycle.

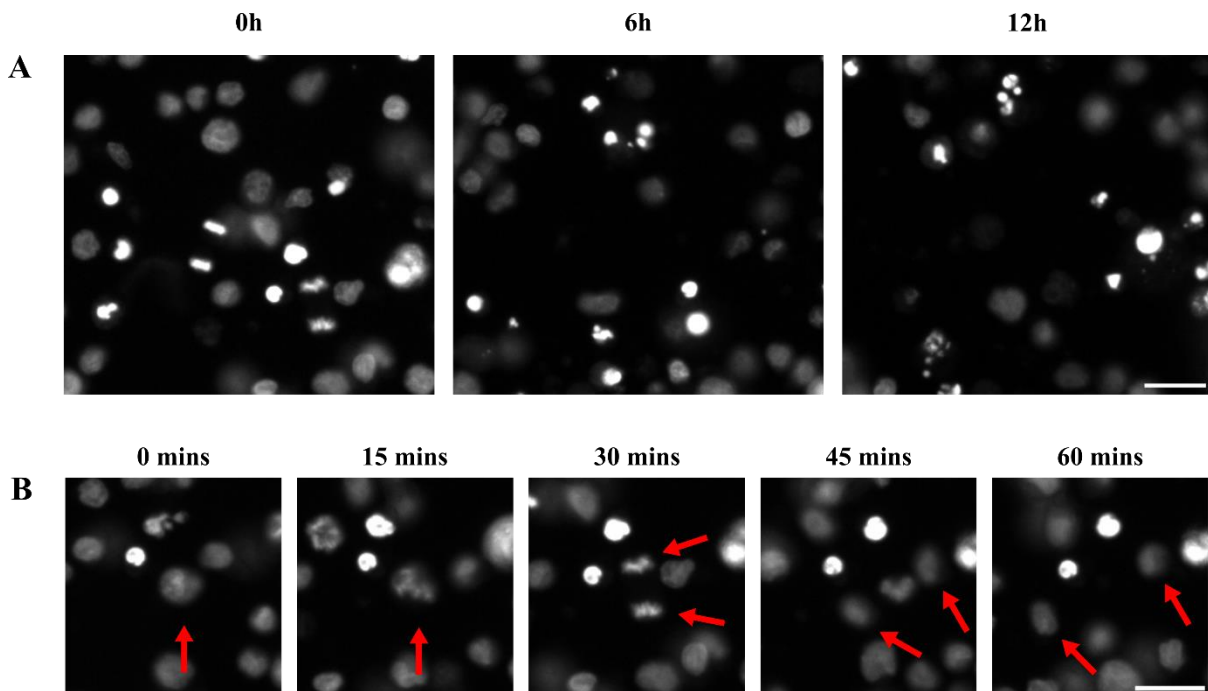


**Figure 5.3. Lymphoblastoid cell adhesion is slightly improved by a CC2 coated surface.** Live imaging of L995 cells on a CC2 coated dish. (A) Images shown in 6h intervals to highlight cell movement over a long time period. (B) Images shown in 15 minute intervals to highlight that a cell division can be tracked across a short time period.

Figure 5.1, Figure 5.2 and Figure 5.3 highlight the difficulty of live imaging lymphoblastoid cells over a full cell cycle. Whilst pre-coated CC2 dishes did reduce cell movement in the short-term, this was not enough for long-term imaging. For observation of a full cell cycle, improvements would still have to be made to keep cells in frame and in focus for at least 24 hours. Some possible improvements are discussed in 5.3.

### 5.2.2 Problem 2 – Lymphoblastoid cells are difficult to transfect

The poor cell adherence is not the only problem when working with lymphoblastoid cells. Lymphoblastoid cells are notoriously difficult to transfect<sup>291,292</sup>. It is thought that suspension cells have a reduced transfection efficiency due to less attachment of the transfection complex to the cell surface and therefore a reduced uptake of DNA<sup>296</sup>. For the studies of rob(15;21)c in L995 and L996 cells throughout a cell cycle, a method must be optimised to successfully transfect lymphoblastoid cells. Ultimately, stable cells would be created that have chromosome 15 and chromosome 21 fluorescently tagged. To create a stable line, we must first be able to transfect cells with target DNA. As conventional methods (e.g. lipofectamine-based transfection) are inefficient for the transfection of lymphoblastoid cells, I hypothesised that using lentivirus for transduction would be most effective for our desired purpose. Although the

process of lentiviral transduction requires more work and time than other methods of transfection, if successful, it should create stable cell lines containing the target gene. The use of lentivirus for lymphoblastoid transduction has also previously been reported<sup>297,298</sup>.

Firstly, L995 and L996 cells were transduced with CENP-A-mCherry containing lentivirus. This experiment was done as proof of principle to confirm that lentivirus transduction could be done in these cells, with the goal of undertaking more complex transductions in future experiments.

HEK293FT cells were used to produce lentivirus. The transfer plasmid pLenti6-CENP-A-mCherry (Addgene #89767), the envelope plasmid pMD2.G-VSV-G and the packaging plasmid pCMV-dR8.91 were all transfected into HEK293FT cells to produce lentivirus-containing medium as in section 2.9. The presence of virus was detected with the use of Takara Lenti-X GoStix and virus-containing supernatants were then used to transduce L995 and L996 cells via spinfection as described in section 2.9. Transduced cells were allowed to grow out for 1 week and then incubated with blasticidin for the selection of cells with stable integration of transgenes (the pLenti6-CENP-A-mCherry plasmid also contained a blasticidin resistance gene). After blasticidin selection, cells were fixed and imaged (Figure 5.4A) and also seeded for live cell imaging (Figure 5.4B). Figure 5.4 highlights the CENP-A-mCherry foci and thus confirms that lentiviral transduction was successful.

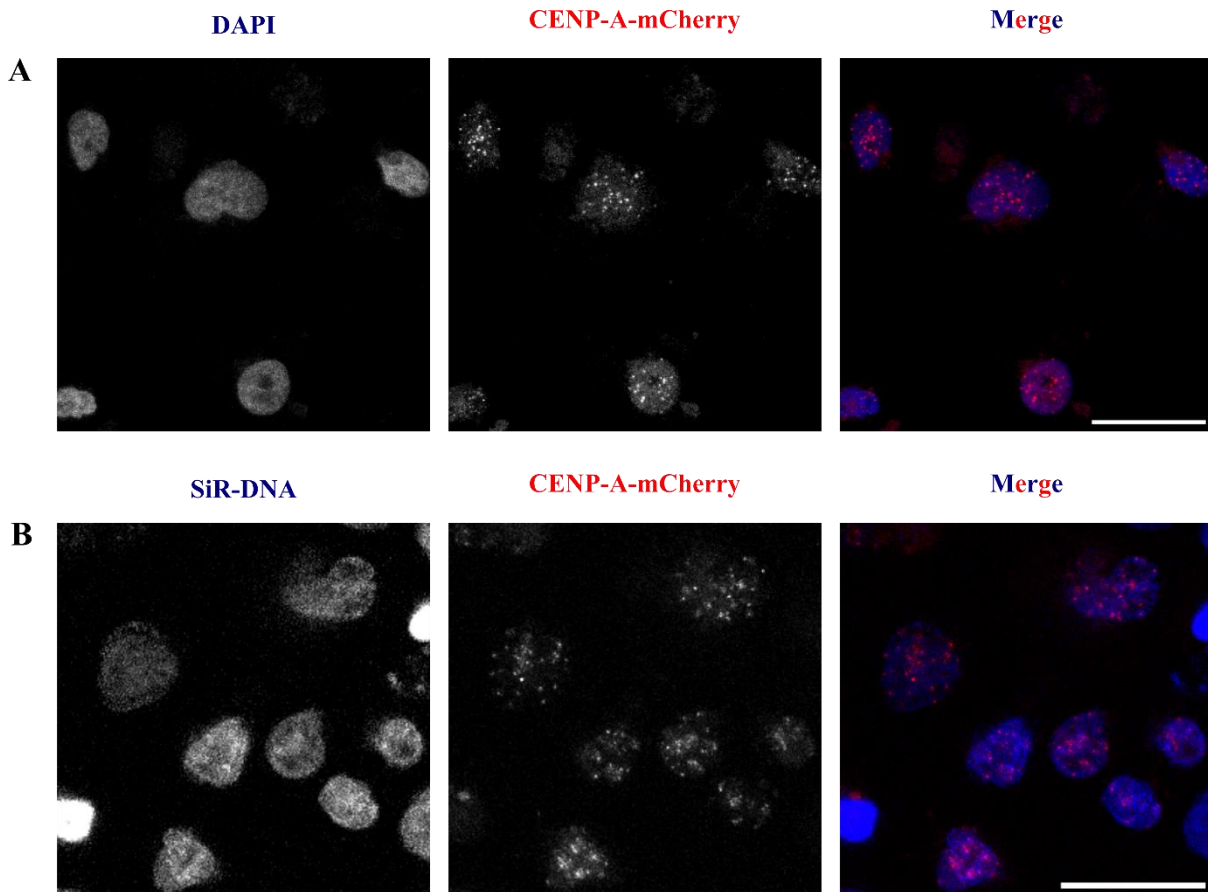


**Figure 5.4. Lymphoblastoid L996 cells can successfully be transduced by lentivirus.** (A) Fixed IF imaging of L996 cells transduced by lentivirus containing transgenic mCherry-tagged CENP-A. (B) Single frame from a live imaging experiment of L996 cells transduced by lentivirus containing transgenic mCherry-tagged CENP-A. Scale bars = 20  $\mu\text{m}$ .

Although transfection of lymphoblastoid cells is difficult by conventional methods, Figure 5.4 shows that our lymphoblastoid cells of interest can successfully be transduced by lentivirus. This transduction created a stable cell line with fluorescent CENP-A proteins; this cell line will hopefully be useful in future experiments to study chromosome segregation.

Studying the chromosome segregation tendencies specifically of rob(15;21)c throughout division was the main goal of the experiments in this chapter. At a minimum, we wanted to study cell division (~1 hour) but ideally, we wanted to study a full cell cycle (~24 hours). To study rob(15;21)c, it would have to be distinguished from other chromosomes in the cell. Initially, I hypothesised that due to the dicentric nature of rob(15;21)c, the stable cell line created in Figure 5.4 with fluorescent CENP-A would contain a chromosome with 4 closely located CENP-A foci and that this would be enough to identify rob(15;21)c. However, as can be seen in Figure 5.4B, during live cell imaging experiments that would be used for

chromosome segregation studies, CENP-A foci were simply too close and there was not high enough resolution to identify a dicentric chromosome from others with any real certainty. It could be hypothesised that by increasing the resolution of the imaging we may see the desired 4 CENP-A foci on rob(15;21)c, however, to observe the somewhat rare mis-segregation events, the field of view needs to be kept wide in order to image multiple cells in one field. For large improvements in resolution, we would have to limit the field of view down to one or few cells.

### **5.2.3 Problem 3 – rob(15;21)c needs to be distinguishable from other chromosomes by live imaging.**

An alternative, albeit more complex, method for identifying rob(15;21)c in a live imaging environment would be to specifically tag this chromosome of interest. Multiple methods exist for locus-specific fluorescent chromosome tagging. The use of fluorescent Zinc Finger Proteins (ZFPs) and the use of fluorescent Transcription Activator-Like Effectors (TALEs) are some of the initial methods used for chromosome tagging<sup>299-301</sup>. However, both of these methods require extremely highly repetitive sequences to get enough observable fluorescence. A more recent technique used for chromosome tagging makes use of the CRISPR-Cas9 system. By using a catalytically dead Cas9 (dCas9) protein to prevent DNA cutting, single guide RNAs (sgRNAs) with specific target sequences can locate this protein to specific loci. The use of hairpin loops on the sgRNA can recruit many fluorescent proteins to one site, reducing the necessary requirement for highly repetitive sequences. Multiple modifications of this technique have been developed that involve a fluorescent protein being conjugated to various components of this system (e.g. to the dCas9 protein itself or to the sgRNA)<sup>293,302-307</sup>. The method that I thought to be most fit for our purpose was that termed CRISPRainbow. Figure 5.5 is a diagram of the components of the CRISPRainbow technique that I use in the rest of this chapter. This technique developed by Thoru Pederson's laboratory involves the addition of hairpin loops on the 3' end of the sgRNA, MS2, PP7 and BoxB. These hairpins can recruit a fluorescent protein conjugated to an RNA hairpin binding domain that specifically recognises each of the hairpins (respectively MCP, PCP and N22). By having multiple copies of these hairpin loops per sgRNA (and therefore recruiting multiple fluorescent proteins) and by combining fluorescent proteins, this technique allows for fluorescent tagging of specific, and multiple, genomic loci in one cell without the need for these loci to be extremely repetitive<sup>293</sup>. The ultimate intention was to tag a chromosome 15 locus in one colour and a chromosome 21 locus in a different colour, such that rob(15;21)c can be tracked throughout a live cell division.

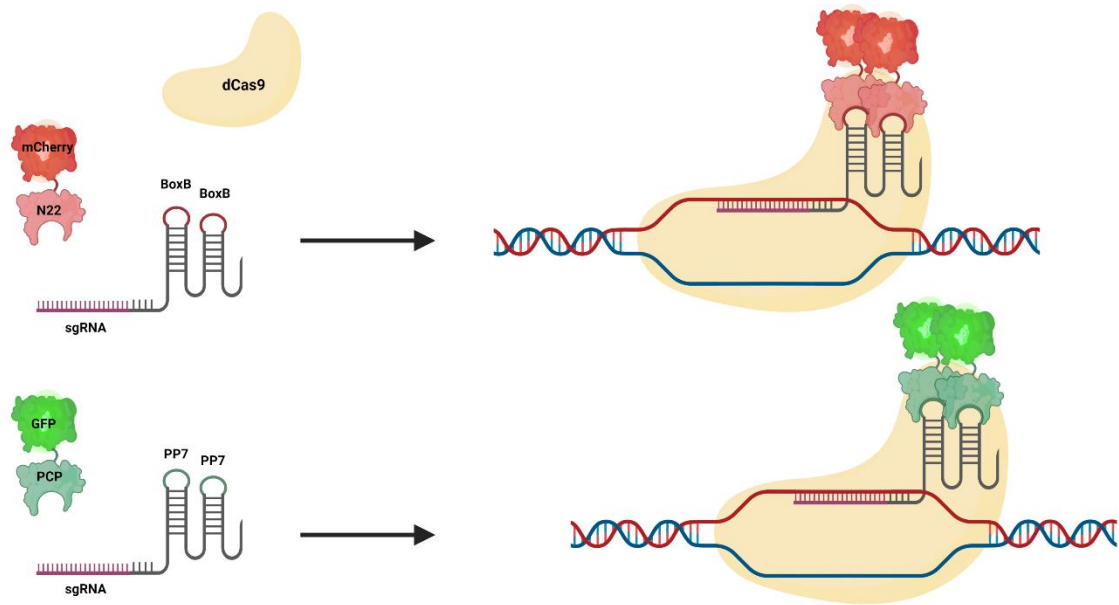


**Figure 5.5. Diagram of the CRISPRainbow technique for fluorescently tagging specific loci.**

Diagram adapted from Ma *et al.* to show how CRISPRainbow can be used to tag specific, repetitive loci in multiple colours for use in live or fixed cell imaging<sup>293</sup>.

### 5.2.3.1 Target identification

This CRISPRainbow project was done in collaboration with Dr Richard Yim, Dr Barbora Badurova, Dr Yuko Takeda, Dr Sarra Ryan and Professor Mary Herbert (Newcastle University).

Although the CRISPRainbow system does not require target sequences as repetitive as TALEs or ZFPs, it requires sequences that are somewhat repetitive for optimal fluorescence (more repeats should give a greater signal to noise ratio), and these sequences also need to be upstream of a Protospacer-Adjacent Motif (PAM) site. The PAM site is required for the targeting of Cas9 proteins and without it, the Cas9 will not bind<sup>308–310</sup>. In order to identify potential target sgRNA sequences on chromosomes 15 and 21, Dr Richard Yim developed a technique in which he used a library of 41-mers from the T2T genome (previously generated for other purposes) to screen for PAM sites on chromosomes 15 and 21. A list was then generated of all 20-mers upstream of these PAMs. Our collaborators on this project were particularly interested in centromeric targets for sgRNA and so these were the first to be mined. If unique centromeric sequences could be found, then centromeric loci would also be our preferred tagging location. The close proximity of the chromosome 15 and chromosome 21 centromere within rob(15;21)c would be easily distinguishable if both centromeres were tagged (as opposed to loci on arms that would

not colocalise as well). However, as previously with centromeric FISH probes, due to the similarity in chromosome 21 and chromosome 13 centromeric repeats, such target sgRNA sequences would bind to both chromosome 21 and chromosome 13.

Dr Barbora Badurova took these potential target sequences and narrowed them down to candidate sequences. Various criteria were used to refine targets, including their absence on other chromosomes, the number of repeats on the desired chromosome and the GC content (this has been reported as a factor that can affect sgRNA efficiency, ~50% GC content is likely optimal<sup>311</sup>). This often produced a small number of candidates that could be tested experimentally (4 on chromosomes 13/21 and 10 on chromosome 15).

Candidates were tested by pooling sgRNAs and injecting 4-6 into a single human oocyte. If fluorescent foci could be seen then 2-3 of the candidate sgRNAs were selected to be injected into a second oocyte. Finally, if this step was successful then single candidate sgRNAs were selected and injected into a further oocyte to find one sgRNA that worked well.

For chromosome 15, 131 potential target 20-mers were found. Following refinement of the candidates, 6 were tested and, finally, one target prevailed (as shown in Figure 5.6A). This successful target sgRNA was injected into a metaphase II human oocyte along with fluorescently tagged (mNeonGreen) dCas9 mRNA (Figure 5.6A). This figure shows the two expected foci from centromeric chromosome 15 targets. As Figure 5.6A is the labelling of an oocyte in meiosis II, there is only one copy of each chromosome, though two chromatids (as can be seen by the two foci). Although the images shown in Figure 5.6 involve a fluorescent dCas9, these targets were also confirmed to work with the CRISPRainbow system by adding PP7 or BoxB loops to sgRNA and then injecting into oocytes with mRNA for PCP-mNeonGreen or N22-mScarlett and dCas9 without a fluorescent tag (not shown).

For chromosomes 21/13, Dr Yim's pipeline found 168 20-mers of interest, though only 4 were not present on other chromosomes. After these were narrowed down by Dr Badurova, one successful target sequence was found (shown in Figure 5.6B). This successful sgRNA was injected into a metaphase II human oocyte with mRNA for dCas9-mNeonGreen, and labelled two chromosomes as expected (Figure 5.6B).

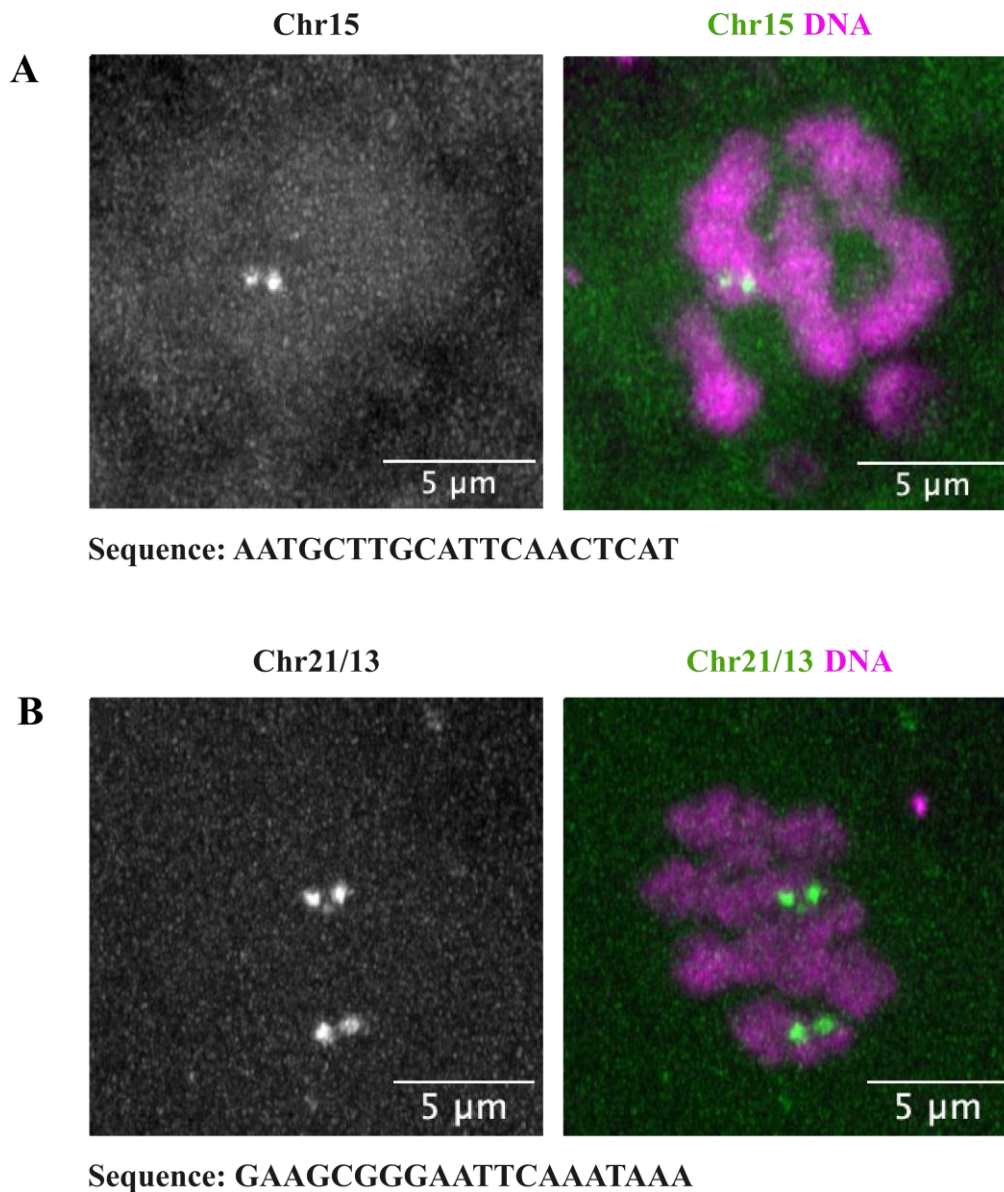


**Figure 5.6. Chromosome 15 and chromosome 21/13 can be tagged in human oocytes.** (A) Chromosome 15 specific foci after injection of the successful target sgRNA and dCas9-mNeonGreen mRNA into a human oocyte in metaphase II. (B) Chromosome 21/13 specific foci after injection of the successful target sgRNA and dCas9-mNeonGreen into a human oocyte in metaphase II. Images provided by Barbora Badurova.

Human oocytes are a good system to validate these sgRNA targets. Extensive cloning is not required as sgRNA and dCas9 mRNA can be produced and directly injected into oocytes. Fluorescence can then be visualised on the same day by live cell imaging. Chromosome 21, chromosome 13 and chromosome 15 were of interest to Dr Badurova (as well as chromosome 16, chromosome 18 and chromosome 22) as they are known “troublemaker” chromosomes due to their frequency to be aneuploid in human meiosis. Human oocytes are likely to have the same sequences as our cell lines. However, due to individual variation, it is possible that the target sequences would not exist or would exist at low copy numbers in L995 and L996 cells. To

confirm their presence and repetitiveness, Dr Yim compared the successful targets from the oocyte study against our Illumina sequencing from L995 and L996 cells. This confirmed that the target sequence for chromosome 21/13 was present with ~195 copies in L995 and ~190 in L996 (on chromosome 21) and the target sequence for chromosome 15 was present with ~147 copies in L995 and ~160 in L996. Whilst this is lower than the number of copies (353 repeats for the chromosome 21 sequence and 344 for the chromosome 15 sequence) in CHM13 (used for the T2T genome), the CRISPRainbow system has previously been used to visualise sequences with >100 repeats<sup>293</sup>. The number of copies of the target sequences in the successfully tagged oocytes is unknown.

Importantly, to confirm that sgRNAs were targeting their desired location, FISH staining was done correlatively on the same cell. Figure 5.7A shows dCas9-mNeonGreen signal in an oocyte that has been co-injected with sgRNA to target chromosome 21 and chromosome 13 (as in Figure 5.6B). These cells were then stained with FISH probes for the  $\alpha$ -satellites of chromosome 21 and 13 (Figure 5.7B). This figure shows the colocalisation between dCas9-mNeonGreen signal and that of the  $\alpha$ -satellite FISH probes. The FISH probes used were labelled with Texas Red and so colocalised staining was undoubtedly from the FISH probes and not from dCas9-mNeonGreen bleed-through (protein fluorescence is also often diminished significantly by the Carnoy's fixative required for FISH staining).

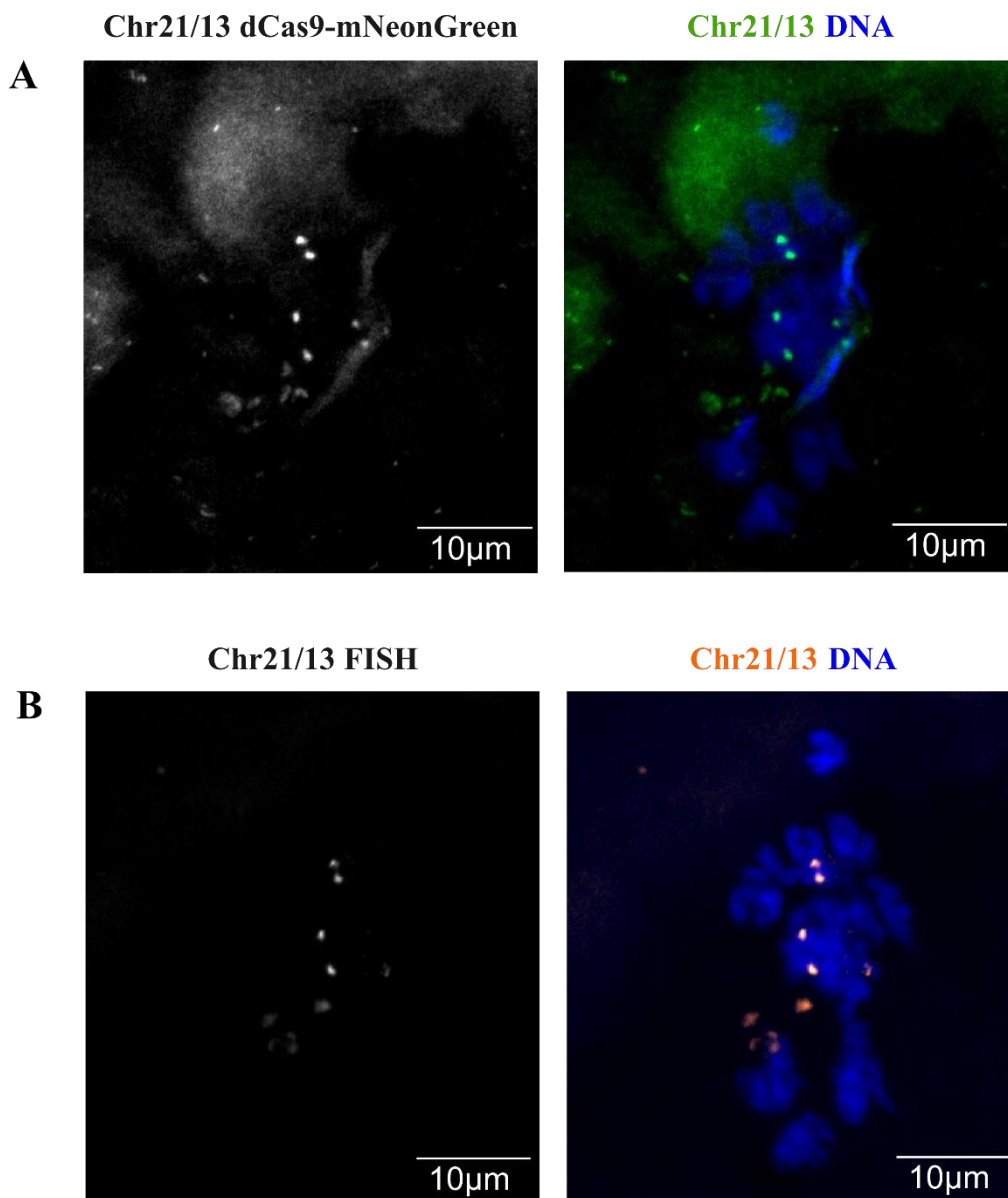


**Figure 5.7. FISH confirms that sgRNA successfully targets chromosome 21 and chromosome 13.**

(A) A metaphase II oocyte after injection with the sgRNA for chromosome 21/13 and dCas9-mNeonGreen mRNA.

(B) The same cell as in (A) stained with FISH probes for the  $\alpha$ -satellites for chromosome 21 and chromosome 13.

Images provided by Barbora Badurova.

### 5.2.3.2 CRISPRainbow optimisation

The first step to optimising the CRISPRainbow system for rob(15;21)c tagging in L995 and L996 cells was to reduce and refine the constructs needed. CRISPRainbow has mostly been done with transient transfection in the past, however for lymphoblastoid cells this system would need to be optimised for lentiviral transduction. The plasmids designed by the Pederson laboratory were made in a backbone that could also be used as lentiviral transfer plasmids. However, if I was to tag rob(15;21)c using the currently available plasmid set (Addgene kit #1000000079), this would involve lentiviral transduction of five different constructs (dCas9,

sgRNA-PP7, PCP-GFP, sgRNA-BoxB, N22-mCherry). In order to streamline these transductions, I made some modifications to the existing plasmids. By combining the sgRNA-PP7 plasmid and the PCP-GFP plasmid, the total number of constructs needed for transduction could be reduced by one. Integrating the sgRNA-BoxB sequence into the N22-mCherry plasmid would again reduce the total number of plasmids by one. The existing dCas9 plasmid has no mammalian cell selection antibiotic resistance gene or fluorescent protein for FACS selection and so cloning in an antibiotic resistance gene was imperative to allow selection of successfully transduced cells. Figure 5.8 shows a plasmid map from full plasmid sequencing of the dCas9 lentiviral transfer plasmid and in yellow the cloned in blasticidin resistance gene and SV40 promoter. Figure 5.9 shows a plasmid map from full plasmid sequencing of the new GFP-1 lentiviral transfer plasmid and highlighted in yellow the cloned in U6 promoter, CCDB gene (for gateway cloning) and PP7. This reduces the need for two separate plasmids for the sgRNA and the fluorescent protein conjugated RNA binding protein. Figure 5.10 shows a plasmid map from full plasmid sequencing of the new mCherry-3 plasmid that contains combined sgRNA-BoxB and N22-mCherry sequences, with the yellow highlighted region showing that the U6 promoter, CCDB and BoxB were cloned in.

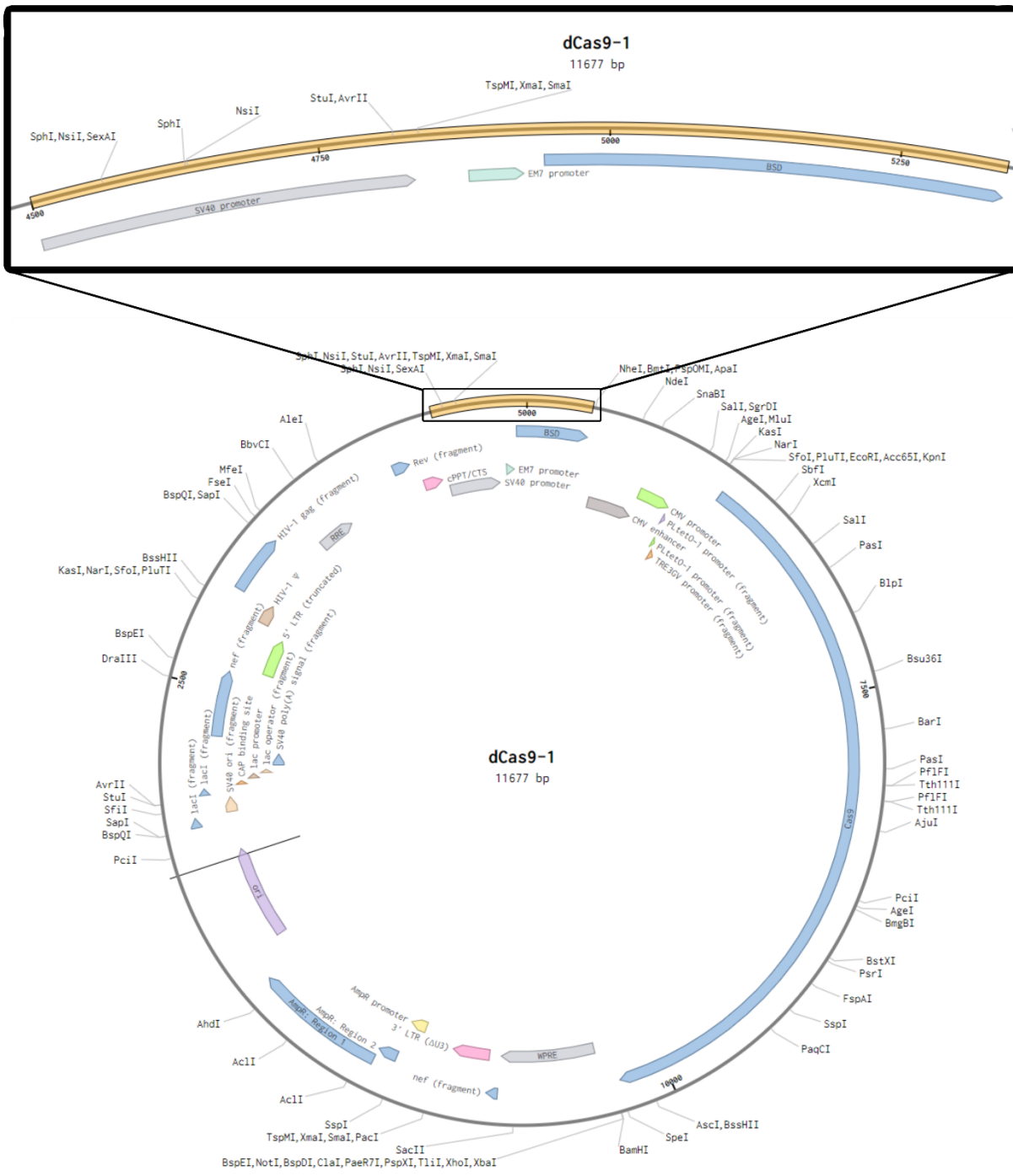


**Figure 5.8. Blasticidin resistance was successfully cloned into a dCas9 containing plasmid.** Long read sequencing from Plasmidsaurus shows that the SV40 promoter and blasticidin resistance gene (BSD) were successfully cloned into the dCas9 containing plasmid from the CRISPRainbow multiplex labelling kit (kit #1000000079) from Addgene. The insert is highlighted in yellow.

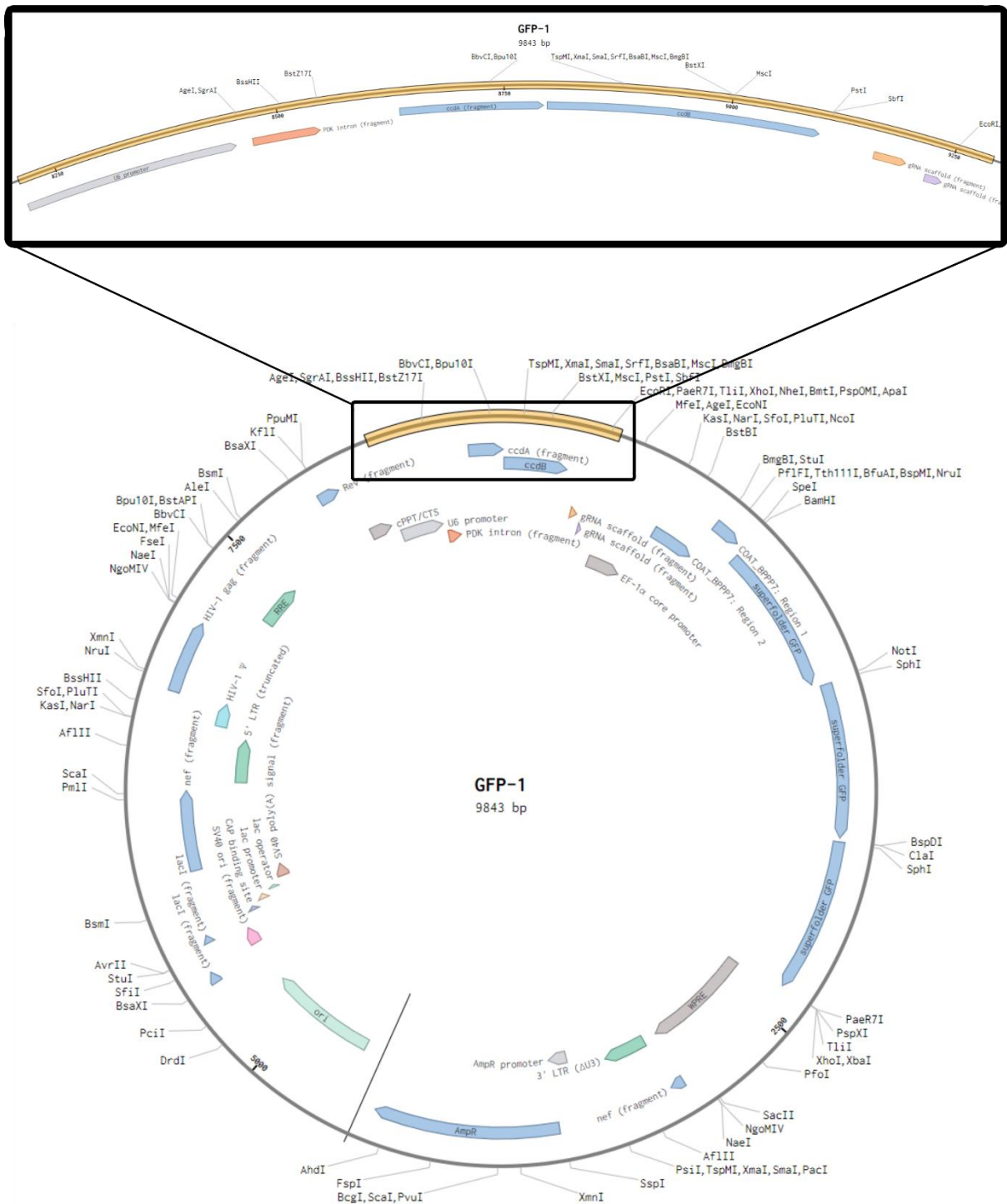


**Figure 5.9.** The U6 promoter, the CCDB gene and 2xPP7 sequences were successfully cloned into a PCP-3xGFP containing plasmid. Long read sequencing from Plasmidsaurus shows that the U6 promoter, the CCDB gene and 2xPP7 sequences were successfully cloned into the PCP-3xGFP containing plasmid from the CRISPRainbow multiplex labelling kit (kit #100000079) from Addgene. The insert is highlighted in yellow.



The modifications of CRISPRainbow plasmids in Figure 5.8, Figure 5.9 and Figure 5.10 allow for cell selection following lentiviral transduction and reduce the total number of transductions needed down from five to three. This should reduce the time needed for sequential lentiviral transduction and selection.

The next step to optimise CRISPRainbow for use in L995 and L996 cells for rob(15;21)c tagging was to first test that we could identify highly repetitive regions. Telomeres have previously been tagged using the CRISPRainbow method and therefore a validated target sgRNA sequence already existed<sup>304</sup>. I sought to clone this same insert into the plasmid made in Figure 5.10 by PCR linearisation and then Gibson assembly. This would allow for the use of the product as a transfer plasmid for lentiviral production. Cells transduced by this lentivirus should then have fluorescent telomeres. However, cloning this product proved difficult. The primers used for linearisation should have removed a region of ~670 bp from the mCherry-3 plasmid from Figure 5.10 (leaving a linearised product of ~8,800 bp and without the CCDB gene used for gateway cloning). However, after full plasmid sequencing of many colonies from this reaction the products were not as desired and ranged from 6-8 kb, showing non-specific primer annealing. After analysing the sequencing results, new primers were designed in the hope of more specific annealing and a gradient PCR was set up to find the optimal annealing temperature of both primer sets. An optimal annealing temperature was found to be 65.5°C; this was used for the attempted linearisation of mCherry-3 for insertion of the previously validated pan-telomeric sgRNA target and the chromosome 13/21 and chromosome 15 targets as developed in Figure 5.6. A similar optimisation process for primer annealing was undertaken for the linearisation of the GFP-1 plasmid designed in Figure 5.9. Ultimately, after attempted PCR linearisation (using various primer pairs) and the use of Gibson assembly for insertion of sgRNA targets of interest, the sequencing of multiple colonies showed incorrect products with variable sizes. This brought concerns about the PCR linearisation of these plasmids and so I then attempted to linearise them using restriction enzyme digest and insert a synthesised gene containing target sgRNAs. However, after initial attempts at restriction digests also gave incorrectly sized products, and due to other problems that were occurring in parallel (difficulty to image lymphoblastoid cells by live imaging in 5.2.1 and difficulty to lentivirally-transduce dCas9 in Figure 5.11), this work was ceased. In the interest of time, I prioritised other experiments for the remainder of my project, as outlined in the Discussion (section 5.3).

### 5.2.3.3 *Attempted CRISPRainbow transduction*

To fully implement the CRISPRainbow system into L995 and L996 cells for tagging of *rob(15;21)c*, transgenes from Figure 5.8, Figure 5.9 and Figure 5.10 would have to be co-expressed. As lentiviral transduction appears to be an efficient method in L995 and L996 cells, the sequential production of stable cell lines would be necessary; co-transduction with multiple lentiviruses would likely be inefficient. The first step in sequential lentivirus transductions was to transduce L995 and L996 cells with the virus containing the dCas9 construct. Producing stable cells with the expression of just dCas9 may also be useful for future experiments which could be attempted transiently.

Virus-containing medium was produced by packaging in HEK293FT cells. To confirm that virus was produced, Takara Lenti-X Gostix were used. These confirmed that a high titre of lentivirus was present in the medium from HEK293FT cells transfected with envelope, packaging and dCas9 plasmids. After spinfection of L996 target cells with virus containing medium, cells were allowed to recover and grow out for ~7 days or until they looked healthy and were growing well. As these viral constructs should have contained both dCas9 and blasticidin resistance, cells were then subject to blasticidin selection and continued to be grown in this media for ~14 days in order to kill untransduced cells and allow dCas9 transduced populations to grow out. In parallel, spinfection of L996 cells with a control GFP plasmid was done. This allowed imaging after 48h to detect GFP fluorescence and therefore whether transduction was successful. In this experiment, GFP fluorescence was seen in population of cells and therefore there were not technical problems with this protocol. GFP fluorescence was being used as a proxy for dCas9 transduction (in the same cell line, virus produced on the same day and spinfection done at the same time) as there were no fluorescent markers in the dCas9 construct that could be detected.

To validate the expression of dCas9 protein, multiple western blots were done with transfected cell lysate, stained for Cas9 (antibody also confirmed to bind dCas9), using purified dCas9 protein as a positive antibody control. An antibody to the abundant protein  $\alpha$ -tubulin was used to confirm equal loading. Figure 5.11 is a representative image of these western blots and shows that no dCas9 expression could be detected in cells that were transduced with dCas9 containing lentivirus. An image is also shown in Figure 5.11 after long exposure of this blot to confirm that there was no weak band in the L996-dCas9 lane. Despite confirmation of virus with Lenti-X Gostix, previous experiments to show L996 can be lentivirally transduced (Figure 5.4) and

the fact that these cells were growing through blasticidin selection, we concluded that dCas9 was not being expressed (and this was confirmed by multiple western blots).

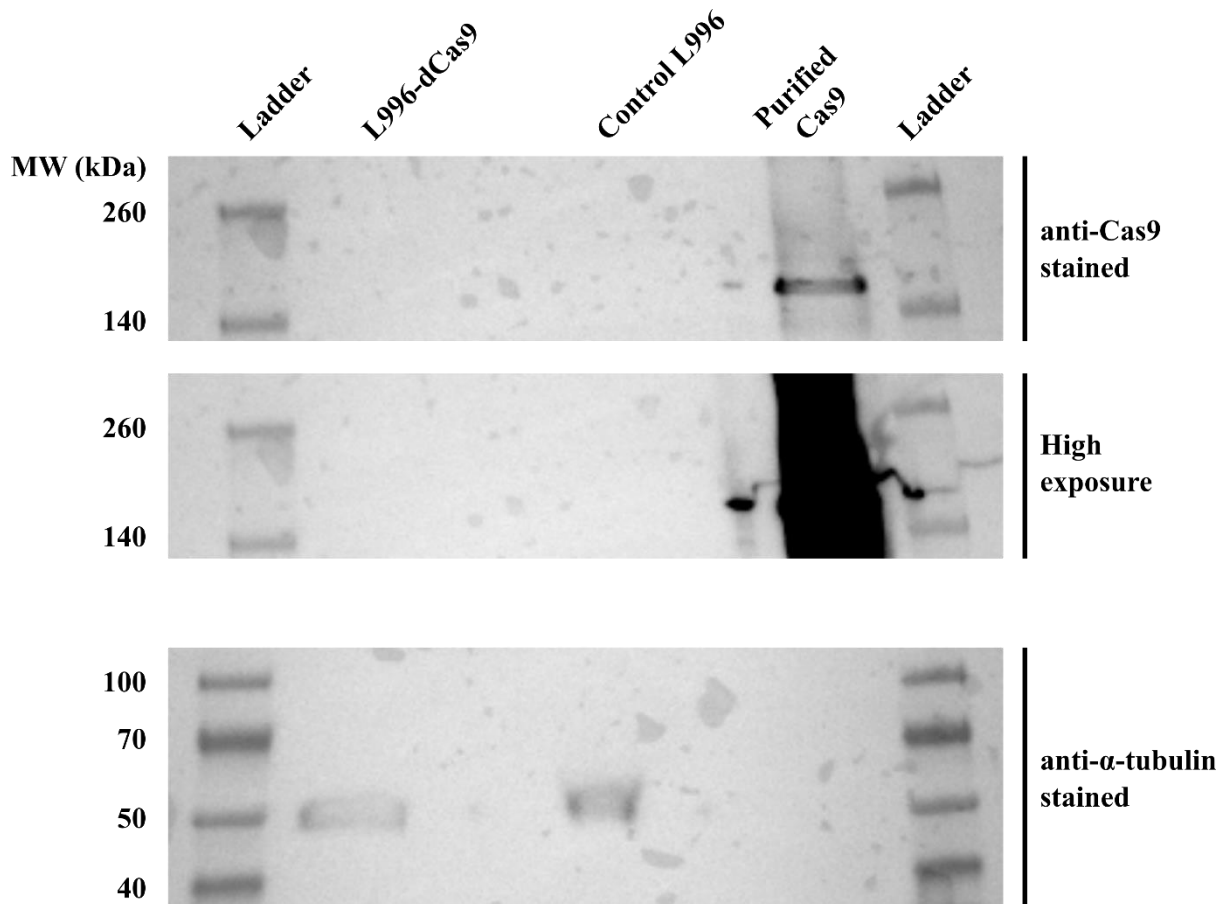


**Figure 5.11. L996 cells transduced with dCas9 containing lentivirus did not express dCas9 protein.**

Western blot of cell lysates from control (untransduced) L996 cells and L996 cells that were transduced with lentivirus containing dCas9 and that have survived blasticidin selection. Purified Cas9 protein was loaded as an antibody positive control.

As an alternative method for plasmid transfection, it has been reported that lymphoblastoid cells can also be successfully nucleofected<sup>291,312</sup>. Nucleofection is an electroporation-based method for transfection that is optimised for each cell type and has been shown to work well with cells that are difficult to transfect<sup>313-315</sup>. As dCas9 lentiviral transduction was proving challenging, optimisation of a protocol for L995 and L996 nucleofection was carried out.

We had access to a nucleofector II and therefore could only use the Amaxa kits designed for this device. Most publications for lymphoblastoid cell nucleofection used kit V, although many of them used different programs on the machine<sup>291,312</sup>. We therefore decided to use kit V and to test multiple different programs to optimise this protocol for best transfection efficiency in L995

and L996 cells. Results from this optimisation experiment are shown in Figure 5.12. All tested programs managed to successfully nucleofect some L996 cells with the small pmaxGFP plasmid supplied with the Amaxa nucleofector kit, though all with very low transfection efficiency. The program that showed highest efficiency was X-001 with ~5-10% of cells expressing the GFP construct after 48 hours. This program, though not as efficient as initially hoped, showed promise that L995 and L996 cells could be nucleofected. This program could then be taken forward to start attempting to nucleofect constructs of interest. If efficiency remained poor, then we reasoned that we could use Fluorescence-Activated Cell Sorting (FACS) to select for fluorescent successfully nucleofected cells.

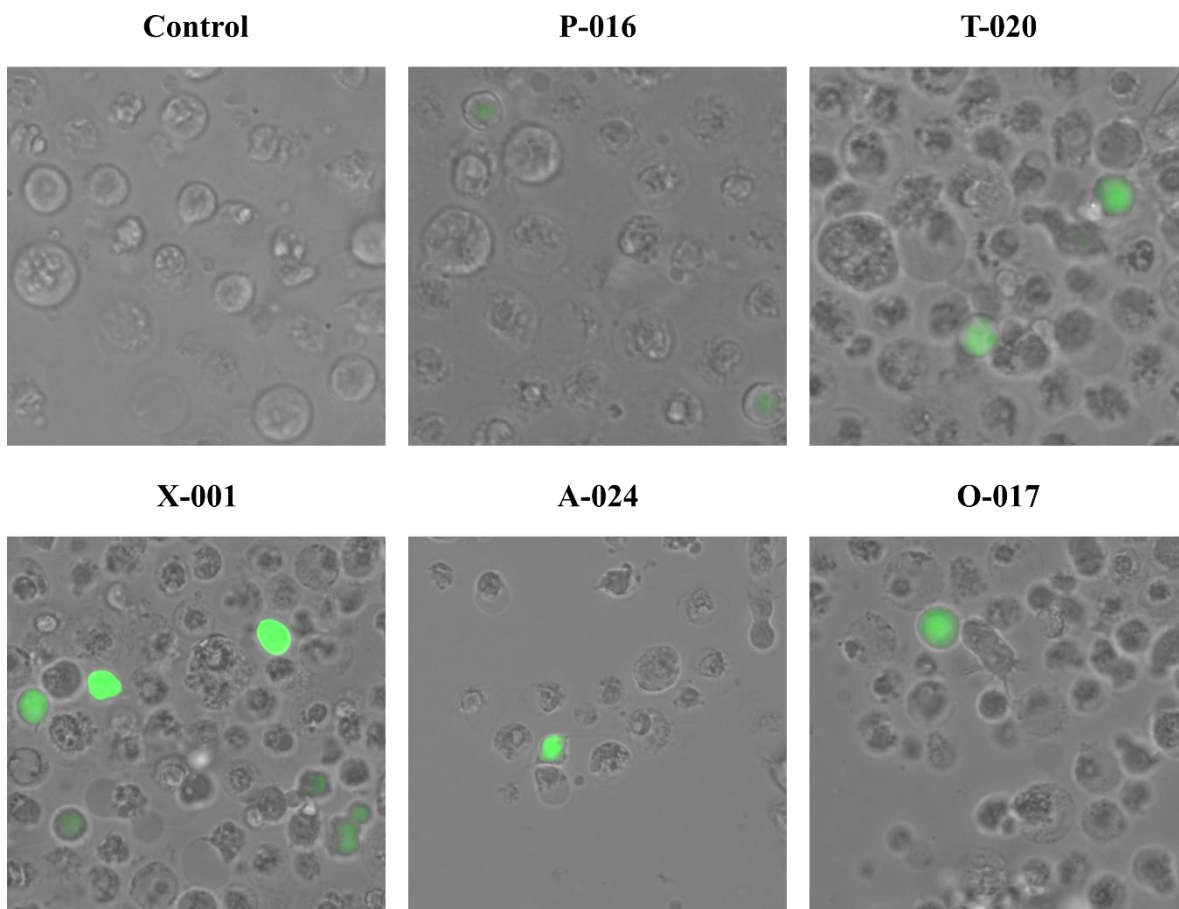


**Figure 5.12. L996 cells can be transfected with a control GFP plasmid by nucleofection.**

Nucleofection optimisation using Amaxa nucleofector Kit V and testing multiple programs which published data suggests might be optimal for lymphoblastoid cell transfection. Cells were transfected with the control 3.5kb pmaxGFP plasmid supplied with nucleofection kits. Imaging highlights the low transfection efficiency in all programs, with X-001 being the most efficient.

The results in Figure 5.12 showed that L996 cells could be nucleofected. However, there is a direct correlation between the size of a plasmid and transfection efficiency and the control pmaxGFP plasmid used in Figure 5.12 is only 3.5 kb<sup>314,316-318</sup>. The three constructs of interest that are required for CRISPRainbow are 9.5-11.7 kb. As these are much larger than the control plasmid there is a chance that they do not nucleofect well. In order to test this hypothesis I used the same nucleofection protocol used for the results in Figure 5.12 but using the three plasmids designed in Figure 5.8, Figure 5.9 and Figure 5.10. After 48 hours from the start of nucleofection, the expression of these transgenes was tested. Figure 5.13 shows imaging of L996 cells 48 hours after nucleofection with the fluorescent protein containing plasmids designed in Figure 5.9 and Figure 5.10. Both cell populations showed no cells that fluoresced after being excited with a laser that should excite GFP and mCherry (Texas Red filter).

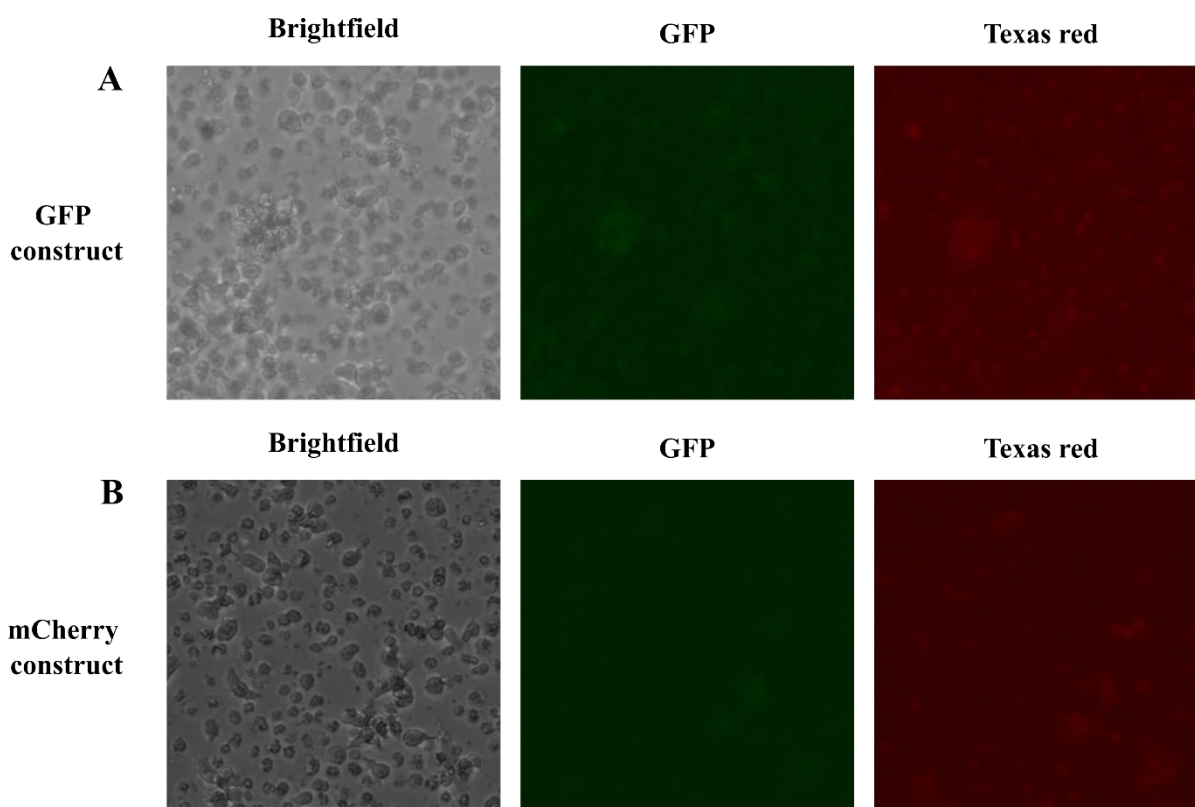


**Figure 5.13. Large fluorescent plasmids were not successfully nucleofected.** (A) L996 cells nucleofected with GFP-1 plasmid and imaged after 48h. (B) L996 cells nucleofected with mCherry-3 plasmid and imaged after 48h.

To test for the presence of dCas9 expression (no fluorescent protein in this plasmid), a western blot was done using cell lysate collected 48 hours after nucleofection with the construct designed in Figure 5.8. Again, purified Cas9 protein was used as a positive control and  $\alpha$ -tubulin used as a loading control. This western blot also confirmed that this nucleofection was

ineffective. It is likely that nucleofection of large plasmids is not efficient in L995 and L996 cells, as supported by the inability to nucleofect 9.5-11.7 kb plasmids in Figure 5.13 and Figure 5.14, but successful nucleofection of the 3.5kb plasmid in Figure 5.12. Although these experiments were not successful, if time was not limited then future work would have included using the original five construct system or making these constructs of interest smaller and attempting nucleofection again, as discussed further in 5.3.

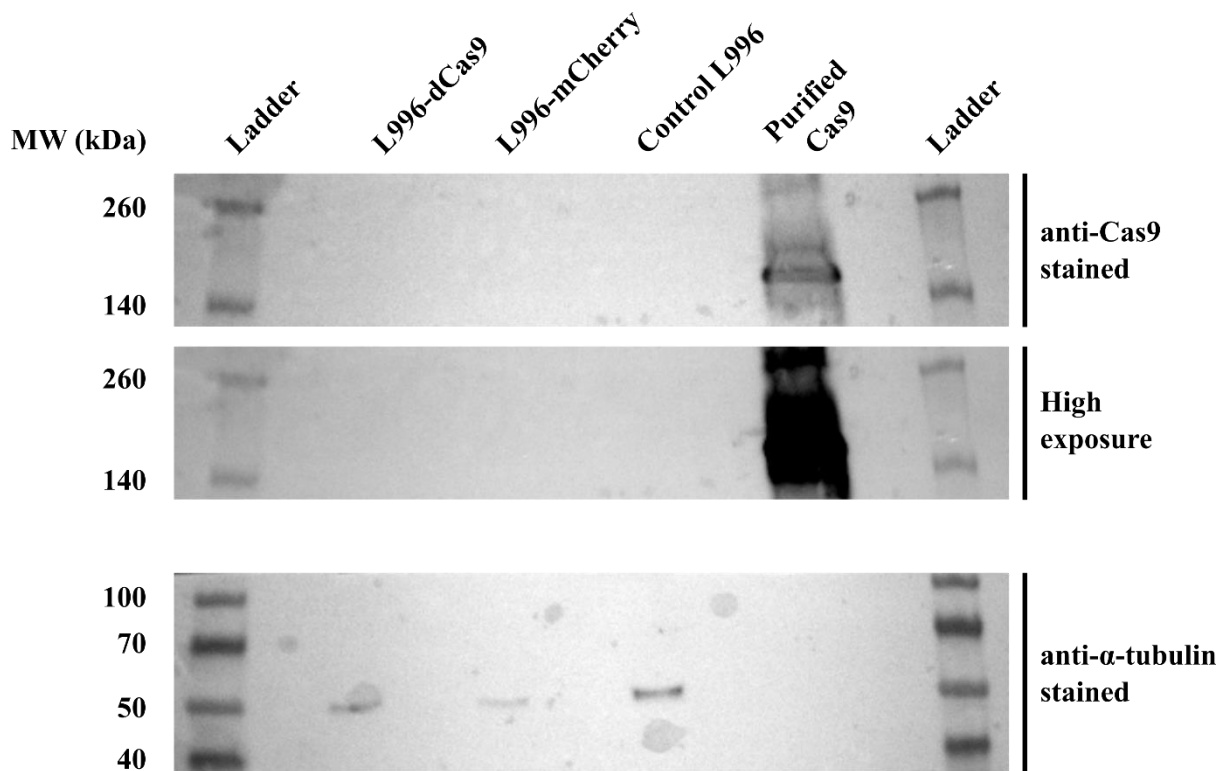


**Figure 5.14. L996 cells nucleofected with dCas9 containing plasmid did not express dCas9 protein.** Western blot of cell lysates from control (untransduced) L996 cells and L996 cells that were nucleofected with a dCas9 containing plasmid and cells that were nucleofected with an mCherry containing plasmid. Purified Cas9 protein was loaded as an antibody positive control.

### 5.3 Discussion

In this chapter I have described attempts to troubleshoot some of the challenges that stand in the way of labelling rob(15;21)c specifically for live cell imaging in L995 and L996 cell lines. The work here has highlighted how it is difficult to image lymphoblastoid cells through an entire cell cycle due to their lack of adherence. This work has also shown by multiple methods that transduction of lymphoblastoid cells is difficult, particularly if the construct of interest is large. Some challenges have been identified and addressed in this chapter and for those that are

yet to be overcome, I propose some possible solutions that would have been attempted if time was not limited.

Figure 5.1, Figure 5.2 and Figure 5.3 demonstrate the challenges that are involved in live cell imaging of cells that are usually in suspension. As adherence of lymphoblastoid cells to glass and plastic is minimal, I attempted to use chemical coating of imaging dishes as a method to promote cell adhesion. In Figure 5.2, poly-L-lysine and Cell-Tak were used with no success in adhering L995 or L996 cells; and causing an increased rate of cell death. In Figure 5.3, pre-coated commercially available imaging dishes (CC2 coating – similar to poly-D-lysine) were used with a slight improvement of adherence in the short term, but long term imaging again showed extensive cell movement. If these experiments for the observation of chromosome dynamics through a full cell cycle were to be done in the future, this imaging protocol would have to be optimised. One possibility is the use of a low percentage agarose medium and with entrapment with the use of an agarose pad on top of cells<sup>319,320</sup>. However, a potential problem with slowing cell movement (by any of the described methods) is that this may cause damage or distress to cells that are usually in suspension and therefore cause a reduction in cell viability.

Through a productive collaboration with the labs of Professor Mary Herbert and Dr Sarra Ryan progress was made on the intended method for tagging our chromosomes of interest (chromosome 15, chromosome 21 and rob(15;21)c). Potential target sgRNA sequences were identified by Dr Richard Yim and then refined and validated by Dr Barbora Badurova. The outcome of this collaboration was that we now have target sgRNA sequences on chromosome 15 and chromosomes 21/13 that have been confirmed to be repetitive enough (in theory due to the number of repeats) for visualisation in L995 and L996 cells. These were confirmed to target dCas9 to the relative loci in human oocytes, which are for most purposes more difficult to image than mammalian cells. Although the chromosome 21 target sequence also labelled chromosome 13, this shouldn't be an insurmountable problem. On rob(15;21)c the colocalisation of chromosome 15 and chromosome 21 foci should be obvious and the normal chromosome 21 and chromosome 13 should be able to be differentiated by both chromosome size and by the size of the fluorescent foci (chromosome 13 is larger than chromosome 21 and contains ~5x the quantity of this specific target sequence, at least in CHM13).

The work done in human oocytes provided a nice proof of concept for this method. However, for use in lymphoblastoid cells, modifications had to be made. The plasmids used in the original CRISPRainbow multiplex labelling kit were refined such that only three plasmids would have

to be transfected to label our chromosomes of interest instead of five. The dCas9 containing plasmid was then used for the initial lentiviral transduction to start this labelling process in L995 and L996 cells. Although preliminary results showed that these cells could be successfully transduced by lentivirus (Figure 5.4), no dCas9 protein was seen by western blot following dCas9 lentiviral spinfection of these cells (Figure 5.11), despite surviving blasticidin selection (dCas9 construct contained blasticidin resistance gene). It is possible that lentivirus particles successfully retained the blasticidin resistance gene but lost the large dCas9 gene or that L995 and L996 cells could not survive when expressing dCas9 and so the only population of cells to survive was the small percentage that managed to retain blasticidin resistance but had lost dCas9. It is known that as the size of a transfer plasmid increases, the viral titre decreases<sup>321-323</sup>. To confirm the presence of virus (though not quantifiably) Lenti-X Gostix were used. This assay only detects p24 capsid protein (and therefore the presence of virus), though this has been shown to be a poor prediction of transduction efficiency due to the high variability in virus production<sup>324</sup>. It is possible that the large size of the dCas9 transfer plasmid (~11.7kb - cloned in Figure 5.8) had led to poor transduction efficiency of L995 and L996 cells. In future work, the original five construct system could be used. The steps I took to try and optimise and streamline the number of constructs needed may have been detrimental due to the size of each construct increasing. However, the size of the original constructs were 8.7kb (GFP) and 8.4kb (mCherry) and after streamlining, the new constructs were 9.8kb and 9.5kb. As there is only a 1.1kb difference, I am not sure that the original system would have been much more successful.

Simultaneously to lentiviral transduction optimisation, nucleofection of plasmids was also tested. Nucleofection has previously been used for many types of difficult-to-transfect cell types<sup>313-315</sup>, including lymphoblastoid cells<sup>291,312</sup>. Preliminary experiments with a small control plasmid (3.5kb) found that L995 and L996 cells could indeed be successfully nucleofected, albeit only with a low transfection efficiency (~5-10%) (Figure 5.12). However, when larger constructs of interest were nucleofected (9.5-11.7kb), they failed to produce fluorescence (Figure 5.13) or proteins that could be detected by western blot (Figure 5.14). As time was limited, these optimisation experiments had to be halted. However, the next logical steps would be to reduce the size of plasmids for nucleofection. Whilst some of the genes of interest are large (e.g. dCas9), they are currently in large backbones that contain the necessary elements for lentiviral work. If the optimisation of nucleofection in L995 and L996 was continued then I would begin by removing unnecessary parts of the constructs made in Figure 5.8, Figure 5.9 and Figure 5.10 or I would instead clone the necessary genes into a much smaller backbone. I

predict that reducing plasmid size would increase transfection efficiency (as has been shown by the 3.5kb plasmid in Figure 5.12).

In summary, the work in this chapter was originally undertaken with the hope of being able to produce a cell line in which rob(15;21)c was fluorescently tagged. Although multiple challenges arose, this chapter provides a summary of the optimisation of multiple techniques required for transfection and imaging of lymphoblastoid cells. Due to time constraints the experiments in this chapter could not be finished. Given more time I believe that it would be possible to successfully tag rob(15;21)c with a fluorescent label and observe its segregation tendencies through a cell cycle in L995 and L996 cells. Above I have outlined some of the next steps which could be taken to facilitate the completion of this set of experiments.

## Chapter 6: Discussion

---

The work in this thesis has characterised the dicentric chromosome rob(15;21)c and its segregation properties. The seminal paper in 2014 from Li *et al.* discovered that carriers of the rob(15;21)c chromosome have a huge ~2700x increased risk of developing the subtype of leukaemia, iAMP21-ALL<sup>145</sup>. The purpose of this thesis has been to build on the work in Li *et al.* by using cell biology approaches to characterise the rob(15;21)c chromosome and understand the mechanism driving the predisposition for the rob(15;21)c chromosome to undergo chromothripsis and drive iAMP21-ALL.

In this chapter I discuss the key findings from the work in Chapters 3, 4, and 5. I consider their implications in the context of current knowledge, their limitations, what can be concluded from them, and some recommendations for future work.

### 6.1 The active dicentricity of the rob(15;21)c chromosome

Robertsonian chromosomes are often dicentric in that they contain centromeric DNA repeats from both of their parent chromosomes. However, surprisingly little work has been done to fully understand these chromosomes, especially considering their high prevalence in the general population (~1 in 800); with a particular lack of research in recent years. Important fundamental knowledge on the centromeres of Robertsonian chromosomes has come from the work of Beth Sullivan and co-workers. In 1994, by analysing chromosome spreads from 48 human lymphocyte samples, Sullivan *et al.* showed that dicentric Robertsonian chromosomes have preferential activity at one centromere<sup>255</sup>. However, whilst the cohort included many cases for the more common Robertsonian translocations (rob(13;14)c and rob(14;21)c), only two cases of rob(15;21)c were investigated. Of the work that has been done in Robertsonian chromosomes, the chromosome rob(15;21)c has rarely been studied. Due to the discovery of a huge predisposition for chromothripsis and iAMP21-ALL development in rob(15;21)c carriers<sup>145</sup>, studying this chromosome became of interest.

In Chapter 3, I studied the rob(15;21)c chromosome in novel lymphoblastoid cell lines containing this chromosome (L995 and L996). Work from this chapter highlighted how this chromosome is most often actively dicentric, with the inner kinetochore protein CENP-C assembling at both centromeres in most cells. I hypothesise that this active dicentricity may be possible due to the short inter-centromeric distance between the two centromeres on each rob(15;21)c sister chromatid. Research from Page and Shaffer on Robertsonians and from

Sullivan *et al.* on dicentric X chromosomes suggests that a short inter-centromeric distance allows for the centromeres to work cooperatively whereas, when the inter-centromeric distance increases, the likelihood for a dicentric chromosome to inactivate one centromere and become functionally monocentric increases<sup>127,137</sup>. I suggest that the short inter-centromeric distance seen in chromosome spreads of rob(15;21)c allow for increased chromosomal stability and a reduced chance of erroneous microtubule attachments when compared with dicentric chromosomes that have a greater inter-centromeric distance. It is possible that a large inter-centromeric distance allows the chromosome to twist and this may cause the two centromeres of one sister chromatid to bind to opposite spindle poles, hence promoting a mis-segregating chromosome. Instead, the short inter-centromeric distance on rob(15;21)c promotes the binding of both kinetochores (on each sister chromatid) to microtubules from the same pole, therefore allowing faithful segregation in the majority of mitoses.

Initially we hypothesised that the activities of the rob(15;21)c centromeres were changing as cells were continuously cultured as a mechanism to improve chromosome segregation fidelity (transitioning from actively dicentric to actively monocentric). However, when assessed, we found no evidence to support this idea, and both phenotypes were seen in similar proportions at all tested passages, with actively dicentric being the predominant phenotype (Figure 3.15 and Figure 3.16). In 2005, Higgins *et al.* showed that centromere activity in a dicentric chromosome is usually clonal, however in some cell lines this centromere activity state can switch in a growing population of cells<sup>129</sup>. A valuable future experiment to add to the work in this thesis would be to grow L995 and L996 cells from a single cell by using Fluorescence-Activated Cell Sorting (FACS) to isolate single cells. Then, by growing out clonal lines, it could be determined if rob(15;21)c has the ability to change state in a clonal population or whether separate stable actively dicentric and actively monocentric clonal lines exist and that their proportion *in vitro* (and presumably *in vivo*) is determined by selection.

Results in Figure 3.14 showed that as well as the inner kinetochore protein CENP-C, outer kinetochore proteins Hec1 (NDC80) and NUF2 also assemble onto actively dicentric rob(15;21)c chromosomes. As members of the NDC80 complex, NDC80 and NUF2 are directly involved in microtubule binding. Therefore it is very likely that both of the kinetochores on rob(15;21)c that assemble these proteins are functional and have the ability to bind spindle microtubules. This is supported by images in Figure 3.20 that show microtubules binding to both kinetochores on what appear to be dicentric chromosomes in rob(15;21)c containing cells. The limitations of these data include that these are images from only two cells and it was not

possible to stain the rob(15;21)c chromosomes with FISH probes in these cells, therefore we have to make the presumption that these chromosomes are rob(15;21)c and not two closely located monocentric chromosomes. One further consideration is that recent work from the Kops lab has highlighted that monocentric chromosomes appear bipartite when imaged at a high resolution<sup>325</sup>. It is possible that the two CENP-C foci that we see in Figure 3.20B and Figure 3.20C are actually that of a monocentric chromosome resolving out to show this bipartite phenotype and bundles of microtubules binding to each subunit.

The predominant centromeric phenotype that we observed in rob(15;21)c chromosomes is actively dicentric. However, the strength of the two centromeres is often not equal. In Figure 3.17 and Figure 3.18 it was shown that rob(15;21)c has quantifiable and centromere-specific dominance in the intensity and size of CENP-C foci. The centromere belonging to the chromosome 15 arm is significantly more intense and larger than that belonging to the chromosome 21 arm within the rob(15;21)c chromosome. In support of this, when a rob(15;21)c chromosome showed to be actively dicentric, the undetectable centromere was very often that of the chromosome 21 arm. This is of particular interest as sequencing results from Li *et al.* identified how the derivative chromosome produced post-chromothripsis from rob(15;21)c chromosomes is monocentric, specifically retaining the chromosome 21 centromere and losing the chromosome 15 centromere<sup>145</sup>. Therefore our results suggest that the chromosome involved in chromothripsis is likely actively dicentric (containing an active chromosome 21 centromere that can be inherited by the derivative chromosome, as opposed to an actively monocentric rob(15;21)c chromosome that loses activity of the chromosome 21 centromere – shown in Figure 3.19). However, whilst it seems unlikely, it cannot be ruled out that an actively monocentric rob(15;21)c chromosome (that has lost activity of the chromosome 21 centromere via epigenetic mechanisms) undergoes chromothripsis, with only the chromosome 21 centromere being retained and then its activity is switched back on. Whilst we believe it to be more likely that an active dicentric rob(15;21)c chromosome undergoes chromothripsis, we presume that the chromosome 15 centromere is lost and the chromosome 21 centromere is retained due to selection, and not due to a direct mechanism driving the specific centromere loss.

Although Chapter 3 characterised the activity of the centromeres of rob(15;21)c, logical future experiments would include further studying the functionality of these centromeres. With the use of correlative IF and then FISH on fixed cells with an actively occurring mis-segregation we could gain further information on the ability of each kinetochore to bind microtubules and

observe any possible mis-attachments that may be causing the mis-segregation. If the method of CRISPRainbow tagging of rob(15;21)c for live imaging could be optimised, then Correlative Light and Electron Microscopy (CLEM) images may also allow for identification of rob(15;21)c via light microscopy and then the high resolution of electron microscopy may be able to identify individual microtubules. This would provide information on how many microtubules bind each kinetochore (and if the centromere dominance correlates with the number of microtubule attachments) and how aberrant attachments may be causing mis-segregation.

## 6.2 The mis-segregation of rob(15;21)c and mechanisms that may be driving it

The results in Chapter 4 highlighted how rob(15;21)c mis-segregates at a much higher rate than expected (16-17% of mis-segregations contain rob(15;21)c). Of particular interest, we found that both sisters mis-segregate together frequently (around half of the rob(15;21)c mis-segregations contain both sister chromatids; Figure 4.4). These data are interesting in the context of Li *et al.*, who inferred that two copies of rob(15;21)c were present in the chromothriptic event that occurs in iAMP21-ALL development (3 of the 4 rob(15;21)c cases with der(15;21) sequenced showed evidence to suggest that two copies were present in the chromothriptic event). Our results indicate how that is likely due to a mechanistic reason that drives co-mis-segregation of sister chromatids into an environment that is susceptible to chromothripsis (a micronucleus). An alternative reason for both sisters undergoing chromothripsis might be due to selective pressure, i.e. a necessity for two copies to be present to drive cell survival and cancer. Although these scenarios are not mutually exclusive, and two copies may help drive cancer, our results suggest a mechanism that directly facilitates a chromothriptic event on two copies of the rob(15;21)c chromosome. One possible limitation to this work is that these mis-segregation rates have likely been influenced by the use of nocodazole. Due to its nature of action, nocodazole induces mis-segregation. This is beneficial for our mis-segregation experiments as, without synchronisation from nocodazole, an asynchronous population has few cells in anaphase and telophase and of these few contain actively occurring mis-segregations. Nocodazole is able to increase both the number of anaphase cells and the proportion of mis-segregations, therefore allowing for the collection of more data. However, nocodazole was previously shown to induce mis-segregation in a non-random manner, with chromosome 1 and chromosome 2 being affected more than other chromosomes<sup>95,97</sup>. These studies however did not show any specific induction of chromosome 15 or chromosome 21 mis-segregation and therefore we presume that the mis-segregation rate

of rob(15;21)c is unlikely to be preferentially induced by nocodazole because of its homologous chromosomes. However, it may be possible that the dicentricity of rob(15;21)c causes it to be more susceptible to nocodazole induced mis-segregation. In these experiments we also use normal chromosome 15 and normal chromosome 21 within the same cells as internal controls and this showed significantly lower rates of mis-segregation for both control chromosomes compared with rob(15;21)c. In the future, the rate of mis-segregation could be assessed in an asynchronous population by developing a high-throughput imaging and imaging analysis pipeline that is able to identify anaphase and telophase cells, similarly to the approach in Figure 4.14 for metaphase cells. This type of analysis was not carried out in the work in this thesis as it proved much more difficult to successfully identify anaphase and telophase cells reliably due to their variability in nuclear morphology. However, with the use of machine learning it may be possible to optimise this process and successfully pick out anaphase and telophase cells, including those with active mis-segregations. Such a pipeline would allow for the input of a large number of images of FISH stained asynchronous cells, therefore providing sufficient data to determine a more accurate rate for rob(15;21)c mis-segregation when compared with chromosome 15 and chromosome 21.

Many experiments were done to try and understand the mechanism driving frequent co-mis-segregation of rob(15;21)c sister chromatids. The staining of proteins involved in the CPC and therefore error correction appeared normal on rob(15;21)c, including Aurora B and one of its downstream phosphosites that was used as a proxy for Aurora B activity. Cohesin staining appeared normal on rob(15;21)c on chromosome spreads (metaphase-like) and therefore if the Cohesin cleavage on this chromosome is also normal then it is unlikely that the rob(15;21)c sister chromatids are being physically held together during anaphase by cohesion. This could be tested experimentally by staining for Cohesin during anaphase to determine if rob(15;21)c has been released from the centromeric Cohesin. Also, the nuclear interphase location of rob(15;21)c appears favourable for faithful segregation. Frequently mis-segregating chromosomes are often closer to the periphery of the cell during interphase, however rob(15;21)c showed to have a central nuclear location. One finding of interest is that rob(15;21)c appears to align late/mis-align on the metaphase plate. This mis-alignment suggests that erroneous microtubule-kinetochore attachments may persist for longer on the dicentric centromeres of rob(15;21)c than on most chromosomes.

Based on the work in section 4.2.4, I hypothesise that the actively dicentric nature of rob(15;21)c causes an increased number of aberrant microtubule-kinetochore attachments

compared with a monocentric chromosome. Despite apparently normal CPC protein recruitment to rob(15;21)c, the normal level of activity sufficient for error correction on a monocentric chromosome may not be enough to resolve all mis-attachments on the dicentric chromosome. In turn, these uncorrected mis-attachments may sometimes allow the mis-segregation of rob(15;21)c chromosomes during anaphase and, if this persists into telophase, then rob(15;21)c may enter a micronucleus, initiating a potential chromothriptic event.

We do not currently fully understand why both sister chromatids are present in mis-segregations so frequently, though a possible mechanism is that erroneous microtubule-kinetochore attachments on the dicentric rob(15;21)c cause chromosome twisting as the two kinetochores of one sister chromatid are bound to microtubules from opposite poles. This twisting may compromise tension-dependent Aurora B regulation, therefore reducing the capacity for error correction and allowing mis-attachments to persist. It is possible that this kind of mechanism would equally affect both sister chromatids and therefore this mechanism may drive the co-mis-segregation of rob(15;21)c sister chromatids as observed in Figure 4.4. To address this hypothesis in the future, further super-resolution imaging experiments could be done to observe any chromosome twisting when rob(15;21)c mis-segregates. I also propose that staining various Aurora B phosphosites related to error correction on anaphase/telophase cells with actively mis-segregating chromosomes may help to understand if the CPC is active or if it is being hindered by the abnormal chromosome morphology. A further protein of interest to study in this same context is MPS1. It has been proposed that MPS1 also plays a role in error correction of incorrect microtubule-kinetochore attachments<sup>326</sup>.

Further, although rob(15;21)c has the most obvious impact on cancer development, other Robertsonian chromosomes may also have segregation defects. An interesting question is why rob(15;21)c causes a much stronger predisposition to this subtype of leukaemia than other Robertsonian chromosomes. One possibility is that many Robertsonian chromosomes have a tendency to mis-segregate, and that the difference in cancer predisposition is determined by the probability that subsequent rearrangements of the chromosome (such as chromothripsis) are oncogenic. It is also possible that other Robertsonians have much more faithful segregation. Regardless of the outcome, characterising other Robertsonian chromosomes and how they act during chromosome segregation are some of the logical next steps for this project.

### 6.3 The difficulty in tagging rob(15;21)c and tracking it throughout cell division

The results in Chapter 5 highlight the difficulties of fluorescently tagging rob(15;21)c in lymphoblastoid cells and live-imaging these cells. Multiple problems were encountered in the CRISPRainbow tagging process. It was quickly discovered that imaging lymphoblastoid cells (that are usually growing in suspension) across multiple hours is challenging. Even with the use of approaches to improve adhesion (e.g. Cell-Tak), cells rapidly moved out of focus and out of frame. One obvious alternative method to live-image non-adherent cells would be to use software to track the movement of a cell during imaging such that the frame moved, and the cell remained in frame. However, one problem with this is that we would be trying to observe relatively rare events (mitosis with a mis-segregation event that contains rob(15;21)c and tracking only allows for the imaging of one or two cells at a time. To improve the chances of observing one of these rare events we would need to image a whole field of many cells. A possible method that could be attempted in future experiments is to use agarose containing media and/or the physical entrapment of cells with an agarose pad. This method has previously been used to image suspension cells<sup>319,320</sup>.

Although experiments to tag of rob(15;21)c with the use of CRISPRainbow encountered multiple obstacles that prevented their success, multiple steps of progress were made that may allow for success in this tagging method in the future. Targets of interest on chromosome 15 and chromosome 21/13 were identified. These were confirmed to be present in sufficient repeat number in our cells of interest. These were also validated for successful use with the CRISPRainbow system in human oocytes. Also, the original CRISPRainbow plasmid system was refined for use in lentiviral transduction for the creation of stable cell lines.

Unfortunately, transduction of the constructs of interest for CRISPRainbow were not successful either lentivirally or transiently by nucleofection. Lymphoblastoid cells are notoriously difficult to transfect, though previous studies have successfully used both nucleofection and lentivirus in lymphoblastoid lines<sup>291,297,298,312</sup>. We also showed that our particular cells of interest could be successfully transduced by lentivirus containing CENP-A-mCherry. The creation of these CENP-A-mCherry lines were mostly as a proof of principle, but there is a possibility that they could be of use of tracking centromere dynamics in a live cell imaging experiment. However CENP-A foci were not sufficiently resolvable at the magnification needed for these experiments to distinguish rob(15;21)c from other chromosomes. The next logical experiments to be done would be to greatly reduce the plasmid size of the CRISPRainbow plasmids. It is possible that

both lentivirus transduction and transient nucleofection were hindered by the size of the plasmids used. As nucleofection worked with a smaller GFP control plasmid in our cells of interest, it is logical to test this theory with nucleofection first. It has been shown that nucleofection is more efficient with smaller plasmids and the ones used here are relatively large (9.5-11.7 kb). As the nucleofection of the small GFP plasmid proved successful, we believe that this could be a factor preventing the efficient transfection of L995/6 cells. While the original plasmids are quite large, the sequences of interest are not (~4 kb). By removing excess DNA, particularly many of the genes required for lentivirus production (the same plasmids were used for lentivirus production and nucleofection and therefore they contained lentiviral genes not necessary for nucleofection), the overall size of the plasmids could be greatly reduced. Similar to the experiments in Figure 5.13 and Figure 5.14, first a test run of nucleofection with dCas9, GFP and mCherry plasmids (after size reduction) could be done. dCas9 presence could be detected by western blot and the GFP and mCherry by microscopy.

Another possible future experiment is to microinject our cells of interest, similar to what is done in oocytes. Although this technique is much easier for oocytes due to their large size, mammalian somatic cells have previously been injected successfully<sup>327</sup>. This could potentially bypass the difficulties in transducing lymphoblastoid cells, although it would be much lower throughput.

While these CRISPRainbow experiments were not successful in this study, we cannot conclude that the technique is not suitable for this application. Given more time, further refinements to this process could be made and it is possible that an optimised protocol would allow for the CRISPRainbow creation of fluorescently tagged rob(15;21)c.

#### 6.4 Concluding remarks

Despite Robertsonian chromosomes being carried in 1/800 individuals, little recent research has been done to examine the cell biology of these chromosomes. In this thesis, I studied a rare, but clinically relevant Robertsonian translocation, rob(15;21)c. The rob(15;21)c chromosome has been shown to give carriers a huge predisposition to iAMP21-ALL development. Here we have shown that this is likely due to the active dicentricity of this chromosome driving frequent mis-segregation. This mis-segregation then may place both rob(15;21)c sister chromatids in a micronucleus, an environment that has previously shown to be a facilitator in chromothripsis<sup>154,156</sup>. Our work has also narrowed down some of the potential mechanisms that may be driving the predisposition of rob(15;21)c to chromothripsis; we suggest that the active

dicentricity of this chromosome may lead to an increased number of microtubule mis-attachments that are occasionally not resolved by error correction. By better understanding the rob(15;21)c chromosome, we have gained insights into Robertsonian chromosomes, chromosome mis-segregation and the roles of dicentric chromosomes in cancer development.

## References

1. Obaya AJ, Sedivy JM. Regulation of cyclin-Cdk activity in mammalian cells. *Cell Mol Life Sci CMLS*. 2002 Jan 1;59(1):126–42.
2. Murray AW. Recycling the Cell Cycle: Cyclins Revisited. *Cell*. 2004 Jan 23;116(2):221–34.
3. Harris B. Investigation of the kinase haspin and mitosis specific histone H3 threonine 3 phosphorylation [PhD thesis]. Newcastle University; 2021.
4. Jallepalli PV, Lengauer C. Chromosome segregation and cancer: cutting through the mystery. *Nat Rev Cancer*. 2001 Nov;1(2):109–17.
5. Bakhoun SF, Cantley LC. The multifaceted role of chromosomal instability in cancer and its microenvironment. *Cell*. 2018 Sep 6;174(6):1347–60.
6. Bakhoun SF, Ngo B, Laughney AM, Cavallo JA, Murphy CJ, Ly P, et al. Chromosomal instability drives metastasis through a cytosolic DNA response. *Nature*. 2018 Jan 25;553(7689):467–72.
7. Ippolito MR, Martis V, Martin S, Tijhuis AE, Hong C, Wardenaar R, et al. Gene copy-number changes and chromosomal instability induced by aneuploidy confer resistance to chemotherapy. *Dev Cell*. 2021 Sep 13;56(17):2440-2454.e6.
8. Lukow DA, Sausville EL, Suri P, Chunduri NK, Wieland A, Leu J, et al. Chromosomal instability accelerates the evolution of resistance to anti-cancer therapies. *Dev Cell*. 2021 Sep 13;56(17):2427-2439.e4.
9. Waizenegger IC, Hauf S, Meinke A, Peters JM. Two Distinct Pathways Remove Mammalian Cohesin from Chromosome Arms in Prophase and from Centromeres in Anaphase. *Cell*. 2000 Oct 27;103(3):399–410.
10. McGuinness BE, Hirota T, Kudo NR, Peters JM, Nasmyth K. Shugoshin prevents dissociation of cohesin from centromeres during mitosis in vertebrate cells. *PLoS Biol*. 2005 Mar;3(3):e86.
11. Zhou L, Liang C, Chen Q, Zhang Z, Zhang B, Yan H, et al. The N-Terminal Non-Kinase-Domain-Mediated Binding of Haspin to Pds5B Protects Centromeric Cohesion in Mitosis. *Curr Biol CB*. 2017 Apr 3;27(7):992–1004.
12. Clute P, Pines J. Temporal and spatial control of cyclin B1 destruction in metaphase. *Nat Cell Biol*. 1999 Jun;1(2):82–7.
13. Hauf S, Waizenegger IC, Peters JM. Cohesin cleavage by separase required for anaphase and cytokinesis in human cells. *Science*. 2001 Aug 17;293(5533):1320–3.
14. Sun Y, Kucej M, Fan HY, Yu H, Sun QY, Zou H. Separase is recruited to mitotic chromosomes to dissolve sister chromatid cohesion in a DNA-dependent manner. *Cell*. 2009 Apr 3;137(1):123–32.

15. Maddox P, Desai A, Oegema K, Mitchison TJ, Salmon ED. Poleward microtubule flux is a major component of spindle dynamics and anaphase a in mitotic *Drosophila* embryos. *Curr Biol CB*. 2002 Oct 1;12(19):1670–4.
16. Steblyanko Y, Rajendraprasad G, Osswald M, Eibes S, Jacome A, Geley S, et al. Microtubule poleward flux in human cells is driven by the coordinated action of four kinesins. *EMBO J*. 2020 Dec;39(23):e105432.
17. Scholey JM, Civelekoglu-Scholey G, Brust-Mascher I. Anaphase B. *Biology*. 2016 Dec 8;5(4):51.
18. Vukušić K, Tolić IM. Anaphase B: Long-standing models meet new concepts. *Semin Cell Dev Biol*. 2021 Sep;117:127–39.
19. Green RA, Paluch E, Oegema K. Cytokinesis in animal cells. *Annu Rev Cell Dev Biol*. 2012;28:29–58.
20. Sender R, Milo R. The distribution of cellular turnover in the human body. *Nat Med*. 2021 Jan;27(1):45–8.
21. Holland AJ, Cleveland DW. Losing balance: the origin and impact of aneuploidy in cancer. *EMBO Rep*. 2012 Jun;13(6):501–14.
22. Gascoigne KE, Cheeseman IM. CDK-dependent phosphorylation and nuclear exclusion coordinately control kinetochore assembly state. *J Cell Biol*. 2013 Apr 1;201(1):23–32.
23. Navarro AP, Cheeseman IM. Kinetochore assembly throughout the cell cycle. *Semin Cell Dev Biol*. 2021 Sep 1;117:62–74.
24. Pesenti ME, Raisch T, Conti D, Walstein K, Hoffmann I, Vogt D, et al. Structure of the human inner kinetochore CCAN complex and its significance for human centromere organization. *Mol Cell*. 2022 Jun 2;82(11):2113–2131.e8.
25. Perpelescu M, Fukagawa T. The ABCs of CENPs. *Chromosoma*. 2011 Oct 1;120(5):425–46.
26. Rago F, Gascoigne KE, Cheeseman IM. Distinct organization and regulation of the outer kinetochore KMN network downstream of CENP-C and CENP-T. *Curr Biol CB*. 2015 Mar 2;25(5):671–7.
27. Hori T, Shang WH, Takeuchi K, Fukagawa T. The CCAN recruits CENP-A to the centromere and forms the structural core for kinetochore assembly. *J Cell Biol*. 2013 Jan 7;200(1):45–60.
28. Varma D, Salmon ED. The KMN protein network – chief conductors of the kinetochore orchestra. *J Cell Sci*. 2012 Dec 15;125(24):5927–36.
29. Petrovic A, Keller J, Liu Y, Overlack K, John J, Dimitrova YN, et al. Structure of the MIS12 Complex and Molecular Basis of Its Interaction with CENP-C at Human Kinetochores. *Cell*. 2016 Nov 3;167(4):1028–1040.e15.
30. Malvezzi F, Litos G, Schleiffer A, Heuck A, Mechtler K, Clausen T, et al. A structural basis for kinetochore recruitment of the Ndc80 complex via two distinct centromere receptors. *EMBO J*. 2013 Feb 6;32(3):409–23.

31. Nishino T, Rago F, Hori T, Tomii K, Cheeseman IM, Fukagawa T. CENP-T provides a structural platform for outer kinetochore assembly. *EMBO J.* 2013 Feb 6;32(3):424–36.
32. Huis in 't Veld PJ, Jeganathan S, Petrovic A, Singh P, John J, Krenn V, et al. Molecular basis of outer kinetochore assembly on CENP-T. *eLife.* 5:e21007.
33. Gaitanos TN, Santamaria A, Jeyaprakash AA, Wang B, Conti E, Nigg EA. Stable kinetochore–microtubule interactions depend on the Ska complex and its new component Ska3/C13Orf3. *EMBO J.* 2009 May 20;28(10):1442–52.
34. McEwen BF, Heagle AB, Cassels GO, Buttle KF, Rieder CL. Kinetochore Fiber Maturation in PtK1 Cells and Its Implications for the Mechanisms of Chromosome Congression and Anaphase Onset. *J Cell Biol.* 1997 Jun 30;137(7):1567.
35. Magidson V, Paul R, Yang N, Ault JG, O’Connell CB, Tikhonenko I, et al. Adaptive changes in the kinetochore architecture facilitate proper spindle assembly. *Nat Cell Biol.* 2015 Sep;17(9):1134–44.
36. Tolić IM. Mitotic spindle: kinetochore fibers hold on tight to interpolar bundles. *Eur Biophys J.* 2018;47(3):191–203.
37. Maiato H, Gomes AM, Sousa F, Barisic M. Mechanisms of Chromosome Congression during Mitosis. *Biology.* 2017 Mar;6(1):13.
38. Dong Y, Vanden Beldt KJ, Meng X, Khodjakov A, McEwen BF. The outer plate in vertebrate kinetochores is a flexible network with multiple microtubule interactions. *Nat Cell Biol.* 2007 May;9(5):516–22.
39. Kuniyasu K, Iemura K, Tanaka K. Delayed Chromosome Alignment to the Spindle Equator Increases the Rate of Chromosome Missegregation in Cancer Cell Lines. *Biomolecules* [Internet]. 2019 Jan 1 [cited 2023 Jun 14];9(1). Available from: /pmc/articles/PMC6359495/
40. Yang Z, Tulu US, Wadsworth P, Rieder CL. Kinetochore Dynein Is Required for Chromosome Motion and Congression Independent of the Spindle Checkpoint. *Curr Biol.* 2007 Jun 5;17(11):973–80.
41. Li Y, Yu W, Liang Y, Zhu X. Kinetochore dynein generates a poleward pulling force to facilitate congression and full chromosome alignment. *Cell Res.* 2007 Aug;17(8):701–12.
42. Shrestha RL, Conti D, Tamura N, Braun D, Ramalingam RA, Cieslinski K, et al. Aurora-B kinase pathway controls the lateral to end-on conversion of kinetochore-microtubule attachments in human cells. *Nat Commun.* 2017 Jul 28;8(1):150.
43. Koshland DE, Mitchison TJ, Kirschner MW. Polewards chromosome movement driven by microtubule depolymerization in vitro. *Nature.* 1988 Feb;331(6156):499–504.
44. Coue M, Lombillo VA, McIntosh JR. Microtubule depolymerization promotes particle and chromosome movement in vitro. *J Cell Biol.* 1991 Mar 15;112(6):1165–75.
45. Cassimeris L, Rieder CL, Salmon ED. Microtubule assembly and kinetochore directional instability in vertebrate monopolar spindles: implications for the mechanism of chromosome congression. *J Cell Sci.* 1994 Jan;107 ( Pt 1):285–97.

46. Rieder CL, Davison EA, Jensen LC, Cassimeris L, Salmon ED. Oscillatory movements of monooriented chromosomes and their position relative to the spindle pole result from the ejection properties of the aster and half-spindle. *J Cell Biol.* 1986 Aug 1;103(2):581–91.
47. Orr B, Maiato H. No chromosome left behind: The importance of metaphase alignment for mitotic fidelity. *J Cell Biol.* 2019 Mar 11;218(4):1086–8.
48. Khodjakov A, Rieder CL. Kinetochores moving away from their associated pole do not exert a significant pushing force on the chromosome. *J Cell Biol.* 1996 Oct 15;135(2):315–27.
49. Toso A, Winter JR, Garrod AJ, Amaro AC, Meraldi P, McAinsh AD. Kinetochores-generated pushing forces separate centrosomes during bipolar spindle assembly. *J Cell Biol.* 2009 Feb 9;184(3):365–72.
50. Vukušić K, Buđa R, Bosilj A, Milas A, Pavin N, Tolić IM. Microtubule Sliding within the Bridging Fiber Pushes Kinetochores Apart to Segregate Chromosomes. *Dev Cell.* 2017 Oct 9;43(1):11–23.e6.
51. FitzHarris G. Anaphase B precedes anaphase A in the mouse egg. *Curr Biol CB.* 2012 Mar 6;22(5):437–44.
52. Satyanarayana A, Kaldis P. Mammalian cell-cycle regulation: several Cdks, numerous cyclins and diverse compensatory mechanisms. *Oncogene.* 2009 Aug 20;28(33):2925–39.
53. Iyer DR, Rhind N. The Intra-S Checkpoint Responses to DNA Damage. *Genes.* 2017 Feb 17;8(2):74.
54. Shaltiel IA, Krenning L, Bruinsma W, Medema RH. The same, only different - DNA damage checkpoints and their reversal throughout the cell cycle. *J Cell Sci.* 2015 Feb 15;128(4):607–20.
55. Foley EA, Kapoor TM. Microtubule attachment and spindle assembly checkpoint signaling at the kinetochore. *Nat Rev Mol Cell Biol.* 2013 Jan;14(1):25–37.
56. London N, Biggins S. Mad1 kinetochore recruitment by Mps1-mediated phosphorylation of Bub1 signals the spindle checkpoint. *Genes Dev.* 2014 Jan 15;28(2):140–52.
57. London N, Ceto S, Ranish JA, Biggins S. Phosphoregulation of Spc105 by Mps1 and PP1 Regulates Bub1 Localization to Kinetochores. *Curr Biol CB.* 2012 May 22;22(10):900–6.
58. Yamagishi Y, Yang CH, Tanno Y, Watanabe Y. MPS1/Mph1 phosphorylates the kinetochore protein KNL1/Spc7 to recruit SAC components. *Nat Cell Biol.* 2012 Jun 3;14(7):746–52.
59. Shepperd LA, Meadows JC, Sochaj AM, Lancaster TC, Zou J, Buttrick GJ, et al. Phospho-dependent recruitment of Bub1 and Bub3 to Spc7/KNL1 by Mph1 kinase maintains the spindle checkpoint. *Curr Biol CB.* 2012 May 22;22(10):891–9.
60. Nilsson J, Yekezare M, Minshull J, Pines J. The APC/C maintains the spindle assembly checkpoint by targeting Cdc20 for destruction. *Nat Cell Biol.* 2008 Dec;10(12):1411–20.

61. Sudakin V, Chan GKT, Yen TJ. Checkpoint inhibition of the APC/C in HeLa cells is mediated by a complex of BUBR1, BUB3, CDC20, and MAD2. *J Cell Biol.* 2001 Sep 3;154(5):925–36.
62. Liu ST, Zhang H. The mitotic checkpoint complex (MCC): looking back and forth after 15 years. *AIMS Mol Sci.* 2016;3(4):597–634.
63. Chao WCH, Kulkarni K, Zhang Z, Kong EH, Barford D. Structure of the mitotic checkpoint complex. *Nature.* 2012 Mar 21;484(7393):208–13.
64. Foe IT, Foster SA, Cheung SK, DeLuca SZ, Morgan DO, Toczyski DP. Ubiquitination of Cdc20 by the APC occurs through an intramolecular mechanism. *Curr Biol CB.* 2011 Nov 22;21(22):1870–7.
65. Ji Z, Gao H, Yu H. Kinetochore attachment sensed by competitive Mps1 and microtubule binding to Ndc80C. *Science.* 2015 Jun 12;348(6240):1260–4.
66. Hiruma Y, Sacristan C, Pachis ST, Adamopoulos A, Kuijt T, Ubbink M, et al. CELL DIVISION CYCLE. Competition between MPS1 and microtubules at kinetochores regulates spindle checkpoint signaling. *Science.* 2015 Jun 12;348(6240):1264–7.
67. Etemad B, Kuijt TEF, Kops GJPL. Kinetochore–microtubule attachment is sufficient to satisfy the human spindle assembly checkpoint. *Nat Commun.* 2015 Dec 1;6:8987.
68. Kuhn J, Dumont S. Spindle assembly checkpoint satisfaction occurs via end-on but not lateral attachments under tension. *J Cell Biol.* 2017 Jun 5;216(6):1533–42.
69. Cimini D, Moree B, Canman JC, Salmon ED. Merotelic kinetochore orientation occurs frequently during early mitosis in mammalian tissue cells and error correction is achieved by two different mechanisms. *J Cell Sci.* 2003 Oct 15;116(20):4213–25.
70. Cimini D, Cameron LA, Salmon ED. Anaphase spindle mechanics prevent mis-segregation of merotelically oriented chromosomes. *Curr Biol.* 2004 Dec 14;14(23):2149–55.
71. Gregan J, Polakova S, Zhang L, Tolić-Nørrelykke IM, Cimini D. Merotelic kinetochore attachment: Causes and effects. *Trends Cell Biol.* 2011 Jun 1;21(6):374–81.
72. Lens SMA, Voest EE, Medema RH. Shared and separate functions of polo-like kinases and aurora kinases in cancer. *Nat Rev Cancer.* 2010 Dec;10(12):825–41.
73. Kelly AE, Funabiki H. Correcting aberrant kinetochore microtubule attachments: an Aurora B-centric view. *Curr Opin Cell Biol.* 2009 Feb;21(1):51–8.
74. Knowlton AL, Lan W, Stukenberg PT. Aurora B is enriched at merotelic attachment sites, where it regulates MCAK. *Curr Biol CB.* 2006 Sep 5;16(17):1705–10.
75. Cimini D, Wan X, Hirel CB, Salmon ED. Aurora kinase promotes turnover of kinetochore microtubules to reduce chromosome segregation errors. *Curr Biol CB.* 2006 Sep 5;16(17):1711–8.
76. Lampson MA, Renduchitala K, Khodjakov A, Kapoor TM. Correcting improper chromosome–spindle attachments during cell division. *Nat Cell Biol* 2004 63. 2004 Feb 8;6(3):232–7.

77. DeLuca JG, Gall WE, Ciferri C, Cimini D, Musacchio A, Salmon ED. Kinetochore microtubule dynamics and attachment stability are regulated by Hec1. *Cell*. 2006 Dec 1;127(5):969–82.
78. Ciferri C, Pasqualato S, Screpanti E, Varetto G, Santaguida S, Reis GD, et al. Implications for Kinetochore-Microtubule Attachment from the Structure of an Engineered Ndc80 Complex. *Cell*. 2008 May 2;133(3):427–39.
79. DeLuca KF, Lens SMA, DeLuca JG. Temporal changes in Hec1 phosphorylation control kinetochore–microtubule attachment stability during mitosis. *J Cell Sci*. 2011 Feb 15;124(4):622–34.
80. Pinsky BA, Kung C, Shokat KM, Biggins S. The Ipl1-Aurora protein kinase activates the spindle checkpoint by creating unattached kinetochores. *Nat Cell Biol*. 2006 Jan;8(1):78–83.
81. Earnshaw WC, Cooke CA. Analysis of the distribution of the INCENPs throughout mitosis reveals the existence of a pathway of structural changes in the chromosomes during metaphase and early events in cleavage furrow formation. *J Cell Sci*. 1991 Apr;98 ( Pt 4):443–61.
82. Adriaans IE, Hooikaas PJ, Aher A, Vromans MJM, Es RM van, Grigoriev I, et al. MKLP2 Is a Motile Kinesin that Transports the Chromosomal Passenger Complex during Anaphase. *Curr Biol*. 2020 Jul 6;30(13):2628-2637.e9.
83. Gruneberg U, Neef R, Honda R, Nigg EA, Barr FA. Relocation of Aurora B from centromeres to the central spindle at the metaphase to anaphase transition requires MKlp2. *J Cell Biol*. 2004 Jul 19;166(2):167–72.
84. Carmena M, Wheelock M, Funabiki H, Earnshaw WC. The Chromosomal Passenger Complex (CPC): From Easy Rider to the Godfather of Mitosis. *Nat Rev Mol Cell Biol*. 2012 Dec;13(12):789–803.
85. Zhai Y, Kronebusch PJ, Borisy GG. Kinetochore microtubule dynamics and the metaphase-anaphase transition. *J Cell Biol*. 1995 Nov 1;131(3):721–34.
86. Gorbsky GJ, Borisy GG. Microtubules of the kinetochore fiber turn over in metaphase but not in anaphase. *J Cell Biol*. 1989 Aug 1;109(2):653–62.
87. Sen O, Harrison JU, Burroughs NJ, McAnish AD. Kinetochore life histories reveal an Aurora-B-dependent error correction mechanism in anaphase. *Dev Cell*. 2021 Nov 22;56(22):3082.
88. Orr B, De Sousa F, Gomes AM, Afonso O, Ferreira LT, Figueiredo AC, et al. An anaphase surveillance mechanism prevents micronuclei formation from frequent chromosome segregation errors. *Cell Rep*. 2021 Nov 9;37(6):109783.
89. Fuller BG, Lampson MA, Foley EA, Rosasco-Nitcher S, Le KV, Tobelmann P, et al. Midzone activation of aurora B in anaphase produces an intracellular phosphorylation gradient. *Nature*. 2008 Jun;453(7198):1132–6.
90. Papini D, Levasseur MD, Higgins JMG. The Aurora B gradient sustains kinetochore stability in anaphase. *Cell Rep*. 2021 Nov 9;37(6):109818.

91. Bolhaqueiro ACF, Ponsioen B, Bakker B, Klaasen SJ, Kucukkose E, van Jaarsveld RH, et al. Ongoing chromosomal instability and karyotype evolution in human colorectal cancer organoids. *Nat Genet.* 2019 May;51(5):824–34.
92. Cimini D, Howell B, Maddox P, Khodjakov A, Degrossi F, Salmon ED. Merotelic kinetochore orientation is a major mechanism of aneuploidy in mitotic mammalian tissue cells. *J Cell Biol.* 2001 Feb 5;152(3):517–27.
93. Cimini D, Fioravanti D, Salmon ED, Degrossi F. Merotelic kinetochore orientation versus chromosome mono-orientation in the origin of lagging chromosomes in human primary cells. *J Cell Sci.* 2002 Feb;115(Pt 3):507–15.
94. Crasta K, Ganem NJ, Dagher R, Lantermann AB, Ivanova EV, Pan Y, et al. DNA breaks and chromosome pulverization from errors in mitosis. *Nature.* 2012 Feb 2;482(7383):53–8.
95. Worrall JT, Tamura N, Mazzagatti A, Shaikh N, van Lingen T, Bakker B, et al. Non-random Mis-segregation of Human Chromosomes. *Cell Rep.* 2018;23(11):3366–80.
96. Henikoff S, Malik HS. Centromeres: Selfish drivers. *Nature.* 2002 May;417(6886):227–227.
97. Dumont M, Gamba R, Gestraud P, Klaasen S, Worrall JT, De Vries SG, et al. Human chromosome-specific aneuploidy is influenced by DNA-dependent centromeric features. *EMBO J.* 2019 Nov 21;e102924.
98. Klaasen SJ, Truong MA, van Jaarsveld RH, Koprivec I, Štimac V, de Vries SG, et al. Nuclear chromosome locations dictate segregation error frequencies. *Nat* 2022 6077919. 2022 Jul 13;607(7919):604–9.
99. Vukušić K, Tolić IM. Polar Chromosomes—Challenges of a Risky Path. *Cells.* 2022 May 3;11(9):1531.
100. Sobecki M, Souaid C, Boulay J, Guerineau V, Noordermeer D, Crabbe L. MadID, a Versatile Approach to Map Protein-DNA Interactions, Highlights Telomere-Nuclear Envelope Contact Sites in Human Cells. *Cell Rep.* 2018 Dec 4;25(10):2891-2903.e5.
101. Chen Y, Zhang Y, Wang Y, Zhang L, Brinkman EK, Adam SA, et al. Mapping 3D genome organization relative to nuclear compartments using TSA-Seq as a cytological ruler. *J Cell Biol.* 2018 Aug 28;217(11):4025–48.
102. Kind J, Pagie L, Ortabozkoyun H, Boyle S, de Vries SS, Janssen H, et al. Single-cell dynamics of genome-nuclear lamina interactions. *Cell.* 2013 Mar 28;153(1):178–92.
103. Kouznetsova A, Kitajima TS, Brismar H, Höög C. Post-metaphase correction of aberrant kinetochore-microtubule attachments in mammalian eggs. *EMBO Rep.* 2019 Aug;20(8):e47905.
104. Hintzsche H, Hemmann U, Poth A, Utesch D, Lott J, Stopper H, et al. Fate of micronuclei and micronucleated cells. *Mutat Res Rev Mutat Res.* 2017;771:85–98.
105. Hatch EM, Fischer AH, Deerinck TJ, Hetzer MW. Catastrophic Nuclear Envelope Collapse in Cancer Cell Micronuclei. *Cell.* 2013 Jul 3;154(1):47.

106. Ben-David U, Amon A. Context is everything: aneuploidy in cancer. *Nat Rev Genet.* 2020 Jan 1;21(1):44–62.
107. Barra V, Fachinetti D. The dark side of centromeres: types, causes and consequences of structural abnormalities implicating centromeric DNA. *Nat Commun [Internet].* 2018 Dec 1 [cited 2021 Jan 13];9(1). Available from: <https://pubmed.ncbi.nlm.nih.gov/30337534/>
108. Hamerton JL, Canning N, Ray M, Smith S. A cytogenetic survey of 14,069 newborn infants: I. Incidence of chromosome abnormalities. *Clin Genet.* 1975 Apr 23;8(4):223–43.
109. Nielsen J, Wohler M. Chromosome abnormalities found among 34,910 newborn children: results from a 13-year incidence study in Arhus, Denmark. *Hum Genet.* 1991 Jan;87(1):81–3.
110. Hochstenbach R, van Binsbergen E, Engelen J, Nieuwint A, Polstra A, Poddighe P, et al. Array analysis and karyotyping: workflow consequences based on a retrospective study of 36,325 patients with idiopathic developmental delay in the Netherlands. *Eur J Med Genet.* 2009;52(4):161–9.
111. Bandyopadhyay R, Heller A, Knox-DuBois C, McCaskill C, Berend SA, Page SL, et al. Parental origin and timing of de novo robertsonian translocation formation. *Am J Hum Genet.* 2002 Dec 1;71(6):1456–62.
112. Stimpson KM, Sullivan LL, Kuo ME, Sullivan BA. Nucleolar Organization, Ribosomal DNA Array Stability, and Acrocentric Chromosome Integrity Are Linked to Telomere Function. *PLoS ONE.* 2014 Mar 24;9(3):e92432.
113. Shaffer LG, Lupski JR. Molecular mechanisms for constitutional chromosomal rearrangements in humans. *Annu Rev Genet.* 2000;34:297–329.
114. Maciejowski J, Li Y, Bosco N, Campbell PJ, de Lange T. Chromothripsis and Kataegis Induced by Telomere Crisis. *Cell.* 2015 Dec 17;163(7):1641–54.
115. Poot M, Hochstenbach R. Prevalence and Phenotypic Impact of Robertsonian Translocations. *Mol Syndromol.* 2021;12(1):1–11.
116. McClintock B. The Stability of Broken Ends of Chromosomes in Zea Mays. *Genetics.* 1941;26(2):234–82.
117. Lopez V, Barinova N, Onishi M, Pobiega S, Pringle JR, Dubrana K, et al. Cytokinesis breaks dicentric chromosomes preferentially at pericentromeric regions and telomere fusions. *Genes Dev.* 2015;29(3):322–36.
118. Gascoigne KE, Cheeseman IM. Induced dicentric chromosome formation promotes genomic rearrangements and tumorigenesis. *Chromosome Res.* 2013 Jul 1;21(4):407–18.
119. Yilmaz A, Zhang XY, Chung JT, Tan SL, Holzer H, Ao A. Chromosome Segregation Analysis in Human Embryos Obtained from Couples Involving Male Carriers of Reciprocal or Robertsonian Translocation. *PLOS ONE.* 2012 Sep 27;7(9):e46046.

120. Engels H, Eggermann T, Caliebe A, Jelska A, Schubert R, Schüler HM, et al. Genetic counseling in Robertsonian translocations der(13;14): Frequencies of reproductive outcomes and infertility in 101 pedigrees. *Am J Med Genet A*. 2008;146A(20):2611–6.
121. Scriven PN, Flinter FA, Braude PR, Ogilvie CM. Robertsonian translocations—reproductive risks and indications for preimplantation genetic diagnosis. *Hum Reprod*. 2001 Nov 1;16(11):2267–73.
122. Schoemaker MJ, Jones ME, Higgins CD, Wright AF, Swerdlow AJ. Mortality and Cancer Incidence in Carriers of Balanced Robertsonian Translocations: A National Cohort Study. *Am J Epidemiol*. 2019 Mar 1;188(3):500–8.
123. Campbell PJ, Yachida S, Mudie LJ, Stephens PJ, Pleasance ED, Stebbings LA, et al. The patterns and dynamics of genomic instability in metastatic pancreatic cancer. *Nature*. 2010 Oct 28;467(7319):1109–13.
124. Nones K, Waddell N, Wayte N, Patch AM, Bailey P, Newell F, et al. Genomic catastrophes frequently arise in esophageal adenocarcinoma and drive tumorigenesis. *Nat Commun*. 2014 Oct 29;5:5224.
125. Wandall A. Kinetochore development in two dicentric chromosomes in man - A light and electron microscopic study. *Hum Genet*. 1989 May;82(2):137–41.
126. Earnshaw WC, Ratrie H, Stetten G. Visualization of centromere proteins CENP-B and CENP-C on a stable dicentric chromosome in cytological spreads. *Chromosoma*. 1989 Jun;98(1):1–12.
127. Sullivan BA, Willard HF. Stable dicentric X chromosomes with two functional centromeres [1]. *Nat Genet*. 1998;20(3):227–8.
128. Stimpson KM, Song IY, Jauch A, Holtgreve-Grez H, Hayden KE, Bridger JM, et al. Telomere Disruption Results in Non-Random Formation of De Novo Dicentric Chromosomes Involving Acrocentric Human Chromosomes. *PLOS Genet*. 2010 Aug 12;6(8):e1001061.
129. Higgins AW, Gustashaw KM, Willard HF. Engineered human dicentric chromosomes show centromere plasticity. *Chromosome Res*. 2005 Dec 8;13(8):745–62.
130. Jeppesen P, Mitchell A, Turner B, Perry P. Antibodies to defined histone epitopes reveal variations in chromatin conformation and underacetylation of centric heterochromatin in human metaphase chromosomes. *Chromosoma*. 1992 Mar;101(5–6):322–32.
131. Belyaev N, Keohane AM, Turner BM. Differential underacetylation of histones H2A, H3 and H4 on the inactive X chromosome in human female cells. *Hum Genet*. 1996 May;97(5):573–8.
132. Koo DH, Han F, Birchler JA, Jiang J. Distinct DNA methylation patterns associated with active and inactive centromeres of the maize B chromosome. *Genome Res*. 2011 Jan 6;21(6):908–14.
133. Fu S, Gao Z, Birchler J, Han F. Dicentric Chromosome Formation and Epigenetics of Centromere Formation in Plants. *J Genet Genomics*. 2012 Mar 20;39(3):125–30.

134. Altemose N, Logsdon GA, Bzikadze AV, Sidhwani P, Langley SA, Caldas GV, et al. Complete genomic and epigenetic maps of human centromeres. *Science*. 2022 Apr;376(6588):eabl4178.
135. MacKinnon RN, Campbell LJ. The Role of Dicentric Chromosome Formation and Secondary Centromere Deletion in the Evolution of Myeloid Malignancy. *Genet Res Int*. 2011;2011.
136. Sullivan BA, Schwartz S. Identification of centromeric antigens in dicentric robertsonian translocations: CENP-C and CENP-E are necessary components of functional centromeres. *Hum Mol Genet*. 1995 Dec 1;4(12):2189–97.
137. Page SL, Shaffer LG. Chromosome stability is maintained by short intercentromeric distance in functionally dicentric human Robertsonian translocations. *Chromosome Res*. 1998;6(2):115–22.
138. Stimpson KM, Matheny JE, Sullivan BA. Dicentric chromosomes: Unique models to study centromere function and inactivation. *Chromosome Res*. 2012 Jul;20(5):595–605.
139. Stratton MR, Campbell PJ, Futreal PA. The cancer genome. *Nature*. 2009 Apr 9;458(7239):719–24.
140. Holland AJ, Cleveland DW. Chromoanagenesis and cancer: Mechanisms and consequences of localized, complex chromosomal rearrangements. *Nat Med*. 2012 Nov;18(11):1630–8.
141. Pellestor F, Gaillard J, Schneider A, Puechberty J, Gatinois V. Chromoanagenesis, the mechanisms of a genomic chaos. *Semin Cell Dev Biol* [Internet]. 2021 Feb [cited 2021 Feb 23]; Available from: <https://linkinghub.elsevier.com/retrieve/pii/S1084952121000124>
142. Pellestor F. Chromoanagenesis: Cataclysms behind complex chromosomal rearrangements. *Mol Cytogenet*. 2019 Feb 11;12(1).
143. Pellestor F, Gatinois V. Chromoanagenesis: A piece of the macroevolution scenario. *Mol Cytogenet*. 2020 Jan 28;13(1).
144. Stephens PJ, Greenman CD, Fu B, Yang F, Bignell GR, Mudie LJ, et al. Massive genomic rearrangement acquired in a single catastrophic event during cancer development. *Cell*. 2011 Jan 7;144(1):27–40.
145. Li Y, Schwab C, Ryan SL, Papaemmanuil E, Robinson HM, Jacobs P, et al. Constitutional and somatic rearrangement of chromosome 21 in acute lymphoblastic leukaemia. *Nature*. 2014;508(1):98–102.
146. Korbel JO, Campbell PJ. Criteria for inference of chromothripsis in cancer genomes. *Cell*. 2013 Mar 14;152(6):1226–36.
147. Liu P, Erez A, Nagamani SCS, Dhar SU, Kołodziejaska KE, Dharmadhikari AV, et al. Chromosome catastrophes involve replication mechanisms generating complex genomic rearrangements. *Cell*. 2011 Sep 16;146(6):889–903.

148. Berger MF, Lawrence MS, Demichelis F, Drier Y, Cibulskis K, Sivachenko AY, et al. The genomic complexity of primary human prostate cancer. *Nature*. 2011 Feb 10;470(7333):214–20.
149. Baca SC, Prandi D, Lawrence MS, Mosquera JM, Romanel A, Drier Y, et al. Punctuated evolution of prostate cancer genomes. *Cell*. 2013 Apr 25;153(3):666–77.
150. Zhang CZ, Leibowitz ML, Pellman D. Chromothripsis and beyond: Rapid genome evolution from complex chromosomal rearrangements. *Genes Dev*. 2013 Dec 1;27(23):2513–30.
151. Hanahan D, Weinberg RA. Hallmarks of cancer: The next generation. *Cell*. 2011 Mar 4;144(5):646–74.
152. Rode A, Maass KK, Willmund KV, Lichter P, Ernst A. Chromothripsis in cancer cells: An update. *Int J Cancer*. 2016 May 15;138(10):2322–33.
153. Cortés-Ciriano I, Lee JJK, Xi R, Jain D, Jung YL, Yang L, et al. Comprehensive analysis of chromothripsis in 2,658 human cancers using whole-genome sequencing. *Nat Genet*. 2020 Feb 5;1–11.
154. Zhang CZ, Spektor A, Cornils H, Francis JM, Jackson EK, Liu S, et al. Chromothripsis from DNA damage in micronuclei. *Nature*. 2015 Jun 11;522(7555):179–84.
155. Sorzano COS, Pascual-Montano A, De Diego AS, Martínez-A C, Van Wely KHM. Chromothripsis: Breakage-fusion-bridge over and over again. *Cell Cycle*. 2013 Jul 1;12(13):2016–23.
156. Umbreit NT, Zhang CZ, Lynch LD, Blaine LJ, Cheng AM, Tourdot R, et al. Mechanisms generating cancer genome complexity from a single cell division error. *Science*. 2020 Apr 17;368(6488):eaba0712.
157. Kisurina-Evgenieva OP, Sutiagina OI, Onishchenko GE. Biogenesis of micronuclei. *Biochem Mosc*. 2016 May 1;81(5):453–64.
158. Bhatia A, Kumar Y. Relevance of microscopic indicators of chromosomal instability in routine reporting of malignancies. *Diagn Cytopathol*. 2014 Feb;42(2):181–8.
159. Torres-Bugarín O, Macriz Romero N, Ramos Ibarra ML, Flores-García A, Valdez Aburto P, Zavala-Cerna MG. Genotoxic Effect in Autoimmune Diseases Evaluated by the Micronucleus Test Assay: Our Experience and Literature Review. *BioMed Res Int*. 2015;2015:194031.
160. Luzhna L, Kathiria P, Kovalchuk O. Micronuclei in genotoxicity assessment: From genetics to epigenetics and beyond. *Front Genet*. 2013;4(JUL).
161. Géraud G, Laquerrière F, Masson C, Arnoult J, Labidi B, Hernandez-Verdun D. Three-dimensional organization of micronuclei induced by colchicine in PtK1 cells. *Exp Cell Res*. 1989 Mar 1;181(1):27–39.
162. Yoshikawa T, Kashino G, Ono K, Watanabe M. Phosphorylated H2AX Foci in Tumor Cells Have No Correlation with Their Radiation Sensitivities. *J Radiat Res (Tokyo)*. 2009 Mar;50(2):151–60.

163. Terradas M, Martín M, Tusell L, Genescà A. Genetic activities in micronuclei: Is the DNA entrapped in micronuclei lost for the cell? *Mutat Res - Rev Mutat Res*. 2010;705(1):60–7.
164. Medvedeva NG, Panyutin IV, Panyutin IG, Neumann RD. Phosphorylation of Histone H2AX in Radiation-Induced Micronuclei. *Radiat Res*. 2007;168(4):493–8.
165. Xu R, Xu Y, Huo W, Lv Z, Yuan J, Ning S, et al. Mitosis-specific MRN complex promotes a mitotic signaling cascade to regulate spindle dynamics and chromosome segregation. *Proc Natl Acad Sci*. 2018 Oct 23;115(43):E10079–88.
166. Hoffelder DR, Luo L, Burke NA, Watkins SC, Gollin SM, Saunders WS. Resolution of anaphase bridges in cancer cells. *Chromosoma*. 2004 Jun;112(8):389–97.
167. Labidi B, Gregoire M, Frackowiak S, Hernandez-Verdun D, Bouteille M. RNA polymerase activity in PtK1 micronuclei containing individual chromosomes. An in vitro and in situ study. *Exp Cell Res*. 1987 Mar 1;169(1):233–44.
168. Terradas M, Martín M, Hernández L, Tusell L, Genescà A. Nuclear envelope defects impede a proper response to micronuclear DNA lesions. *Mutat Res - Fundam Mol Mech Mutagen*. 2012 Jan 3;729(1–2):35–40.
169. Dechat T, Gajewski A, Korbei B, Gerlich D, Daigle N, Haraguchi T, et al. LAP2alpha and BAF transiently localize to telomeres and specific regions on chromatin during nuclear assembly. *J Cell Sci*. 2004 Dec 1;117(Pt 25):6117–28.
170. Haraguchi T, Kojidani T, Koujin T, Shimi T, Osakada H, Mori C, et al. Live cell imaging and electron microscopy reveal dynamic processes of BAF-directed nuclear envelope assembly. *J Cell Sci*. 2008 Aug 1;121(Pt 15):2540–54.
171. Liu S, Kwon M, Mannino M, Yang N, Renda F, Khodjakov A, et al. Nuclear envelope assembly defects link mitotic errors to chromothripsis. *Nature*. 2018 Sep 27;561(7724):551–5.
172. Walther TC, Alves A, Pickersgill H, Loiodice I, Hetzer M, Galy V, et al. The conserved Nup107-160 complex is critical for nuclear pore complex assembly. *Cell*. 2003 Apr 18;113(2):195–206.
173. Liu S, Pellman D. The coordination of nuclear envelope assembly and chromosome segregation in metazoans. *Nucleus*. 2020 Jan 1;11(1):35–52.
174. Kutay U, Jühlen R, Antonin W. Mitotic disassembly and reassembly of nuclear pore complexes. *Trends Cell Biol*. 2021 Dec 1;31(12):1019–33.
175. Afonso O, Castellani CM, Cheeseman LP, Ferreira JG, Orr B, Ferreira LT, et al. Spatiotemporal control of mitotic exit during anaphase by an aurora B-Cdk1 crosstalk. *eLife*. 8:e47646.
176. Afonso O, Matos I, Pereira AJ, Aguiar P, Lampson MA, Maiato H. Feedback control of chromosome separation by a midzone Aurora B gradient. *Science*. 2014 Jul 18;345(6194):332–6.

177. Maiato H, Afonso O, Matos I. A chromosome separation checkpoint: A midzone Aurora B gradient mediates a chromosome separation checkpoint that regulates the anaphase-telophase transition. *BioEssays News Rev Mol Cell Dev Biol*. 2015 Mar;37(3):257–66.
178. Maiato H, Silva S. Double-checking chromosome segregation. *J Cell Biol* [Internet]. 2023 May 5 [cited 2023 Apr 12];222(5). Available from: /pmc/articles/PMC10082326/
179. Carmena M, Ruchaud S, Earnshaw WC. Making the Auroras glow: regulation of Aurora A and B kinase function by interacting proteins. *Curr Opin Cell Biol*. 2009 Dec;21(6):796–805.
180. Uehara R, Tsukada Y, Kamasaki T, Poser I, Yoda K, Gerlich DW, et al. Aurora B and Kif2A control microtubule length for assembly of a functional central spindle during anaphase. *J Cell Biol*. 2013 Aug 19;202(4):623–36.
181. Ly P, Teitz LS, Kim DH, Shoshani O, Skaletsky H, Fachinetti D, et al. Selective y centromere inactivation triggers chromosome shattering in micronuclei and repair by non-homologous end joining. *Nat Cell Biol*. 2017 Jan 1;19(1):68–75.
182. Roberts SA, Lawrence MS, Klimczak LJ, Grimm SA, Fargo D, Stojanov P, et al. An APOBEC cytidine deaminase mutagenesis pattern is widespread in human cancers. *Nat Genet*. 2013 Sep 14;45(9):970–6.
183. Nik-Zainal S, Alexandrov LB, Wedge DC, Van Loo P, Greenman CD, Raine K, et al. Mutational processes molding the genomes of 21 breast cancers. *Cell*. 2012 May 25;149(5):979–93.
184. Gisselsson D, Pettersson L, Höglund M, Heidenblad M, Gorunova L, Wiegant J, et al. Chromosomal breakage-fusion-bridge events cause genetic intratumor heterogeneity. *Proc Natl Acad Sci U S A*. 2000 May 9;97(10):5357–62.
185. Maher CA, Wilson RK. Chromothripsis and human disease: Piecing together the shattering process. *Cell*. 2012 Jan 20;148(1–2):29–32.
186. El Achkar E, Gerbault-Seureau M, Muleris M, Dutrillaux B, Debatisse M. Premature condensation induces breaks at the interface of early and late replicating chromosome bands bearing common fragile sites. *Proc Natl Acad Sci U S A*. 2005 Dec 13;102(50):18069–74.
187. Jones MJK, Jallepalli PV. Chromothripsis: Chromosomes in Crisis. *Dev Cell*. 2012 Nov 13;23(5):908–17.
188. Tubio JMC, Estivill X. Cancer: When catastrophe strikes a cell. *Nature*. 2011 Feb 24;470(7335):476–7.
189. Lin YF, Hu Q, Mazzagatti A, Valle-Inclán JE, Maurais EG, Dahiya R, et al. Mitotic clustering of pulverized chromosomes from micronuclei. *Nat* 2023. 2023 May 10;1–8.
190. Trivedi P, Steele CD, Au FKC, Alexandrov LB, Cleveland DW. Mitotic tethering enables inheritance of shattered micronuclear chromosomes. *Nature*. 2023 Jun;618(7967):1049–56.
191. Misteli T, Soutoglou E. The emerging role of nuclear architecture in DNA repair and genome maintenance. *Nat Rev Mol Cell Biol*. 2009 Apr;10(4):243–54.

192. Hu Q, Valle-Inclan JE, Dahiya R, Guyer A, Mazzagatti A, Maurais EG, et al. Non-homologous end joining shapes the genomic rearrangement landscape of chromothripsis from mitotic errors. *bioRxiv*. 2023 Aug 11;2023.08.10.552800.
193. Chiang C, Jacobsen JC, Ernst C, Hanscom C, Heilbut A, Blumenthal I, et al. Complex reorganization and predominant non-homologous repair following chromosomal breakage in karyotypically balanced germline rearrangements and transgenic integration. *Nat Genet*. 2012;44(4):390–1.
194. Pellestor F, Gatinois V, Puechberty J, Geneviève D, Lefort G. Chromothripsis: potential origin in gametogenesis and preimplantation cell divisions. A review. *Fertil Steril*. 2014 Dec 1;102(6):1785–96.
195. Kloosterman WP, Guryev V, van Roosmalen M, Duran KJ, de Bruijn E, Bakker SCM, et al. Chromothripsis as a mechanism driving complex de novo structural rearrangements in the germline. *Hum Mol Genet*. 2011 May;20(10):1916–24.
196. Kloosterman WP, Tavakoli-Yaraki M, Van Roosmalen MJ, Van Binsbergen E, Renkens I, Duran K, et al. Constitutional Chromothripsis Rearrangements Involve Clustered Double-Stranded DNA Breaks and Nonhomologous Repair Mechanisms. *Cell Rep*. 2012 Jun 28;1(6):648–55.
197. De Pagter MS, Van Roosmalen MJ, Baas AF, Renkens I, Duran KJ, Van Binsbergen E, et al. Chromothripsis in healthy individuals affects multiple protein-coding genes and can result in severe congenital abnormalities in offspring. *Am J Hum Genet*. 2015 Apr 2;96(4):651–6.
198. Ma X, Liu Y, Liu Y, Alexandrov LB, Edmonson MN, Gawad C, et al. Pan-cancer genome and transcriptome analyses of 1,699 paediatric leukaemias and solid tumours. *Nature*. 2018 Mar;555(7696):371–6.
199. Gröbner SN, Worst BC, Weischenfeldt J, Buchhalter I, Kleinheinz K, Rudneva VA, et al. The landscape of genomic alterations across childhood cancers. *Nature*. 2018 Mar 15;555(7696):321–7.
200. Rausch T, Jones DTW, Zapatka M, Stütz AM, Zichner T, Weischenfeldt J, et al. Genome sequencing of pediatric medulloblastoma links catastrophic DNA rearrangements with TP53 mutations. *Cell*. 2012 Jan 20;148(1–2):59–71.
201. Aaltonen LA, Abascal F, Abeshouse A, Aburatani H, Adams DJ, Agrawal N, et al. Pan-cancer analysis of whole genomes. *Nature*. 2020 Feb;578(7793):82–93.
202. Kim TM, Xi R, Luquette LJ, Park RW, Johnson MD, Park PJ. Functional genomic analysis of chromosomal aberrations in a compendium of 8000 cancer genomes. *Genome Res*. 2013 Feb;23(2):217–27.
203. Cai H, Kumar N, Bagheri HC, von Mering C, Robinson MD, Baudis M. Chromothripsis-like patterns are recurring but heterogeneously distributed features in a survey of 22,347 cancer genome screens. *BMC Genomics*. 2014 Jan 29;15(1).
204. Stiller CA, Kroll ME, Boyle PJ, Feng Z. Population mixing, socioeconomic status and incidence of childhood acute lymphoblastic leukaemia in England and Wales: analysis by census ward. *Br J Cancer*. 2008 Mar 11;98(5):1006–11.

205. Pieters R, de Groot-Kruseman H, Van der Velden V, Fiocco M, van den Berg H, de Bont E, et al. Successful Therapy Reduction and Intensification for Childhood Acute Lymphoblastic Leukemia Based on Minimal Residual Disease Monitoring: Study ALL10 From the Dutch Childhood Oncology Group. *J Clin Oncol Off J Am Soc Clin Oncol*. 2016 Aug 1;34(22):2591–601.
206. Vora A, Goulden N, Wade R, Mitchell C, Hancock J, Hough R, et al. Treatment reduction for children and young adults with low-risk acute lymphoblastic leukaemia defined by minimal residual disease (UKALL 2003): a randomised controlled trial. *Lancet Oncol*. 2013 Mar;14(3):199–209.
207. Mörücke A, Zimmermann M, Valsecchi MG, Stanulla M, Biondi A, Mann G, et al. Dexamethasone vs prednisone in induction treatment of pediatric ALL: results of the randomized trial AIEOP-BFM ALL 2000. *Blood*. 2016 Apr 28;127(17):2101–12.
208. Harewood L, Robinson H, Harris R, Jabbar Al-Obaidi M, Jalali GR, Martineau M, et al. Amplification of AML1 on a duplicated chromosome 21 in acute lymphoblastic leukemia: A study of 20 cases. *Leukemia*. 2003 Mar 1;17(3):547–53.
209. Robinson HM, Broadfield ZJ, Cheung KL, Harewood L, Harris RL, Jalali GR, et al. Amplification of AML1 in acute lymphoblastic leukemia is associated with a poor outcome. *Leukemia*. 2003 Sep 18;17(11):2249–50.
210. Rand V, Parker H, Russell LJ, Schwab C, Ensor H, Irving J, et al. Genomic characterization implicates iAMP21 as a likely primary genetic event in childhood B-cell precursor acute lymphoblastic leukemia. *Blood*. 2011 Jun 23;117(25):6848–55.
211. Hong D, Fritz AJ, Gordon JA, Tye CE, Boyd JR, Tracy KM, et al. RUNX1-dependent mechanisms in biological control and dysregulation in cancer. *J Cell Physiol*. 2019 Jun 1;234(6):8597–609.
212. Sood R, Kamikubo Y, Liu P. Role of RUNX1 in hematological malignancies. *Blood*. 2017 Apr 13;129(15):2070–82.
213. Hormann FM, Hoogkamer AQ, Boeree A, Sonneveld E, Escherich G, den Boer ML, et al. Integrating copy number data of 64 iAMP21 BCP-ALL patients narrows the common region of amplification to 1.57 Mb. *Front Oncol*. 2023;13:1128560.
214. Rabin KR. Insights into the genomics of iAMP21-ALL. *Blood*. 2023 Aug 24;142(8):682–4.
215. Koleilat A, Smadbeck JB, Cinthya |, Zepeda-Mendoza J, Williamson CM, Pitel BA, et al. Characterization of unusual iAMP21 B-lymphoblastic leukemia (iAMP21-ALL) from the Mayo Clinic and Children’s Oncology Group. *Genes Chromosomes Cancer* [Internet]. 2022 Jul 19 [cited 2022 Jul 26]; Available from: <https://onlinelibrary.wiley.com/doi/full/10.1002/gcc.23084>
216. Harrison CJ. Blood Spotlight on iAMP21 acute lymphoblastic leukemia (ALL), a high-risk pediatric disease. *Blood*. 2015 Feb 26;125(9):1383–6.
217. Moorman AV, Richards SM, Robinson HM, Strefford JC, Gibson BES, Kinsey SE, et al. Brief report: Prognosis of children with acute lymphoblastic leukemia (ALL) and

- intrachromosomal amplification of chromosome 21 (iAMP21). *Blood*. 2007 Mar 15;109(6):2327–30.
218. Attarbaschi A, Mann G, Panzer-Grümayer R, Röttgers S, Steiner M, König M, et al. Minimal residual disease values discriminate between low and high relapse risk in children with B-cell precursor acute lymphoblastic leukemia and an intrachromosomal amplification of chromosome 21: The Austrian and German Acute Lymphoblastic Leukemia Berl. *J Clin Oncol*. 2008;26(18):3046–50.
  219. Moorman AV, Robinson H, Schwab C, Richards SM, Hancock J, Mitchell CD, et al. Risk-Directed Treatment Intensification Significantly Reduces the Risk of Relapse Among Children and Adolescents With Acute Lymphoblastic Leukemia and Intrachromosomal Amplification of Chromosome 21: A Comparison of the MRC ALL97/99 and UKALL2003 Trials. *J Clin Oncol*. 2013;31(27):3389–96.
  220. Heerema NA, Carroll AJ, Devidas M, Loh ML, Borowitz MJ, Gastier-Foster JM, et al. Intrachromosomal amplification of chromosome 21 is associated with inferior outcomes in children with acute lymphoblastic leukemia treated in contemporary standard-risk children's oncology group studies: A report from the children's oncology group. *J Clin Oncol*. 2013 Sep 20;31(27):3397–402.
  221. Robinson HM, Harrison CJ, Moorman AV, Chudoba I, Strefford JC. Intrachromosomal amplification of chromosome 21 (iAMP21) may arise from a breakage-fusion-bridge cycle. *Genes Chromosomes Cancer*. 2007 Apr;46(4):318–26.
  222. Lo AWI, Sprung CN, Fouladi B, Pedram M, Sabatier L, Ricoul M, et al. Chromosome Instability as a Result of Double-Strand Breaks near Telomeres in Mouse Embryonic Stem Cells. *Mol Cell Biol*. 2002 Jul 1;22(13):4836–50.
  223. Sabatier L, Ricoul M, Pottier G, Murnane JP. The loss of a single telomere can result in instability of multiple chromosomes in a human tumor cell line. *Mol Cancer Res*. 2005 Mar;3(3):139–50.
  224. Jacobs PA, Browne C, Gregson N, Joyce C, White H, Jacobs C Browne N Gregson C Joyce H White PA. Estimates of the frequency of chromosome abnormalities detectable in unselected newborns using moderate levels of banding. *J Med Genet*. 1992;29:103–8.
  225. Bashton M, Hollis R, Ryan S, Schwab CJ, Moppett J, Harrison CJ, et al. Concordance of copy number abnormality detection using SNP arrays and Multiplex Ligation-dependent Probe Amplification (MLPA) in acute lymphoblastic leukaemia. *Sci Rep*. 2020 Jan 8;10:45.
  226. Creasey T, Enshaei A, Nebral K, Schwab C, Watts K, Cuthbert G, et al. Single nucleotide polymorphism array-based signature of low hypodiploidy in acute lymphoblastic leukemia. *Genes Chromosomes Cancer*. 2021 Sep;60(9):604–15.
  227. Liffner B, Absalon S. Expansion Microscopy Reveals Plasmodium falciparum Blood-Stage Parasites Undergo Anaphase with A Chromatin Bridge in the Absence of Mini-Chromosome Maintenance Complex Binding Protein. *Microorganisms*. 2021 Nov 6;9(11):2306.

228. Schindelin J, Arganda-Carreras I, Frise E, Kaynig V, Longair M, Pietzsch T, et al. Fiji: an open-source platform for biological-image analysis. *Nat Methods*. 2012 Jul;9(7):676–82.
229. Bankhead P, Loughrey MB, Fernández JA, Dombrowski Y, McArd DG, Dunne PD, et al. QuPath: Open source software for digital pathology image analysis. *Sci Rep*. 2017 Dec 4;7(1):16878.
230. Schmidt U, Weigert M, Broaddus C, Myers G. Cell Detection with Star-Convex Polygons. In: Frangi AF, Schnabel JA, Davatzikos C, Alberola-López C, Fichtinger G, editors. *Medical Image Computing and Computer Assisted Intervention – MICCAI 2018*. Cham: Springer International Publishing; 2018. p. 265–73. (Lecture Notes in Computer Science).
231. Wickham H. *ggplot2: Elegant Graphics for Data Analysis* [Internet]. Springer-Verlag New York; 2016. Available from: <https://ggplot2.tidyverse.org>
232. Antonarakis SE. Short arms of human acrocentric chromosomes and the completion of the human genome sequence. *Genome Res*. 2022 Apr;32(4):599–607.
233. McStay B. The p-Arms of Human Acrocentric Chromosomes Play by a Different Set of Rules. *Annu Rev Genomics Hum Genet*. 2023 Aug 25;24(1):63–83.
234. Gao Q, Ryan SL, Iacobucci I, Ghatge PS, Cranston RE, Schwab C, et al. The genomic landscape of acute lymphoblastic leukemia with intrachromosomal amplification of chromosome 21. *Blood*. 2023 Aug 24;142(8):711–23.
235. Martin S, Santaguida S. Understanding Complexity of Cancer Genomes: Lessons from Errors. *Dev Cell*. 2020 Jun 8;53(5):500–2.
236. MacDonald JR, Ziman R, Yuen RKC, Feuk L, Scherer SW. The Database of Genomic Variants: a curated collection of structural variation in the human genome. *Nucleic Acids Res*. 2014 Jan 1;42(Database issue):D986–92.
237. Abruzzo MA, Hunt PA, Mayer M, Jacobs PA, Wang JCC, Erbe RW. Cytogenetic analysis of lymphoblastoid cell lines. *Cytogenet Genome Res*. 1986;42(3):169–73.
238. Scheinfeldt LB, Hodges K, Pevsner J, Berlin D, Turan N, Gerry NP. Genetic and genomic stability across lymphoblastoid cell line expansions. *BMC Res Notes*. 2018 Aug 3;11(1).
239. Toritsuka M, Makinodan M, Yamauchi T, Yamashita Y, Ikawa D, Komori T, et al. Altered gene expression in lymphoblastoid cell lines after subculture. *Vitro Cell Dev Biol - Anim*. 2018 Aug 1;54(7):523–7.
240. Bunda S, Heir P, Metcalf J, Li ASC, Agnihotri S, Pusch S, et al. CIC protein instability contributes to tumorigenesis in glioblastoma. *Nat Commun*. 2019 Feb 8;10(1):661.
241. Lee CJ, Chan WI, Scotting PJ. CIC, a gene involved in cerebellar development and ErbB signaling, is significantly expressed in medulloblastomas. *J Neurooncol*. 2005 Jun;73(2):101–8.

242. Tan Q, Brunetti L, Rousseaux MWC, Lu HC, Wan YW, Revelli JP, et al. Loss of Capicua alters early T cell development and predisposes mice to T cell lymphoblastic leukemia/lymphoma. *Proc Natl Acad Sci U S A*. 2018 Feb 13;115(7):E1511–9.
243. Lacoste S, Wiechec E, Dos Santos Silva AG, Guffei A, Williams G, Lowbeer M, et al. Chromosomal rearrangements after ex vivo Epstein-Barr virus (EBV) infection of human B cells. *Oncogene*. 2010 Jan;29(4):503–15.
244. Beh TT, MacKinnon RN, Kalitsis P. Active centromere and chromosome identification in fixed cell lines. *Mol Cytogenet*. 2016;9(1).
245. Maiato H, DeLuca J, Salmon ED, Earnshaw WC. The dynamic kinetochore-microtubule interface. *J Cell Sci*. 2004 Nov 1;117(23):5461–77.
246. Wegel E, Göhler A, Lagerholm BC, Wainman A, Uphoff S, Kaufmann R, et al. Imaging cellular structures in super-resolution with SIM, STED and Localisation Microscopy: A practical comparison. *Sci Rep*. 2016 Jun 6;6(1):27290.
247. Trifonov AS, Jaskula JC, Teulon C, Glenn DR, Bar-Gill N, Walsworth RL. Chapter 5 - Limits to Resolution of CW STED Microscopy. In: Arimondo E, Berman PR, Lin CC, editors. *Advances In Atomic, Molecular, and Optical Physics* [Internet]. Academic Press; 2013 [cited 2023 Dec 5]. p. 279–302. (*Advances in Atomic, Molecular, and Optical Physics*; vol. 62). Available from: <https://www.sciencedirect.com/science/article/pii/B9780124080904000050>
248. Tomkiel J, Cooke CA, Saitoh H, Bernat RL, Earnshaw WC. CENP-C is required for maintaining proper kinetochore size and for a timely transition to anaphase. *J Cell Biol*. 1994;125(3):531–45.
249. Page SL, Earnshaw WC, Choo KH, Shaffer LG. Further evidence that CENP-C is a necessary component of active centromeres: studies of a dic(X; 15) with simultaneous immunofluorescence and FISH. *Hum Mol Genet*. 1995 Feb;4(2):289–94.
250. McAinsh AD, Meraldi P. The CCAN complex: Linking centromere specification to control of kinetochore-microtubule dynamics. *Semin Cell Dev Biol*. 2011;22(9):946–52.
251. Hara M, Fukagawa T. Critical Foundation of the Kinetochore: The Constitutive Centromere-Associated Network (CCAN). In: Black BE, editor. *Centromeres and Kinetochores: Discovering the Molecular Mechanisms Underlying Chromosome Inheritance* [Internet]. Cham: Springer International Publishing; 2017 [cited 2024 Jan 20]. p. 29–57. (*Progress in Molecular and Subcellular Biology*). Available from: [https://doi.org/10.1007/978-3-319-58592-5\\_2](https://doi.org/10.1007/978-3-319-58592-5_2)
252. Stirpe A, Heun P. The ins and outs of CENP-A: Chromatin dynamics of the centromere-specific histone. *Semin Cell Dev Biol*. 2023 Feb;135:24–34.
253. Afreen S, Varma D. Cell Division: Molecular Pathways for KMN Kinetochore Recruitment. *Curr Biol*. 2015 Apr 20;25(8):R332–5.
254. DeLuca JG, Dong Y, Hergert P, Strauss J, Hickey JM, Salmon ED, et al. Hec1 and Nuf2 Are Core Components of the Kinetochore Outer Plate Essential for Organizing Microtubule Attachment Sites. *Mol Biol Cell*. 2005 Feb;16(2):519–31.

255. Sullivan BA, Wolff DJ, Schwartz S. Analysis of centromeric activity in Robertsonian translocations: implications for a functional acrocentric hierarchy. *Chromosoma*. 1994 Dec;103(7):459–67.
256. Warburton PE, Cooke CA, Bourassa S, Vafa O, Sullivan BA, Stetten G, et al. Immunolocalization of CENP-A suggests a distinct nucleosome structure at the inner kinetochore plate of active centromeres. *Curr Biol*. 1997 Nov 1;7(11):901–4.
257. Earnshaw WC, Migeon BR. Three related centromere proteins are absent from the inactive centromere of a stable isodicentric chromosome. *Chromosoma*. 1985 Aug;92(4):290–6.
258. Fisher AM, Al-Gazali L, Pramathan T, Quaipe R, Cockwell AE, Barber JCK, et al. Centromeric inactivation in a dicentric human Y;21 translocation chromosome. *Chromosoma*. 1997 Aug 1;106(4):199–206.
259. Nicklas RB. How Cells Get the Right Chromosomes. *Science*. 1997 Jan 31;275(5300):632–7.
260. Ly P, Brunner SF, Shoshani O, Kim DH, Lan W, Pyntikova T, et al. Chromosome segregation errors generate a diverse spectrum of simple and complex genomic rearrangements. *Nat Genet*. 2019 Apr 1;51(4):705–15.
261. Tang S, Stokasimov E, Cui Y, Pellman D. Breakage of cytoplasmic chromosomes by pathological DNA base excision repair. *Nature*. 2022 Jun;606(7916):930–6.
262. Thompson SL, Bakhoun SF, Compton DA. Mechanisms of Chromosomal Instability. *Curr Biol*. 2010 Mar 23;20(6):R285–95.
263. Miyazaki K, Ichikawa Y, Saitoh N, Saitoh H. Three Types of Nuclear Envelope Assemblies Associated with Micronuclei. *CellBio*. 2020 Jan 14;09(01):14–28.
264. Tovini L, Johnson SC, Andersen AM, Carolina Johanna Spierings D, Wardenaar R, Foijer F, et al. Inducing Specific Chromosome Mis-Segregation in Human Cells. [cited 2022 Apr 21]; Available from: <https://doi.org/10.1101/2022.04.19.486691>
265. Drpic D, Almeida AC, Aguiar P, Renda F, Damas J, Lewin HA, et al. Chromosome Segregation Is Biased by Kinetochore Size. *Curr Biol*. 2018 May 7;28(9):1344–1356.e5.
266. Bolzer A, Kreth G, Solovei I, Koehler D, Saracoglu K, Fauth C, et al. Three-Dimensional Maps of All Chromosomes in Human Male Fibroblast Nuclei and Prometaphase Rosettes. [cited 2023 Jan 18]; Available from: [www.plosbiology.org](http://www.plosbiology.org)
267. Peters JM, Tedeschi A, Schmitz J. The cohesin complex and its roles in chromosome biology. *Genes Dev*. 2008 Nov 15;22(22):3089–114.
268. Sapkota H, Wasiak E, Daum JR, Gorbisky GJ. Multiple determinants and consequences of cohesion fatigue in mammalian cells. *Mol Biol Cell*. 2018 Aug 1;29(15):1811–24.
269. Hauf S, Roitinger E, Koch B, Dittrich CM, Mechtler K, Peters JM. Dissociation of Cohesin from Chromosome Arms and Loss of Arm Cohesion during Early Mitosis Depends on Phosphorylation of SA2. *PLoS Biol*. 2005 Mar;3(3):e69.

270. Sumara I, Vorlaufer E, Gieffers C, Peters BH, Peters JM. Characterization of Vertebrate Cohesin Complexes and Their Regulation in Prophase. *J Cell Biol.* 2000 Nov 13;151(4):749–62.
271. Losada A, Hirano M, Hirano T. Identification of *Xenopus* SMC protein complexes required for sister chromatid cohesion. *Genes Dev.* 1998 Jul 1;12(13):1986–97.
272. Klaasen SJ, Kops GJPL. Chromosome Inequality: Causes and Consequences of Non-Random Segregation Errors in Mitosis and Meiosis. *Cells.* 2022 Nov 11;11(22):3564.
273. Pachis ST, Kops GJPL. Leader of the SAC: molecular mechanisms of Mps1/TTK regulation in mitosis. *Open Biol.* 2018 Aug 15;8(8):180109.
274. Kops GJPL, Shah JV. Connecting up and clearing out: how kinetochore attachment silences the spindle assembly checkpoint. *Chromosoma.* 2012 Oct;121(5):509–25.
275. London N, Biggins S. Signaling dynamics in the spindle checkpoint response. *Nat Rev Mol Cell Biol.* 2014 Nov;15(11):736–47.
276. Hindriksen S, Lens SMA, Hadders MA. The Ins and Outs of Aurora B Inner Centromere Localization. *Front Cell Dev Biol.* 2017 Dec 22;5:112.
277. Liu D, Vader G, Vromans MJM, Lampson MA, Lens SMA. Sensing chromosome bi-orientation by spatial separation of aurora B kinase from kinetochore substrates. *Science.* 2009 Mar 6;323(5919):1350–3.
278. DeLuca KF, Meppelink A, Broad AJ, Mick JE, Peersen OB, Pektas S, et al. Aurora A kinase phosphorylates Hec1 to regulate metaphase kinetochore–microtubule dynamics. *J Cell Biol.* 2018 Jan 2;217(1):163–77.
279. Auckland P, McAinsh AD. Building an integrated model of chromosome congression. *J Cell Sci.* 2015 Sep 15;128(18):3363–74.
280. Maiato H, Gomes AM, Sousa F, Barisic M. Mechanisms of Chromosome Congression during Mitosis. *Biology.* 2017 Mar;6(1):13.
281. Itoh G, Ikeda M, Iemura K, Amin MA, Kuriyama S, Tanaka M, et al. Lateral attachment of kinetochores to microtubules is enriched in prometaphase rosette and facilitates chromosome alignment and bi-orientation establishment. *Sci Rep.* 2018 Mar 1;8(1):3888.
282. Ye AA, Deretic J, Hoel CM, Hinman AW, Cimini D, Welburn JP, et al. Aurora A Kinase Contributes to a Pole-Based Error Correction Pathway. *Curr Biol.* 2015 Jul 20;25(14):1842–51.
283. Ly P, Cleveland DW. Rebuilding Chromosomes After Catastrophe: Emerging Mechanisms of Chromothripsis. *Trends Cell Biol.* 2017 Dec 1;27(12):917–30.
284. Stear JH, Roth MB. Characterization of HCP-6, a *C. elegans* protein required to prevent chromosome twisting and merotelic attachment. *Genes Dev.* 2002 Jun 15;16(12):1498–508.
285. Cimini D. Merotelic kinetochore orientation, aneuploidy, and cancer. *Biochim Biophys Acta BBA - Rev Cancer.* 2008 Sep 1;1786(1):32–40.

286. McVey SL, Cosby JK, Nannas NJ. Aurora B Tension Sensing Mechanisms in the Kinetochore Ensure Accurate Chromosome Segregation. *Int J Mol Sci.* 2021 Aug 16;22(16):8818.
287. Chen GY, Renda F, Zhang H, Gokden A, Wu DZ, Chenoweth DM, et al. Tension promotes kinetochore–microtubule release by Aurora B kinase. *J Cell Biol.* 2021 Apr 27;220(6):e202007030.
288. Crosetto N, Bienko M. Radial Organization in the Mammalian Nucleus. *Front Genet* [Internet]. 2020 [cited 2024 Jan 29];11. Available from: <https://www.frontiersin.org/articles/10.3389/fgene.2020.00033>
289. Girelli G, Custodio J, Kallas T, Agostini F, Wernersson E, Spanjaard B, et al. GPSeq reveals the radial organization of chromatin in the cell nucleus. *Nat Biotechnol* 2020 3810. 2020 May 25;38(10):1184–93.
290. Das P, Shen T, McCord RP. Inferring chromosome radial organization from Hi-C data. *BMC Bioinformatics.* 2020 Nov 10;21(1):511.
291. Johnston AD, Simões-Pires CA, Suzuki M, Grealley JM. High-efficiency genomic editing in Epstein-Barr virus-transformed lymphoblastoid B cells using a single-stranded donor oligonucleotide strategy. *Commun Biol* [Internet]. 2019 [cited 2024 Feb 6];2. Available from: <https://www.ncbi.nlm.nih.gov/pmc/articles/PMC6694121/>
292. Ewunkem AJ, Agee K. Optimization of transfection methods for human lymphoblast TK6 cell line. *Gene Protein Dis.* 2023 May 29;2(2):0353.
293. Ma H, Tu LC, Naseri A, Huisman M, Zhang S, Grunwald D, et al. Multiplexed labeling of genomic loci with dCas9 and engineered sgRNAs using CRISPRainbow. *Nat Biotechnol.* 2016 May 1;34(5):528–30.
294. Waite JH, Tanzer ML. Polyphenolic Substance of *Mytilus edulis*: Novel Adhesive Containing L-Dopa and Hydroxyproline. *Science.* 1981 May 29;212(4498):1038–40.
295. Yu C, Zhao W, Duan C, Xie J, Yin W. Poly-l-lysine-caused cell adhesion induces pyroptosis in THP-1 monocytes. *Open Life Sci.* 2022 Jan 1;17(1):279–83.
296. Basiouni S, Fuhrmann H, Schumann J. High-efficiency transfection of suspension cell lines. *BioTechniques.* 2012 Aug;53(2):1–4.
297. La J, Y S, R C, Cc H, J G. Robust imaging and gene delivery to study human lymphoblastoid cell lines. *J Hum Genet* [Internet]. 2018 Sep [cited 2024 Feb 6];63(9). Available from: <https://pubmed.ncbi.nlm.nih.gov/29925960/>
298. Gebre M, Nomburg JL, Gewurz BE. CRISPR–Cas9 Genetic Analysis of Virus–Host Interactions. *Viruses.* 2018 Feb;10(2):55.
299. Casas-Delucchi CS, Becker A, Bolius JJ, Cardoso MC. Targeted manipulation of heterochromatin rescues MeCP2 Rett mutants and re-establishes higher order chromatin organization. *Nucleic Acids Res.* 2012 Dec;40(22):e176.
300. Lindhout BI, Fransz P, Tessadori F, Meckel T, Hooykaas PJJ, van der Zaal BJ. Live cell imaging of repetitive DNA sequences via GFP-tagged polydactyl zinc finger proteins. *Nucleic Acids Res.* 2007 Aug;35(16):e107.

301. Ma H, Reyes-Gutierrez P, Pederson T. Visualization of repetitive DNA sequences in human chromosomes with transcription activator-like effectors. *Proc Natl Acad Sci U S A*. 2013 Dec 24;110(52):21048–53.
302. Chen B, Gilbert LA, Cimini BA, Schnitzbauer J, Zhang W, Li GW, et al. Dynamic imaging of genomic loci in living human cells by an optimized CRISPR/Cas system. *Cell*. 2013 Dec 19;155(7):1479–91.
303. Chen B, Hu J, Almeida R, Liu H, Balakrishnan S, Covill-Cooke C, et al. Expanding the CRISPR imaging toolset with *Staphylococcus aureus* Cas9 for simultaneous imaging of multiple genomic loci. *Nucleic Acids Res*. 2016 May 5;44(8):e75.
304. Ma H, Naseri A, Reyes-Gutierrez P, Wolfe SA, Zhang S, Pederson T. Multicolor CRISPR labeling of chromosomal loci in human cells. *Proc Natl Acad Sci U S A*. 2015 Mar 10;112(10):3002–7.
305. Ma H, Tu LC, Naseri A, Chung YC, Grunwald D, Zhang S, et al. CRISPR-Sirius: RNA scaffolds for signal amplification in genome imaging. *Nat Methods*. 2018 Nov 1;15(11):928–31.
306. Tanenbaum ME, Gilbert LA, Qi LS, Weissman JS, Vale RD. A protein tagging system for signal amplification in gene expression and fluorescence imaging. *Cell*. 2014 Oct 23;159(3):635–46.
307. Shao S, Zhang W, Hu H, Xue B, Qin J, Sun C, et al. Long-term dual-color tracking of genomic loci by modified sgRNAs of the CRISPR/Cas9 system. *Nucleic Acids Res*. 2016 May 19;44(9):e86.
308. Mojica FJM, Díez-Villaseñor C, García-Martínez J, Almendros C. Short motif sequences determine the targets of the prokaryotic CRISPR defence system. *Microbiol Read Engl*. 2009 Mar;155(Pt 3):733–40.
309. Sternberg SH, Redding S, Jinek M, Greene EC, Doudna JA. DNA interrogation by the CRISPR RNA-guided endonuclease Cas9. *Nature*. 2014 Mar 6;507(7490):62–7.
310. Mali P, Esvelt KM, Church GM. Cas9 as a versatile tool for engineering biology. *Nat Methods*. 2013 Oct;10(10):957–63.
311. Konstantakos V, Nentidis A, Krithara A, Paliouras G. CRISPR–Cas9 gRNA efficiency prediction: an overview of predictive tools and the role of deep learning. *Nucleic Acids Res*. 2022 Apr 22;50(7):3616–37.
312. Jiang S, Wang LW, Walsh MJ, Trudeau SJ, Gerdt C, Zhao B, et al. CRISPR/Cas9-Mediated Genome Editing in Epstein-Barr Virus-Transformed Lymphoblastoid B-Cell Lines. *Curr Protoc Mol Biol*. 2018 Jan 1;121(1):31.12.1-31.12.23.
313. Aluigi M, Fogli M, Curti A, Isidori A, Gruppioni E, Chiodoni C, et al. Nucleofection is an efficient nonviral transfection technique for human bone marrow-derived mesenchymal stem cells. *Stem Cells Dayt Ohio*. 2006 Feb;24(2):454–61.
314. Søndergaard JN, Geng K, Sommerauer C, Atanasoai I, Yin X, Kutter C. Successful delivery of large-size CRISPR/Cas9 vectors in hard-to-transfect human cells using small plasmids. *Commun Biol*. 2020 Jun 19;3(1):1–6.

315. Gresch O, Altrogge L. Transfection of difficult-to-transfect primary mammalian cells. *Methods Mol Biol Clifton NJ*. 2012;801:65–74.
316. Lesueur LL, Mir LM, André FM. Overcoming the Specific Toxicity of Large Plasmids Electrotransfer in Primary Cells In Vitro. *Mol Ther - Nucleic Acids* [Internet]. 2016 Jan 1 [cited 2024 Feb 8];5. Available from: [https://www.cell.com/molecular-therapy-family/nucleic-acids/abstract/S2162-2531\(17\)30082-3](https://www.cell.com/molecular-therapy-family/nucleic-acids/abstract/S2162-2531(17)30082-3)
317. Lukacs GL, Haggie P, Seksek O, Lechardeur D, Freedman N, Verkman AS. Size-dependent DNA Mobility in Cytoplasm and Nucleus \*. *J Biol Chem*. 2000 Jan 21;275(3):1625–9.
318. Pezzoli D, Giupponi E, Mantovani D, Candiani G. Size matters for in vitro gene delivery: investigating the relationships among complexation protocol, transfection medium, size and sedimentation. *Sci Rep*. 2017 Mar 8;7(1):44134.
319. Yost S, De Wolf B, Hanks S, Zachariou A, Marcozzi C, Clarke M, et al. Biallelic TRIP13 mutations predispose to Wilms tumor and chromosome missegregation. *Nat Genet*. 2017 Jul 1;49(7):1148.
320. Ivanusic D, Madela K, Denner J. Easy and low-cost stable positioning of suspension cells during live-cell imaging. *J Biol Methods*. 2017 Oct 17;4(4):e80–e80.
321. Counsell JR, Asgarian Z, Meng J, Ferrer V, Vink CA, Howe SJ, et al. Lentiviral vectors can be used for full-length dystrophin gene therapy. *Sci Rep*. 2017 Mar 6;7(1):79.
322. M K, B K, N M, Re S. Systematic determination of the packaging limit of lentiviral vectors. *Hum Gene Ther* [Internet]. 2001 Oct 10 [cited 2024 Feb 17];12(15). Available from: <https://pubmed.ncbi.nlm.nih.gov/11589831/>
323. Sweeney NP, Vink CA. The impact of lentiviral vector genome size and producer cell genomic to gag-pol mRNA ratios on packaging efficiency and titre. *Mol Ther - Methods Clin Dev*. 2021 Jun 11;21:574–84.
324. Geraerts M, Willems S, Baekelandt V, Debyser Z, Gijssbers R. Comparison of lentiviral vector titration methods. *BMC Biotechnol*. 2006 Jul 12;6:34.
325. Sacristan C, Samejima K, Ruiz LA, Lambers MLA, Buckle A, Brackley CA, et al. Condensin reorganizes centromeric chromatin during mitotic entry into a bipartite structure stabilized by cohesin. *bioRxiv*. 2022 Aug 1;2022.08.01.502248.
326. Hayward D, Bancroft J, Mangat D, Alfonso-Pérez T, Dugdale S, McCarthy J, et al. Checkpoint signaling and error correction require regulation of the MPS1 T-loop by PP2A-B56. *J Cell Biol*. 2019 Oct 7;218(10):3188–99.
327. Es L, Af P. Assessing mRNA nuclear export in mammalian cells by microinjection. *Methods San Diego Calif* [Internet]. 2017 Aug 15 [cited 2024 Mar 11];126. Available from: <https://pubmed.ncbi.nlm.nih.gov/28577934/>